Zirconium-89 Complexes for Cell Tracking with Positron Emission Tomography

Trevor John Ferris
School of Physical Sciences, University of Kent at Canterbury

A thesis is submitted to the University of Kent at Canterbury in partial fulfilment of the requirements for the degree of Doctor of Philosophy

DECLARATION

No part of this thesis has been submitted by me or anyone else in support of an application for any other degree or qualification at the University of Kent or at any other University.

Signed: Trevor Ferris

Date: 18/03/2015

Abstract

Tracking cell migration *in vivo* by scintigraphy using cells labelled with gamma-emitting radionuclides (especially indium-111) is a well-established clinical and research tool. Positron emission tomography offers improved sensitivity and resolution, but there are no established cell labelling methods using suitable long-lived isotopes. The long half-life positron emitter zirconium-89 (half-life 78.4 h) is a strong candidate for cell labelling and cell tracking, and is becoming increasingly available. It has no known biological role or transport mechanisms.

The aim of this research was to produce a range of candidate neutral zirconium L_4 lipophilic complexes that could be prepared under radiopharmaceutical conditions and used in cell labelling. This aim was achieved with the ligands; oxine, tropolone and ethyl maltol. The resulting complexes can be prepared in high yield from zirconium precursors in hydrochloric or oxalic acid solution. A deferiprone complex was prepared from deferiprone and zirconium tetrachloride, but was found to lack lipophilic properties and it was not possible to prepare the deferiprone complex under radiopharmaceutical conditions.

Analytical techniques such as carbon, hydrogen and nitrogen elemental analysis, nuclear magnetic resonance spectroscopy, fourier transform infrared spectroscopy, and Raman spectroscopy have been used to characterise the complexes. The oxine and tropolone complexes were the most amenable to chromatographic characterisation and high performance liquid chromatography and instant thin layer chromatography protocols have been established to monitor radiochemical purity.

Cell uptake and efflux of zirconium-89 tetrakisoxine, tropolone and ethyl maltol utilising the following cell lines was determined; HCT116: colon cancer, J774: mouse macrophage and MDA-MB-231: breast cancer. Zirconium-89 tetrakisoxine has emerged as a lead compound. Zirconium-89 tetrakisoxine labelled myeloma cells retained the radiotracer *in vivo* for up to 7 days. Zirconium-89 tetrakisoxine was found to be a promising cell tracking agent for long term cell tracking studies.

Publications and Presentations

Peer-Reviewed Journal Articles:

Synthesis and Characterisation of Zirconium Complexes for Cell Tracking with Zr-89 by Positron Emission Tomography. T. J. Ferris, P. Charoenphun, L. K. Meszaros, G. E. D. Mullen, P. J. Blower and M. J. Went, *Dalton Trans*, 2014, **43**, 14851-14857.

[^{89}Zr]-Zr(oxinate)4 for long term in vivo cell tracking by positron emission tomography. P. Charoenphun, L.K. Meszaros, K. Chuamsaamarkkee1, E. Sharif-Paghaleh, J. R. Ballinger, T. J. Ferris, M. J. Went, G. E.D. Mullen, P. J. Blower, *Eur J Nucl Med Mol Imaging*, 2015, **42**, 2, 278-287.

Conference Abstracts:

^{89}Zr-Oxine Complex: a Long-Lived Radiolabel for Cell Tracking Using PET. L. K. Meszaros, P. Charoenphun, K. Chuamsaamarkkee, J. R. Ballinger, G. E. D. Mullen, T. J. Ferris, M. J. Went and P. J. Blower, 2013 World Molecular Imaging Conference, http://www.wmis.org/abstracts/2013/data/index.htm, Accessed 26 June 2014.

Medical Imaging utilising Zirconium Complexes. T. J. Ferris, P. Charoenphun, M. J. Went and P. J. Blower, *Nucl Med Commun*, 2013, **34**, 362.

Poster Presentations:

Medical Imaging utilising Zirconium Complexes. T. J. Ferris, P. Charoenphun, M. J. Went and P. J. Blower, *Nucl Med Commun*, 2013, **34**, 362.

Zirconium-89 Complexes for Positron Emission Tomography. Metal ions in medical imaging optical, radiopharmaceutical and MRI contrast. Dalton Discussion 15 08-SEP-2014 to 10-SEP-2014 University of York, UK.

Acknowledgements

I'd like to say thank you to the following people for their help and support with my research and production of this thesis.

My supervisor Professor Michael Went for his outstanding support over the years as a lecturer during my undergraduate time at Kent through to my postgraduate research. His knowledge of the chemical sciences has been invaluable in guiding my research. His support has kept me motivated and inspired me to produce this work to the best of my ability.

Our collobrator Professor Phil Blower from Kings College London for helping to guide my research and introducing me to nuclear medicine, his field of expertise. Without his knowledge, support and genorousity this research project would not have been possible and I am very gratefull.

Sarah for her unending patience, understanding and encouragement not just through the course of this PhD but over the last 10 years.

Watkin, Kitten and Bill Jenner Ferris for their quiet understanding and constant companionship.

Liv for her honesty and words of support.

Aaron, Alex (Chief), Christina (Red Ross) Christine Rogers, Emma, Holly, Jon James, Kate, Nanami (Nana), Ollie and Simon (Sensei) for making my time at Kent an enjoyable chapter in my life.

I would like to finish with one of my favourite quotes that I have found most illuminating and inspirational; *"Everything is determined, the beginning as well as the end, by forces over which we have no control. It is determined for the insect, as well as for the star. Human beings, vegetables, or cosmic dust, we all dance to a mysterious tune, intoned in the distance by an invisible piper."* **Albert Einstein**

To

Sarah Jane Jenner

CONTENTS

CHAPTER 2

Synthesis and Nuclear Magnetic Resonance Spectroscopic Characterisation of Zirconium Compounds

CHAPTER 4

Synthesis of Zirconium Tetrakis Complexes under Conditions Compatible with Radiopharmacy

CHAPTER 6

The *In Vitro* and *In Vivo* Analysis of Zirconium Compounds

APPENDIX

FIGURE INDEX

Chapter 1

Chapter 2

Chapter 4

Chapter 5

Chapter 6

Chapter 7

Abbreviations

Carbon-11:	**^{11}C**
Carbon-ion radiotherapy:	**CIRT**
Central nervous system:	**CNS**
Computational fluid dynamics:	**CFD**
Computed tomography:	**CT**
Computerised axial tomography:	**CAT**
Deoxyribonucleic acid:	**DNA**
Department of energy:	**DOE**
Dimethyl sulfoxide:	**DMSO**
Electroluminescence:	**EL**
Electron:	**e^-**
Emission computed tomography:	**ECT**
Epidermal growth factor receptor 2:	**HER2**
Fluorine-18:	**^{18}F**
Fluorodeoxyglucose:	**FDG**
Food and Drugs Administration:	**FDA**
Heteronuclear Multiple Quantum Coherence:	**HMQC**
High Performance Liquid Chromatography:	**HPLC**
Immuno-positron emission tomography:	**Immuno-PET**
Indium-111:	**^{111}In**
Instant Thin Layer Chromatography:	**ITLC**
International Union of Pure and Applied Chemistry:	**IUPAC**
Iodine-123:	**^{123}I**
Iodine-124:	**^{124}I**
Kerma area product:	**KAP**
Kiloelectronvolt:	**keV**
Magnetic resonance imaging:	**MRI**
Megabecquerel:	**MBq**
Molybdenum-99:	**^{99}Mo**
Monoclonal antibodies:	**mAB**
Neutron absorption cross section:	**NAC**

Nitrogen-13 ammonia:	**^{13}N-NH_3**
Nitrogen-13:	**^{13}N**
Optical coherence tomography:	**OCT**
Organic Light Emitting Diode:	**OLED**
Oxygen-15:	**^{15}O**
Phosphorus-30:	**^{30}P**
Photomultiplier tube:	**PMT**
Polysilicic Acid:	**SA**
Positron emission tomography:	**PET**
Prostate specific membrane antigen:	**PMSA**
Regional cerebral blood flow:	**rCBF**
Regional myocardial blood flow:	**rMBF**
Rubidium-82 Chloride:	**$^{82}RbCl$**
Rubidium-82:	**^{82}Rb**
Silica Gell:	**SG**
Single photon emission computed tomography:	**SPECT**
Super paramagnetic iron oxide:	**SPIO**
Technetium-99m:	**^{99m}Tc**
Thallium-201:	**^{201}TI**
The University of Kent at Canterbury:	**UKC**
Ultraviolet Visible:	**UV-Vis**
Xenon-133:	**^{133}Xe**
Yttrium-89:	**^{89}Y**
Zirconium-89:	**^{89}Zr**

CHAPTER 1
Introduction

1.1. Medical Imaging

Medical imaging refers to several different technologies that are used to view the human body in order to diagnose, monitor, or treat medical conditions. Each type of technology gives different information about the area of the body being studied or treated, related to possible disease, injury, or the effectiveness of medical treatment.

Methods of medical imaging that are based on X-ray technology include traditional X-ray, mammography, computed tomography (CT) fluoroscopy and angiography.
If there is a need to enhance an X-ray image it is possible to enhance the image with contrast agents. These contrast agents are used in angiography examinations.[1]

Diagnostic ultrasound methods employ high-frequency sound waves which produce images of internal body organs and soft tissues.[2] This is a painless test which is commonly used to monitor the growth of an unborn child, detect abnormalities of heart structures and detect abnormal widening of blood vessels (aneurysms).[2]

Magnetic resonance imaging (MRI) operates without the use of ionizing radiation unlike conventional X-ray, CT and Molecular Imaging. MRI uses strong magnetic fields to visualize internal structures of the body in more detail than X-rays. MRI produces no known irreversible biological effects in humans.[1]

Nuclear imaging is a method of producing images of different parts of the body after a radioactive tracer material is administered. Radiation is detected and the images are recorded on computer and on film. In the majority of cases radioactive tracers used in nuclear medicine are injected intravenously.[3] During a typical nuclear imaging scan the amount of radiation a patient receives is very low. Molecular imaging in nuclear medicine uses methods to visualize biological processes in the cells of organisms. Radioactive markers, called radiopharmaceuticals, are used for molecular imaging[3], to study molecular biological events under their full range of conditions.

1.1.1 X-ray Imaging (Radiography)

Medical X-rays are used in various types of diagnostic examinations and procedures. X-ray energy is high enough to pass through materials such as body tissues, internal organs and clothing[4]. The energy is absorbed in different amounts which is dependent on the density of the material they pass through. Dense materials, such as bone show up as white on X-rays whereas air in lungs shows up as black. Fat and muscle appear as varying shades of grey.[5] X-ray radiography can be used to locate tumours, orthopaedic injuries, pneumonias and foreign objects. Experienced physicians can read these images to diagnose medical conditions or injuries.[4] Advantages of X-ray imaging include easy mobility of certain types of equipment, a lower cost compared to other imaging methods and no complicated preparation of the patient, resulting in quick diagnosis and high bone resolution.[6] Disadvantages of X-ray imaging include the small potential for ionising radiation to damage living tissue, although only at very high levels of radiation exposure and in the minority of procedures[6], and the possibility that a person who has been exposed to X-rays could develop cancer, but this risk is minimal and depends on factors such as quantity of radiation dose administered, sex and age of the person exposed.[5]

1.1.2 Contrast Radiography

In some cases the use of conventional radiography may not be able to provide a diagnosis. Bones absorb radiation efficiently which is why they show up excellently on X-rays.[7] Other tissues and organs do not absorb radiation as effectively. Contrast radiography is in some cases a solution to this problem as it can be used to outline and highlight the exact anatomy of the area under investigation. An example of this technique in use is when a patient is suspected to have a bladder tumour that does not show up on a conventional radiograph. A contrast agent is injected into the patient that accumulates at the tumour thus it becomes visible.[8] Kidney function can also be evaluated using this technique. In this case the contrast agent is administered *via* intravenous pyelography (IVP). The kidneys excrete the contrast agent and depending on the efficiency of the process, the functional efficiency of the kidneys can be determined.[8]

1.1.3 Mammography

Mammography is a technique that uses X-rays to create images of breast tissue. The technique is undertaken to detect and evaluate any anomalies that may be found such as cysts and tumours.[9] Two forms of mammography exist; diagnostic and screening. Screening mammogram are used to look for cancer when the patient has no history of cancer, breast surgery or symptoms. Between 2 to 4 screening mammograms out of every 1,000 lead to the diagnosis of breast cancer. Diagnostic mammograms are tailored to examine a specific area in the breast.[9] The X-rays in diagnostic mammograms are taken at a range of angles so that a specific area can be targeted. Magnification views or spot comparisons can also be used to aid in a diagnosis. Diagnostic mammography cannot however provide a definitive diagnosis of cancer, it can be used to assess if any discovered anomalies have the potential of being benign or whether further investigative procedures should be undertaken to determine whether cancer is present.

1.1.4 Computed Tomography

Computed tomography (CT) imaging also known as computerized axial tomography (CAT) scanning can present a form of imaging commonly known as cross-sectional imaging. These cross sectional images or slices of a patient's anatomy can be used in a range of diagnostic and therapeutic treatments. CT techniques are based on mathematical algorithms originally developed by Radon in 1917. In the 1970s CT techniques were introduced to the radionuclide imaging methods of the time.[10] Radiopharmaceuticals administered to a patient decay and positrons or gamma rays are emitted. These emissions are recorded by detectors and can be used to provide cross sectional images of a patient. The technique is known as emission computed tomography (ECT).[10] When radiopharmaceuticals are used that emit γ-rays the technique is known as single photon emission computed tomography (SPECT). When a positron emitting radiopharmaceutical is used the technique is known as positron emission tomography/computed tomography (PET/CT).

1.1.5 Angiography

Angiography is a medical imaging technique which is used to image blood vessels. The technique utilises an X-ray contrast agent that is water soluble and ionic or non-ionic. The water soluble agent is injected into the blood stream of arteries known as arteriography or veins known as venography.[11] When imaging lymph vessels contrast agents of an oily nature are used. This technique is used to investigate the normal and pathological nature of a vessel. Diseases such as tumours, sources of bleeding, arteriovenous inflammations and arteriovenous fistulae can be investigated with this technique. Digital subtraction angiography is used to produce images but it is also possible to take single shot images with rapid film changers in a process known as cine angiography for coronary arteries. The image in figure 1.1 is of a 45 year old female who had the symptom of weakness in her right arm. Head CT both with and without contrast agent was performed. The computed tomography image illustrates a subarachnoid haemorrhage with a left middle cerebral arterial aneurysm.[11]

Figure 1.1: Cerebral Angiogram[11]

1.1.6 Ultrasound Imaging

Ultrasound imaging (sonography) is a technique that has been in use for over 20 years. The technique uses high-frequency sound waves to view soft tissues such as muscles and internal organs. The images are captured in real time and as such they can show blood flowing through vessels and movement of internal organs.[12] During an ultrasound exam a hand-held device (transducer) is placed against the patient's skin. High frequency sound waves are sent out of the transducer and these reflect off various structures. The sound waves return and are displayed as an image which is based on the time taken for the signal to return and the frequency and strength of the signal. It can also be used to view a fetus in pregnancy and monitor its heart beat. The optical equivalent of ultrasound is Optical Coherence Tomography (OCT), and uses a beam of infrared shone from a laser instead of sound waves.[12]

1.1.7 Fluoroscopy

Fluoroscopy is a technique that is used to visualize the motion of internally found items in the body such as fluids, structures, and devices. The X-ray images provided by this technique are in real time and as such are very useful in a range of investigatory and diagnostic procedures. The level of X-ray exposure that is required for a single fluoroscopic image is relatively low in comparison to radiography but a patient usually requires a series of images to be taken and higher total exposure can be the result of this. During the procedure the X-rays are moved over different areas of the patient.[13] Two important factors to be considered during the procedure are firstly the areas that are exposed the most to the X-rays because these areas will have the highest absorbed doses. Secondly the total amount of radiation that the patient has been exposed to. This is directly related to the Kerma Area Product (KAP) *or* *(P_{AK})*. Fluoroscopy is used in a wide variety of examinations and procedures to diagnose or treat patients. Examples of the technique in use are; viewing the placement of devices such as stents that open blocked or narrow vessels within the patient, angiograms which allow the visualization of organs and blood vessels[13] and orthopaedic surgery to help guide the treatment of fractures and joint replacements.

1.1.8 MRI

MRI is an imaging technique that utilises strong magnetic fields and radio waves. This in turn can produce cross sectional images of internal structures and the organs of a patient. The signal detected by the MRI apparatus will vary depending on the amount of water contained in a particular area of the body and the magnetic properties of that area.[14] MRI scans can produce detailed images of ligaments and cartilage which are not possible to be imaged using any other medical imaging technique. The technique is used to detect abnormalities of the brain and spinal cord, identify diseases of the liver and abdominal organs and diagnose uterine problems in women who are being evaluated for possible infertility.[14] A benefit of MRI imaging is that it does not use ionization radiation so damage to deoxyribonucleic acid (DNA) can be avoided, there are also no reported harmful side effects related to exposure to the strong magnetic fields used in MRI scanners.

1.2 Nuclear Medicine and Imaging

Diagnostic nuclear medicine is an area of medical imaging that utilises radionuclides to produce an image of the distribution of radiopharmaceuticals *in vivo.*[15] This technique and resultant images can provide a range of useful information about both structure and function of various diseases due to the fact that it principally relies on the functional changes of the disease.[16] It is a method used to gather medical information that would otherwise be unavailable, require a range of more expensive diagnostic tests or necessitate surgical procedures. Nuclear medicine imaging can in many cases identify abnormalities very early in the progress of the disease. Nuclear medicine determines the cause of a disease or medical issue based on the function of the organ. This can be achieved by using the technique to analyse metabolism, physiological changes and molecular alterations of the disease.[16] The images obtained with this technique can be combined with MRI or more commonly CT to provide greater information regarding the lesions and tissues being assessed. Nuclear medicine has advantages over investigatory procedures such as surgery because it is non-invasive, there is the possibility to monitor the patient over a few minutes to a few days and quantitative information can be obtained when imaging instruments are in conjunction with computers.[16]

Nuclear medicine has become invaluable to a range of medical disciplines including neurology, cardiology, oncology and urology. The technique is used to locate tumours that may be found deep in the body, assess the normal functionality of organs and monitor the progress of medical or surgical treatments.[17] A few examples include; assessing the blood flow to the brain, detection of infection within bones and the assessment of a patients liver, cardiac or renal transplant function.[17]

Radiopharmaceuticals can be used in the treatment of diseases by being developed to target a specific organ or lesion. The radiopharmaceutical will be able to deliver enough radiation to a target which will destroy the diseased tissue. For example the treatment of thyroid cancer and overactive thyroid gland hyperthyroidism.[18]

1.3 Basis of Nuclear Medicine

1.3.1 Atomic structure

An atom is comprised of three different types of subatomic particles. The neutron has no electric charge and it has mass that is almost equivalent to the mass of a hydrogen atom, it can be found in the nucleus.[19] The proton carries a charge of $+e$, and is almost equivalent to the mass of a hydrogen atom, it is also located within the nucleus. The electron carries a charge of $-e$, has a mass that is approximately 1/1837 of a hydrogen atom, and occupies most of the volume of the atom.[19]

1.3.2 Isotopes

When atoms of the same element contain different numbers of neutrons, the different versions of the element are known as isotopes. The most common isotope of hydrogen contains no neutrons, the isotope of hydrogen, deuterium has one neutron and tritium has two neutrons as illustrated below.

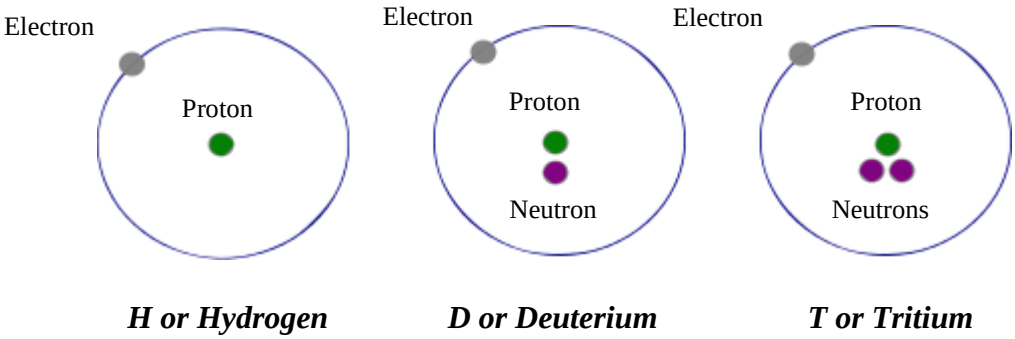

Figure: 1.2 Isotopes of Hydrogen

1.3.3 *Radioisotopes*

A number of isotopes are radioactive and are commonly referred to as radionuclides or radioisotopes. Stable isotopes are those which have never been observed to undergo radioactive decay. For example carbon-12 and carbon-13 are stable isotopes of the element carbon. Carbon-12 is the more common of the two accounting for 98.89% of carbon. Carbon-14 is a radioactive form of carbon and is used as a radiopharmaceutical to monitor a patient's absorption of glucose.[19]

1.4 Radiopharmaceuticals

Radiopharmaceuticals are drugs that are used for a range of examinations *via* the use of gamma cameras or used for internal radiation therapy to combat a range of diseases.[20] They are synthesised with radioactive components and these radioactive drugs can be specifically designed to target and accumulate in certain areas of the body. Gamma cameras can then be employed to detect and image the distribution of the radioactivity of the administered radiopharmaceutical. The radioactivity also allows the determination of the amount of drug that remains in the liver and other organs as well as the quantity that is excreted by the kidneys.[16] Most radiopharmaceuticals are employed in the detection of diseases *via* diagnostic procedures. Around 10% of radiopharmaceuticals are used for the treatment of diseases.[20] This is in the majority of cases, treatment of pain in cancer patients. There is a high level of interest in the pharmaceutical industry to develop a curative treatment for cancer. There are four areas of physiological measurement that radiopharmaceuticals are used to detect; the physiological function of organs, metabolism of tissues, intercellular/intracellular communications, and regional blood flow, cellular transport and localisation of assorted molecules.[16]

1.5 Steps of Imaging Agent Development

1.5.1 Introduction

The process of imaging agent development is long and extremely costly. It can take approximately 10 years at a cost around 90 million pounds.[21] There are several stages in the development ranging from the discovery of a molecule that may have potential to become a new radiopharmaceutical to marketing and drug monitoring.[22] It should be noted that on average only one molecule will become a drug out of between 4000 – 5000. The process is complex and requires specialist knowledge from a range of disciplines such as medicinal chemistry, molecular biology, pharmacology and regulatory science.[23] The journey of a drug from its discovery to marketing is often found to be difficult and the majority of drugs will not make this journey successfully to completion.

The development of a new radiopharmaceutical requires a great deal of time and the investment of money.. Once a suitable compound has been developed it is then tested in pharmacological and preclinical studies which are undertaken *in vitro.*[22] Pharmacokinetics looks at the absorption, distribution, metabolism and elimination of the new compound. The toxicity of the compound at high and low doses is then determined. Three stages of clinical studies are then undertaken and if the new compound passes, registration can be completed. Marketing and continued monitoring finalises the development of a new radiopharmaceutical.[22]

1.5.2 Discovery

An imaging agent discovery project is initiated when a need or gap has been identified, whether it is related to a disease, clinical condition or lack of suitable medical compound. The primary research in the early stages of imaging agent discovery is usually undertaken in academia. This research results in data that are valuable and can be utilized in the further stages of the new compounds development. The need for a positron emitting radiolabel for cells was identified at the early stages of this PhD research. There are positron emitters available that can be used to radiolabel cells such as gallium-68[24] however its short half-life of 68 minutes imposes considerable limitations. Copper-64 has a longer half-life of 12 hours and copper complexes such as copper bis diethyldithiocarbamate[25] suffer efflux problems over a period of hours; probably the result of biological mechanisms in place to control cellular copper levels, so a longer biological half-life would be preferable. ^{89}Zr has properties that make it an ideal candidate as a cell tracking radionuclide. The data obtained during the discovery phase has been very promising and as such the Zr oxine, tropolone and ethyl maltol complexes progressed to the pharmalogical phase of development.

1.5.3 Preclinical Testing

During the preclinical testing stages properties of the drug candidate such as safety, bioactivity and efficacy are investigated.

The experiments designed to test these properties at this stage are developed to support clinical testing at later stages of development.[26] An imaging agent candidate will first go through a series of quick tests known as screening tests. If successful it will progress to more substantial testing such as testing the imaging agent candidate on an isolated organ. Final testing at this stage involves the use of preconditioned animals. In the field of oncology test are conducted using mice which carry tumours originating from humans.

1.5.4 Pharmacokinetics

Pharmacokinetics is an area of research which deals with the action of drugs/imaging agents within the body such as; absorption, distribution, metabolism, and excretion. These properties are paramount in determining whether a drug candidate has the potential to progress through further stages of imaging agentsdevelopment successfully.[26] Tests to determine these properties include *in vitro* assays which provide information on the drug candidate's metabolism and permeation. If the drug candidate demonstrates potential it will be studied using *in vivo* animal models.[27] Of the complexes reported in this thesis zirconium tetrakisoxine has demonstrated the properties required to progress to *in vivo* animal models as reported in chapter 6.

1.5.6 Toxicological Analysis

It is very important to identify the dose limiting organ for toxicity and radiation exposure of a new imaging agent candidate. Toxicity and radiation exposure from an imaging agent can have damaging effects to an organism as a whole, its organs or at a cellular level (cytotoxicity). Testing at this stage usually involves *in vitro* testing and/or *in vivo* tests which involve small animal studies results of which can be translated to humans.[21] Dependant on whether any of these effects are found and the extent to which they occur may result in the termination of further investigation and development of the imaging agent candidate.

1.5.7 Clinical Trials

New imaging agent candidates must progress through clinical trials to ascertain whether they are safe and function as intended. Proof of mechanism/concept and the issues of translation to human subjects are addressed at this stage.[21] Radio tracers do tend to have fairly low levels of toxicity due to the small dose administered. Proof of mechanism studies will demonstrate the mechanism by which the imaging agent is functioning. Proof of concept studies should be able to demonstrate the ability of the new imaging agent to compete against existing agents. PET and SPECT imaging agents should not/do not evoke a pharmacological response and as such measuring pharmacodynamics is not possible.[21] To prove that the imaging agent candidate is reaching its intended target the amount of uptake of the imaging agent at the target site is determined. Uptake at other sites is also recorded to ensure that the imaging agent is arriving at its intended target due to discriminative binding to an intended target rather than by other mechanisms.[21] Clinical trials are arduous and it is imperative that the potential imaging agent is understood and is safe. If successful the imaging agent candidate will move on to registration.[22]

1.5.8 Registration

If the drug candidate passes the aforementioned stages an application for registration with the country's health regulative authority can be submitted. In Europe a market authorization application would be registered with the European Agency for the Evaluation of Medical Products.[28] A complete description of manufacturing processes along with all data obtained is submitted. If successful the new drug can be marketed and sold under the recognized label of the regulative authority.[28]

1.5.9 Post Marketing

This phase is on-going and provides important information related to the use of the drug.[22] Trials are conducted that ascertain the long term benefits, any risks and the ideal dose for patients. The trials themselves are conducted utilising thousands of patients and can continue for multiple years.[28]

1.6 Therapeutic Nuclear Medicine

Therapeutic nuclear medicine can be used to treat a number of diseases such as thyroid hyperactivity, tumours in the form of lymphomas, thyroid cancer, blood pathologies and bone pain that is a result of metastases. Treatment in many cases uses single, large doses of radioactive materials and side effects do occur. Cells that divide quickly as is the case with cancers are very susceptible to damage by radiation.[22] Hence radiation may be used to irradiate areas of the body containing cancers and these cancers may be eradicated or inhibited.[16] Therapeutic nuclear medicine treatments can be administered either internally or externally. Internal radionuclide therapy is undertaken by placing or dosing a gamma or beta emitter in the area requiring treatment. Internal radiotherapy is becoming more common and is called brachytherapy. The two types of brachytherapy are – seed implantation and low dose rates. Both types are used to treat prostate cancer with radiation from inside the prostate gland. Perhaps the most successful cancer treatment to date is the treatment of thyroid cancer using Iodine-131.[16] External treatment uses strong beams of radioactivity either photons or particle radiation to destroy tumours.[22]

1.7 Diagnostic Nuclear Medicine

There are currently over 10,000 hospitals worldwide that use radioisotopes in the field of nuclear medicine and 89-95% of these medical procedures are diagnostic. Diagnostic nuclear medicine generally uses small amounts of radioisotopes, but certain diagnostic tests such as heart scans need to use much higher doses. In order to target a specific organ or type of disease a radioisotope, or tracer, is combined with a chemical that is known to accumulate at that specific organ or disease. This compound is known as a radiopharmaceutical agent. The most common radioisotope is technetium-99m with over 30 million diagnostic procedures conducted with this radioisotope worldwide annually. Radiopharmaceutical agents are administered to a patient either orally, intravenously or by inhalation. The photons emitted from the isotope are detected by cameras and this information can be fed to a computer and specific software can generate an image of the area of interest.

1.8 Scintigraphy

Scintigraphy is a technique which detects and measures gamma radiation released from the body as a radiopharmaceutical decays. The radiopharmaceutical becomes concentrated in certain tissues; hence the tissues themselves become the source of the radiation.[22] The technique is used commonly in medicine for anatomical research and to assess organ function. The majority of organs can be analysed using this technique and most importantly their function or structure can be investigated without the need to perform surgery or a biopsy.[22] The images produced from this technique may be dynamic, providing information about function, or static, providing information about structure.

An example of scintigraphy is reported in the Journal of Physiology which reports the effects of dynamic and isometric muscle contractions on the lymph flow in human skeletal muscle.[29] The studies were conducted using scintigraphy and ^{99m}Tc was used to radio label human serum albumin. The findings suggest that lymph propulsion by working muscle is most efficient when the muscle is able to shorten close to its minimum length.[29] Other examples of scintigraphy techniques include: Gastroesophageal Scintigraphy a technique used to investigate the oesophagus and stomach. Once a radioisotope had been introduced into the stomach, scintillation measurements are taken over both the oesophagus and the stomach. This can be used to determine the level of gastroesophageal reflux. Myocardial perfusion scintigraphy is undertaken by utilising a radiotracer (normally thallium-201)[30] which negotiates the myocardial capillary system and enters myocardial cells. Myocardial blood flow and the viability of cells can be determined utilising delayed and real-time images.[30] Research undertaken by Junjie Li *et al*[31] compared the necrosis seen *in vivo* by contrast-enhanced MRI against the hot spots found on planar scintigraphy.[31]

Figure 1.3[31] illustrates *in vivo* MRI (A) and planar gamma imaging (B) of necrosis in tumour models. Planar gamma scintigraphy radiography exposed a hotspot in the necrotic regions of the liver (B). Findings show that radioiodinated hypericin is a promising tracer of necrosis utilising scintigraphy.[31]

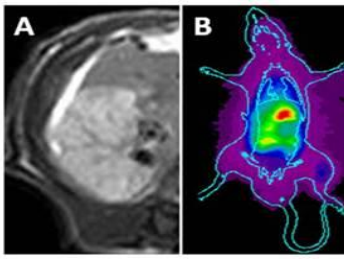

Figure 1.3: *In Vivo* Liver Necrosis[31]

1.9 Single Photon Emission Computed Tomography (SPECT)

Single Photon Emission Computed Tomography (SPECT) is a type of nuclear imaging technique that has a range of uses including imaging blood flow to tissues and organs in the body. It is advantageous over other imaging techniques such as X-rays because it has unlimited depth penetration and intrinsic sensitivity.[10] SPECT analysis requires the combination of two different technologies, a radiotracer and CT. The radiotracer emits gamma rays that are detected by a scanner; in the majority of instances two to three of these revolve around the patient. SPECT is an excellent, proven technique for analysing areas of the body[22] that are limited in size or less well defined, such as the brain.[22] A computer collects the information and produces two dimensional cross sectional images which can be reconstructed together to produce a 3D image. The acquisition time to obtain images in SPECT is relatively long and as such organs that are in motion such as the heart are significantly difficult to image and interpret. A method to overcome this problem is to take images of the heart according to its rhythm.[22] The time period between two beats is divided into thirty separate sequences and the gamma impacts detected within each of these sequences are collected separately. This results in thirty different images of the heart corresponding to a precise moment of the heartbeat. They are then displayed in the correct sequence and looped in a technique known as gated SPECT.[22] Commonly used radiotracers in SPECT include: technetium-99m (^{99m}Tc), iodine-123 (^{123}I), fluorine-18 (^{18}F), thallium-201 (^{201}TI) and xenon-133 (^{133}Xe). A range of compounds and drugs can be labelled with these isotopes forming a range of radiopharmaceuticals. The type of radiopharmaceutical used in a diagnostic exam is dependent on the area of interest. For example ^{18}F can be used to radiolabel fludeoxyglucose (FDG) forming ^{18}F-FDG; a radiopharmaceutical that can be used to analyse the glucose metabolism of tumours.[22] The SPECT nuclear medicine technique differs from another technique that utilises gamma rays; positron emission tomography (PET).[16] PET utilises positron decay which produces two gamma rays which results in the ability to locate the radiopharmaceuticals more accurately than SPECT which only tracks a single photon. SPECT however is more readily available and cheaper to conduct.[16]

1.10 Positron Emission Tomography (PET)

1.10.1 Early History

Carl David Anderson was an American physicist who discovered the positron in 1932. He received the 1936 Nobel Prize in Physics for this outstanding discovery. Shortly after this discovery Jean Frédéric Joliot and Irène Curie produced the first positron emitting nuclide.[32] This was a achieved by bombarding aluminium-27 (^{27}Al) with alpha partcals resulting in the formation of phosphorus-30 (^{30}P)[33], a positron emitter with a half-life of 2.5 minutes.[34] Ernest Orlando an American physicist invented the first cyclotron, an instrument that accelerates nuclear particles to very high velocities without the use of high voltages. Using his newly invented cyclotron Ernest Orlando produced nitrogen-13 (half-life <10 minutes) and carbon-11 (half-life 24 minutes) within the same year. These discoveries led to the production and utilization of positron emitting tracers.[34]

The first commercial PET scanners were developed at the end of the 1960s and utilized analogue electronics which in turn generated tomographic images. In 1968 The Royal Adelaide Hospital investigated this technology for bone scanning.[35] Results showed that the technique was too slow and inefficient for clinical use. It was determined that the fluorine-18 (^{18}F) isotope was unusable with rectilinear scanners and gamma cameras. At the time it was also difficult to source the isotope.[35] At the beginning of the 1970s at Washington University's school of medicine Michel Ter-Pogossian, Michael E. Phelps and Edward J. Hoffman developed the principles by which modern PET imaging systems are based. At the end of the 1970s detectors with greater sensitivities and better tomographic properties began to appear, capable of brain imaging and imaging the torsos of narrow patients.[36] The 1980s saw the commercial availability of whole body PET tomographs leading to research into the application of this technology to analyse organs such as the heart and extra cranial neoplasms. The 1990s saw a generation of full ring commercial tomographs introduced that were capable of whole body clinical applications.[36] Today's modern PET tomographs continue to develop and image time continues to be reduced with improved image quality.

1.11 Positron Emitters for use in PET

There are a large number of radiotracers available to clinicians to aid in the diagnosis of diseases. Common examples of these are reported below.

1.11.1 Oxygen-15

Oxygen-15 (^{15}O) half-life ($t_{½}$ =2 minutes) is used to quantify regional cerebral blood flow (rCBF) [10]. This information can be used to characterise altered brain perfusions in patients who are suffering from cerebrovascular disease.[37] Regional myocardial blood flow (rMBF) can be quantified using ^{15}O in patients' studies of myocardial perfusion in various pathological and physiological conditions.[38]

1.11.2 Rubidium-82 Chloride

Rubidium-82 Chloride ($^{82}RbCl$) commonly known as CardioGen-82 is used in PET for the diagnosis of myocardial infarction. This PET radiotracer is used to distinguish between normal and abnormal regions of myocardial perfusion in patients with suspected myocardial infarction.[39] It is also used to diagnose coronary artery disease and determine the extent and severity of this disease in the patient.[40]

1.11.3 Fluorine-18 Fluorodeoxyglucose

^{18}F half-life ($t_{½}$ = 109.8 minutes) is a commonly used radioisotope in nuclear medicine. Fluorine has very favorable properties such as its ability to replace other atoms that are in an active compound with relative ease, without altering the biological properties of these compounds.[22] Cancer cells require high levels of glucose and will consume higher quantities than normal cells. Hence radiolabeling glucose can aid in the identification of cancerous cells. Once injected in to a patient (dose ~ 350 megabecquerel (MBq)) Fluorine-18 Fluorodeoxyglucose (^{18}F-FDG) will accumulate at cells which are under a state of rapid growth and proliferation such as tumours and their metastases.[22] As the brain and heart also have a high level of glucose uptake ^{18}F-FDG can be used to image these organs as well.

1.11.4 Carbon-11 Methionine

Carbon-11 methionine is also used in oncology where it acts as a marker for protein synthesis. The metabolism of methionine is altered in cancer and it is possible to use methionine labelled with ^{11}C to image brain, lung, and breast cancer and lymphomas.[41] It has been reported that head and neck cancer can be effectively imaged with carbon-11 methionine and its use in PET imaging could be useful in measuring cancers for therapy treatment plans.[41] Carbon-11 methionine has also been studied in the detection and PET imaging of chordoma, a rare malignant bone tumour.[42] The findings of the studies indicated that carbon-11 methionine PET is viable for the imaging of this pathology and can provide valuable information on the therapeutic treatment of chordoma after carbon-ion radiotherapy (CIRT).[42]

1.11.5 Nitrogen-13 Ammonia

Nitrogen-13 ammonia (^{13}N-NH_3) has a half-life of 10 minutes and has been evaluated as a tracer for myocardial perfusion (the flow of blood to the heart). Using this tracer in a PET scan can provide information that can result in the diagnosis of coronary heart disease or aid in the decision of whether a patient would benefit from coronary bypass surgery.[43] Results of work undertaken by Warren F. Walsh *et al*[44] show that the uptake (in animal studies) of this tracer is proportional to regional tissue perfusion. Clearance of this radiotracer once administered intravenously is rapid and excretion occurs *via* the liver, lungs, myocardium, kidney and bladder.[44]

1.11.6 Iodine-124

Iodine-124 (^{124}I) is a positron emitting halogen and is a popular long lived radionuclide used for the design and synthesis of new PET radiotracers. With a half-life of 4.2 days it is possible to use longer radio synthesis methods and longer PET imaging studies.[45] The labelling methods and chemistry are well established for ^{124}I and there is a large range of compounds that have used ^{124}I for imaging techniques.[45] An example of ^{124}I in use in PET is in the form of iodide salt (^{124}I)NaI that can be used to image the thyroid.

1.12 Physical Principles of PET

The main principles of imaging tissue function *in vivo* with PET are illustrated and summarised in figure 1.4 below. There are multiple steps involved in the PET process to produce an image that can be used for diagnostic purposes.

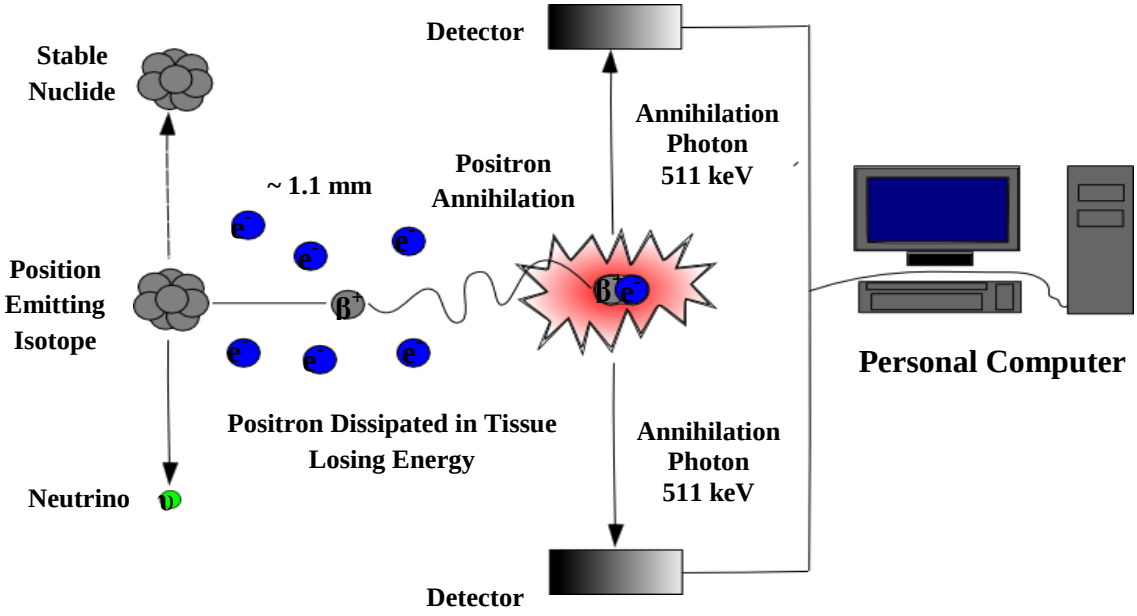

Figure 1.4: The PET Scanning Process[46]

Firstly the patient is positioned on a flat-bed which is moved into the large circular scanner at one end when the procedure is ready to be conducted. The patient needs to be placed into the field of view of the PET detectors which can detect and register incident gamma rays.[22] A positron (β^+) emitting radionuclide is administered to the patient and the radionuclide component of the radio tracer decays and the resulting positrons (β^+) travel a short distance ~ 1 mm in the body. After traveling this short distance the positrons will combine with electrons (e^-) in the absorbing matter causing annihilation to occur[10] and produce two 511 kilo electron volt (keV)[22] photons that travel in opposite directions of each other. The detectors surrounding the patient detect these photons and they are linked so that two events distinctly occurring within a specific time frame are known as a coincident and it can be said that these photons originated from the same annihilation. The coincident events can be stored in arrays and reconstructed using a form of digital image processing.[16] The resulting images show the tracer distribution throughout the patient.

1.13 PET Detector

The detection system is an indispensable component of any imaging apparatus. It is key that the properties of the detection are fully understood to devise an appropriate operating protocol that allows the collection of quantitative information. Since the introduction of PET the design and performance of the utilized detectors have evolved and improved dramatically. The overall axial field view has increased from 2 cm to 20 cm and the total number of detector elements has increased from 20 to 20,000.[47] The spatial resolution is the capacity of an imaging system to determine the difference between two adjacent high-contrast objects. There has been a drastic improvement to the PET detectors properties increasing the spatial resolution from 25 mm to 5 mm alongside over a thousand fold increase in sensitivity.[47] Scintillation detection systems are used in nearly all PET tomographs. The conversion of high-energy photons into visible light occurs due to an interaction with a scintillating material.[48] First a photon incident creates an energetic electron on the scintillator, then the electron travels along through the scintillator and as it excites other electrons it loses its energy. The electrons that have been excited give off light as they decay back to their ground state. The scintillator is optically connected to a photomultiplier tube (PMT). Once light makes contact with the PMT an electrical signal is generated.[10] An array is used to generate a timing signal then used in the coincidence circuitry. Due to finite time resolution of the detector and the computational fluid dynamics (CFD) system there is usually a time difference between the two timing pulses generated by a coincident. To combat this timing pulses are transferred to a gate generator, creating an electronic pulse.[48] Properties required for camera configuration in PET that lead to the production of high resolution images include the detected localisation of annihilation protons achieved by utilising small detectors. Dead time is the time period after each coincident and in which a PET system is not able to record another event, meaning some events will be missed. At high count-rates these losses, known as dead-time losses can become very significant. Every coincident event that is detected during an imaging session is recorded by the PET computer as raw data sets.

In both PET and SPECT the coincident data is reconstructed with computer software resulting in cross-sectional images in the coronal, sagittal and tranverse plains.[48] These planes are illustrated in the diagram below.[49]

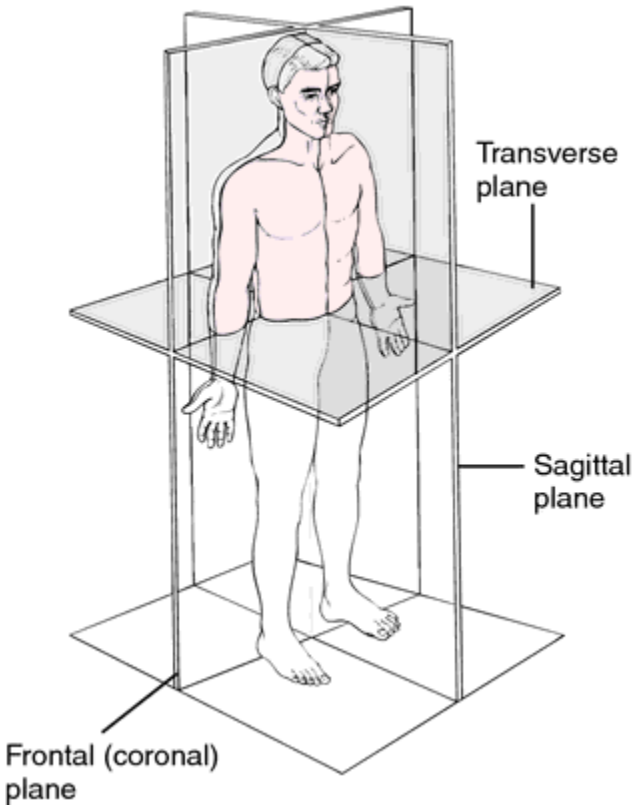

Figure 1.5: Coronal, Sagittal and Transverse Plains[49]

1.14 Application of PET

1.14.1 Oncology

PET has a variety of distinctive uses in clinical fields such as cancers; lymphoma, melanoma and colon cancer, and strokes. A common PET radiotracer is ^{18}F - fluorodeoxyglucose (^{18}F-FDG) which is used to image a wide range of malignant tumours. The specify and sensitivity of this radiotracer is in the majority of instances in the high 90s %. ^{18}F-FDG[50] has been used to detect and image tumours located in the head and neck, musculoskeletal system, neuroendocrine system, ovaries and breasts. In oncology PET is an extremely reliable method for differentiating between benign and malignant primary tumours as well as recurring pathologies.[50] Staging (extent of spread) of the disease depends on several factors. PET can be used to determine the presence or absence of metastasis, the amount that the disease has spread to the lymph nodes in the region, the number of tumours (this includes the primary tumour and the presence of metastatic tumours, or metastases) the tumour grade (how closely the cancer cells and tissue resemble normal cells and tissue) and the actual size of the primary neoplasm.[51] Staging is extremely important because it can be used to estimate a patient's prognosis, assist in the development of a treatment plan and identify suitable clinical trials for which the patient may be eligible.[51] Researchers are also able to exchange information using a common terminology using the information obtained by the use of PET.[16]

1.14.2 Cardiology

PET is the most common form of diagnostic testing used in cardiology. ^{18}F-FDG is a glucose analogue that is widely used as a metabolic imaging tracer in clinical oncology. The radionuclide Nitrogen-13 (^{13}N) can be used to image myocardial perfusion utilising a dynamic scanning protocol to calculate the absolute blood flow within a patient.[52] PET cardiology viability imaging determines the extent of heart muscle damaged by heart disease or a heart attack. If a patient is suspected to be suffering from either a stunned or hibernating myocardium PET scans can help to identify this.[52]

1.14.3 Neurology

In the field of neurology PET is employed to differentiate recurrent brain tumours from radiation fibrosis or necrosis, which is essential for neurological studies.[53] Radionuclides such as ^{15}O which are produced from nitrogen ($^{15}N_2$) can be used to measure the flow of blood to the main or upper sections of the brain. The carbon isotope ^{11}C which is produced from nitrogen ($^{14}N_2$) can be used as a PET radiotracer to scan, image and subsequently study both normal and abnormal brain functions.[53] This method has been successfully used to identify areas of the brain which are affected by epileptic seizures.

1.14.4 Neuropsychology and Cognitive Neuroscience

In the medical field of neuropsychology and cognitive neuroscience PET can be employed to investigate a range of psychiatric disorders. It can be used to evaluate neurological activity in patients suffering with amnesia.[54] Research has been undertaken that links direct visualisation of blunted brain responses to serotonin release with major depression sufferers. PET has been used to investigate Fahr's disease, an inherited neurological disorder that has the symptom of unnatural calcium deposits in the areas of the brain that control movement. ^{18}F-FDG has been used to investigate this disease, findings showed that there was a reduced glucose uptake in the areas of calcium deposits and in the temporal and parietal cortices.[55]

1.14.5 Pharmacology

During pre-clinical trials PET can be employed to provide researchers with the information required to produce radiolabeled drugs. Radiotracers such as ^{18}F-3-fluorothymidine (^{18}F-FLT) can be used to assess specific synthetic rates of DNA, in turn functional state or integrity of a tissue can be assessed.[56] Pharmalogical activity of a newly developed radiotracer for potential use in PET depends on the free concentration that can be achieved in the target tissue. This can be assessed *in vivo* utilising PET after a molecule has been labelled with a positron emitting isotope that does not change the properties of the chemical structure of the molecule.[56]

1.15 PET Vs SPECT

The two dominant molecular imaging techniques in the field of nuclear medicine are positron emission tomography (PET) and single photon emission computed tomography (SPECT). Both techniques have strengths and limitations in hardware and software design and the actual radiotracers that are used with these techniques. Both of these techniques have suffered from setbacks over the years with radiopharmaceutical supply problems such as the supply shortage of the most commonly used nuclear medicine radioisotope precursor for ^{99m}Tc; molybdenum-99 (^{99}Mo).[57]

PET imaging has a far greater sensitivity than SPECT and this is around ~ 2 to 3 times greater. There is a difference in the ability of the techniques to detect and record a higher percentage of emitted events during a procedure. Physical collimators are needed in SPECT to reject photons that are not within an acceptable small angular range. If this is not done it will not be possible to determine the angle of incidence.[58] SPECT is more available, widely utilized and cheaper than PET. The overall cost of PET equipment is much more expensive than SPECT equipment. SPECT tracers are a lot cheaper than PET tracers and are more widely available but this is changing.[59] SPECT has problematic issues such as long scan times, low resolution images and susceptibility to interference from artifacts and attenuation. It is easy to misdiagnose artifacts such as perfusion defects when using SPECT and the technique does not allow the amount of blood flow to be measured, while PET does.

There have been significant advances in the development of Rubidium-82 (^{82}Rb) technology which has enabled new levels of excellence in the assessment of myocardial perfusion against which the next generation of cardiac imaging agents can be tested for their specificity and sensitivity.[60] The data that are being produced from studies involving ^{82}Rb are expected to illustrate the cost-effectiveness of cardiac PET over SPECT. PET also has other advantages over SPECT such as higher spatial resolution and the ability to perform quantitative measurements.[61] PET scan times are around 30-40 minutes quicker than the two or more hours required for a SPECT scan.

1.16 Immuno PET

Immuno-positron emission tomography (immuno-PET) is a non-invasive imaging technique utilising intact antibodies labelled with a positron emitter. The technique can provide information in target therapy such as where the target is and where the antibody is located. Immuno PET has the potential to have an important role in cancer staging and can improve the diagnostic characterisation of tumours.[62]

The combination of immuno-PET with mABs can be used to provide support and improve a range of treatment areas. It can be used to determine the most favourable dose for radio immunotherapy treatment or to determine the most efficient times to administer mAB doses.[62] The efficiency of drug delivery across the blood brain barrier and methods to improve this can also be determined using this technique. Biodistribution and quantification of mABs at target locations can be visualised using immuno-PET.[62]

Immuno-PET scans can be tremendously predictive of colorectal disease and slightly less so with recurrent ovarian cancers.[63] The requirements of immuno-PET are a suitable positron emitter with a half-life that is relatable to the time required to achieve optimal tumour to non-tumour ratios and be able to latch onto the targeting compound securely.[64] Zirconium-89 (^{89}Zr) has the potential to fulfil these requirements.

The combination of imaging and drug targeting can be used to pre select patients and tailor treatment plans accordingly.[65] This process is the way forward for the development of personalised medicine. Personalised medicine itself is the customisation of healthcare whereby medical practices, decisions and products are developed for the individual which leads to greater levels of successful treatments.[65]

1.17 Cell Tracking in Cancer

Cancer treatment in the form of cell based therapies provides a range of methods that have great potential.[66] Non-invasive tracking and imaging of a range of therapeutic cells that have been labelled non-destructively such as stem cells and T cells can provide valuable information on the mechanisms of cancer development.[66] The technique can provide information such as the location, viability, cell lineage expansion and response to drugs, movement, or other behaviours of cancers *in vivo*.

There are two methods for the tracking of cells, direct and indirect. In the direct method of tracking, therapeutic cells are labelled directly with tags that can be detected[67], for example radioisotopes as is the case with PET and SPECT. Direct cell labelling methods are cost effective, widely available and are easier to conduct when compared to indirect cell labelling methods. The indirect method of tracking cells involves cell labelling utilising reporter genes[67] and immune cells such as T Cells.[66] The indirect method allows for a greater level of sensitivity and specificity.

Figure 1.5 illustrates direct imaging involving the labelling of stem cells with PET or MRI tracers, 111-In oxine and super paramagnetic iron oxide (SPIO) respectively.[61] In Indirect imaging a detectable signal is the product of reporter genes encoding a reporter protein that metabolizes a substrate.[61]

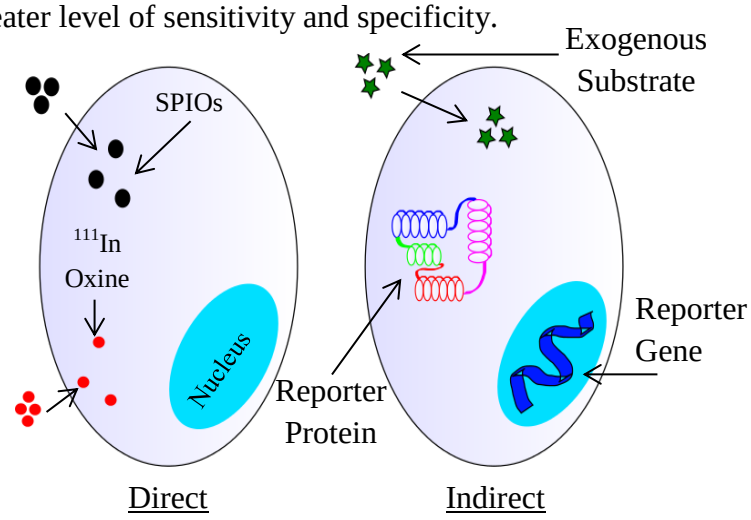

Figure 1.6: Cell Tracking Methods[68]

Another example of a direct cell labelling complex is 64-Cu-pyruvaldehydebis (N^4-methylthiosemicarbazone which can be used to label cells non-invasively to image tumours using PET. The compound has a strong binding affinity to human serum and is being studied as potential marker of perfusion.[69] Perfusion is an important factor in the physiology of tumours. Perfusion can have serious implications in the diagnosis, prognosis, planning and responses of treatments.[69]

1.18 Indium-111 Oxine and Indium-111 Tropolone

White blood cells have been labelled with success for many years to detect areas of infection and inflammation. Complexes such as indium-111 oxine (^{111}In-oxine) and indium-111 tropolone (^{111}In-tropolone) have been used in scintigraphy for this purpose.[70] Although they are being replaced by radiotracers such as ^{99m}Tc-hexamethylpropyleneamine oxime (^{99m}Tc-HMPAO).[71] ^{99m}Tc-HMPAO is preferred to image abscesses in the gastrointestinal tract but ^{111}In-oxine and ^{111}In-tropolone are still used to image patients at a number of facilities.[70] ^{111}In-oxine is known to be superior to ^{99m}Tc-HMPAO when imaging a range of clinical indicators including lung infections, diabetic foot, postoperative abscesses and bowel disease.[70]

1.18.1 Indium-111 Oxine

^{111}In oxine has been used to track radiolabelled lymphocytes in cancer patients, this radiotracer has been approved by the FDA since 1988.[66] It is known that Indium (In) forms a complex with oxine in the ratio of 1:3.[72] The resulting complex is lipid soluble and neutral and as such it is able to enter cells *via* penetration of the cell membrane.[73] Once the complex has entered a cell indium becomes irreversibly attached to cytoplasmic constituents within the cell.[72] The oxine is released from the complex and leaves the cell. The probable mechanism of labelling cells with ^{111}In oxine involves an exchange reaction between subcellular constituents that chelate indium more actively than oxine.[73]

1.18.2 Indium-111 Tropolone

^{111}In tropolone has properties very similar to that of ^{111}In oxine. However ^{111}In tropolone is soluble in isotonic saline whereas ^{111}In oxine is not. It has also been reported that less time is required for the labelling of lymphocytes when using ^{111}In tropolone.[74] ^{111}In tropolone has the advantage that it can label lymphocytes in plasma whereas ^{111}In oxine cannot. This is due to the fact that indium is found to bind more strongly to the transferrin contained within the plasma than oxine.[71]

1.19 Zirconium

1.19.1 An Introduction to Zirconium

The element zirconium (Zr) has an atomic mass of 91.224 amu and an atomic number of 40. It is a strong transition metal which is both malleable and ductile with properties similar to that of titanium. It is greyish/white in appearance and is resistant towards corrosion due to an oxide film on its surface. It is found to be solid at room temperature and becomes brittle at lower purity levels.[75]

Zr ore (commonly known as zircon, $ZrSiO_4$) is a by-product of the mining and processing of tin and the titanium minerals rutile and ilmenite, and is the most important form of Zr in use. Zircons main use is that of a refractor and an opacifier. It is also used in alloys such as zircaloy.[76] Zr has an important role in nuclear applications because it has low thermal neutron absorption cross section (NAC) properties. This coupled with the fact that it possesses high thermal stability, does not readily absorb neutrons and has anti corrosive properties, makes it an ideal candidate to be used as cladding material for nuclear fuel rods. Zr is known to form a range of organometallic and inorganic compounds, for example zirconocene dichloride and zirconium dioxide. Impure Zr and baddeleyite are utilized in lab crucibles and other well-known uses of Zr include furnace bricks, percussion caps and catalytic converters.[76]

Zr has no known biological properties or transport mechanisms and in most cases its salts have low systemic toxicity. The estimated average daily dietary intake in humans is 50 µg and absorption by the gut does not occur. Any Zr which is absorbed on average accumulates at a slightly greater percentage in the skeleton than in any other tissue.[76] Zr is very biocompatible with minimal biological availability and electro catalytic activity in the human body. This is due to Zr's passive oxide layers with very low solubility and exceptional protective properties.[77] Because of the tolerance of human tissues to Zr, it makes the metal suitable for use in some artificial joints and limbs.

1.20 Zirconium Chemistry

1.20.1 Zirconium Coordination Chemistry

When Zr is in a compound it is normally in the oxidation state IV, compounds where Zr is in lower oxidation states such as III, II or I are less common.[78] Compounds of Zr tend to commonly display coordination numbers and shapes of the following; 4 (tetrahedral), 6 (octahedral), 7 (pentagonal pyramidal) and 8 (dodecahedral).[79] Zr exhibits tetrahedral coordination in compounds such as gaseous $ZrCl_4$.[80] In solid state molecular compounds the coordination number is commonly be found to be 6 or above. Octahedral Zr complexes include solid $ZrCl_4$ and Rb_2ZrCl_6.[81] Zr complexes of coordination number 6 such as dimethyl benzamidinate Zr (Zr anchored via benzamidate ligands) have been reported to have catalytic properties that can be used in the polymerization of α-olefins.[82] An example of a pentagonal pyramidal Zr complex of coordination number 7 is ZrF_7^{3-} in $(NH_4)_3ZrF_7$.[83] Dodecahedral Zr complexes of coordination number 8 include $ZrF_4.H_2O$, a halide whereby the coordination around the Zr(IV) atom is comprised of six F atoms and two water molecules.[84] Coordination numbers of 7 or 8 can be found in crystalline structures with capped trigonal prismatic and square antiprismatic conformations which have respectively been reported.[81] The relatively high charge and large size of the Zr(IV) ion results in the preference for compounds of a higher coordination number. Zr's $4d^0$ configuration is the reason for the range of coordination geometries as stereochemical inclination due to a partly filled d-shell does not exist in Zr(IV).[85]

Zr is commonly known to form ionic bonds. The majority of Zr ions have a charge of +4 and will form a neutral complex when a bond with one or more ions totals a charge of -4 as is the case with the formation of zirconium tetrafluoride.[86] Zr complexes also exhibit dative covalent bonding such as in the platinum Zr adduct $[(Cy_3P)_2Pt–ZrCl_4]$.[87]

1.21 Zirconium Isotopes

1.21.1 Zirconium Isotopes

Zr is known to have four naturally occurring isotopes which are stable. It also has one extremely long lived naturally occurring radioisotope zirconium-96 with a half-life of 3.9×10^{20} years.[88] The properties of these isotopes are reported below. [89, 90]

Isotope	Atomic Mass	No of Neutrons	Natural Abundance	Nuclear Spin	Magnetic Moment (μ/μ_N)
^{90}Zr	89.905	50	51.45	0	N/A
^{91}Zr	90.906	51	11.22	5/2	-1.304
^{92}Zr	91.905	52	17.15	0	N/A
^{94}Zr	93.906	54	17.38	0	N/A

Table 1.1

1.21.2 Zirconium Radioisotopes

Apart from ^{96}Zr, radioisotopes of Zr are synthesised.[86] Currently twenty seven of these exist and the majority of them have half-lives of less than one day.[86] Properties and uses of two common radioisotopes; ^{89}Zr and ^{93}Zr are reported below. [91, 92, 93]

Isotope	Atomic Mass	Half Life	Decay mode	Decay Energy	Daughter Nuclide
^{89}Zr	89.9089	3.27 Days	β^+	396.9 keV	^{89}Y
^{93}Zr	92.9064	1.5 Million Years	*B*	91.24 keV	^{93}Nb

Table 1.2

^{93}Zr is commonly found in used nuclear fuel (UNF) cladding, U.S. light water reactor fuel assemblies, spent nuclear fuels and reprocessed wastes.[94] It is a concern to the Department of Energy (DOE) of America because of its 1.5 million year half-life.[95] ^{89}Zr has properties that are extremely useful in the field of PET imaging. Its half-life of 3.27 days is a good fit to the circulation half-lives of antibodies which are also in the magnitude of days.[96] ^{89}Zr has been of interest in the field of PET for a number of years particularly in the area of labelling monoclonal antibodies.[97]

1.22 The Synthesis and Uses of ^{89}Zr in PET

1.22.1 ^{89}Zr Production

The most common method of ^{89}Zr production uses a low-energy cyclotron utilising the nuclear process; [^{89}Y (p, n) ^{89}Zr].[98] This method involves the bombardment of ^{89}Y with deuterons or protons.[99] ^{89}Y is the preferred target material due to it being one of 26 chemical elements having only a solitary stable isotope (known as monoisotopic) hence its isotopic abundance is 100%.[98] The use of ^{89}Y avoids processes involving the preparation and enrichment of other isotopes for conversion into ^{89}Zr. These processes can be costly and problematic[98] and are involved in neutron activation for the synthesis of ^{89}Zr[100] and the alpha catalysed nuclear synthesis of ^{89}Zr.[98]

1.22.2 ^{89}Zr PET Tracers

Currently PET medical imaging based around ^{89}Zr has been explored in regards to a range of cancer related targets. Examples include epidermal growth factor receptor 2 (HER2) which is related to cell survival, metastasis, angiogenesis, differentiation and proliferation.[101] There is a direct correlation of the over expression of HER2 and a variety of human cancers[96] and because of this it is an important target for cancer diagnosis and treatment. Zirconium-89 trastuzumab has been designed as a PET imaging agent, used to determine and localize HER2 over expressing tumours with excellent results.[102] Prostate specific membrane antigen (PMSA) is one of the foremost characterised targets in the field of oncology.[96] ^{89}Zr-labeled anti-PSMA mAb, J591 has been reported to quantify PMSA expression *in vivo*.[103] Research has shown that this radiotracer has excellent potential for the imaging of PMSA.[103]

^{89}Zr has been used to successfully label antibodies, proteins and peptides for diagnostic purposes in the field of medical imaging utilising PET for some time. However non-biological ligands have not been used in complexes with the ^{89}Zr radioisotope in the attempt to label cells. It may be more cost effective and efficient to utilise non-biological ligands to label ^{89}Zr for diagnostic purposes in PET.

1.23 Bodily Clearance of Yttrium-89

^{89}Zr decays into the stable isotope yttrium-89, which has no decay products. Yttrium (Y) is found in a variety of common household equipment such as colour televisions, energy saving light bulbs and fluorescent lamps. Yttrium cannot be found in nature as a free element. It is in the majority of cases found in rare earth minerals and in uranium ores.[104] The element is at its most dangerous in the working environment because it can be inhaled with air as gasses or danger-associated molecular pattern molecules[105] which can be the direct cause of lung embolisms, even more so if a person is exposed long term.

No biological role has yet to be determined for this element yet it can be found in most living organisms. Human breast milk contains a concentration of 4 ppm and plants that are commonly eaten by humans have a range of between 20 -100 ppm.

Y is a known cause of cancer and causes the chance of cancer to increase if inhaled. It can also be very damaging to the liver if it accumulates in the body in significant quantities. Research has been under taken and findings show that yttrium is poorly absorbed in the gastrointestinal tract and 90% of ingested or absorbed Y is excreted *via* the faeces in rats however guinea pigs excreted 0% in the faeces. Exposure to mice and rats of the element resulted in an uptake of 25% and 50% respectably *via* inhalation. Human studies results show 11 – 55% retention after inhalation.[104]

Y injected intravenously into rats resulted in an accumulation in the liver lung and spleen. Half-life time clearance of the Y *via* the liver was 144 days. Experimental results also indicated that there is a limited maximum level uptake in the bones, excretion from the bones is slow and the accumulation in the bones is considerably less than other organs.[104] These findings demonstrate that that ^{89}Zr has the potential to be useful in PET applications.

1.24 Properties Required for New Zirconium Radiopharmaceuticals

There are currently over 100 PET radioisotopes but the larger part of these lack properties that are required for use in the field of cell tracking by PET imaging. Problems include high production costs, low availability and lack of established radiochemistry. Additionally many isotopes have half-lives that do not match the required times for cell tracking applications.[96] ^{89}Zr may be a solution to these problems and there has been a recent increase in the availability of positron emitters such as ^{89}Zr (78.4hours/3.26 days).[96] ^{89}Zr offers new possibilities for PET isotopes as it has properties that are ideal for cell tracking and possibly immunoPET.

1.24.1 Half Life

The half-life of ^{89}Zr (3.26 days) is an excellent fit for the time required for intact monoclonal antibodies (mAbs) to obtain an ideal tumour to non-tumour ratio.[97] The problem with this is the lack of methods available to couple ^{89}Zr to mAbs with high stability.[97] Established PET methods may be able to use ^{89}Zr for longer study times.

1.24.2 Biological Properties

The action and transport mechanisms of Zr in biological systems are unknown. It is retained firstly within soft tissues and then gradually within the bone.[106] In cytological and histological investigations, Zr has been shown to have low levels of toxicity.[107] Zr is able to cross the blood brain barrier and become deposited within the brain.[106] Human uptake of Zr has been reported to be as high as 125 mg per day.[106]

1.24.3 Diffusion into Cells and Stability

Small neutral polar molecules, such as water and urea can easily diffuse across the lipid bilayer of a cell.[108] The ligands chosen to complex with Zr must be uninegative and bidentate so that they can form a neutral complex with the zirconium ion as its charge will be +4. When the ^{89}Zr complexes are within the cells they must be able to dissociate in a manner analogous to well established ^{111}In complexes.[73]

1.25 An Overview of the Zirconium Precursor Complexes

When the radioactive Zr isotope is received from the supplier it arrives in the form of potassium zirconium tetrakisoxalato in oxalic acid. The Zr isotope can also be in the form of zirconium tetrachloride in hydrochloric acid. Because of this it was important to understand the chemistry of these precursor compounds. As the Zr isotope behaves chemically exactly the same as the stable form of Zr it was possible to investigate these complexes without the need for radiation safety procedures.

1.25.1 Zirconium Tetra Chloride

Zirconium tetrachloride, ($ZrCl_4$) is a white crystalline solid. Commonly used as a source of pure zirconium in analytical chemistry it is also used to make water repellent textiles. $ZrCl_4$ is easily decomposed by water and is very corrosive to metals and living tissue when in the presence of moisture. It has been used as a chemoselective catalyst compound under mild reaction conditions for the acetalization of carbonyl.[109]

1.25.2 Zirconium Tetrakisoxalato

Zirconium tetrakisoxalato, known as its potassium salt, tetra potassium zirconium tetra oxalate or potassiumoxalatozirconate (IV) has a chemical formula of $C_8O_{16}\,Zr\,.4\,K$. The ^{89}Zr isotope is supplied from manufacturers, such as iba Molecular, in the form of the potassium salt of zirconium-89 tetrakisoxalato in 1M oxalic acid solution. This form of the ^{89}Zr complex is due to the process of isolating high purity and high specific-activity ^{89}Zr complex using a small cyclotron.[110] ^{89}Zr is isolated in a high level of both radiochemical and radionuclidic purity in the form of zirconium-89 oxalate by employing the use of a solid-phase hydroxamate resin which results in >99.5% recovery of the radioactivity.[110]

1.26 An Overview of the Ligands to be Complexed with Zirconium

1.26.1 Introduction

The ligands, oxine, tropolone, deferiprone and ethyl maltol were chosen to form complexes with the ^{89}Zr ion. It is desirable to have neutral lipophilic complexes and this can be achieved by combining Zr(IV) with four bidentate uninegative ligands. The ligands chosen can form lipophilic complexes and it is necessary to surround the zirconium metal ion with such ligands as it is a goal of this work to label cells with ^{89}Zr and as such the ^{89}Zr metal isotope must be able to cross cell membranes.

1.26.2 Oxine

Oxine has the chemical formula C_9H_7NO and is an organic compound. It is a known derivative of the heterocycle quinoline by the employment of an OH group on the number eight carbon.

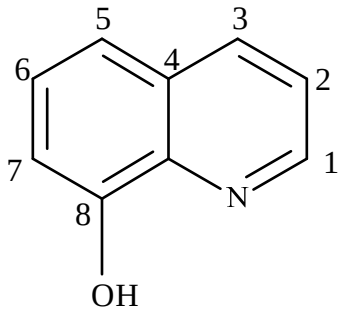

Figure 1.7: Structure of Oxine

Synthesis of oxine can be achieved either by the use of its precursor quinoline or by Skraup synthesis.[111] Skraup synthesis methods are known to be volatile and have been reported to lead to explosions even when inhibitors are employed such as boric acid. The reaction between 2-aminophenol (i) and glycerol (ii) in figure 1.7. The reactants are heated with sulphuric acid (H_2SO_4) and nitrobenzene ($PhNO_2$) which results in the formation of oxine (iii).[112] This process is expensive due to the cost of the raw materials involved and the low yields obtained.[111]

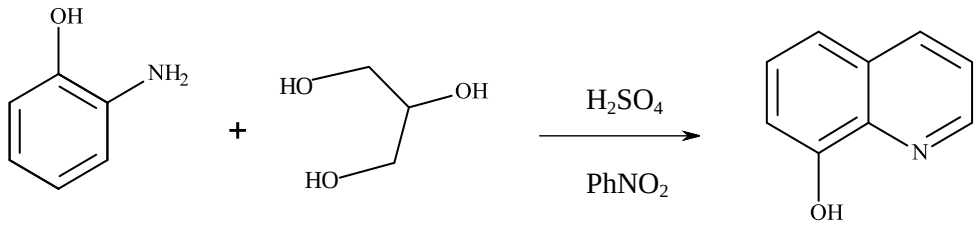

i ii iii

Figure 1.8: **Skraup Synthesis of Oxine**[112]

In a neutral solution the hydroxyl is found to be in the protonated form (pKa=9.89) and the nitrogen itself is not protonated (pKa=5.13). A zwitterionic isomer (also known as inner salts) in the excited state is reported to exist. In this case the H^+ is transferred from the oxygen (resulting in an oxygen anion) to the nitrogen (resulting in a protonated nitrogen cation) [113] illustrated below.

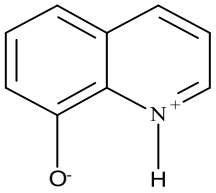

Figure 1.9: Zwitterionic Isomer of Oxine

Once oxine or its derivatives have lost a proton, it is possible for them to form complexes with a large variety of main group and transition metal ions.[114] Oxine and its related compounds have parasitical, bactericidal and fungicidal properties. Recent research has also been undertaken to utilise oxine in the manufacture of electroluminescent devices.[114] The complexes of oxine have also been used as a contraceptive (quinosol) and in a solution of alcohol it can be used as a liquid bandage.[111] In the past there was an interest in the compound for use as a chemotherapeutic. For example there was an interest in Mannich bases of oxine as possible anticancer drug candidates.[115] The interest in these complexes resulted from the fact that experimental results have shown them to express a high potency against human cancer cells. Further research has found that some of the derivatives of oxine such as 7-diethylaminomethyl-oxine exhibit considerable cytotoxic activity against leukaemia. Another oxine derivative, clioquinol has been used to identify cellular targets for zinc ionophores.[116]

1.26.3 Tropolone

Tropolone (Figure 1.9) IUPAC name 2-Hydroxy-2, 4, 6-cycloheptatrien-1-one has the chemical formula; $C_7H_6O_2$ is a derivative of tropone that has hydroxyl group in the number 2-position.[117] It was first characterized in 1945 by M.J.S Dewar and published in Nature.[118] The compound is one from the group of α-hydroxyl ketones that are known to undergo a tautomeric hydrogen shift. The two degenerate forms of tropolone in solution only require low activation energy for the hydrogen transfer to occur. This tautomeric proton transfer illustrated in figure 1.9 is extremely fast and as such NMR spectra only show the averaged signal results for both of the forms.[119]

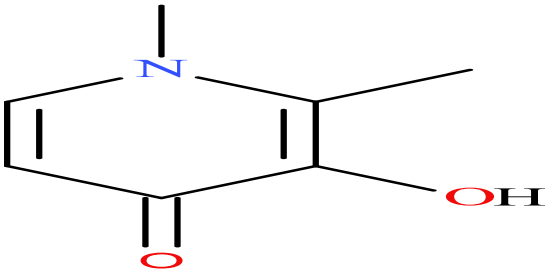

Figure 1.10: Tropolone and its Tautomeric Proton Transfer[119]

It can be synthesized by either acyloin condensation of the ethyl ester of pimelic acid and then oxidising with bromine, or bromination of 1, 2-cycloheptanedione using N-bromosuccinimide and then the use of elevated temperatures resulting in dehydrohalogenation.[117] Tropolone has resonance structures with various characteristics that are similar to polyones and polyenes but it does not have any aromatic characteristic which is unusual due to its structure. The compound is a viable starting material for greater ring structures such as steroids and has been used in Diels Alder reactions.[117] Some of the family of tropolones have anti-bacterial properties and may have the potential for use in antimalarial treatments. Tropolone has been shown to be bacteriostatic and bactericidal for a wide range of bacterial species.[119] Colchicine is an alkaloid compound with a tropolone ring and it demonstrates strong antitumour properties. Cancer cells undergo increased mitosis, hence they are more susceptible to colchicine poisoning than normal cells. The therapeutic properties of colchicine against cancer are limited by its toxicity to normal cells.[120]

1.26.4 *Ethyl Maltol*

Ethyl maltol, IUPAC name; 2-Ethyl-3-hydroxy-4-pyranone has the chemical formula $C_7H_8O_3$. Ethyl maltol was discovered in the 1970s.[121] It was originally isolated from larch tree bark and is produced through fermentation-organic synthesis. It is possible to extract ethyl maltol crystals from natural products or they can be produced by semi synthetic or synthetic methods. Synthetic and industrial production of ethyl maltol causes serious pollution to the environment; it has low production yields with a high cost of production.[121]It is commonly used as a flavour enhancer because it has the ability to cover up the bad taste of chemicals and is found in wine, chocolate, sweets, cosmetics, medicines, fruit flavored drinks and tobacco.[121] It has been reported that the pyrones, maltol (3-hydroxy-2-methyl-4-pyrone, Hma) and ethylmaltol (2-ethyl-3-hydroxy-4-pyrone, Hema), are extremely proficient in increasing the bio-availability and absorption of metal complexes. This is because they deprotonate very easily. A low pK_a value indicates that the compound is acidic and will easily give up its proton to a base, and the pK_a value for maltol is 8.46 and the pK_a value for ethyl maltol is 8.53.[121, 122] Ethyl maltol is a non-toxic anionic bidentate uninegative ligand which can form thermodynamically stable metal complexes with various metal ions that have the required charge necessary for chelation and formation of neutral complexes.[123] Six membered heterocycles such as ethylmaltol have one readily ionisable proton from its hydroxyl group which gives it a zwitter-ionic aromatic type property. These formed ethylmaltol complexes are stable at pH ranges that are found in a physiological environment. Ethyl maltol has been chelated to a number of metals including iron, aluminium, indium molybdenum and gallium.[122] The compound has had its biocompatibility thoroughly studied and findings show a positive toxicity profile.[123] Ethyl maltol has been chelated to iron with high affinity and selectivity, the resulting complex has been investigated in firstly the iron absorption from rats small intestines[124] and secondly investigated within patients to restore iron balance in anaemia.[123] Requirements for an iron ligand in the treatment of anemia are; high affinity for Fe^{3+}, highly aqueous, giving good solubility of the complex, and non-toxicity of the ligand. Ethyl maltol fulfills these requirements.[123]

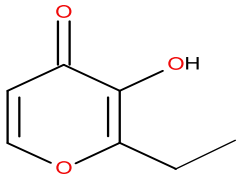

Figure 1.11: Ethyl Maltol

1.26.5 *Deferiprone*

Deferiprone, IUPAC name; 3-hydroxy-1, 2-dimethylpyridin-4(1*H*)-one, common trade name Ferriprox has the chemical formula $C_7H_9NO_2$. Deferiprone is an iron chelator that is orally active.[125] The compound was first designed and synthesised in 1978 at Professor R.C. Hider's laboratories at the University of Essex. Subsequent studies of the complex showed that deferiprone was capable of achieving effective short-term iron chelation[125]. Iron excretion was found to be directly related to the dose of deferiprone administered to the patient within the range of of 25 to 100 mg/kg body weight per day and to the iron load of the patient. However it is possible that deferiprone can cause the number of white blood cells made by bone marrow to decrease (Agranulocytosis) occurring in approximately 1% of patients.[125] Deferiprone is stable in conditions that exist in the human digestive system. It can successfully remove iron from patients suffering from iron overload from a range of organs and locations within the body including the heart and liver. Iron is needed for life to exist in the majority of species but conditions of primary iron overload such a hemochromatosis can lead to a build-up of this element.[126] There is no excretory pathway for iron and a build-up of this element can result in free radical damage which can lead to disease and death.[126] The complex has excellent binding properties with iron, and research has shown a high degree of relative specificity for the tris form of the deferiprone complex. Deferiprone has a molecular weight of 139 Da and is water soluble so it is able to move through cell membranes throughout the body without resistance. The complex is quickly eliminated from the body and has a half-life of about 2 hours with around 90% of the complex excreted in the urine.[126] It can also be used to detoxify patients that have been exposed to other metals such as plutonium and uranium and remove excess aluminum in hemodialysis patients. Deferiprone exhibits potent cyclotoxic activity in human hepatoblastoma cell line HepG2 and neuroblastoma cell line HL-60.[127] Tested against human oral tumour cells results showed that deferiprone exhibited tumour specific cyclotoxicity against cell line HSC-2 however the sensitivity of deferiprone in the experiments against the different cell lines differed remarkably from cell to cell.[127]

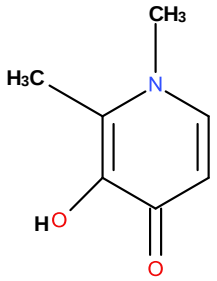

Figure 1.12: Deferiprone

1.27 Zirconium Complexes

There is a distinct lack of information in regards to the mechanisms of ligand coordination and interchange for Zr complexes. The published papers used throughout this thesis tend to focus on the characterisation of a specific complex rather than discuss the reasons behind the various methods used to synthesise the Zr compounds themselves. The extent of controlling the reaction to synthesise a two, three or four coordinated complex is not discussed in any of the published papers. Stoichiometric ratios of the metal and ligand involved in the synthesis process are a key factor in controlling the resulting coordination complex.

Zr can form stable complexes with hydroxamates. For immono-PET purposes Zr Desferrioamine is used in the radiolabelling of antibodies[128]. However there seems to be *in vivo* stability problems with this complex and research has been conducted to provide data that will help to develop new improved hydroxamate based ligands for chelation to ^{89}Zr.[128]

1.27.1 Zirconium Tetrakisoxine

The first Zr complex to be synthesised used the monoprotic bidentate chelating agent oxine. It is a colourless compound that is also commonly known as 8-quinolinol and oxyquinoline.[129] There is very little information available in regards to the zirconium tetrakisoxine complex at present. The first paper reporting findings on this complex was published by David F. Lewis and Robert C. Fay in 1974.[130] The paper reports that the stereochemistry of dodecahedral complexes of the transition metal type $M(AB)_4$ is found to be dependent upon the electronic configuration of the transition metal involved, in this case Zr.

A stereochemical rule was proposed by L. E. Orgel in 1960 that was related to the geometry of eight coordinated d^0, d^1 and d^2 transition metal complexes.[131] The rule states that complexes of the form MX_4Y_4 (M = a d^0, d^1 or metal ion and X, Y = monodentate ligands) are compelled to assume dodecahedral stereochemistry.[132]

Structures of dodecahedral $M(AB)_4$ complexes which have asymmetric bidentate ligands such as zirconium tetrakisoxine have been used to confirm Orgel's proposal for d^0 and d^2 complexes.[130]

Advances were made to this proposed rule[133] and the revised rule states that the structures of dodecahedral complexes of the form $M(AB)_4$ can be predicted because of the way in which the ligands can be sorted into their applicable co-ordination sites according to the electronic configuration of the central transition metal ion and the relative π donor acceptor properties of the ligands.[133] The structure of zirconium tetrakisoxine (prepared by a method not reported) was determined by the use of X-ray diffraction. It is reported that the Zr atom occupies a position at the intersection of three twofold axes. The complex itself assumes a dodecahedral geometry.

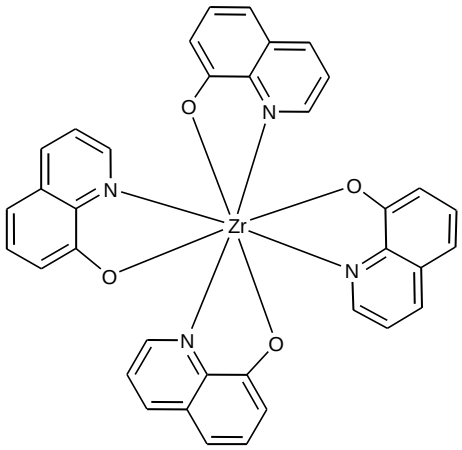

Figure 1.13: Zirconium Tetrakisoxine

The paper concludes that the structures of zirconium tetrakis (oxine) and the previous reported structure of [W(5-bromo-quinoline-8-olate) $_4$][133] provide conclusive evidence that the actual choice of stereoisomer for a dodecahedral molecule can be governed by the electronic configuration of the metal ion.[130]

When there is a lack of unreasonable steric interactions Orgel's hypothesis can be used as a guide to the stereochemistry of eight coordinated d^0 and d^2 transition metal complexes.[131]

The third paper was published by Poopathy Kathrigamanathan and Sivagnanasundram Surenendrakumar in the Journal of Materials Chemistry more recently in 2010.[134] The paper reports the findings of experimental work under taken resulting in two phases of zirconium tetrakisoxine. The research focuses on the possible uses of this complex in new organic light emitting diode (OLED) technology.

The research team had been working on charge transporting material for OLED's for over a decade and their research has shown that zirconium tetrakisoxine has excellent properties that are required for OLED instruments.

It should be noted that the oxine ligand was used by C W Tang and S A Van Slyke in 1987 to produce the first OLED[135], in the form tris oxine aluminium and is a green light emmiter.[136] The properties of the ziconium tetrakisoxine complex include good electron transport which also lowers the operating voltage and increases the lifespan and performance of OLED instruments when compared to the similar compound tris (8-hydroxyquinolinolate) aluminium.[136]

1.27.2 Zirconium Tropolone Complexes

There is very little information available in regards to the zirconium tetrakistropolone complex at present. The first paper reporting findings on this complex was published by Alan R. Davis and Frederick W. B. Einstein in 1978.[137]

1.27.3 Zirconium Ethyl Maltol Complexes

There is very little information or published work available in regards to the complexing of Zr to 2-ethyl-3-hydroxy-4-pyrone (ethyl maltol) in a ratio of 1:4 forming a zirconium tetrakisethyl maltol complex at present.

However research has been published that investigates dichlorobis (2-ethyl-3-hydroxy-4-pyrone) Zr (IV) as a new catalyst for the polymerisation of ethylene.[138]

The paper reports that the complex has four isomers and the cis configuration occurs most often with it being the most stable of the four. This paper is the only found report of Zr being complexed with ethyl maltol.[138] Ethyl maltol has also been chelated to tin and titanium in the form bis-ethylmaltolatodichloro-tin(IV) and bis-ethylmaltolatodichloro-titanium(IV).[139]

Ethyl maltol has been reported to chelate to iron with a high level of selectivity and affinity. The resulting complex has the ratio of 1:3 metal to ligand. It is a neutral complex and as such can easily cross membranes.[140]

1.27.4 Zirconium Deferiprone Complexes

There is currently no information or published work available in regards to the complexing of Zr to deferiprone in the form of a tetrakis complex or any other complex formed with this metal and ligand.

This is to be expected due to the fact that deferiprone was designed for oral chelation therapy in patients with iron over load and has been used for this purpose in over 15 countries in the last 7 years.[141] It has also been successfully investigated in the treatment of aluminium overload in patients undergoing renal dialysis.[141]

Zr is a metal which has no known biological function and as such it is to be expected that there would not be an excess of it within the body. Research investigating the effectiveness of deferiprone chelating to Zr in the body is clearly not required. The affinity deferiprone has with other metals such as magnesium (Mg), copper (Cu) and zinc (Zn) has been investigated[142] but Zr has not.

CHAPTER 2

Synthesis and Nuclear Magnetic Resonance Spectroscopic Characterisation of Zirconium Compounds

2.1 Introduction

Zirconium complexes with the common form of ZrL_4 where L is a bidentate uninegative ligand are the focus in this thesis for the development of new zirconium radiometal complexes for the diagnosis and treatment of diseases. These complexes are neutral and can to diffuse into cells in a manner analogous to InL_3 complexes.

All of the synthesis methods reported in this chapter took place in the laboratories located in the Ingram building at the University of Kent at Canterbury. All compounds and equipment used in this chapter can be found in the appendix section. (Compounds: Table A1, p 225, Equipment A.1.1, p 220)

NMR analysis was undertaken at the University of Kent at Canterbury utilising a JEOL NMR *ECS-400* a 2-channel NMR console, JEOL STAC MAN auto sample changer and JEOL Delta v5.02 software. Full specifications and settings can be found in the appendix section of this thesis.

CHN analysis was undertaken at firstly the University of Kent at Canterbury. Samples of the oxine ligand and the zirconium tetrakisoxine complex were analysed by Dr David Smith utilising an EMA Syst 1106 elemental analyser data system manufactured by Elemental Microanalysis Limited. Secondly CHN analysis was undertaken by Stephen Boyer at the Science Centre London Metropolitan University utilising a Carlo Erba Flash 2000 elemental analyser, configured for % CHN.

2.2 Synthesis Methods of Zr Complexes

2.2.1 Synthesis of Zirconium Tetrakisoxine

The reported method to synthesise zirconium tetrakis 8-hydroxyquinolinate, (reported as zirconium tetrakisoxine in this thesis) has been adapted from supplementary material relating to previously published work[134] in which the complex has been synthesised for use in organic light emitting diodes (OLED).

Oxine (5.0g; 0.0345mol) was completely dissolved in ethanol, (35 mL) in 150 mL glass conical flask. Zirconium tetrachloride (2.01g; 0.0085mol) was completely dissolved in ethanol, (25 mL) in a 150 mL glass conical flask. This solution was cooled to 10^{o}C with an ice water bath. The solution of oxine (5.0 g; 0.0345 mol) in ethanol, was added carefully to solution of zirconium tetrachloride (2.01 g; 0.0085 mol) in ethanol, drop wise with a narrow mouth bottle pipette. The solution was then stirred utilising the magnetic stirrer function of an electric hotplate and an octagon magnetic stirrer. The solution was stirred for 20 minutes at room temperature (20^{o}C). The solution was then heated to 50^{o}C in a water bath and piperidine (10 mL; 0.10 mol) was added drop wise with a narrow mouth bottle pipette. This addition of piperidine to the solution caused a yellow precipitate to form. This suspension was then refluxed for 1 hour and was allowed to cool to room temperature. The resulting precipitate was collected by the use of a Büchner funnel, filter paper and vacuum conical flask. The resulting product was then washed with ethanol, (15 mL), tetrahydrofuran, (15 mL) and diethyl ether (15 mL). The product was then dried at 70^{o}C for 1 hour in an electric oven. Crude yield 5.057 g (89%). Soxhlet extraction was undertaken (5.057 g) with 1,4-dioxane, purifying the compound for 8 hrs. 1, 4-dioxane was removed by use of a rotavap. The resulting yellow precipitate was further dried and collected by the use of a Büchner funnel, filter paper and vacuum conical flask. This collected compound was washed a final time with ethanol, (15 mL). The compound was then dried for 2 hrs in an electric oven at 50^{o}C and once dry was immediately placed into a glass air tight screw top storage container.

Carbon, hydrogen and nitrogen (CHN) analysis results for:
zirconium tetrakisoxine; $C_{36}H_{24}N_4O_4Zr$

Formula Weight: 667.82 g/mol

	Expected	1st Analysis	2nd Analysis
C %	64.75	64.12	63.55
H %	3.62	3.77	3.67
N %	8.69	8.59	8.35

Table 2.2

Theoretical Yield: 5.678 g,
Actual Yield: 4.012 g
Percentage of Theoretical Yield: 70.7%

2.2.2 Synthesis of Zirconium Tetrakistropolone

The reported method to synthesise zirconium tetrakistropolone has been adapted from published work which reports the method used to synthesise zirconium tetrakis isopropyltropolone.[143]

Tropolone (3.8 g; 0.031 mol) was completely dissolved in chloroform (75 mL) in a 250 mL glass conical flask. Zirconium tetrachloride (1.78 g; 0.0076 mol) was completely dissolved in chloroform (75 mL) in 250 mL glass conical flask. The solution of tropolone was added carefully to the solution of zirconium tetrachloride drop wise with a narrow mouth bottle pipette. The resulting solution was then stirred utilising the magnetic stirrer function of an electric hotplate and an octagon magnetic stirrer for 20 minutes at room temperature (~20^{o}C). The solution became pale yellow in colour. The solution was then heated in a water bath at between 50^{o}C and 55^{o}C for 2 hrs. The overall volume of the solution was reduced to ~40 mL during this period. The remaining chloroform was removed by use of a rotavap for 30 minutes.

The compound was then dried at 40^{o}C for 2 hrs in an electric oven and once dry was immediately placed into a glass air tight screw top storage container.

Carbon, hydrogen and nitrogen (CHN) analysis results for $C_{28}H_{20}O_8Zr$

Formula Weight: 575.34 g/mol

	Expected	1st Analysis	2nd Analysis
C %	58.40	53.24	53.33
H %	3.50	3.50	3.51
N %	0	0	0

Table 2.3

The CHN results suggest a formula for the complex of;
$C_{28}H_{20}O_8Zr \cdot 0.55\ CHCl_3$

	Expected	1st Analysis	2nd Analysis
C %	53.47	53.24	53.33
H %	3.23	3.50	3.51
N %	0	0	0

Table 2.4

Formula Weight:	658.91 g/mol
Theoretical Yield:	5.008 g
Actual Yield:	4.179g
Percentage of Theoretical Yield:	83.45 %

2.2.3 Synthesis of Zirconium Dichlorobis Ethyl Maltol

The reported method to synthesise zirconium dichlorobis ethyl maltol has been adapted from published work which reports the method used to synthesise zirconium dichlorobis ethyl maltol for use as a catalyst for ethylene polymerization.[138]

Tetrahydrofuran, (50 mL) was added drop wise with a narrow mouth bottle pipette to ethyl maltol (2-ethyl-3-hydroxy-4-pyrone), (2.00 g; 0.01428 mol) contained in a 150 mL glass conical flask. The ethyl maltol was completely dissolved in the tetrahydrofuran. Tetrahydrofuran, (50 mL) was added drop wise with a narrow mouth bottle pipette to zirconium tetrachloride (1.66 g; 0.00712 mol) contained in a 150 mL glass conical flask. The zirconium tetrachloride was completely dissolved in the tetrahydrofuran. The solution of ethyl maltol was added carefully to the solution of zirconium tetrachloride in drop wise with a narrow mouth bottle pipette. The resulting solution was then stirred utilising the magnetic stirrer function of an electric hotplate and an octagon magnetic stirrer for 60 minutes at room temperature (~20^{o}C). The solution was then heated in a water bath at between 50^{o}C and 55^{o}C for 1.5 hrs. The overall volume of the solution was reduced to ~30 mL during this period. Hexane (30 mL) was added to the solution and a pale yellow precipitate was formed. The resulting precipitate was collected by the use of a Büchner funnel, filter paper and vacuum conical flask. The product was washed with hexane (4x15 mL) and was then dried at 55^{o}C for 2 hrs in an electric oven. Once dry the zirconium dichlorobis ethyl maltol was immediately placed into a glass air tight screw top storage container.

Carbon, hydrogen and nitrogen (CHN) analysis results for:
zirconium dichlorobis ethyl maltol; $C_{14}H_{14}Cl_2O_6Zr$

Formula Weight: 440.39 g/mol

	Expected	1st Analysis	2nd Analysis
C %	38.18	38.26	38.27
H %	3.20	3.13	3.19
N %	0	0	0

Table 2.5

Theoretical Yield: 3.316 g
Actual Yield: 2.958 g
Percentage of Theoretical Yield: 89.2%

2.2.4 Synthesis of Zirconium Tetrakisethyl maltol

The reported method to synthesise zirconium tetrakisethyl maltol has been adapted from published work which reports the method used to synthesise zirconium dichlorobis ethyl maltol for use as a catalyst for ethylene polymerization.[138] The method reported for the synthesis of zirconium dichlorobis ethyl maltol above is based on the stoichiometric ratio of 2:1 where there are two ethyl maltol ligands for one zirconium tetra chloride molecule.

The method for the synthesis of zirconium tetrakisethyl maltol has been adapted so that there is a stoichiometric ratio of 4:1, so that there are four ethyl maltol ligands for one $ZrCl_4$ molecule.

Tetrahydrofuran, (100mL) was added drop wise with a narrow mouth bottle pipette to ethyl maltol (2-ethyl-3-hydroxy-4-pyrone), (4.00 g; 0.02856 mol) contained in a 250 mL glass conical flask.

The ethyl maltol was completely dissolved in the tetrahydrofuran. Tetrahydrofuran, (50 mL) was added drop wise with a narrow mouth bottle pipette to zirconium tetrachloride (1.66 g; 0.00712 mol) contained in a 250 mL glass conical flask. The zirconium tetrachloride was completely dissolved in tetrahydrofuran. The solution of ethyl maltol was added carefully to solution of zirconium tetrachloride drop wise with a narrow mouth bottle pipette. The solution was then stirred utilising the magnetic stirrer function of an electric hotplate and an octagon magnetic stirrer. The solution was stirred for 2 hrs at room temperature (~20^{o}C). The solution was then heated in a water bath at between 50^{o}C and 55^{o}C for 3 hrs. The overall volume of the solution was reduced to ~30 mL during this period. Hexane (50 mL) was added to the solution and a pale yellow precipitate was formed. The resulting precipitate was collected by the use of a Büchner funnel, filter paper and vacuum conical flask. The product was washed with hexane (4x20 mL) and was then dried at 55^{o}C for 3 hrs in an electric oven. Once dry the zirconium tetrakisethyl maltol was immediately placed into a glass air tight screw top storage container.

Carbon, hydrogen and nitrogen (CHN) analysis results for $C_{28}H_{28}O_{12}Zr$

Formula Weight: 647.74 g/mol

	Expected	1st Analysis	2nd Analysis
C %	51.92	51.74	51.82
H %	4.36	4.26	4.30
N %	0	0	0

Table 2.6

Theoretical Yield:	4.612g
Actual Yield:	4.199g
Percentage of Theoretical Yield:	91.0%

2.2.5 Synthesis of Zirconium Tetrakisdeferiprone

The method used to synthesise zirconium tetrakisdeferiprone was adapted from the method reported by Wen-Yuan Hsieh and Shuang Liu to synthesise chromium tris deferiprone.[144] Weights of the metal compound and ligand required were altered accordingly.

Glassware used during the synthesis of zirconium tetrakisdeferiprone was soaked in a 1% solution of nitric acid and 1% solution of hydrochloric acid for 24 hrs. The soaked glass wear was rinsed with millipore water and dried with an electric oven before use.

Deferiprone (0.561 g; 0.004 mol) was added to a solution of methanol (70 mL) in a 250 mL glass round bottom flask. The solution was then warmed to ~32^{o}C until the deferiprone had completely dissolved. Zirconium tetrachloride (0.242 g; 0.001 mol) was completely dissolved in the solution containing deferiprone in a fume cupboard. The addition of zirconium tetrachloride resulted in a release of hydrogen chloride which was allowed to disperse. The solution was then refluxed for 5 hrs, no precipitate had formed at this stage.

The solution was then allowed to cool to room temperature. Diethyl ether (150 mL) was then added to the solution and a white precipitate was immediately formed. The precipitate was filtered with the use of a Büchner funnel. The solid was washed with diethyl ether then recrystallized 3 times (methanol/diethyl ether). The compound was then dried for 18 hrs in a vacuum oven and once dry was immediately placed into a glass air tight screw top storage container.

Carbon, hydrogen and nitrogen (CHN) analysis results for $C_{28}H_{32}N_4O_8Zr$

Formula Weight: 643.45 g/mol

	Expected	1st Analysis	2nd Analysis
C %	52.24	38.94	38.84
H %	5.01	6.49	6.48
N %	8.70	6.60	6.63

Table 2.7

The CHN results suggest a formula for the complex of;

$C_{28}H_{32}N_4O_8Zr \cdot 12H_2O$

	Expected	1st Analysis	2nd Analysis
C %	39.02	38.94	38.84
H %	6.57	6.49	6.48
N %	6.50	6.60	6.63

Table 2.8

Formula Weight:	859.99 g/mol
Theoretical Yield:	0.859 g
Actual Yield:	0.767 g
Percentage of Theoretical Yield:	89.3 %

2.3 Results and Discussion, Synthesis

The zirconium tetrakisoxine complex was synthesised by adapting a previously reported method.[134] The synthesis method of zirconium tetrakistropolone was devised adapting a previously reported method stating the synthesis of zirconium tetrakis isopropyltropolone.[143] The zirconium dichlorobis ethyl maltol complex was also synthesised by adapting a previously reported method.[138] The method previously reported to synthesise zirconium dichlorobis ethyl maltol was adapted and the synthesis of tetrakisethyl maltol was undertaken. The method to synthesise zirconium tetrakisdeferiprone was developed using an amalgamation of the previously developed methods for the synthesis of the zirconium tetrakis complexes.

The CHN analysis results of the zirconium tetrakisoxine, zirconium dichlorobis ethyl maltol and zirconium tetrakisethyl maltol complexes demonstrate that the expected percentage composition values of these three compounds were extremely close to the results of the analysis undertaken. The analysis result values are within ±0.3% of the expected results.

The CHN results for the zirconium tetrakistropolone complex suggest a formula of $C_{28}H_{20}O_8Zr \cdot 0.55\ CHCl_3$. It has been previously reported[137] that a tropolone ligand can be disordered when in a complex between two positions due to close contact with a partially occupied chloroform molecule.[137] This would explain the presence of the chloroform.

The CHN results for the zirconium tetrakisdeferiprone suggest the formula $C_{28}H_{32}N_4O_8Zr.\ 12H_2O$ for the complex which shows an incorporation of water into the structure. Complexes of the form M tris deferiprone (M= Cr, Al, Ga, Fe, In and Mn) are known to be significantly hydrated incorporating 12 water molecules per complex in their crystal structures.[144] Mass spectrometry results confirmed the synthesis of the zirconium tetrakisdeferiprone complex. Zirconium tetrakisethyl maltol and zirconium tetrakisdeferiprone are novel complexes and it has not been possible to find previous accounts of these two complexes.

2.4 Mass Spectrometric Analysis of Zirconium Tetrakisdeferiprone

Zirconium tetrakisdeferiprone is a novel complex with no previously reported close approximations. Mass spectrometry was used to further characterise the zirconium tetrakisdeferiprone complex.

2.4.1 Mass Spectrometry

It is possible to deflect molecules by magnetic fields if the molecule has been converted into an ion as electrically charged particles are affected by magnetic fields.[145]

The mass spectrometric process involves several steps. Firstly an atom is ionised by knocking off one or more electrons which results in a positive ion. The ions are all accelerated so that they all have the same kinetic energy. Depending on the mass of the ion it will be deflected accordingly.[145] Deflection of ions also relies upon the magnitude of the positive charge of the ion. A higher charge equals a greater amount of deflection from the magnetic field. Finally the beams of ions pass through the apparatus and are detected electrically.[146]

Two mass spectrometry techniques were used during these experiments; Matrix-assisted laser desorption/ionization time of flight (MALDI-TOF) and electrospray. MALDI-TOF mass spectrometry is a technique that allows the analysis of compounds which are inclined to be fragile and fragment when ionized by more traditional ionization methods.[146] Electrospray mass spectrometry was used employing direct infusion where by a liquid sample is introduction and continually flowed into a mass spectrometer ion source. The electrospray technique uses high voltage electricity to create an aerosol from a liquid resulting in the production of ions.[145]

2.4.2 Experimental Method

Experimental work was carried out by Kevin Howland, Biomolecular Science Facility Manager, School of Biosciences, University of Kent. MALDI-TOF and electrospray mass spectrometry were both used to analyse the zirconium deferiprone compound. MALDI-TOF mass spectra was recorded on a ultraflexTOF/TOM mass spectrometer. Electro spray mass spectra were recorded on a Bruker micrOTOF-Q II mass spectrometer. The sample was injected as a 0.01 mg/mL infusion into the electro spray source, operating in positive ion mode, at 4.5 kV and mass spectra recorded from 50-1250 m/z. Data was analysed with Bruker's Compass Data Analysis software.

2.4.3 Results and Discussion

MALDI-TOF mass spectrometry, which is the softest ionisation technique available at the University of Kent resulted is a spectra showing only the zirconium tris deferiprone complex (figure 2.1) However a cationising agent was not used which may have enhanced the ionization efficiency.

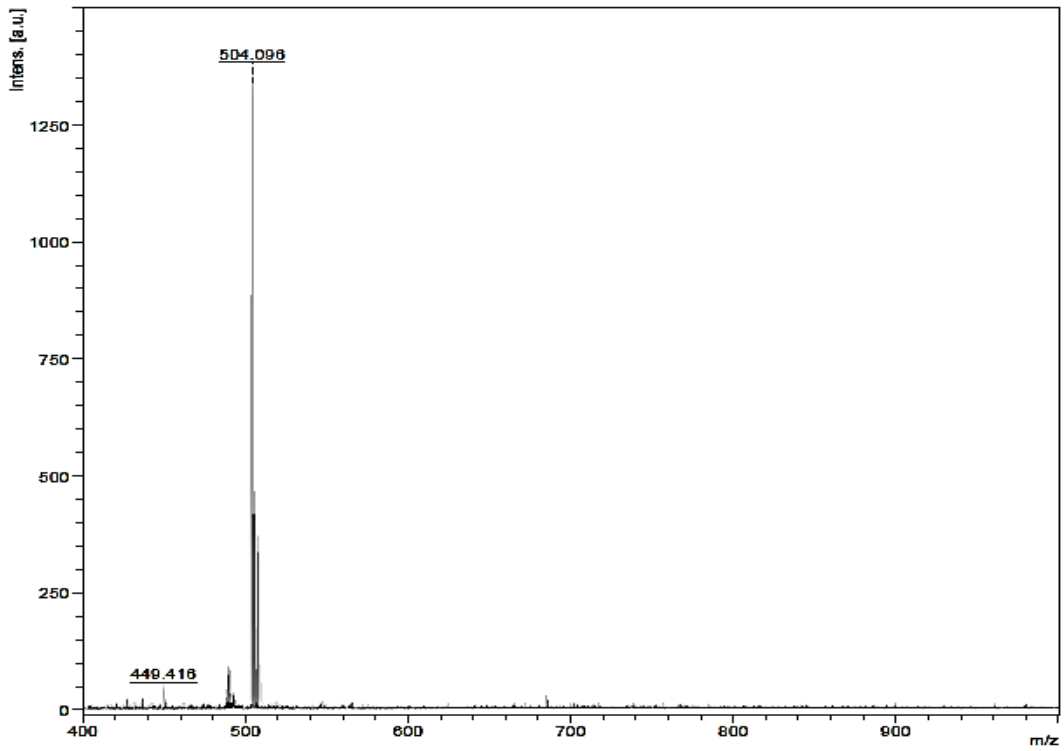

Figure 2.1: MALDI-TOF mass spec of Zirconium Deferiprone Complex

Electrospray mass spectrometry using direct infusion was also used to analyse the zirconium deferiprone complex. Results showed that the predominant ion is the zirconium tris deferiprone, however there is a peak at 665 m/z which could be explained by a zirconium tetrakisdeferiprone sodium adduct. Expansion of this region along with the theoretical isotope pattern for the zirconium tetrakisdeferiprone can be seen in figure 2.3.

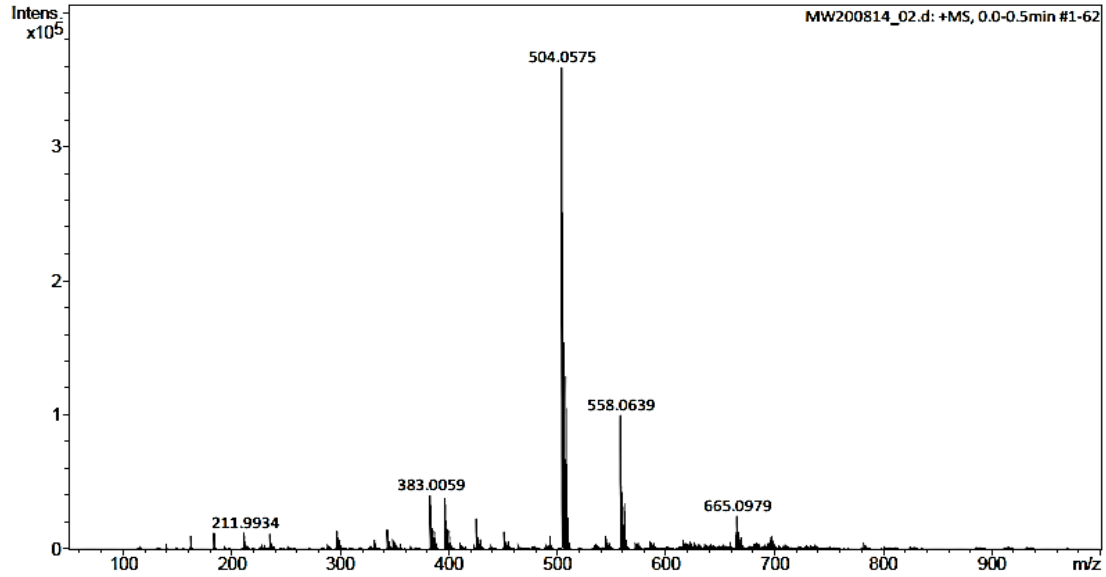

Figure 2.2: MALDI-TOF Spectra of Zirconium Tetrakisdeferiprone

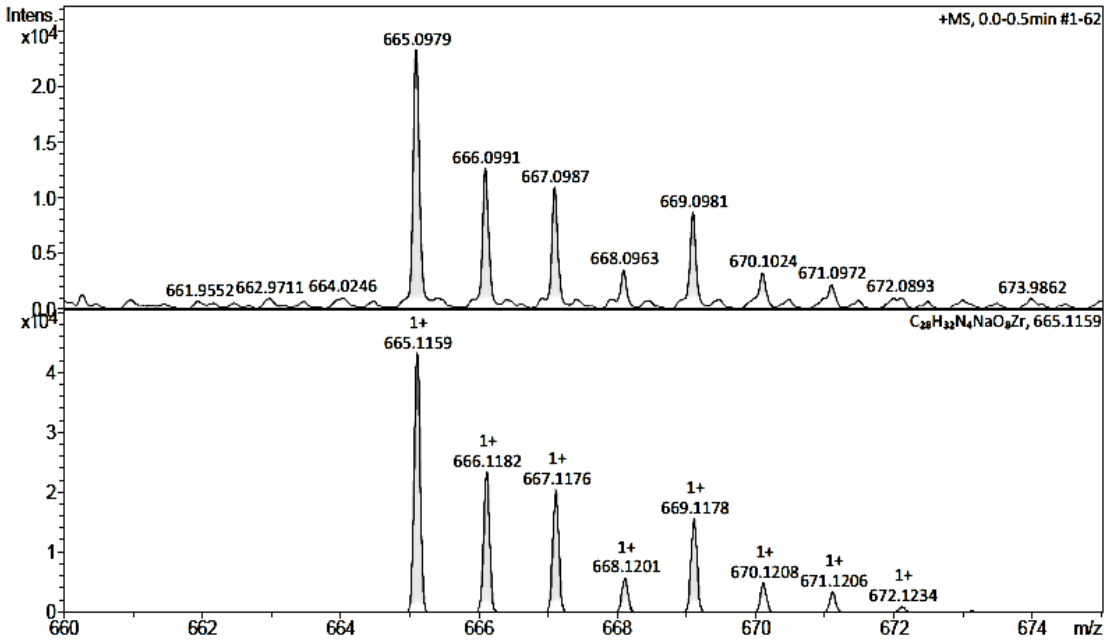

Figure 2.3: Actual and Predicted Spectra of Zirconium Tetrakisdeferiprone

2.4.4 Conclusion

Both of the mass spectrometry techniques have shown that there appears to be zirconium complexes with either three or four deferiprone ligands attached to the zirconium metal.

2.5 Crystal Growth and X-ray Analysis of Deferiprone Complex

2.5.1 Introduction

To confirm the structure of the zirconium tetrakisdeferiprome complex it was decided to grow crystals of a nature that could be analysed with single-crystal X-ray diffraction.[147]

2.5.2 Crystal Growing

A variety of methods to grow crystals was undertaken over a period of six months. Methods included, slow evaporation (22^{o}C and 5^{o}C), solvent diffusion by layering, vapour diffusion, reactant diffusion and sublimation.[148] All of these methods failed to yield crystals of a quality that could be analysed with single-crystal X-ray diffraction apart from slow evaporation at 5^{o}C.

2.5.3 Method

Crystals were grown in two batches. Batch 1; zirconium tetrakisdeferiprone (0.1g) was dissolved in the minimum amount of methanol possible until saturated (<10mL). Once saturated the solution was heated to dissolve the entire remaining compound. This was then placed in a glass test tube, and sealed with parafilm with a small needle sized hole to allow slow evaporation over a number of months at a temperature of 5^{o}C. Batch 2 follows the same method with methanol exchanged for dimethyl sulfoxide.

2.5.4 Results and Discussion

Two batches of crystals were grown by was slow evaporation at 5^{o}C that yielded crystals suitable for analysis. These crystals were sent to University College London for Single-Crystal X-ray Diffraction analysis.

2.5.5 Single-Crystal X-ray Diffraction

All single-crystal X-ray diffraction experiments were undertaken by Professor Derek A. Tocher, deputy head, department of chemistry, University College London.

2.5.6 Crystal Batch 1

Two data sets were collected; the first was with a crystal from batch 1 with Cu radiation. This could not be solved so a second crystal form batch 1 was analysed with Mo radiation and was found to be the hydrochloride salt of deferiprone as the monohydrate, $[C_7H_8N_1(OH)_2]^+Cl^-.H_2O$. Once the Mo dataset had been solved it was possible to use Cu radiation on another crystal from batch 1. Unit cell parameters of crystals were analysed and it was found with certainty that all three of the crystal samples from batch 1 are the same organic salt as seen in figure 2.4.

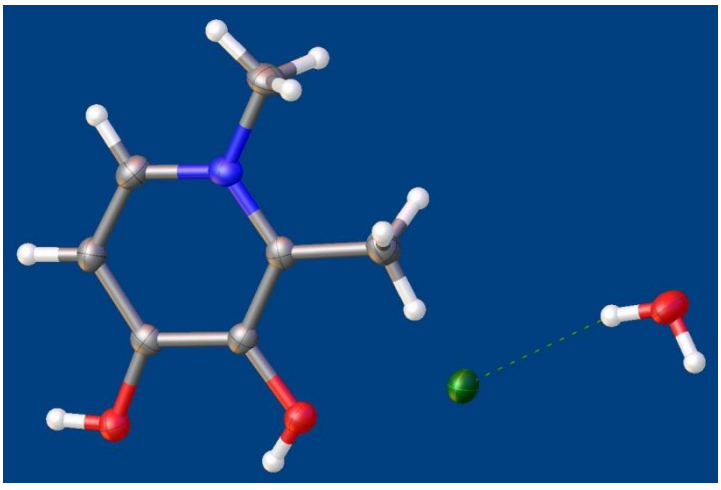

Figure 2.4: Hydrochloride Salt of Deferiproneas a Monohydrate $[C_7H_8N_1(OH)_2]^+Cl^-.H_2O$.

2.5.7 Crystal Batch 2

A fragment from a crystal from batch 2 was placed on the diffractometer and showed no spots. A thinner sample was placed on the diffractometer with the same results. A larger (> 3mm long) crystal was placed on the diffractometer and there was only diffuse scattering. From these results it can be concluded that the crystals from batch 2 are in fact completely amorphous.

2.5.7 Conclusion

All of the crystals analysed from batch 1 were found to be protonated ligand without any zirconium. All of the crystals from batch 2 were found to be completely amorphous. Results indicate that it has not been possible to grow any crystals of the zirconium tetrakisdeferiprone complex. As such it has not been possible to use single-cystal X-ray diffraction to obtain information about the structure of the zirconium tetrakisdeferiprone complex.

2.6 Nuclear Magnetic Resonance Spectroscopy

Nuclear magnetic resonance (NMR) spectroscopy is a widely used analytical technique which can provide useful data that can be used to build models of the compounds being investigated. The technique depends on the magnetic properties of the atomic nucleus. When nuclei are deposited in a strong magnetic field, certain nuclei will resonate at a distinctive frequency located in the radio frequency area of the electromagnetic spectrum.[149] When there is a difference in the resonance frequency it is possible to derive detailed information about the molecular structure in which the atom is located. This information can then be compared to simulation predictions to ascertain whether a predetermined hypothesis was correct.

- Chemical shift data provides information about the local surroundings of the atom. The resonant frequency varies slightly depending on the position of an atom within a molecule, known as the chemical environment. Bonding electrons establish their own small scale magnetic field and this in turn alters the external magnetic field in the proximity of the nucleus, in the order of one part per million.[149]
- Signal intensity, which is measured as the integral of the signal, is derived from the number of equivalent atoms which are present in the given environment. The absorption signal in the NMR spectra is in most cases proportional to the number of protons that are advancing into resonance at the frequency of the signal.[150] Hence the area which is under the absorption peaks is directly proportional to the number of protons which have been detected.[150]
- Spin-spin coupling and through-space interactions can be used to determine distances/spacing. In high resolution NMR spectroscopy the splitting of NMR signals into multiplets is due to scalar or indirect coupling of nuclear spins facilitated by covalent bonding.[151]

NMR spectroscopy will be employed and findings will be reported in this chapter. The technique will be used to determine the loss of a proton from each of the ligands which would have occurred once binding of the ligand to the zirconium ion has occurred. There will be a chemical shift once the ligand has bound to the metal ion and the differences between the spectra of the ligand and the metal complex are compared and findings reported.

2.7 Experimental Method

For ^{1}H NMR analysis of the compounds the quantity of material to be dissolved was between about 5 to 25 mg depending on solubility of the complex into the deuterated solvent. For ^{13}C NMR analysis of the compounds as much compound was dissolved as possible in to the deuterated solvent (as ^{13}C is *six thousand times* less sensitive).

The complex was dissolved in 1 mL of deuterated solvent in a clean sample vial at room temperature ~22^{o}C. Once fully dissolved the deuterated solvent had become saturated with the compound and the solution was drawn up into a sterile syringe fitted with a sterile microlance 3 needle. Between the needle and the sterile syringe a ministart single use filter unit (0.45 µm) was used. The solution was then pushed through the filter and needle into a clean and sterile NMR tube; O.D: 5 mm, thin walled, length 20 cm. The height of the solution contained in the NMR tube was between 4.5 cm and 5.5 cm in all experiments to ensure accurate shimming of the apparatus. The NMR tube cap was then securely place onto the NMR tube.

The NMR tube was then placed into the sample carriage and the position number was noted. The JEOL Delta software (v.5.0.1) controlling the NMR spectrometer was set according to experimental requirements and the experiment was run. Results were automatically saved on to the PC controlling the NMR spectrometer.

Tables of equipment, equipment settings and reagents used throughout this chapter can be located in the appendix section of this thesis.

2.7.1 ^{1}H and ^{13}C NMR of Oxine and Zirconium Tetrakisoxine

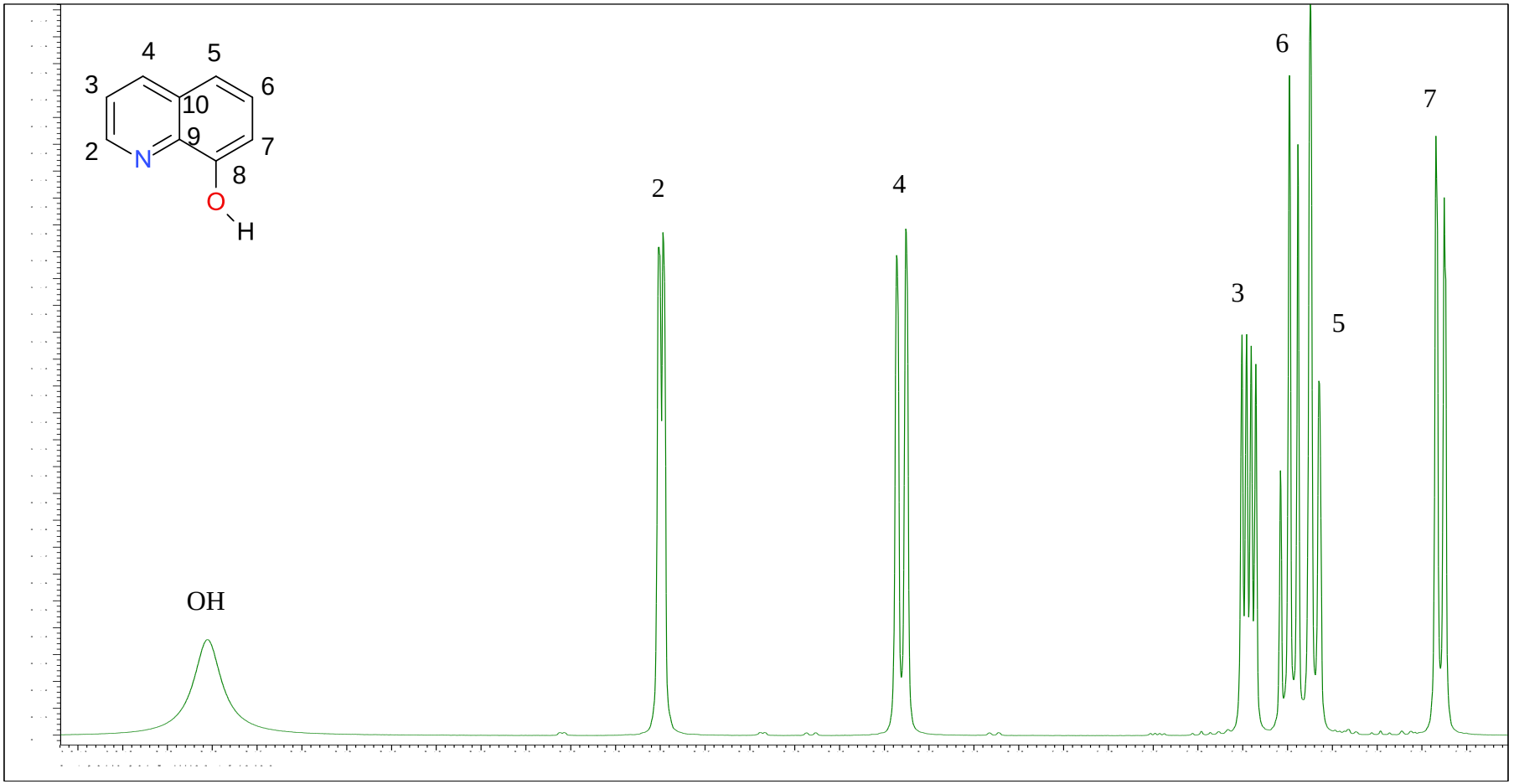

Figure 2.5: ^{1}H NMR of Oxine in DMSO-*d6*

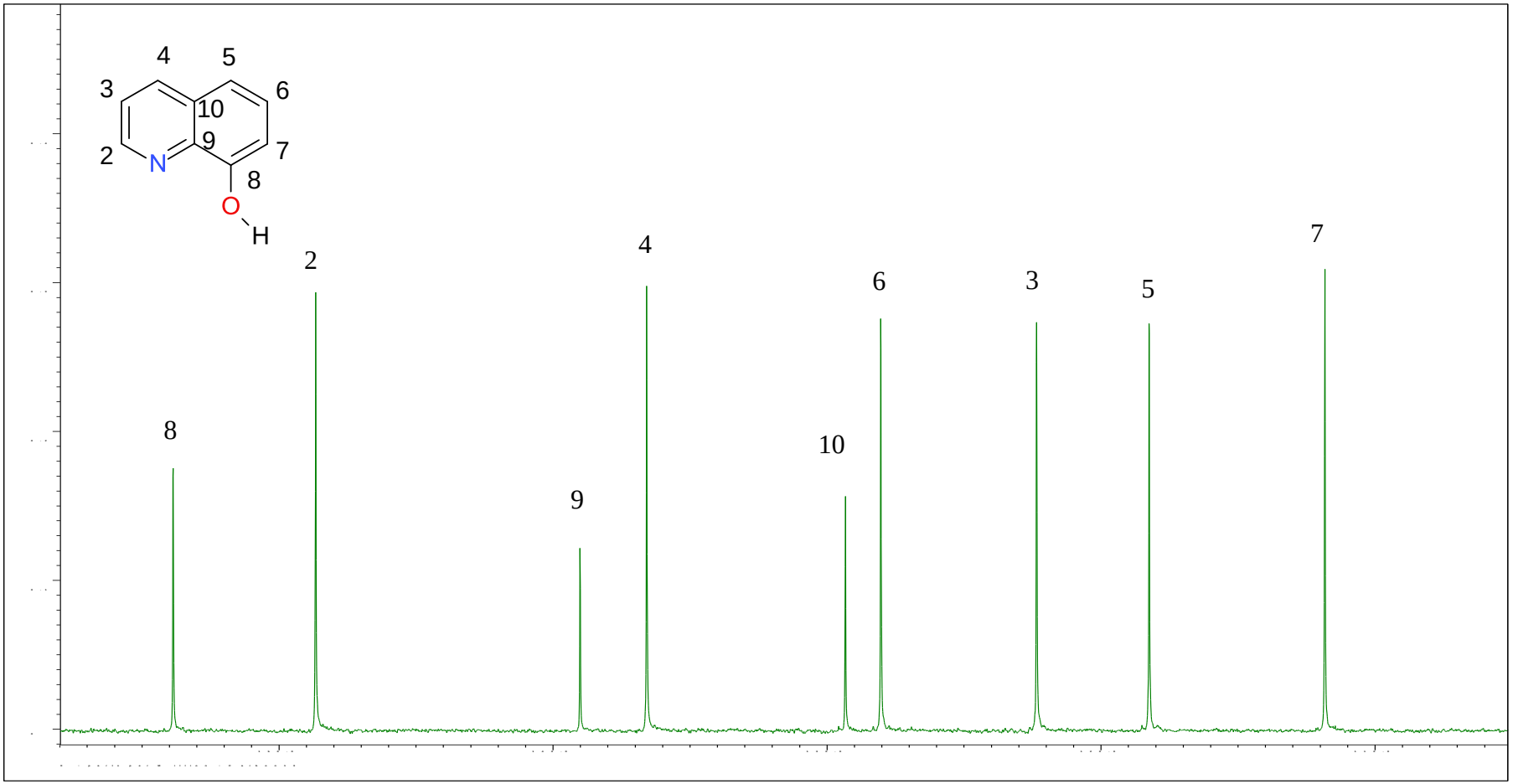

Figure 2.6: ^{13}C NMR of Oxine in DMSO-*d6*

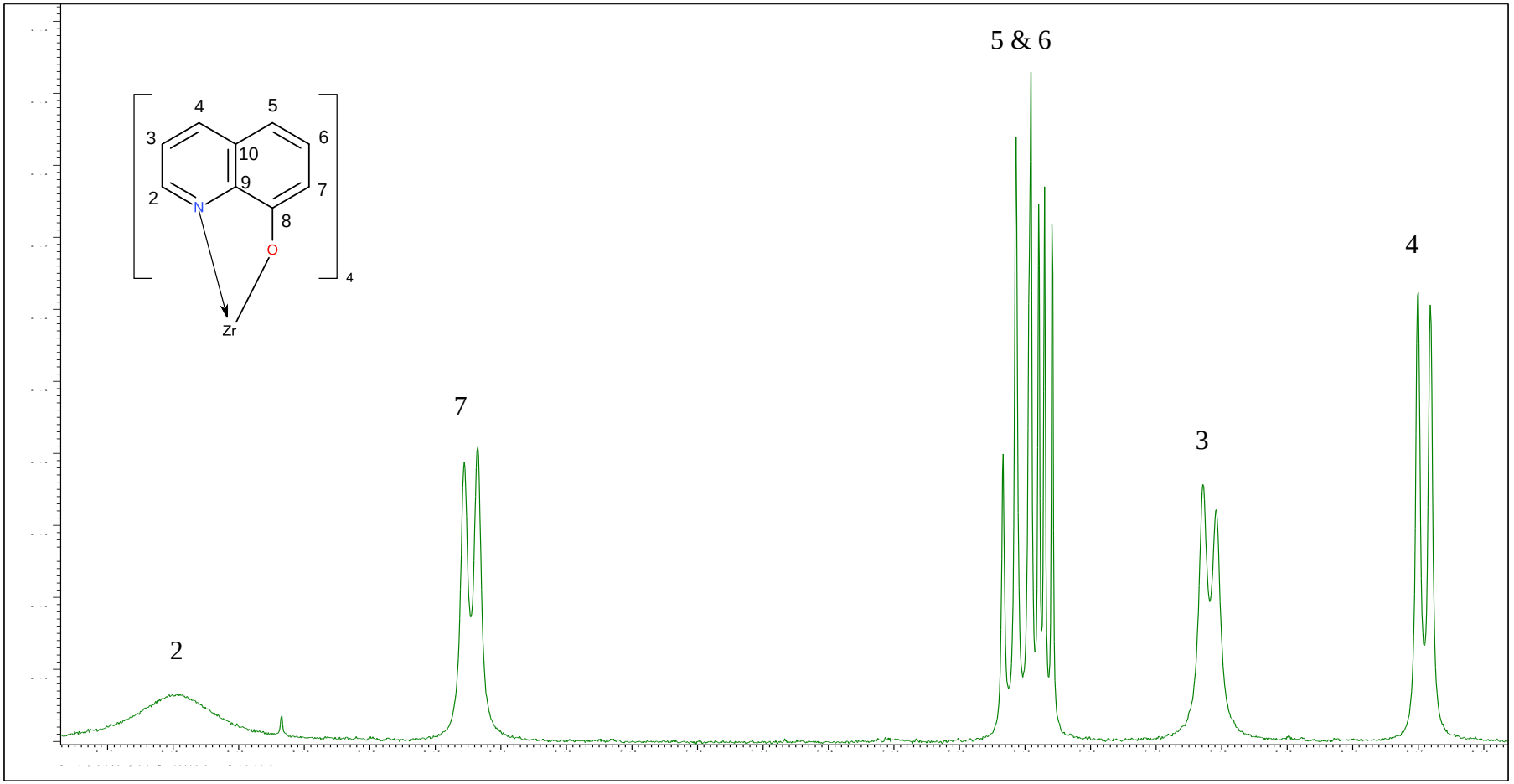

Figure 2.7: ^{1}H NMR of Zirconium Tetrakisoxine in DMSO-*d6*

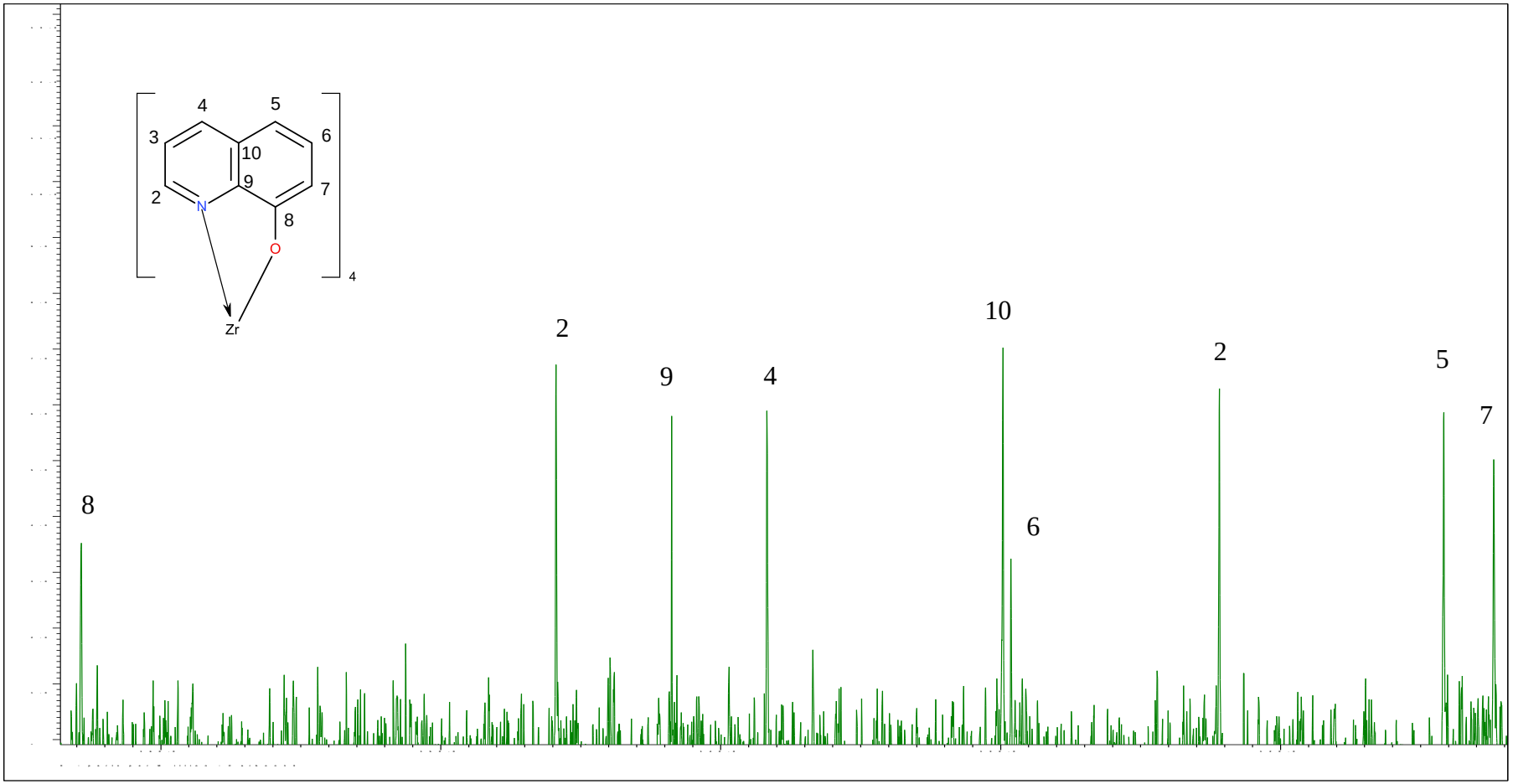

Figure 2.8: ^{13}C NMR of Zirconium Tetrakisoxine in DMSO-*d6*

2.7.2 ^{1}H and ^{13}C NMR of Tropolone and Zirconium Tetrakistropolone

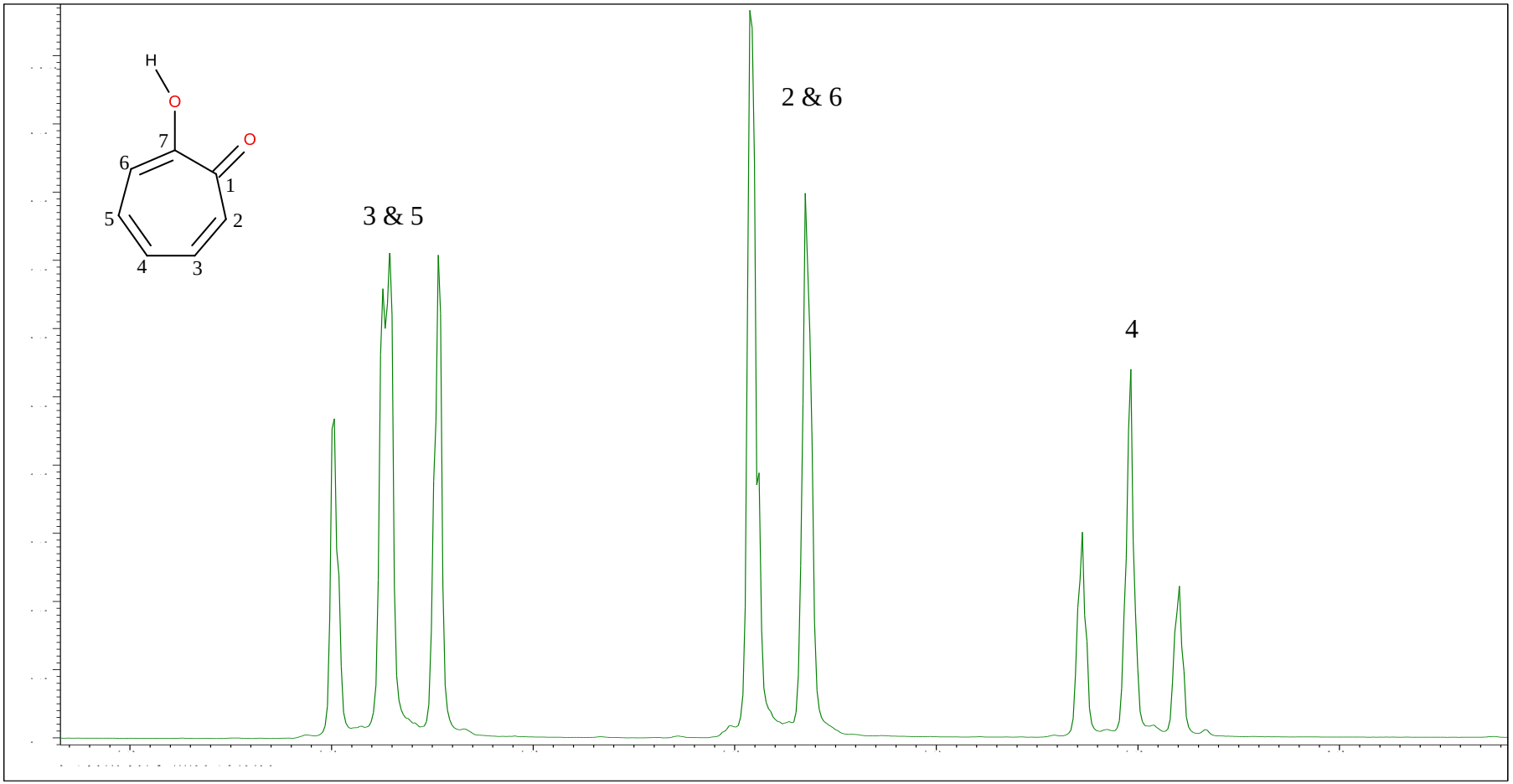

Figure 2.9: ^{1}H NMR of Tropolone in DMSO-*d6*

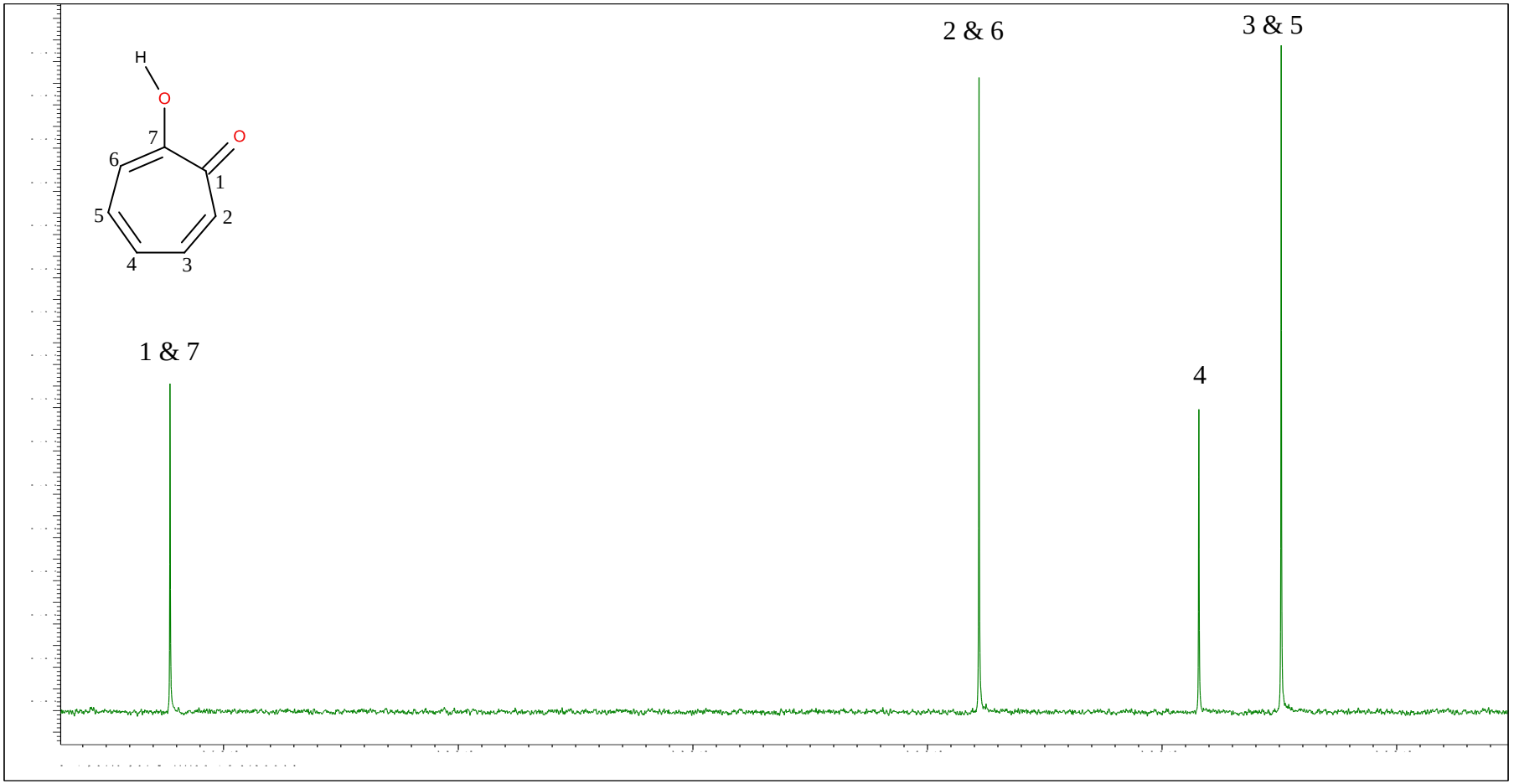

Figure 2.10: ^{13}C NMR of Tropolone in DMSO-*d*

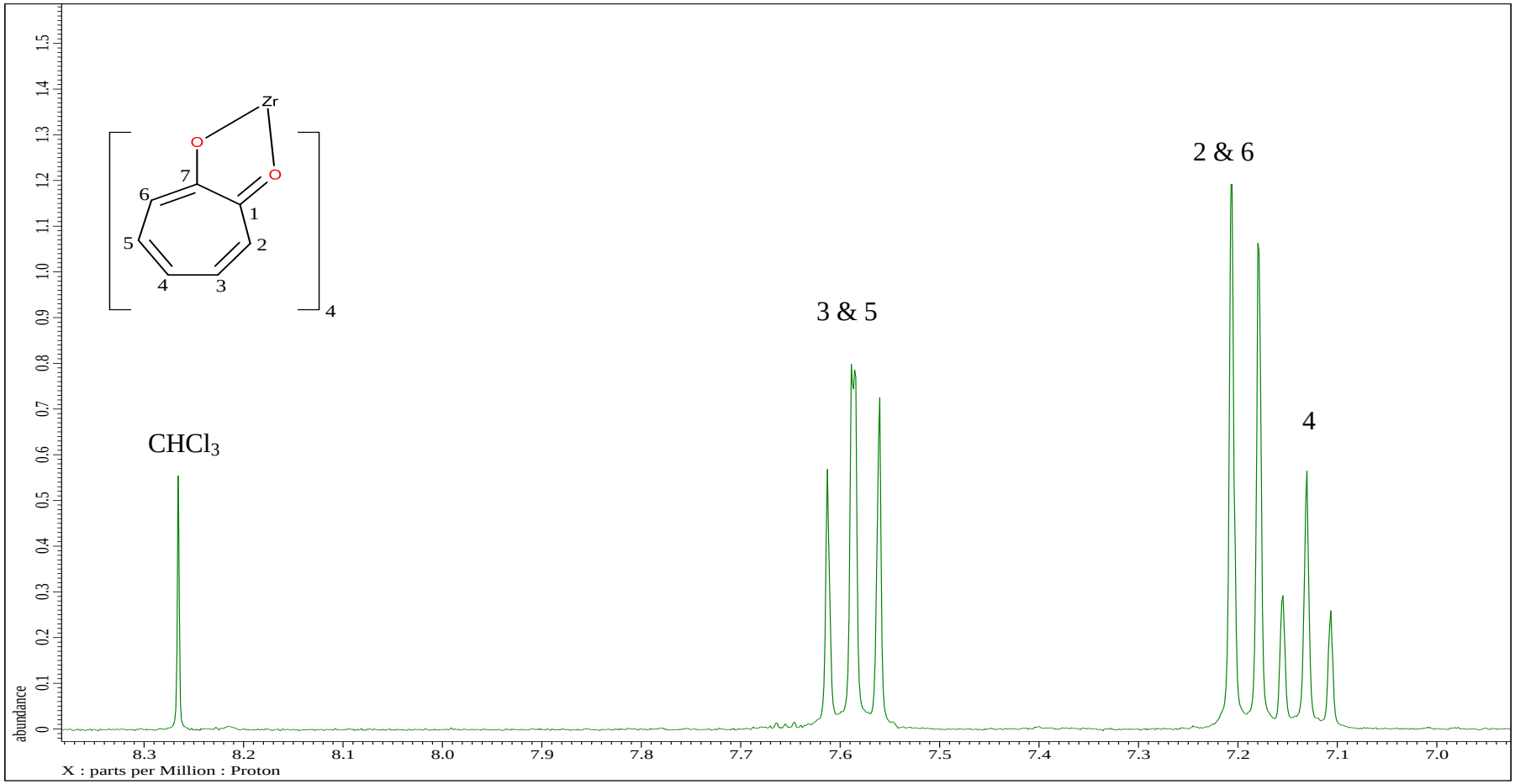

Figure 2.11: ^{1}H NMR of Zirconium Tetrakistropolone in DMSO-*d6*

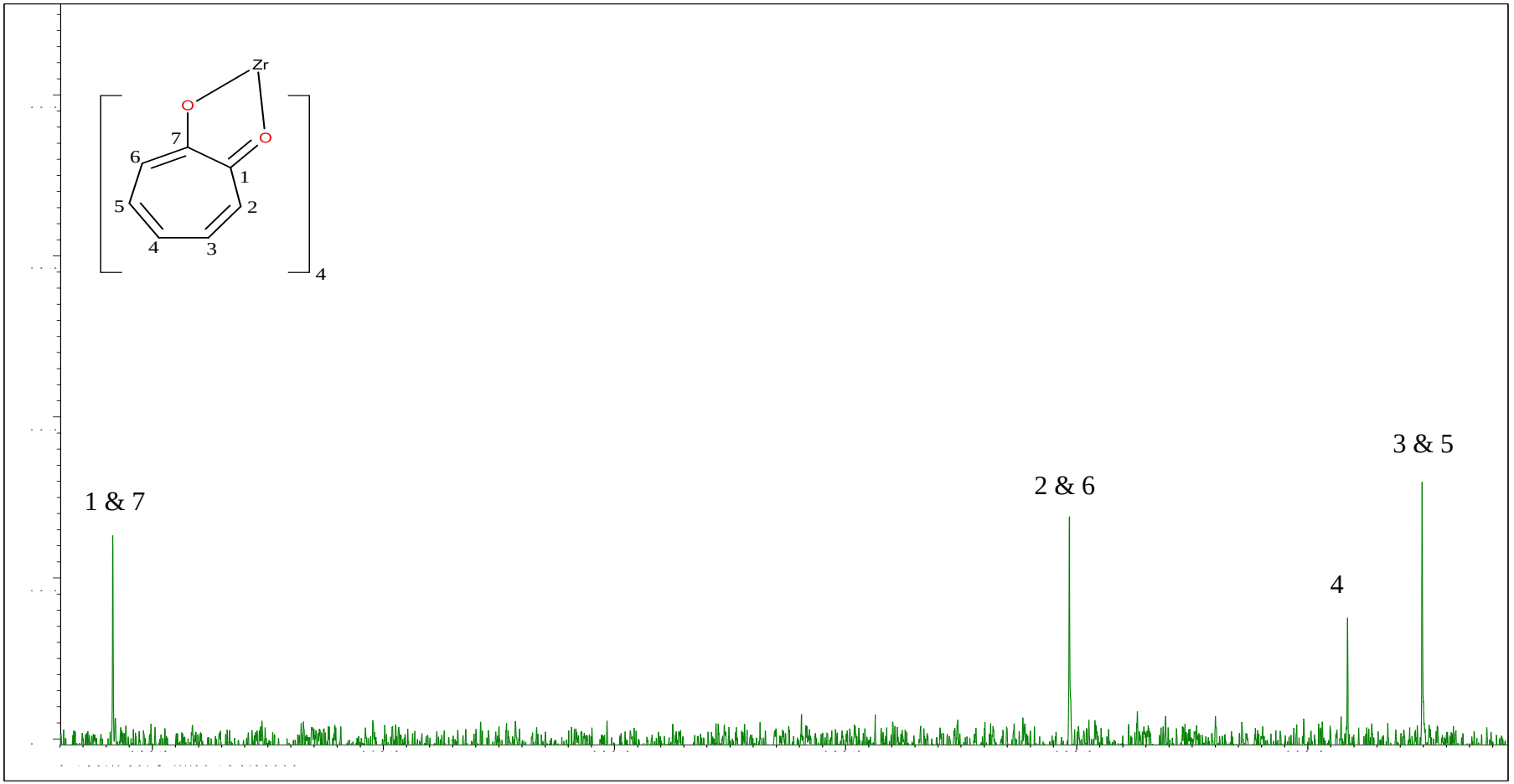

Figure 2.12: ^{13}C NMR of Zirconium Tetrakistropolone in DMSO-*d6*

2.7.3 ^{1}H and ^{13}C NMR Ethyl Maltol, Zirconium Dichlorobis Diethyl Maltol and Zirconium Tetrakisethyl Maltol

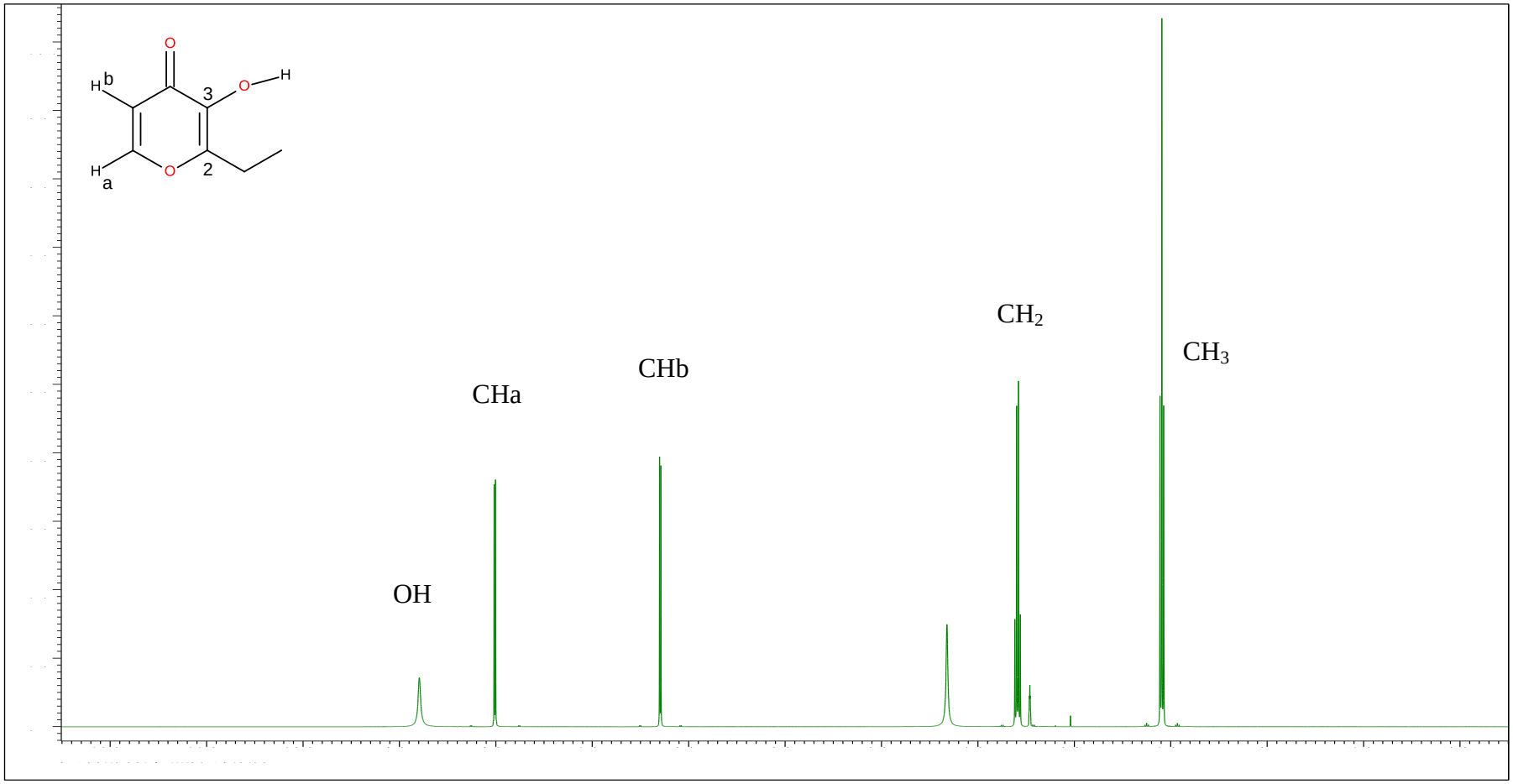

Figure 2.13: ^{1}H NMR of Ethyl Maltol DMSO-*d6*

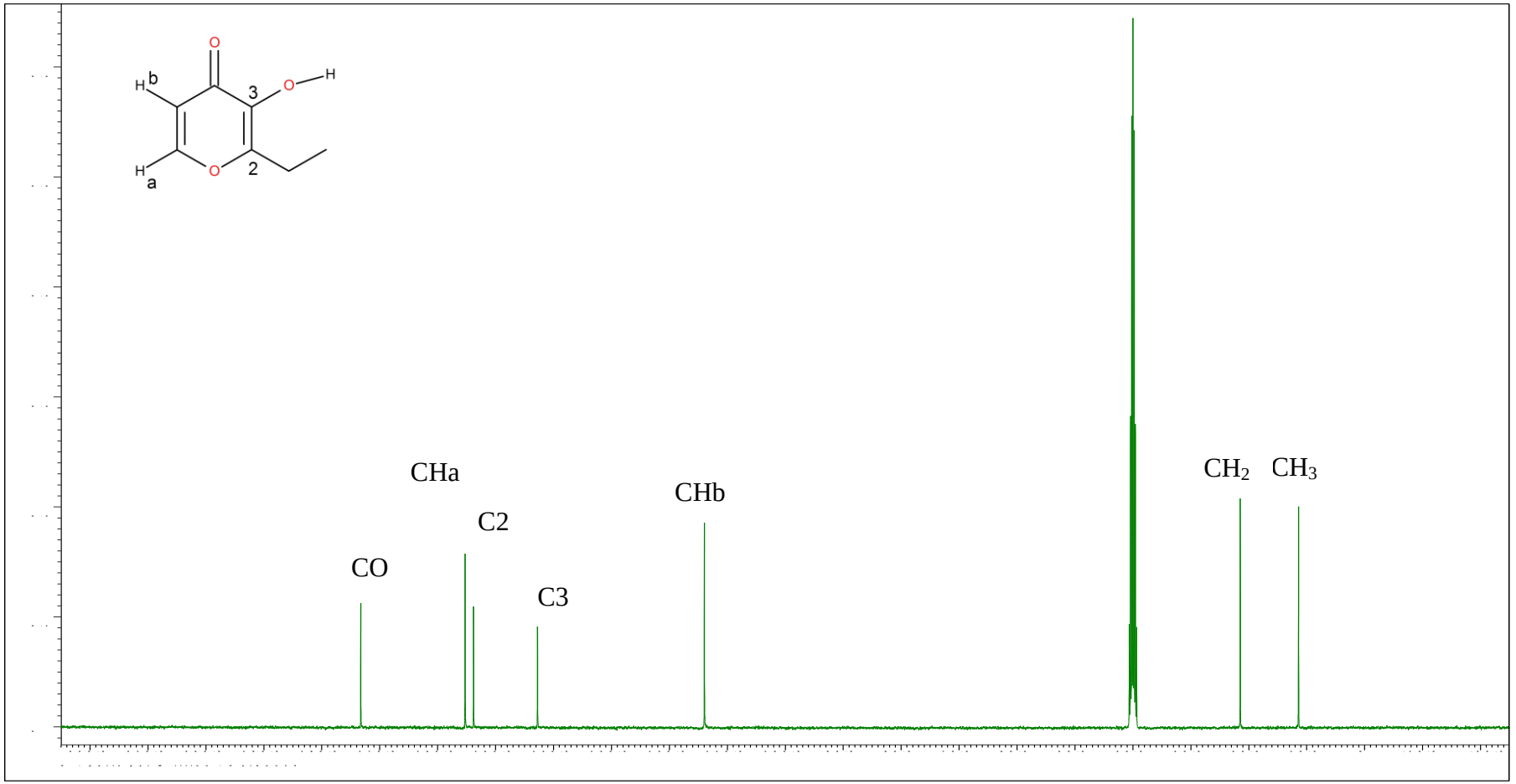

Figure 2.14: ^{13}C NMR of Ethyl Maltol in DMSO-*d6*

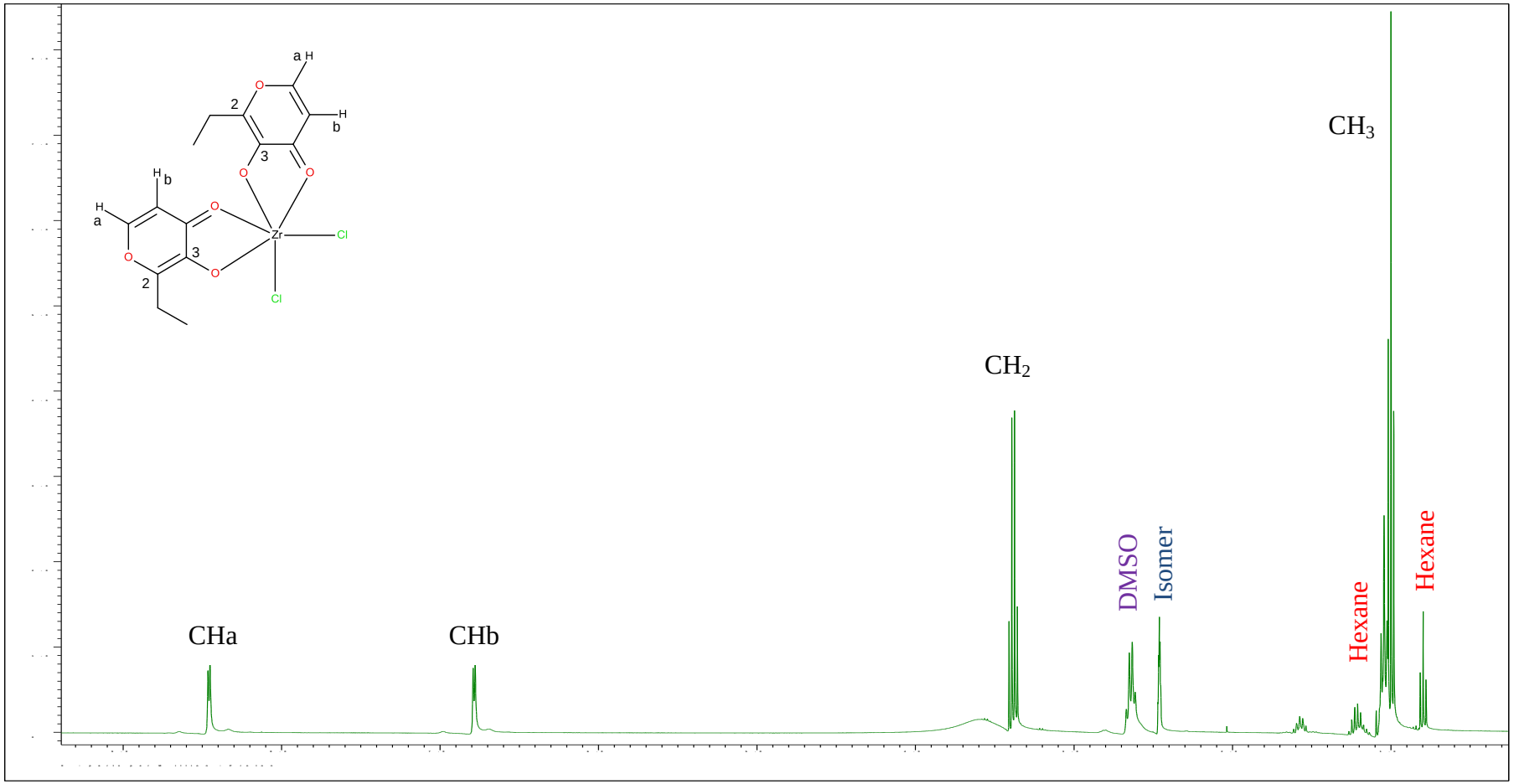

Figure 2.15: ^{1}H NMR of Zirconium Dichlorobis Ethyl Maltol in DMSO-*d6*

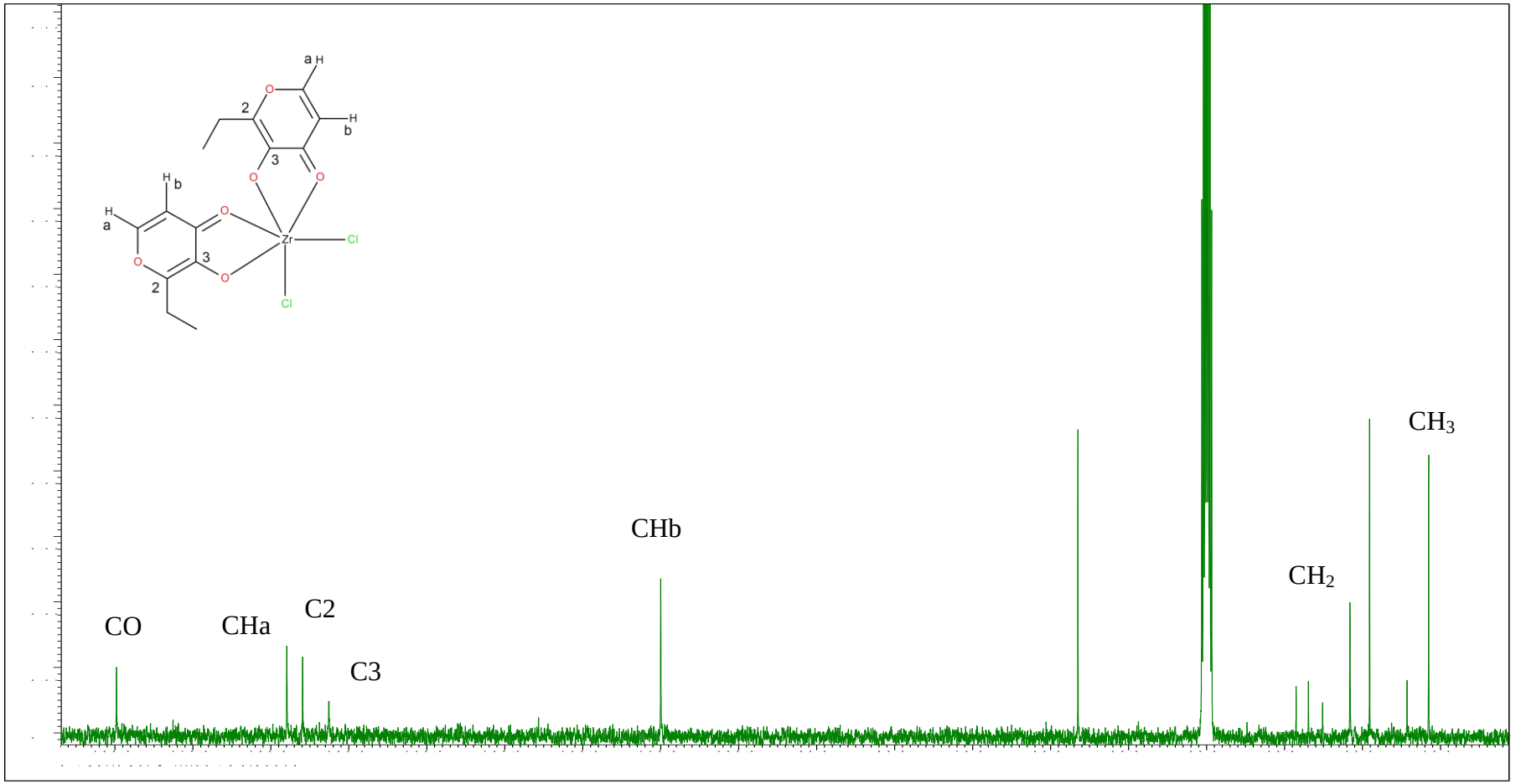

Figure 2.16: ^{13}C NMR of Zirconium Dichlorobis Ethyl Maltol in DMSO-*d6*

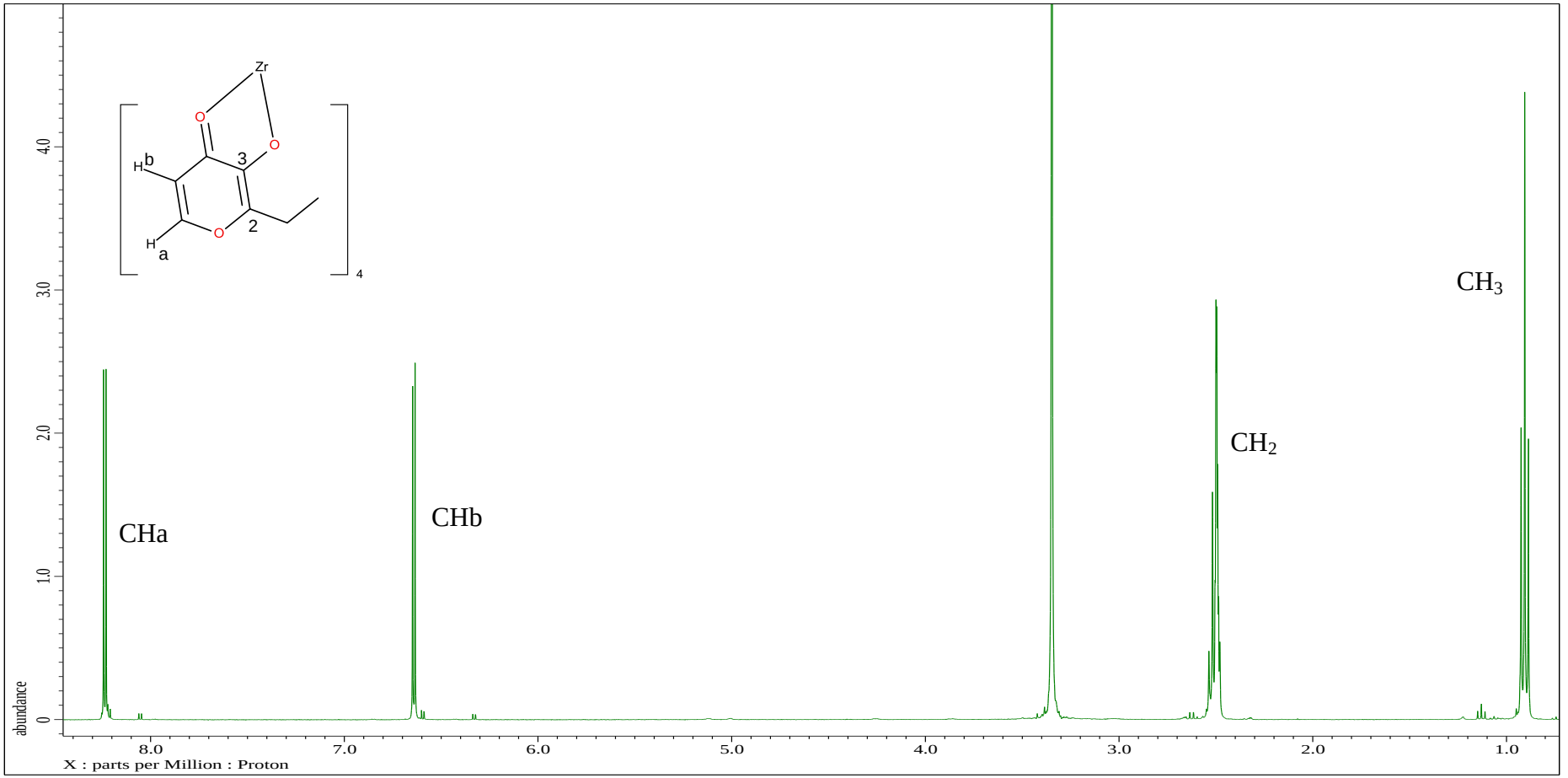

Figure 2.17: ^{1}H NMR of Zirconium Tetrakisethyl Maltol in DMSO-*d6*

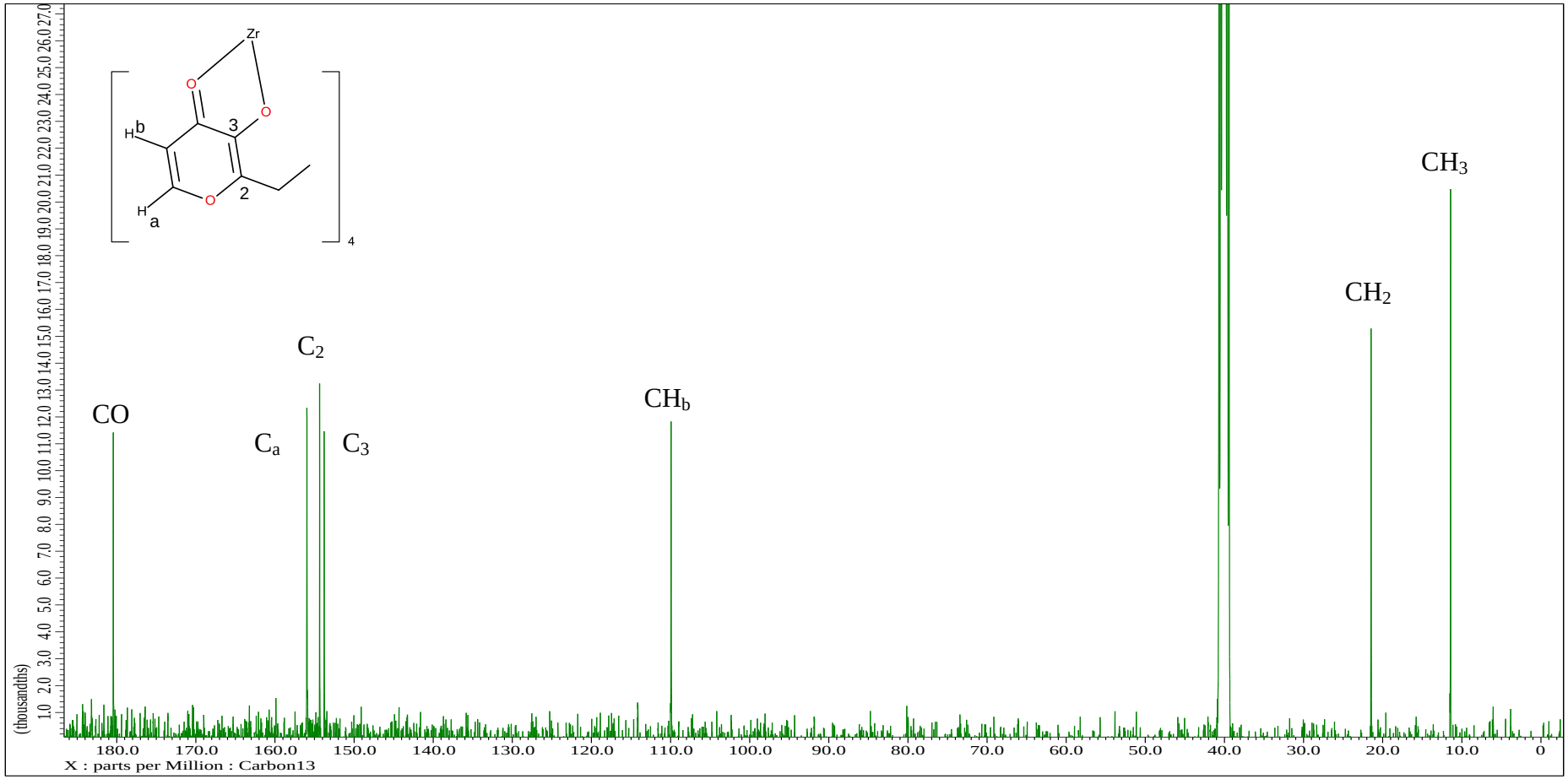

Figure 2.18: ^{13}C NMR of Zirconium Tetrakisethyl Maltol in DMSO-*d6*

2.7.4 ^{1}H & ^{13}C NMR of Deferiprone and Zirconium Tetrakis Deferiprone

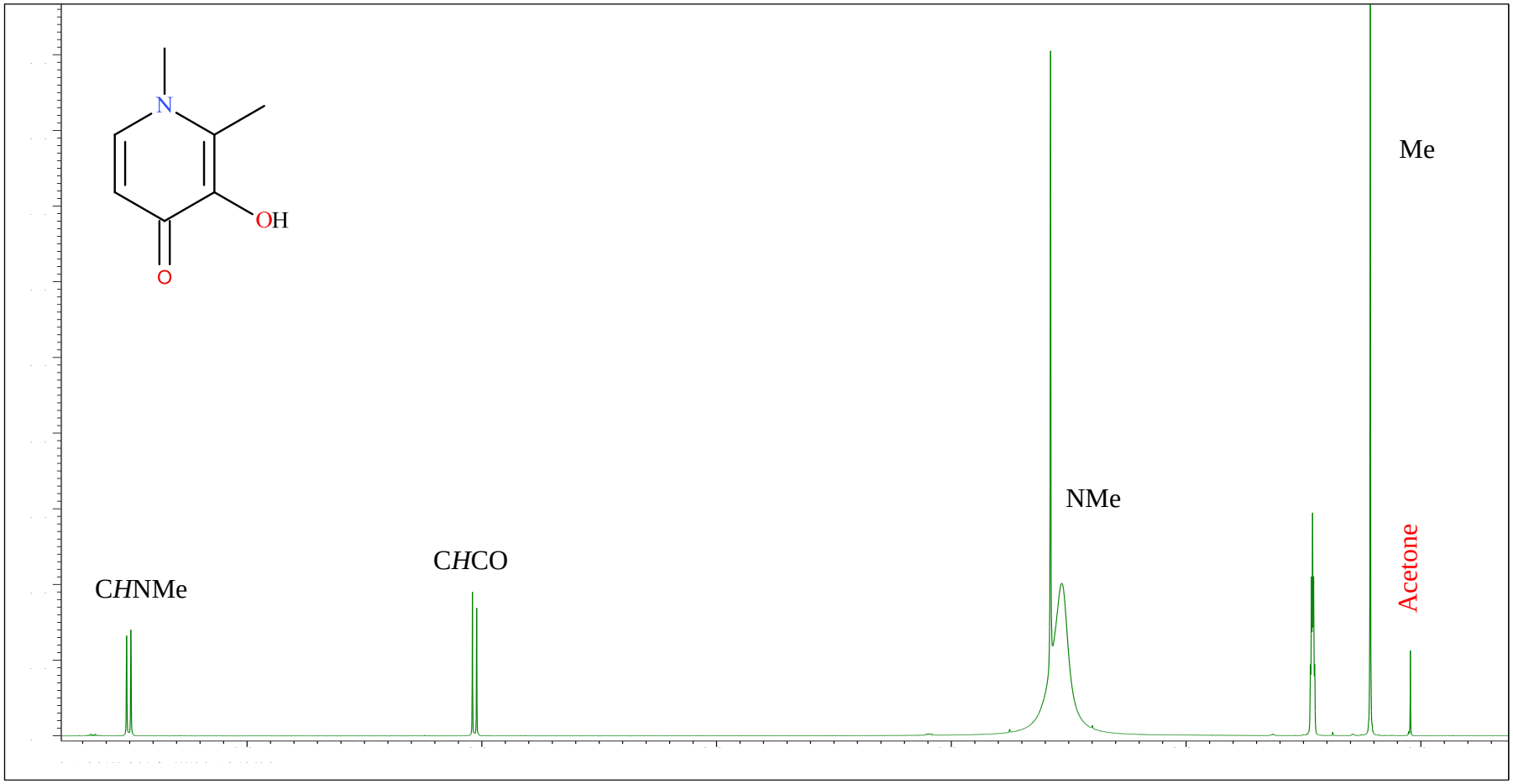

Figure 2.19: ^{1}H NMR of Deferiprone in DMSO-*d6*

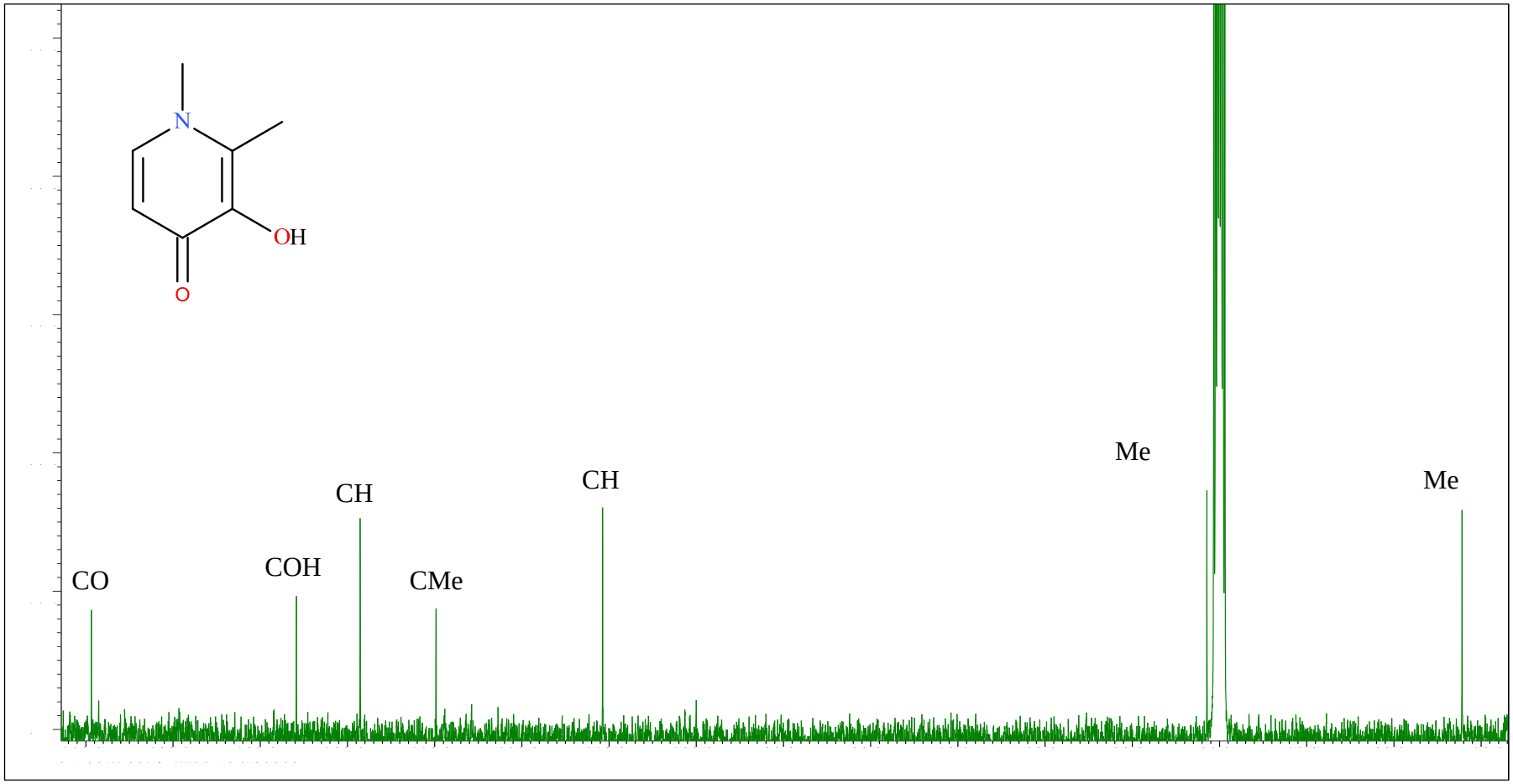

Figure 2.20: ^{13}C NMR of Deferiprone in DMSO-*d6*

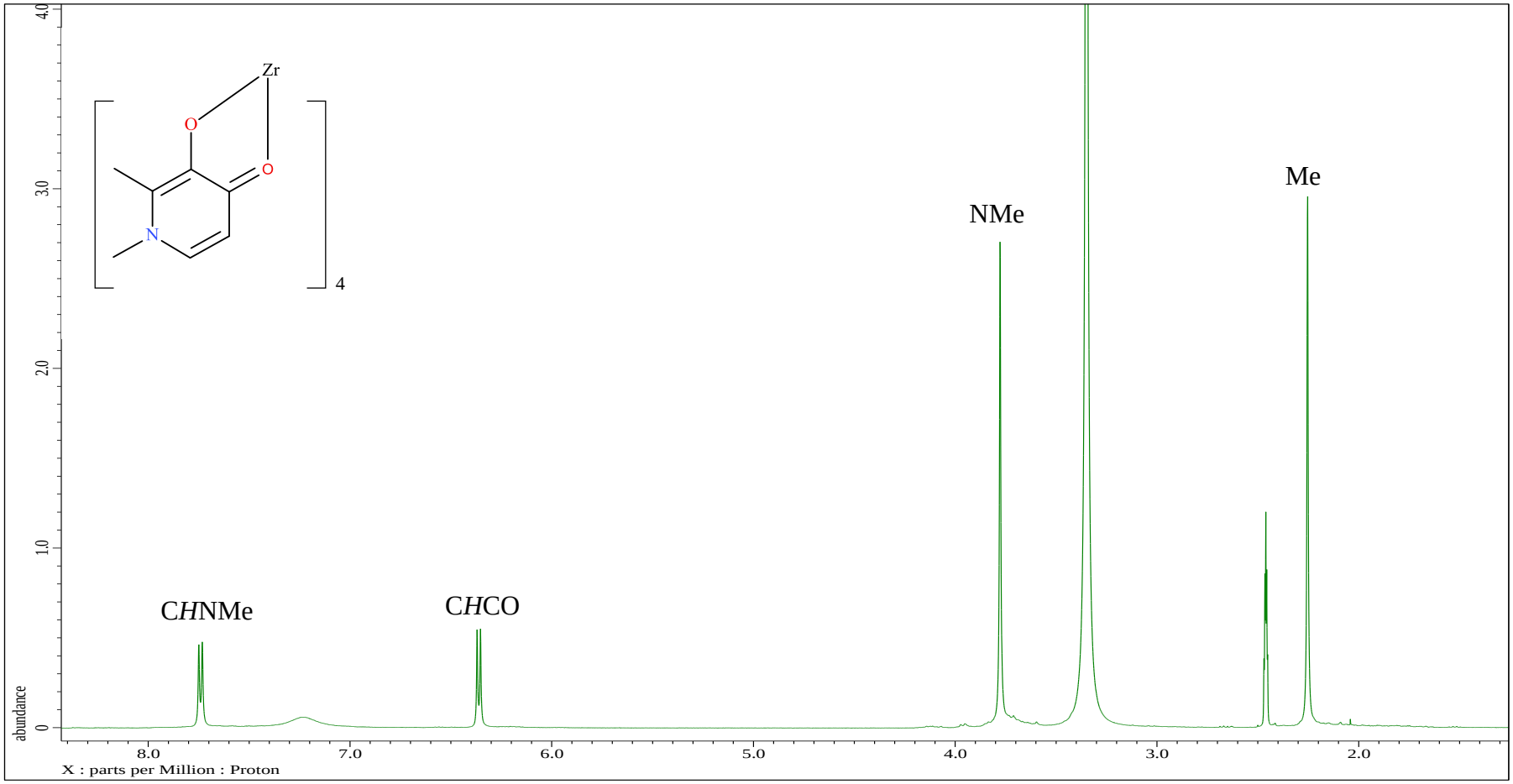

Figure 2.21: ^{1}H NMR of Zirconium Tetrakisdeferiprone in DMSO-*d6*

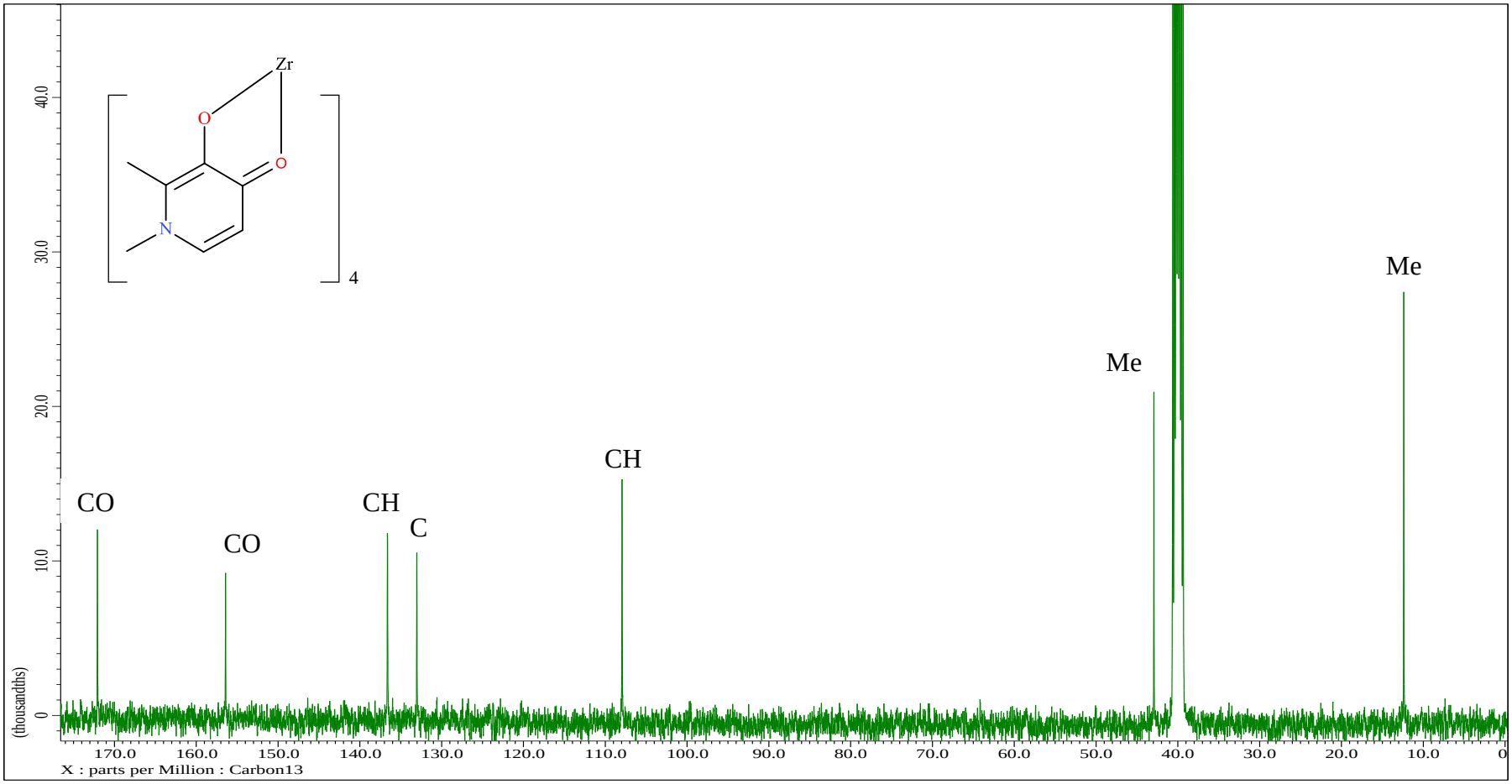

Figure 2.22: ^{13}C NMR of Zirconium Tetrakisdeferiprone in DMSO-*d6*

2.8 Results and Discussion

For NMR sample preparation all compounds were dissolved in d^6-DMSO. All NMR spectra have been referenced to a d^6-DMSO NMR residual proton peak at 2.46 ppm and NMR carbon peak at 40.00 unless stated otherwise.

2.8.1 Oxine

The NMR results were in agreement with previously published findings.[152] This paper reports the findings of proton nuclear magnetic resonance studies of 8-quinolinol and several of its metal complexes. However the paper is over 40 years old and it reports the shifts relative to DMSO. In the cases of the spectra reported in this thesis the NMR spectrometer has assigned the centre of the DMSO quintet to 2.46, hence to correct the values and compare the results reported from the paper to the recent experimental findings 2.46 needs to be added to all NMR values as illustrated in the table below.

	Baker *et al*	Baker (+2.46)	Current Results
2-H	6.27	8.73	8.78
3-H	4.95	7.41	7.47
4-H	5.71	8.17	8.26
5-H	4.82	7.28	7.34
6-H	4.87	7.33	7.40
7-H	4.58	7.04	7.06

Table 2.8

The assignment of the peaks is as follows:

δ_H(400 MHz, d^6-DMSO), 9.81 (1 H, br s, OH), 8.78 (1 H, d, $J_{2,3}$ 3.7 Hz, 2-H), 8.26 (1 H, d, $J_{3,4}$ 8.3 Hz, 4-H), 7.47 (1 H, dd, $J_{2,3}$ 4.1 Hz , $J_{3,4}$ 8.3 Hz, 3-H), 7.40 (1 H, dd, $J_{5,6}$ 7.8 Hz, $J_{6,7}$ 7.4 Hz, 6-H) 7.34 (1 H, d, $J_{5,6}$ 7.8 Hz, 5-H), 7.06 (1 H, d, $J_{6,7}$ 7.4 Hz, 7-H)

To assign the ^{13}C peaks of the analysed oxine, previously published work by J.K. Howie *et al*[153] was utilized. The published work shows the DMSO peak assigned as 40.018 which is in agreement with this research assigning the peak as 40.00.

δ_c(100 MHz, d^6-DMSO) 153.86 (C8), 148.66 (C2), 139.02 (C9), 136.58 (C4), 129.33 (C10), 128.04 (C6), 122.35 (C3), 118.25 (C5), 111.83 (C7)

2.8.2 Zirconium Tetrakisoxine

The method used to synthesise the compound was adapted from supplementary data provided from the previously published work by Kathirgamanathan *et al*.[134] The paper claims to report the discovery of two new phases of zirconium tetrakis 8-hydroxyquinolinate (reported in this thesis as zirconium tetrakisoxine). The supplementary data provided gives NMR spectra for both an alpha and beta form of the zirconium tetrakisoxine complex.[134] However from this supplementary data it is not possible to identify a difference between the alpha and beta forms. The supplementary data provided by Kathirgamanathan *et al*[134] only shows the proton chemical shifts for the alpha form of the complex and the carbon chemical shifts for the beta form of the complex. The proton NMR chemical shift data and allocation of peaks to the complex are reported below and is closely related to the supplementary data reported by Kathirgamanathan [134] regarding the alpha form of the complex.

δ_H(400 MHz, d^6-DMSO), 8.64 (1 H, b s, 2-H), 8.19 (1 H, d, $J_{3,4}$ 8.3 Hz, 4-H), 7.37-7.30 (2 H, m, 5-H and 6-H), 7.06 (1 H, d, $J_{3,4}$ 8.2 Hz, 3-H), 6.73 (1 H, d, $J_{6,7}$ 7.3 Hz, 7-H)

The carbon NMR chemical shift data and allocation of peaks to the complex is reported below and is effectively identical to the supplementary data reported by Kathirgamanathan [134] in regards to the beta form of the complex.

δ_c(100 MHz, d^6-DMSO) 162.82 (C8), 145.88 (C2), 141.73 (C9), 138.37 (C4), 129.90 (C10), 129.61 (C6), 122.17 (C3), 114.15 (C5), 112.37 (C7)

For NMR sample preparation, tropolone and zirconium tetrakistropolone were dissolved in pure d^6-DMSO. During the ^{1}H analysis of the compounds the NMR spectrometer assigned the centre of the DMSO quintet to 2.462.

2.8.3 Tropolone

The ^{1}H and ^{13}C spectra of tropolone illustrate the protons as expected for the complex. The ^{1}H allocation of peaks for tropolone is as follows:

δ_H(400 MHz, d^6-DMSO), 7.41 (2H, dd, J 9.7, 11.0 Hz, H3 & 5), 7.22 (2 H, d, $J_{2,3}$ $J_{5,6}$ 11.0 Hz, H2 & 6), 7.04 (1 H, t, J 9.7 Hz, H4).

The ^{13}C allocation of peaks for tropolone is as follows; (100 MHz, d^6-DMSO) 172.27 (C1 &C7), 137.79 (C2 & C6), 128.41 (C4), 124.90 (C3 & C5).

2.8.4 Zirconium Tetrakistropolone

The ^{1}H and ^{13}C spectra of zirconium tetrakistropolone illustrate the protons as expected for the complex. The ^{1}H assignment of peaks for zirconium tetrakistropolone is as follows:

δ_H (400 MHz, d^6-DMSO), 8.31 (0.125H, s, $CHCl_3$), 7.63 (2H, dd, J 9.6 Hz, 11.0, H3 & 5), 7.23 (2 H, d, $J_{2,3}$ $J_{5,6}$ 11.0 Hz, H2 & 6), 7.17 (1 H, t, J 9.6 Hz, H4).

The ^{13}C assignment of peaks for tropolone is as follows: δ_c (100 MHz, d^6-DMSO) 181.70 (C1 &C7), 140.29 (C2 & C6), 128.26 (C4), 125.03 (C3 & C5).

2.8.5 Ethyl Maltol

The ^{1}H spectrum of ethyl maltol illustrates the protons as expected for the complex. The ^{1}H assignment of peaks for ethyl maltol are as follows: δ_H (400 MHz, d^6-DMSO), 8.83 (1 H, br s, OH), 8.06 (1H, d, $J_{a, b}$ 5.5 Hz, CHa), 6.34 (1 H, d, $J_{a, b}$ 5.5 Hz, CHb), 2.63 (2 H, q, J 7.3 Hz, CH_2), 1.09 (3 H, t, J 7.8 Hz, CH_3)

The ^{13}C assignment of peaks for ethyl maltol is as follows: (100 MHz, d^6-DMSO) 173.26 (CO), 155.25 (CHa), 153.79 (C2), 142.74 (C3), 113.95 (CHb), 21.45 (CH_2), 11.39 (CH_3)

2.8.6 Zirconium Dichlorobisethyl Maltol

Published research on the synthesis of a new zirconium catalyst for ethylene polymerization[138,154] reports that depending of the synthesis method they have found four isomers of the zirconium dichlorobisethyl maltol complex and are as follows;

1H-NMR (300 MHz, DMSO-d6): 8.56ppm (d, 2Ha, JHH 5 Hz, Ha - isomer A), 8.51 (d, 2Ha, JHH 5 Hz, Ha - isomer B), 8.42 (d, 2Ha, JHH 5 Hz, Ha – isomer C), 8.36 (d, 2Ha, JHH 5 Hz, Ha – isomer D), 6.81 (d, 2Hb, JHH 5.1 Hz, Hb - isomer B), 6.76 (d, 2Hb, JHH 5.1 Hz, Hb - isomer A), 6.72 (d, 2Hb, JHH 5.1 Hz, Hb - isomer D), 6.63 (d, 2Hb, JHH 5.1 Hz, Hb - isomer C); 2.68 (q, 4H, JHH 6 Hz, CH_2), 2.61 (q, 4H, JHH 6 Hz, CH_2); 1.08 (t, 6H, JHH 6 Hz, CH_3), 1.04 (t, 6H, JHH 6 Hz, CH_3).

Experimental results are similar to the published research that relates to the third synthesis method[138]; The ^{1}H assignment of peaks for dichlorobisethyl maltol are as follows; δ_H (400 MHz, d^6-DMSO), 8.46 (1H, d, $J_{a,b}$ 5 Hz, CHa), 6.79 (1 H, d, $J_{a,b}$ 5 Hz, CHb), 3.38 (2 H, q, J 7.3 Hz, CH_2), 1.04 (3 H, t, J 6.9 Hz, CH_3).

Residual hexane from the synthesis of the compound has resulted in the following peaks; δ_H (400 MHz, d^6-DMSO), 1.21 (6 H, m, CH_3), 0.80 (8 H t, CH_2).

A weak isomer signal is assigned to,(2.61 q, 4H, JHH 6, CH_2).

Previous published research on the synthesis of a new zirconium catalyst for ethylene polymerization[138,154] the ^{13}C assignment of peaks for ethyl maltol are as follows: 13C-NMR (100 MHz, DMSO-d6): 180.97 (Cc CO, isomer C), 180.19 (Cc CO, isomer B),179.91 (Cc CO, isomer D), 158.06(Ca), 157.08 (Ca); 156.10 (Cd), 155.22 (Cd); 153.65 (Ce), 153.26 (Ce); 110.16 ppm (Cb), 109.88 (Cb); 21.77 (CH_2), 21.63 (CH_2), 21.49 (CH_2); 11.66 (CH_3).

Experimental results and the ^{13}C assignment of peaks for zirconium dichlorobis ethyl maltol are as follows: (100 MHz, d^6-DMSO) 179.78 (CO), 157.93 (CHa), 155.91 (C2), 152.55 (C3), 109.98 (CHb), 21.58 (CH_2), 11.49 (CH_3).

2.8.7 Zirconium Tetrakisethyl maltol

The ^{1}H spectrum of zirconium tetrakisethyl maltol illustrates the protons as expected for the complex. The NMR spectra of the free ligand displays a resonance relating to the hydroxyl group ligand which is absent from the NMR spectra of the zirconium tetrakisethyl maltol complex. This indicates that there has been deprotonation of the free ligand because of metal insertion which was expected. Complexing of the ligand to Zr has also resulted in a shift of the Ha and Hb protons to a higher chemical shift.

The ^{1}H assignment of peaks for zirconium tetrakisethyl maltol is as follows: δ_H (400 MHz, d^6-DMSO), 8.28 (1H, d, $J_{a,b}$ 5.2 Hz, Ha), 6.68 (1 H, d, $J_{a,b}$ 4.8 Hz, Hb), 2.54 (2 H, q, J 7.3 Hz, CH_2), 0.95 (3 H, t, J 7.6 Hz, (CH_3)

The ^{13}C assignment of peaks for zirconium tetrakisethyl maltol is as follows: δ_c(100 MHz, d^6-DMSO), 180.28 (CO), 155.95 (Ca), 154.34 (C2), 153.77 (C3), 109.92 (Cb), 21.44 (CH_2), 11.40, CH_3)

2.8.9 Deferiprone

For NMR sample preparation, deferiprone was dissolved in pure d^6-DMSO. During the ^1H analysis of deferiprone the NMR spectrometer assigned the centre of the DMSO quintet to 2.462. The exact splitting patterns are not observed because the un-equivalent protons are very similar and the NMR spectrometer is unable to differentiate them clearly from each other. The NMR spectra of deferiprone do not show a resonance relating to the hydroxyl group. It is presumed that this is obscured by the other peaks in the NMR spectra. NMR prediction software was utilised (Copyright: Luc Patiny - Ecole Polytechnique Fédérale de Lausanne) to predict possible ^1H assignments of the deferiprone complexes. These are as follows; 7.63 (1 H), 5.65 (1 H), 3.98 (3 H), 2.07 (3 H). This information was utilised to assist in the assignment of the ^1H peaks the following obtained results are within close agreement with previously published findings[85].

The ^1H allocation of peaks for deferiprone is as follows: δ_H (400 MHz, d^6-DMSO), 7.78 (1 H, d, *J* 6.8 C*H*NMe), 6.40 (1 H, *J 6.8* C*H*CO), 3.82 (3 H, s, NMe), 2.29 (3 H, s, Me)

The ^{13}C allocation of peaks for deferiprone is as follows: (100 MHz, d^6-DMSO) 172.06 (CO), 156.40 (CO), 136.60 (CH), 133.01 (C), 107.92 (CH), 42.91 (Me), 12.36 (Me).

2.8.10 Zirconium Tetrakisdeferiprone

The H^1 and ^{13}C spectra of zirconium tetrakisdeferiprone illustrate the protons and carbons as expected for the complex.

The ^1H allocation of peaks for zirconium tetrakisdeferiprone is as follows: δ_H(400 MHz, d^6-DMSO), 7.94 (1 H, br s, C*H*NMe), 6.79 (1 H, br s, C*H*CO), 3.86 (3 H, s, NMe), 2.37 (3 H, s, Me)

The ^{13}C allocation of peaks for zirconium tetrakisdeferiprone is as follows: δ_c(100 MHz, d^6-DMSO) 163.82(CO), 144.40 (CO), 138.77 (CH), 136.82 (C), 110.76 (CH), 43.10(Me), 12.77 (Me)

2.9 Results and Discussion

Both the ^{1}H and ^{13}C NMR spectra of the oxine ligand and the zirconium tetrakisoxine complex are in agreement with previously published work.[134,152] This confirms that the ligand used in the synthesis is as expected and the complex synthesised is zirconium tetrakisoxine. There is a notable difference when comparing the proton NMR spectra of the free oxine ligand (Figure 2.1) against the metal complex, (Figure 2.3). The broad singlet representing the H bound to O has disappeared in the spectrum of the complex indicating deprotonation and binding of the ligand to the Zr metal. The broad singlet in the spectrum of the complex is possible due to the result of an asymmetric isomer being present that is still undergoing fairly rapid interconversion of the oxine ligand sites. This is in agreement with work undertaken by Green *et al* relating to the molecular structure of indium tris oxine.[155]

The exchange of free and coordinated oxine ligands is fairly slow compared to the NMR time scale. It should be further noted that not all of the rings are equivalent so there must be a fluxional process at work.

The 3D images shown in figure 2.5 below were produced by utilising previously published single crystal X-ray crystallographic studies data[3] and Jmol software, an open-source Java viewer for chemical structures in 3D.

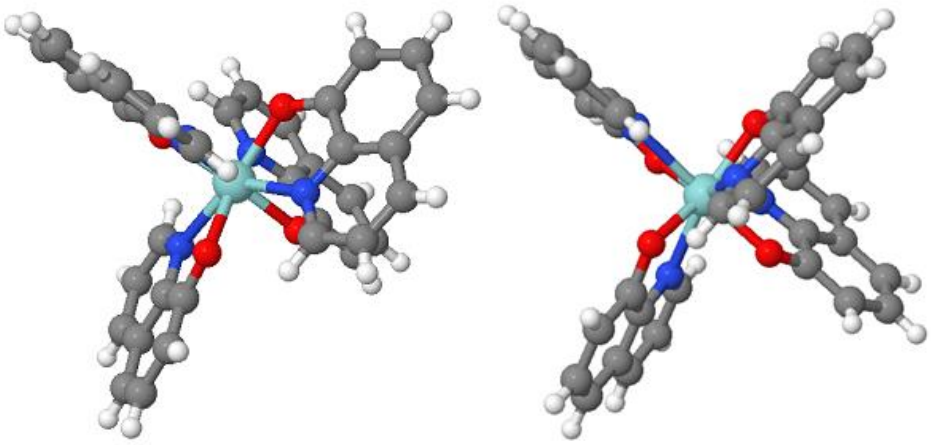

Figure 2.23: 3D Illustration of Zirconium Tetrakisoxine

The 3D images show that the zirconium tetrakisoxine complex has adopted the dodecahedral geometry. This is the most sterically efficient geometric arrangement for eight equivalent ligands and the complex is not symmetrical. The nitrogen atom on the oxine ligand in some instance is found to be close to a hydrogen atom found on an adjacent oxine ligand.

This is not always the case and can have an effect on the NMR spectra with their proton forming a hump on the spectra instead of a peak due to interactions with the nitrogen atom. It is possible for geometric isomerism[156] to come into effect. Ligand binding can occur at different sites through either the nitrogen or oxygen atom. Hence in some instances in the zirconium tetrakisoxine complex there will be pairs of ligands that have nitrogen atoms in close proximity to each other and in other instances there will be pairs of ligands which have a nitrogen and oxygen atom close proximity to each other.

The ^{1}H and ^{13}C NMR spectra of the tropolone ligand and the zirconium tetrakistropolone complex are in agreement with predicted spectra. There is a distinctive shift in the spectra when comparing the tropolone ligand against the zirconium tetrakistropolone complex indicating binding of the ligand to the metal ion. The peak seen in the spectrum of the zirconium tetrakistropolone complex at 8.27 ppm is identified as the proton in $CHCl_3$. This is in agreement with CHN analysis results suggesting a formula of $C_{28}H_{20}O_8Zr \cdot 0.55\ CHCl_3$.

Both the ^{1}H and ^{13}C NMR spectra of the ethyl maltol ligand and the zirconium dichlorobis ethyl maltol complex are in agreement with previously published work.[138] However there seems to be some confusion and the paper has allocated two peaks for DMSO when there should only be one. The use of Heteronuclear Multiple Quantum Coherence (HMQC) NMR allowed the allocation of the C2 and C3 peaks which was not possible with ^{13}C NMR alone. The resonance of the OH group at 8.79 disappears on the spectra of the dichlorobis and tetrakis complex indicating deprotonation of the ligand due to the insertion of Zr.

The ^{1}H and ^{13}C NMR spectra of the zirconium dichlorobis ethyl maltol indicate that isomers are present. These isomers vary in proportion in relation to the synthesis method used.

The ^{1}H NMR spectrum for the deferiprone ligand does not show a peak for the proton that is bound to an adjacent oxygen in the complex. This is because the peak is obscured under one of the other ^{1}H peaks in the spectrum. This is the proton that becomes deprotonated when chelation to the metal complex occurs. However there is a distinct shift in the peaks of the complex when compared to the free ligand indication ligand binding to the metal ion.

2.10 Conclusion

Four zirconium tetrakis complexes and zirconium dichlorobis ethyl maltol have been synthesised from a starting complex of zirconium tetrachloride. Zirconium tetrakisethyl maltol and zirconium tetrakisdeferiprone are novel complexes. NMR spectroscopy results are in agreement with predicted results.

The four tetrakis zirconium complexes are in the general form ZrL_4 where L is a bidentate uninegative ligand. Each of the following ligands; oxine, tropolone, ethyl maltol or deferiprone has been successfully chelated to the Zr ion. The ZrL_4 complexes are neutral and it is hypothesised that they will be able to diffuse into cells in a similar manner analogous to confirmed InL_3 complexes.[157]

CHAPTER 3

Fourier Transform Infrared, Raman Spectroscopy Characterisation and Physical Properties of Zirconium Compounds

3.1. Introduction

3.1.1 Fourier Transform Infrared Spectroscopy

Fourier Transform Infrared Spectroscopy (FTIR) has become the favoured method of infrared spectroscopy and is a chemically specific analytical technique. The technique is based on passing infrared (IR) radiation through a sample. An amount of this IR radiation is transmitted and another amount is absorbed.[150] A PC connected to the apparatus uses software algorithms to produce a spectrum which directly represents the molecular transmission and absorbance of the sample being analysed. The spectrum is comprised of two regions; between 4000-1000 cm^{-1} is known as the *functional group region*, and < 1000 cm^{-1} is known as the *fingerprint region*.[158] As functional groups have vibrational frequencies that are distinctive it is possible to identify these groups using this portion of the spectra. The fingerprint region consistently contains a very complicated series of absorptions. These are essentially due to all manner of bending vibrations within the molecule. This is unique to a sample and like a fingerprint no two unique molecular structures will produce the same infrared spectrum. Because of this infrared spectroscopy is useful for several types of analysis.[150]

FTIR is a non-destructive analytical technique that can be used to determine the consistency or quality of a sample, identify unknown materials and determine the quantity of components.[158] This is due to the fact that the size of the peak in the spectrum is directly proportional to the amount of material that is present. FTIR can be used to positively identify *via* qualitative analysis a large range of materials.[158]

FTIR was used during this research to firstly ensure that the spectra of the zirconium tetrakis complexes indicated a lack of an O-H group when compared to the spectra of the free ligands.

This would indicate a bonding between the ligand and metal ion as de-protonation must occur for the ligand to bind to the zirconium ion. Important functional groups of each of the compounds and ligands were identified using this technique. The fingerprint regions of the free ligand and zirconium tetrakis complexes were compared to ensure uniqueness between the free ligand and the complex.

3.1.2 Raman Spectroscopy

Raman spectroscopy is a technique that is based on inelastic scattering of monochromatic light which is provided in the majority of cases in the form of a laser source. Inelastic scattering occurs when the frequency of photons in monochromatic light is altered after interaction with a sample. It may be absorbed, reflected or scattered. It is the wavelength of the scatted radiation that is analysed. The change in wavelength of the scattered photon provides the structural and chemical information.

Raman spectroscopy was used alongside FTIR spectroscopy to analyse the ligands and complexes. This was undertaken to help confirm functional group assignment as the Raman spectrum and the FTIR spectrum for a given species resemble each other quite closely. Hence for a certain bond type the energy shift that is observed in a Raman spectrum should be identical to the energies seen in its infrared absorption bands. This is provided that the vibrational modes involved are active in both Raman scattering and in infrared absorption. During the process of Raman scattering a brief distortion of electrons that are distributed around a bond in a molecule occurs, directly followed by a discharge of radiation as the bond is restored to its normal state. When the molecule is distorted it is polarized for a brief amount of time, during which an induced dipole is established that disappears upon reemission. In contrast infrared absorption depends upon a vibrational mode of the molecule to have a change in dipole moment or a charge distribution related to it.

Raman spectroscopy has advantages over FTIR, such as water does not cause interference with the analysis of a species. Vibrations that may not be active in FTIR spectroscopy may be visible in Raman spectroscopy due to different selection properties. Because of this Raman spectroscopy complements FTIR spectroscopy.

3.2 Methods

3.2.1 FTIR Spectroscopy

Tables of equipment, equipment settings and reagents used throughout this chapter can be located in the appendix section of this thesis.

The FTIR spectra were obtained by using a Shimadzu IRAffinity-1 FTIR Spectrometer with a Specac Golden Gate single reflection diamond ATR accessory. These were interfaced with a Viglen E7600 personal computer (PC), with Microsoft Windows 7 Professional installed as the operating system. Software used to collate and interpret the FTIR data was in the form of the licensed program: Shimadzu I Resolution 1.5.

Before each of the precursor compounds, ligands and Zr complexes were analysed using the FTIR spectrometer, a background spectrum was taken which was then automatically subtracted from each of the spectra *via* the Shimadzu I Resolution 1.5 software. A small quantity of each of the samples was placed onto the diamond surface of the Specac Golden Gate single reflection diamond ATR accessory individually. The solid samples were pressed into direct contact with the diamond using the pressure tower and using only minimal force. The FTIR spectrometer was set using Shimadzu I Resolution 1.5 software to set a parameter of 8 foreground scans and 8 background scans, 16 scans in total. The software was pre-set to a resolution of 2 cm^{-1}, transmission mode T%. Preliminary scans of each sample were run to decide whether the sample was in acceptable contact with the Specac Golden Gate single reflection diamond ATR accessory. Once it was confirmed that all of the samples were in acceptable contact, the instrument was in each case set to collect the sample scans. None of the sample spectra underwent any smoothing. This was to ensure accurate spectra. Sensitivity was not adjusted with any of the spectra taken. The peak function of the Shimadzu I Resolution 1.5 software was used to identify any important peaks of the various spectra (known as a threshold function). The spectra were then saved using the Viglen E7600 PC to be interpreted further and reported in this thesis.

3.2.2 Raman Spectroscopy

The Raman spectra were obtained by utilising a Horiba LabRAM-HR Raman spectrometer. This was interfaced with a Dell Optiplex 780 personal computer (PC), with Microsoft XP Professional installed as the operating system. Software used to collate and interpret the Raman data was in the form of the licenced program by Horiba Scientific: LAB Spec 6 spectroscopic suite, version 6.1.197.

Calibration of the Raman spectrometer was undertaken before any of the experiments were conducted by utilising the silicon line at 520.6 cm^{-1}. The experiments utilised a laser operating at a wavelength of 784.15 nm. The Raman spectrometer has a Peltier cooled charge coupled device detector incorporated which operated at -70 ^{o}C. Edge filters of high quality were used to enable the analysis of the region closer to the excitation line. An x50 objective lens was used throughout the experiments in turn giving a beam of ~ 2 µm optically focused on the sample. The power of the laser directed at the sample was 20.1 mW with the 784.15 nm laser at full power. The power of the laser was measured by utilising an ASSY LaserCheck handheld power meter with an accuracy of ± 5%. A neutral density filter was used during the experiments which blocked 25 % of the lasers intensity at the sample. A diffraction grating of 600 gr/mm was used in turn achieving a spectral resolution of 2 cm^{-1}. The slit width during all experiments was 100 µm.

A minimum of 3 spectra were obtained during the FTIR and Raman experiments from different samples/parts of the sample to ensure reproducibility.

3.3 FTIR and Raman Specrtroscopy of Compounds

3.3.1 FTIR and Raman Spectroscopy of Zirconium Tetrachloride

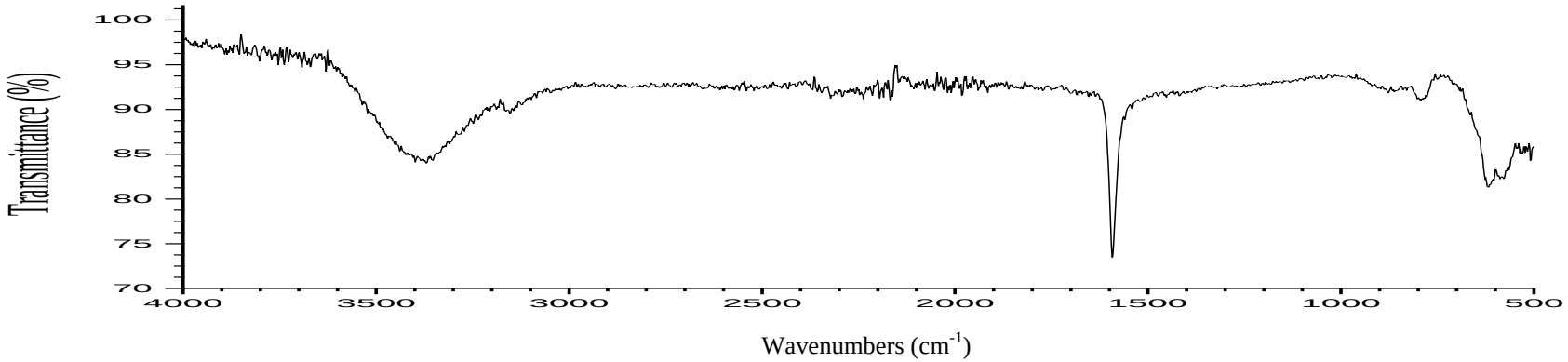

Figure 3.1: FTIR Spectrum of Zirconium Tetrachloride

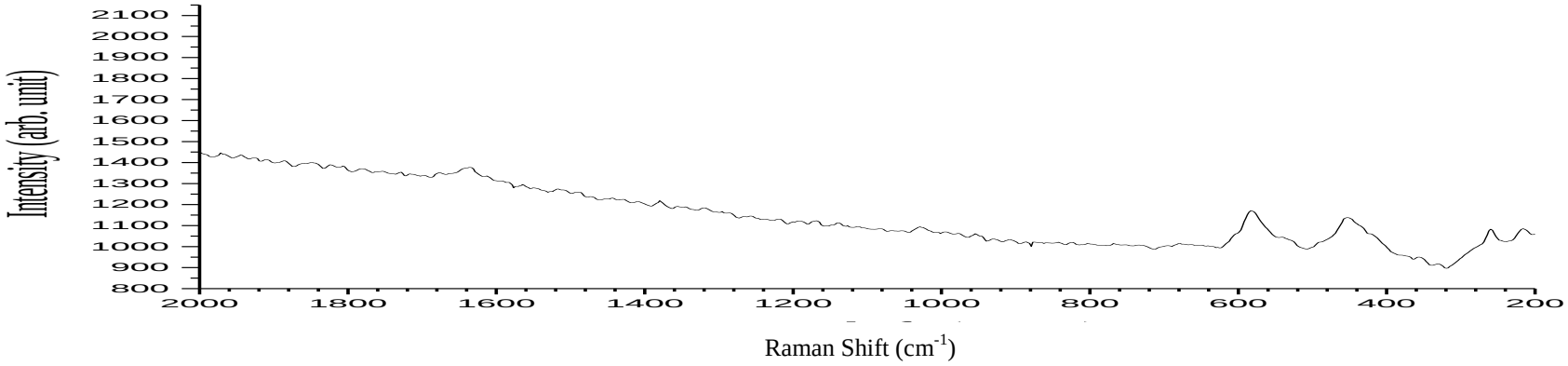

Figure 3.2: Raman Spectrum of Zirconium Tetrachloride

3.3.2 FTIR and Raman Spectroscopy of Zirconium Tetrakisoxalato

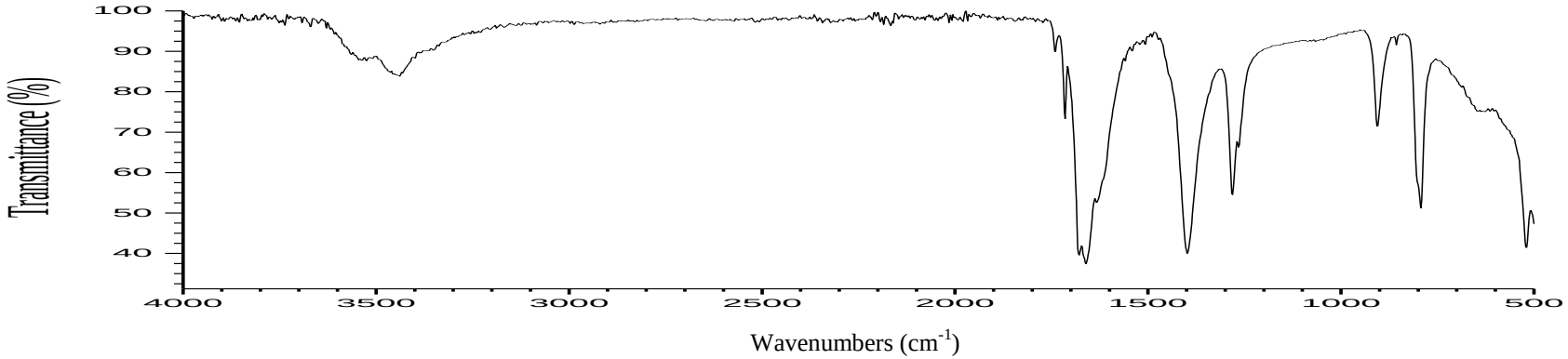

Figure 3.3: FTIR Spectrum of Zirconium Tetrakisoxalato

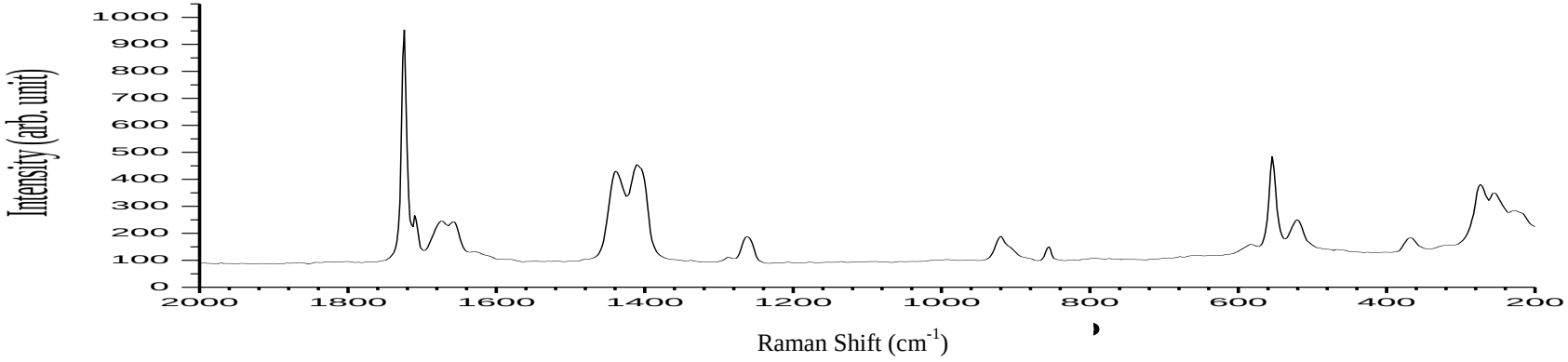

Figure 3.4: Raman Spectrum of Zirconium Tetrakisoxalato

3.3.3 FTIR and Raman Spectroscopy of Oxine and Zirconium Tetrakisoxine

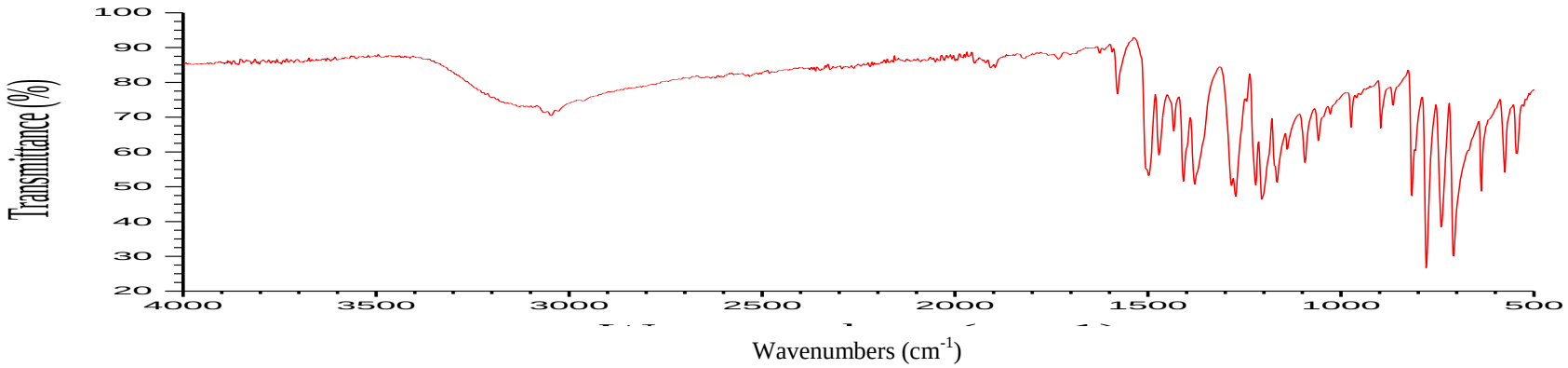

Figure 3.5: FTIR Spectrum of Oxine

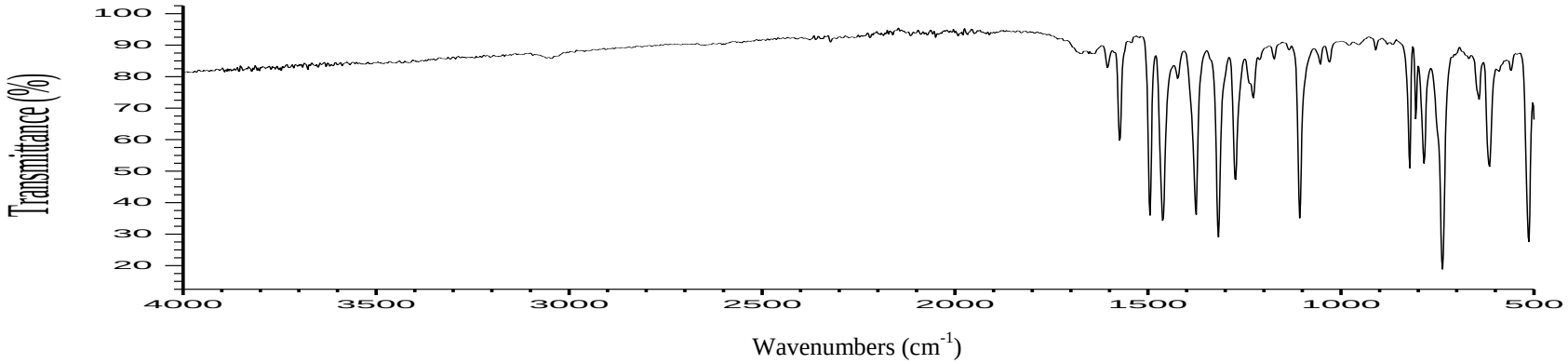

Figure 3.6: FTIR Spectrum of Zirconium Tetrakisoxine

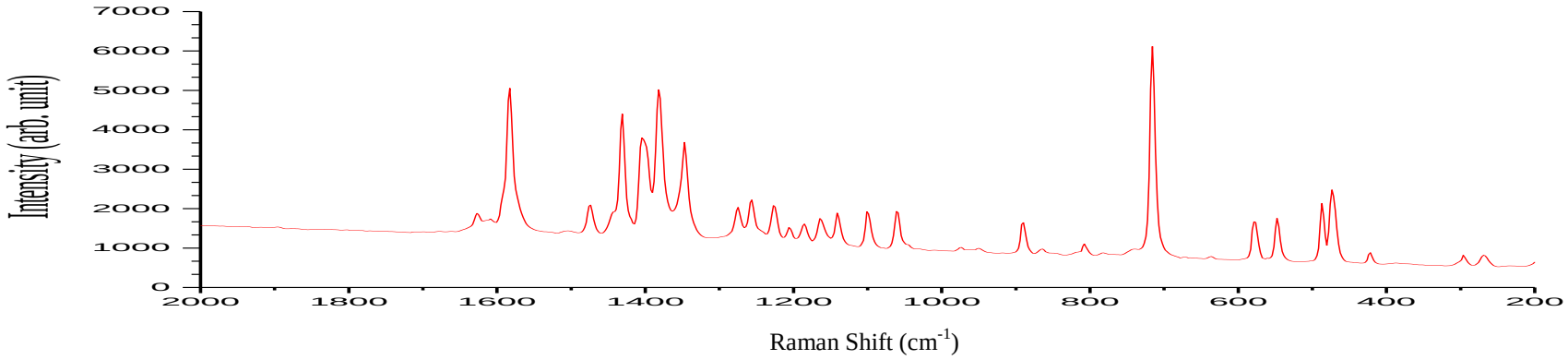

Figure 3.7: Raman Spectrum of Oxine

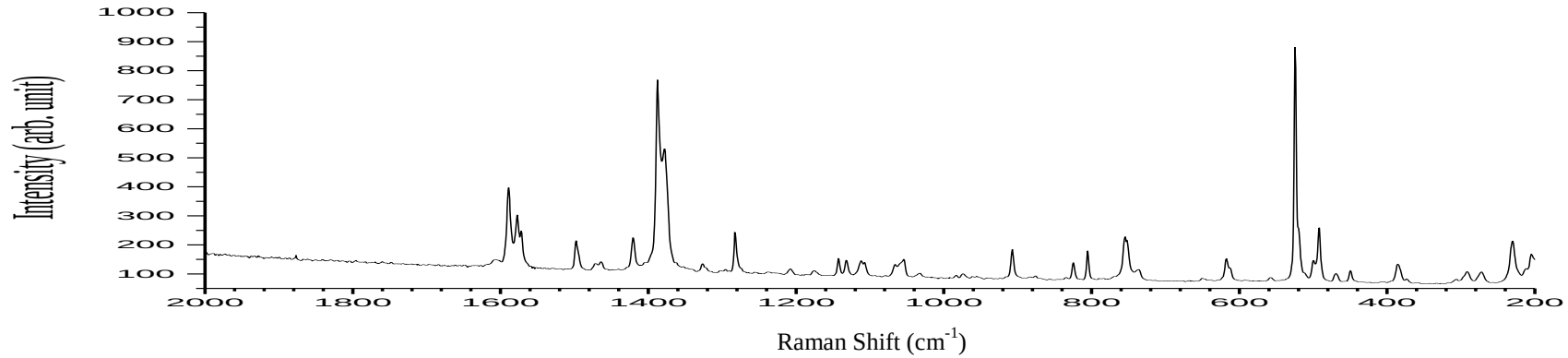

Figure 3.8: Raman Spectrum of Zirconium Tetrakisoxine

3.3.4 FTIR and Raman Spectroscopy of Tropolone and Zr Tetrakistropolone

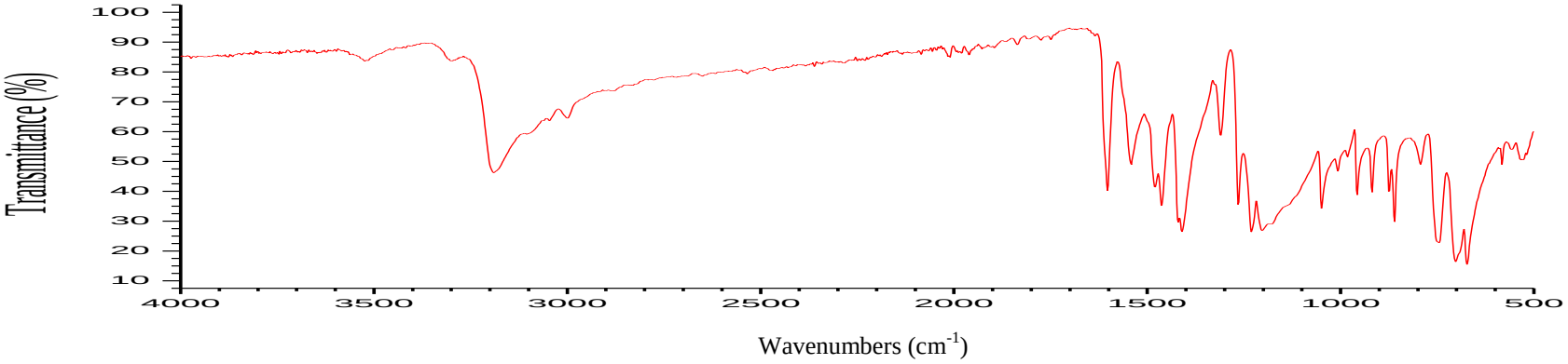

Figure 3.9: FTIR Spectrum of Tropolone

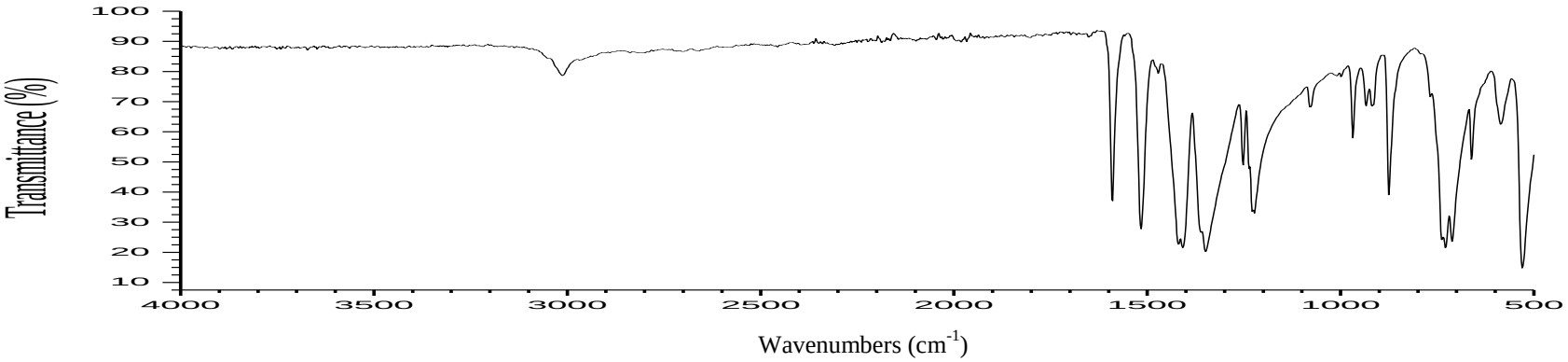

Figure 3.10: FTIR Spectrum of Zirconium Tetrakistropolone

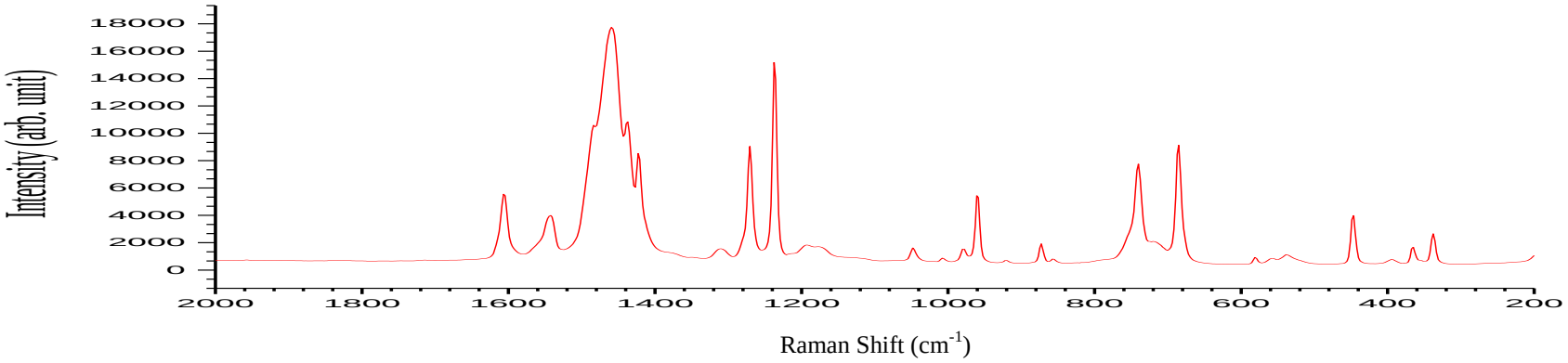

Figure 3.11: Raman Spectrum of Tropolone

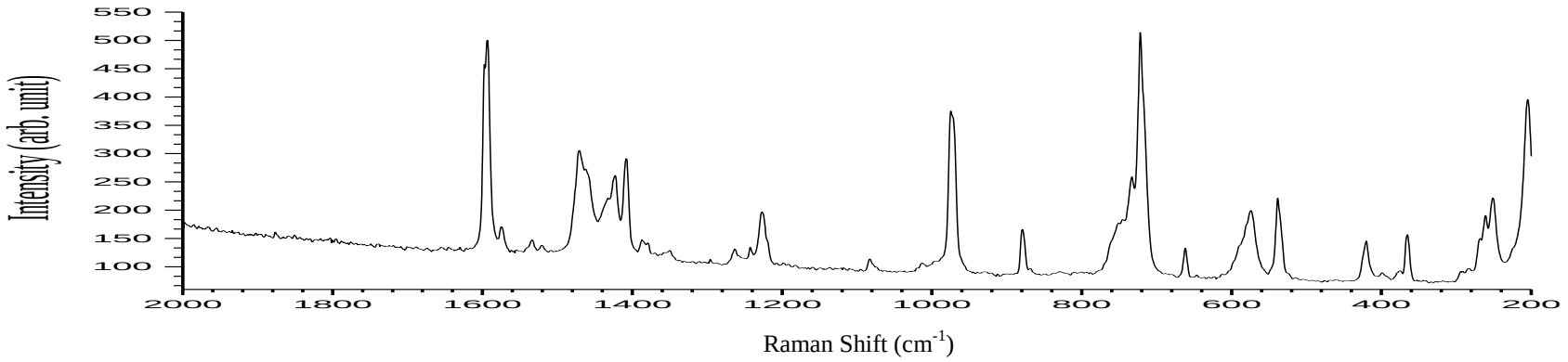

Figure 3.12: Raman Spectrum of Zirconium Tetrakistropolone

3.3.5 FTIR and Raman Spectroscopy of Ethyl Maltol and Zirconium Tetrakisethyl maltol

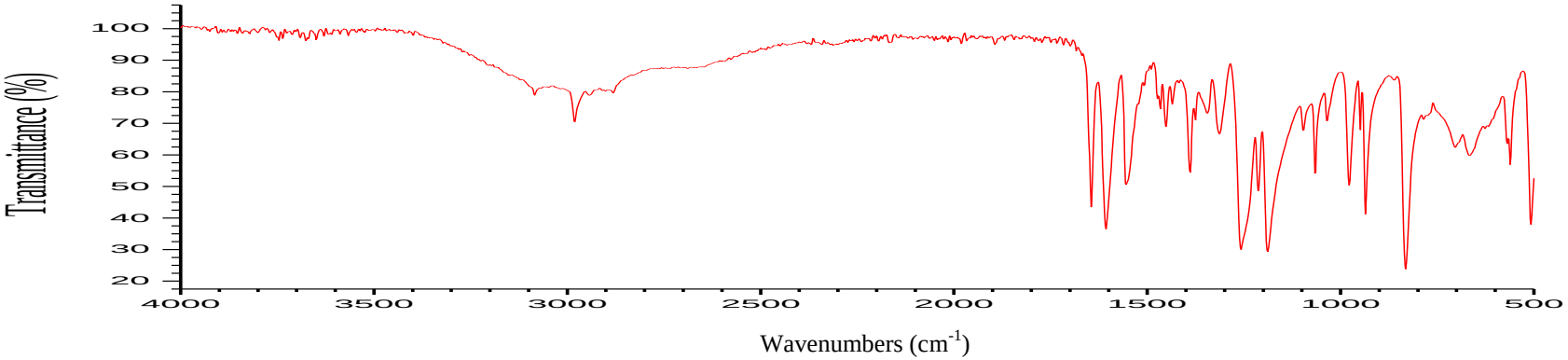

Figure 3.13: FTIR Spectrum of Ethyl Maltol

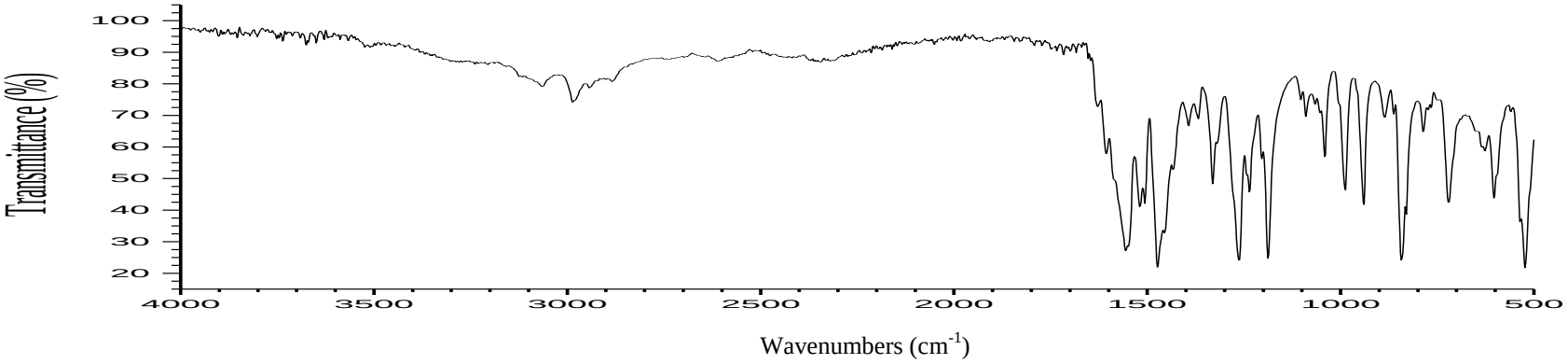

Figure 3.14: FTIR Spectrum of Zirconium Tetrkis Ethyl Maltol

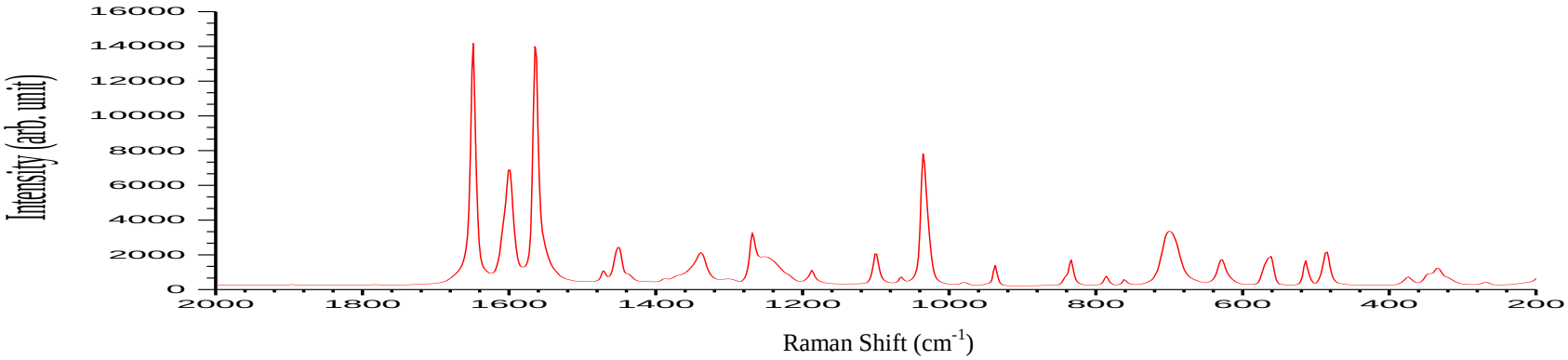

Figure 3.15: Raman Spectrum of Ethyl Maltol

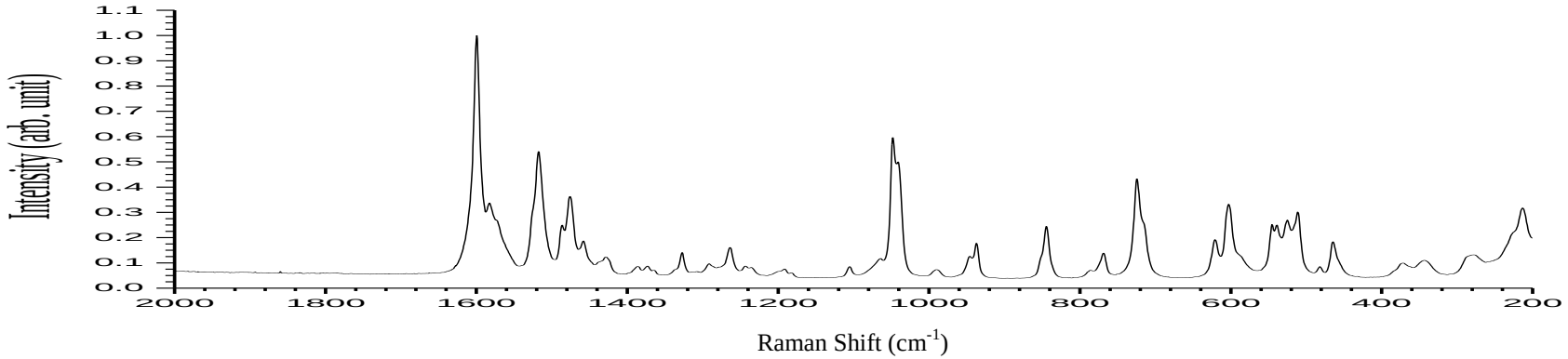

Figure 3.16: Raman Spectrum of Zirconium Tetrakisethyl maltol

3.3.6 FTIR and Raman Spectroscopy of Deferiprone and Zirconium Tetrakisdeferiprone

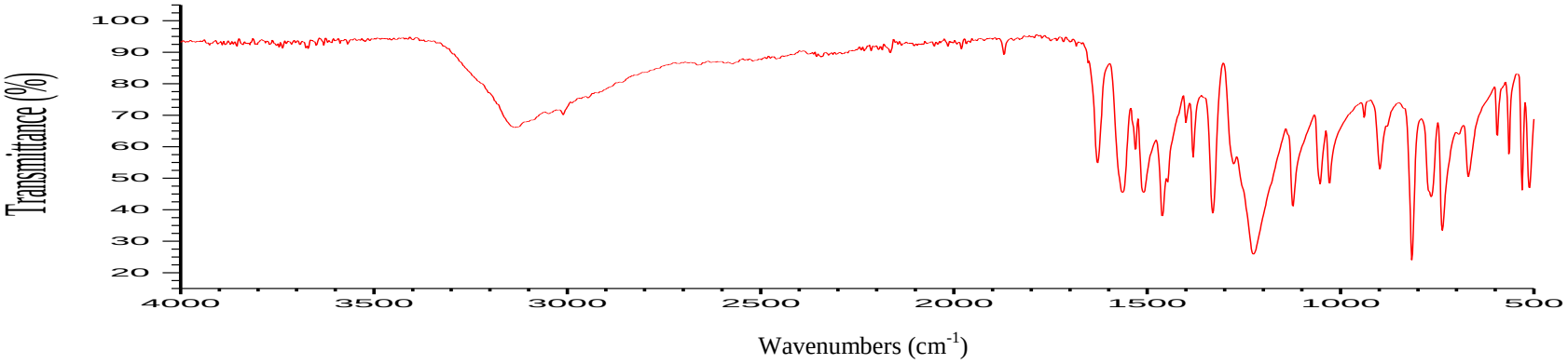

Figure 3.17: FTIR Spectrum of Deferprone

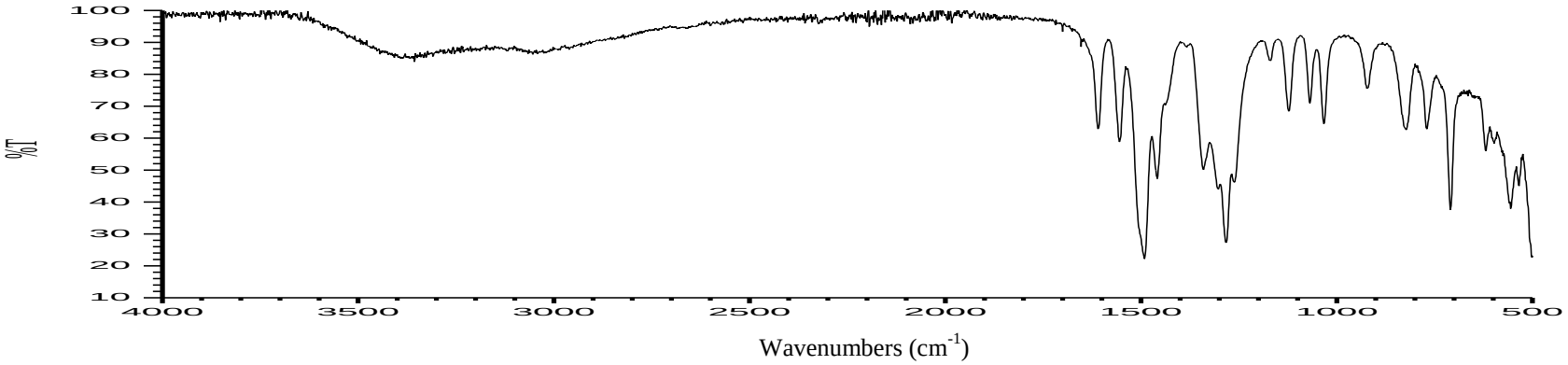

Figure 3.18: FTIR Spectrum of Zirconium Tetrakisdeferiprone

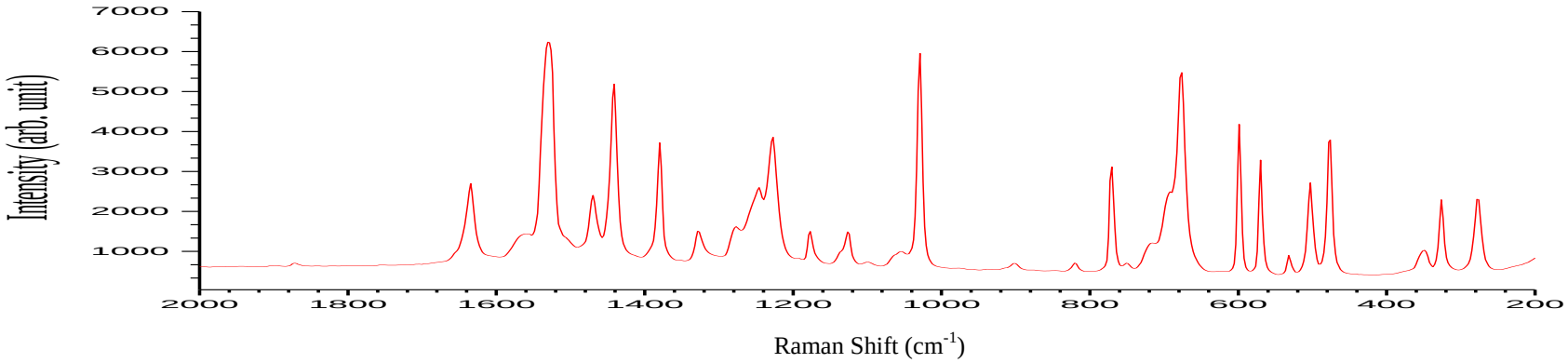

Figure 3.19: Raman Spectrum of Deferiprone

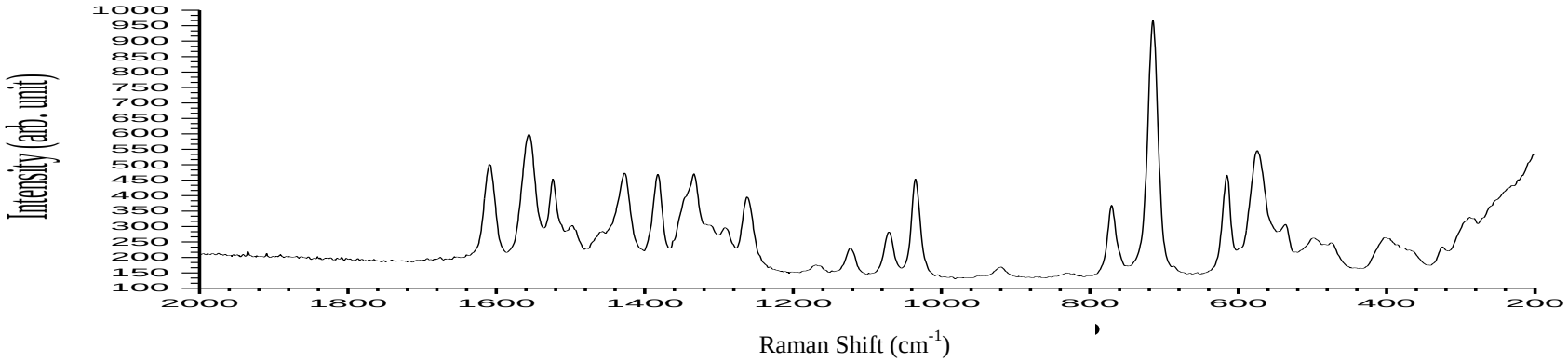

Figure 3.20: Raman Spectrum of Zirconium Tetrakisdeferiprone

3.4 Significant Wavenumbers from FTIR and Raman Analysis of compounds and Possible Functional Group Assignment

3.4.1 Assignment Key

The following abbreviations were used when analysing the spectral peaks of both the FTIR and Raman experiments:

vw:	very weak	s:	strong	sh:	shoulder
w:	weak	vs:	very strong	*ν*:	stretching
m:	medium	br	broad	δ:	bending
ω:	wagging	τ:	twisting	γ:	out of plane deformation

3.4.2 Zirconium Tetrachloride

IR υ_{max} (cm^{-1}): 3435 br (OH), 3393 br (OH), 1590 s (OH), 792 br, 617 m, 581 m (ZrCl), 506 w (ZrCl)

Raman υ_{max} (cm^{-1}): 1638 w, 1379 w, 1029 w, 583 w, 453 w (ZrCl), 259 w (ZrCl), 216 w (ZrCl)

3.4.3 Zirconium Tetrakisoxalato

IR υ_{max} (cm^{-1}): 3537 sh (OH), 3440 br (OH), 1730 s (C=O), 1709 sh, 1679 s (C=O), 1660 vs (C=O), 1399 s (C=O), 1280 m, 1267 sh, 905 m, 792 s (C-O), 519 s

Raman υ_{max} (cm^{-1}): 1724 s (C=O), 1710 w, 1674 w, 1439 m (C-O), 1410 m, 1262 w, 920 w *ν*(C-C), 855 w, 554 m (Zr-O), 520 w (OCO), 367 w, 273 w, 255 w

3.4.4 Oxine

IR υ_{max} (cm^{-1}): 3050 br (O-H), 1947 w, 1906 w, 1892 w, 1818 w, 1731 w, 1625 w $_{(C=N)}$, 1592 sh, 1579 m ($\upsilon_{C=C}$), 1496 s, 1473 s (C-C ring skeleton), 1431 m, 1409 s, 1380 s (CH ring skeleton), 1283 sh, 1272 s, 1241 sh, 1222 s, 1205 s, 1163 s, 1138 m, 1093 m (C-O), 1057 w (υ_{C-O}), 1028 w, 896 w, 864 w, 818 m (δ_{CH} out of plane), 777 vs (CH) , 738 s, 709 vs, 638 m, 572 m, 544 m (ring deformations).

Raman υ_{max} (cm^{-1}): 1626 sh ($\upsilon_{C=N}$), 1582 s($\upsilon_{C=C}$), 1473 m, 1431 s, 1404 s, 1381 s, 1347 m (υ_{C-C}), 1274 w, 1256 w, 1226 w, 1206 w, 1185 w, 1164 w, 1141 w, 1101 w(C-O), 1061 w (υ_{C-O}), 889 w, 864 w, 807 vw (δ_{CH} out of plane), 715 vs (ring breathing), 578 w, 547 w, 487 m, 473 m, 421 vw (ring deformations), 269 vw

3.4.5 Zirconium Tetrakisoxine

IR υ_{max} (cm^{-1}): 3045 w (υ_{CH}), 1604 m ($\upsilon_{C=N}$), 1573 s ($\upsilon_{C=C}$), 1495 vs, 1462 vs, 1423 m, 1378 vs, 1318 vs (υ_{C-C}), 1274 s, 1227 m, 1173 w, 1107 vs (δ_{CH} in plane), 1054 m (υ_{C-O}), 1030 m, 910 w, 822 s, 806 m (δ_{CH} out of plane), 785 s, 737 vs (ring breathing), 643 m, 616 s, 560 w, 514 vs (ring deformations).

Raman υ_{max} (cm^{-1}): 1606 w ($\upsilon_{C=N}$), 1589 m, 1578 m 1572 sh ($\upsilon_{C=C}$), 1498 m, 1463 w, 1421 m, 1388 vs, 1378 s, 1327 w (υ_{C-C}), 1284 m, 1209 w, 1175 w, 1143 w, 1137 w, 1112 w (δ_{CH} in plane), 1054 w (υ_{C-O}) , 1032 w, 907 m, 824 w, 805 m (δ_{CH} out of plane), 754 m, 736 w (ring breathing), 650 w, 617 m, 558 w, 524 vs (Zr-O), 500 sh, 492 m, 469 w, 449 w (ring deformations).

3.4.6 Tropolone

IR υ_{max} (cm^{-1}): 3521 w (OH) , 3298 w, 3188 br, 2998 sh (υ_{CH}), 2012 w, 1976 w, 1960 w, 1924 w, 1892 w, 1837 w, 1773 w, 1750 w, 1602 s ($\upsilon_{C=C}$ and $\upsilon_{C=O}$), 1541 m ($\upsilon_{C=O}$ and $\upsilon_{C=C}$), 1479 sh, 1463 s, 1421 sh, 1408 s, 1309 m($\upsilon_{C=C}$), 1263 m, 1231 s(υ_{C-O}), 1202 br, 1176 sh, 1051 m (υ_{C-C} and δ_{CH}), 1005 w, 983 vw, 957 m, 918 m (υ_{C-C}), 873 w, 860 m, 793 m, 747 m (υ_{C-C} and δ_{CH}), 702 sh (υ_{CH}), 673 vs (υ_{C-C}), 583 w, 557 w, 531 w, 519 sh

Raman υ_{max} (cm^{-1}): 1606 m ($\upsilon_{C=C}$ and $\upsilon_{C=O}$), 1542 w ($\upsilon_{C=O}$ and $\upsilon_{C=C}$), 1459 vs ($\upsilon_{C=O}$ and $\upsilon_{C=C}$), 1437 sh (OH and CH) , 1422 sh (CH and υ_{C-C}), 1309 vw, 1270 m , (OH and CH), 1237 s (CH), 1193 w (CH), 1048 vw (υ_{C-C}), 977 sh, 960 m (υ_{C-C}), 872 w (υ_{C-C}), 739 m (υ_{CH}), , 685 m, 446 w, 365 w, 337 w

3.4.7 Zirconium Tetrakistropolone

IR υ_{max} (cm^{-1}): 3013 m (υ_{CH}) , 1590 vs ($\upsilon_{C=C}$ and $\upsilon_{C=O}$), 1516 vs ($\upsilon_{C=O}$ and $\upsilon_{C=C}$), 1418 sh, 1408 vs, ($\upsilon_{C=O,}$ υ_{C-C} and δ_{CH}), 1349 vs ($\upsilon_{C=C}$), 1223 vs (υ_{C-O}), 1079 m (υ_{C-C} and δ_{CH}), 968 m, 934 m, 919 m (υ_{C-C}), 875 s, 728 vs (υ_{C-C} and δ_{CH}), 712 vs (υ_{CH}), 661 m (υ_{C-C}), 586 m, 530 vs (υ_{Zr-O})

Raman υ_{max} (cm^{-1}): 1593 vs ($\upsilon_{C=C}$ and $\upsilon_{C=O}$) , 1533 w, 1521 w ($\upsilon_{C=O}$ and $\upsilon_{C=C}$), 1471 m (δ_{CH}), 1422 m, 1408 m ($\upsilon_{C=O,}$ υ_{C-C} and δ_{CH}), 1390 w, 1350 w ($\upsilon_{C=C}$), 1227 m (υ_{C-O}), 1082 m (υ_{C-C} and δ_{CH}), 975 s (υ_{C-C}), 879 m (υ_{C-C} and δ_{CH}), 722 vs (υ_{CH}), 662 w (υ_{C-C}), 575m, 538 m (υ_{Zr-O})

3.4.8 Ethyl Maltol

IR υ_{max} (cm^{-1}): 3085 w, 2982 br (υ_{CH}), 2940 w (υ_{CH}), 2879 w, 2163 w, 1892 w, 1644 s, 1606 vs ($\upsilon_{C=O}$), 1557 s ($\upsilon_{C=C}$), 1505 sh, 1467 w, 1450 m, 1434 w (υ_{C-C}), 1389 m, 1376 sh, 1344 w, 1315 m, 1257 s, 1212 m, 1189 s, 1096 w, 1067 m, 1034 w, 976 m, 947 w, 935 s, 860 w, 831 vs, 783 sh, 702 br (γ ring), 667 br, 570 sh, 650 m, 509 s (δ ring)

Raman υ_{max} (cm^{-1}): 1648 s, 1598 m ($\upsilon_{C=O}$), 1564 s ($\upsilon_{C=O}$), 1451 w (υ_{C-C}), 1338 w (ω_{CH}) , 1268 w (τ_{CH}), 1101 w, 1035 m (υ_{C-O-C}), 937 w, 833 w, 700 w, 627 w, 560 w, 514 w, 484 w, 335 w

3.4.9 ***Zirconium Tetrakisethyl maltol***

IR υ_{max} (cm^{-1}): 3065 w, 2986 m (υ_{CH}), 2943 w (υ_{CH}), 2885 w, 1628 sh ($\upsilon_{C=O}$), 1606 sh ($\upsilon_{C=O}$), 1556 vs ($\upsilon_{C=C}$) , 1519 s, 1507 sh, 1473 vs, 1456 sh, 1433 sh (υ_{C-C}), 1393 m, 1368 m, 1331 s, 1262 vs, 1235 s, 1187 vs, 1102 w, 1087 w, 1069 w, 1050 sh, 1040 m, 990 m, 936 m, 885 w, 859 vw, 840 vs, 828 sh, 786 w, 771 m, 624 w, 602 m, 558 w, 522 vs s (δ ring)

Raman υ_{max} (cm^{-1}): 1599 vs ($\upsilon_{C=O}$), 1582 sh ($\upsilon_{C=O}$), 1518 s, 1476 m, 1428 w(υ_{C-C}), 1327 w (ω_{CH}), 1264 w (τ_{CH}), 1048 s (C-O-C), 938 w, 845 m, 769 w, 725 s, 621 w, 603 m, 546 m, 539 m ($_{Zr-O}$), 525 m, 511 m

3.4.10 Deferiprone

IR υ_{max} (cm^{-1}): 3134 br (OH), 3011 sh (υ_{CH} aromatic ring), 2163 vw, 2015 vw, 1979 vw, 1870 w, 1628 s ($\upsilon_{C=O}$), 1563 s, 1531 w ($\upsilon_{C=C}$ aromatic ring), 1508 m, 1460 s, 1444 sh ($\upsilon_{C=C}$ aromatic ring), 1402 w, 1380 m, 1331 s (C-N), 1208 sh, 1225 br (C-O), 1122 m, 1054 m, 1028 m, 938 w, 899 m, 876 sh, 815 vs, 767 m (υ_{CH}), , 738 s, 693 sh, 669 m, 593 m, 564 m, 531 s, 512 s

Raman υ_{max} (cm^{-1}): 1633 m ($\upsilon_{C=O}$), 1530 s ($\upsilon_{C=C}$ aromatic ring), 1470 m, 1380 m, 1329 w (C-N), 1245 sh, 1226 m (C-O), 1177 w, 1126 w, 1029 s, 901 vw, 821 vw, 771 m (υ_{CH}) , 676 s, 599 m, 531 w, 503 m, 476 m, 349 w, 326 w, 278 w

3.4.11 Zirconium Tetrakisdeferiprone

IR υ_{max} (cm^{-1}): 3500-2500 br, 1610 m ($\upsilon_{C=O}$), 1555 m ($\upsilon_{C=C}$ aromatic ring), 1491 s, 1458 m ($\upsilon_{C=C}$ aromatic ring), 1438 w, 1341 m, 1283 s (υ_{C-N}), 1261 m, 1169 w, 1123 m, 1069 m, 1034 m, 923 w, 823 m, 770 m, 710 s, 619 w, 556 m, 498 s

Raman υ_{max} (cm^{-1}): 1609 m ($\upsilon_{C=O}$), 1556 m, 1524 m ($\upsilon_{C=C}$), 1498 w, 1427 m, 1382 m 1334 m (υ_{C-N}), 1292 w, 1262 m (υ_{C-O}), 1169 w, 1123 w, 1071 m, 1035 m, 920 w, 771 m (υ_{CH}), 715 vs, 615 m, 574 m (Zr-O), 536 w, 499 m, 404 m, 325 m, 288 m

3.5 Discussion of FTIR and Raman Spectroscopy Results

3.5.1 Zirconium Tetrachloride

The FTIR spectrum shows broad peaks at 3435 cm^{-1} and 3393 cm^{-1} relating to an O-H group which is due to a small amout of moisture in the zirconium tetrachloride complex. The peak at 1590 cm^{-1} relates to an O-H bend. Zr to Cl bonding peaks are located in the fingerpring region of the spectra at 581 cm^{-1}, and 506 cm^{-1}. Published work by Taylor[159] reports Zr-Cl bonding peaks in the low frequency region of the IR spectra between 220 cm^{-1} and 415 cm^{-1} however the FTIR apparatus used during this work has a lower limit of 500 cm^{-1}. The Raman spectrum of zirconium tetrachloride shows peaks at 453 cm^{-1}, 259 cm^{-1} and 216 cm^{-1} which can all be attributed to bonding between the Zr and Cl of the complex. The allocation of these peaks was based on published work by Photiadis and Papatheodorou[160] investigating vibrational modes of zirconium tetrachloride.

3.5.2 Zirconium Tetrakisoxalato

The broad peak at 3537 cm^{-1} and 3440 cm^{-1} relates to an O-H group which is due to a small amout of moisture in the zirconium tetrakisoxalato complex. The values obtained for the zirconium tetrakisoxalate are in in agreement with those that have been previously described for the oxalate ligand in published work by Yan-Tuan Li and Cui-Wei Yan *et al.*[161] The peaks at 1730 cm^{-1}, 1679 cm^{-1}, 1660 cm^{-1} and 1399 cm^{-1} can all be attributed to C=O bonds in the zirconium tetrakisoxalato complex. The peak at 792 cm^{-1} can be attributed to a C-O bond in the complex. The Raman spectrum of the zirconium tetrakisoxalato complex shows a peaks at 1724 cm^{-1} which can be can be attributed to a C=O bond. A wavenumber of 1439 cm^{-1} may be asssigned to a ν(CO) stretching mode as reported by Frost[162] when investigating oxalates utilising Raman spectroscopy. The bands at 920 cm^{-1} may be attributed to a v(C-C) stretching mode. A symmetric OCO bending mode may be attributed to 520

3.5.3 Oxine and Zirconium Tetrakisoxine

Previously published papers report the FTIR spectroscopic findings of the both oxine and complexes of a similar nature such as aluminium tris oxine[163], metal complexes with oxine as a primary ligand and vitamin U as a secondary ligand[164] and vibrational spectra of some solid oxine metal complexes in correlation with their coordination bond length and type of metal ion.[165] The proposed assignment of wavenumbers to functional groups from the Raman analysis of the compounds was undertaken utilising standard correlation tables and work published by Wagner *et al* regarding vibrational spectra of Ga(III) complexes with oxine and clioquinol.[166]

FTIR analysis of oxine and the zirconium tetrakisoxine complex shows that the groups/structures which are to be expected are present. The OH group which is located at ~ 3045 cm^{-1} on the spectrum of oxine is not present in the spectrum of zirconium tetrakisoxine, due to deprotonation of the ligand at the O-H functional group region. Chelatation occurs *via* covalent linkage between the zirconium metal ion to the phenolic oxygen of the oxine ligand. The band at ~ 1625 cm^{-1}, assigned to the C=N group, has shifted slightly to 1604 cm^{-1} in the chelated complex.

Raman analysis of the oxine and zirconium tetrakisoxine complexes yielded similar results to the FTIR analysis of both the ligand and the complex. The band at located at 1626 cm^{-1} is assigned to C=N in the spectrum of oxine. In the spectrum of the zirconium tetrakisoxine complex this has shifted to a lower energy of 1606 cm^{-1}. The band located at 1582 cm^{-1} assigned to C=C has also shifted to a lower energy of 1573 cm^{-1} in oxine when compared to zirconium tetrakisoxine. There is also a notable shift to lower energies of the peak assigned to C-C in plane from 1347 cm^{-1} in oxine to 1327 cm^{-1} in the zirconium tetrakisoxine complex. The assigned bands have values that are in close agreement with the work reported by Wagner *et al*.[166] A band at 524 cm^{-1} can be tentatively assigned to Zr-O.

cm^{-1} and has been reported by Frost[162] in regards to oxalate complexes. A band at 554 cm^{-1} can be tentatively assigned to Zr-O.

3.5.4 Tropolone and Zirconium Tetrakistropolone

The FTIR values obtained for the tropolone ligand are in agreement with those previously described in published work by Yusaku Ikegami.[167] When comparing the spectra of both the tropolone ligand and the zirconium tetrakistropolone complex it is clear that the complex has a distinct lack of a broad peak found between ~ 3521 cm^{-1} and ~ 2998 cm^{-1} which is found in the spectrum of the tropolone ligand. This broad peak is due to hydrogen bonding which alters the electron cloud and in turn alters the resonance frequency of the O-H bond. As the complex does not have an O-H group that is hydrogen bonded the broad peak is distinctly reduced. The small peak relating to a O-H group is due to a small amout of moisture in the zirconium tetrakistropolone complex. The bands found at 2998 cm^{-1} and 3013 cm^{-1} can be atributed to C-H stretching vibrations of both the ligand and complex respectably. The C=O and C=C functional groups can be attributed to 1602 cm^{-1} and 1541 cm^{-1} for the ligand. These values are found to be at lower energies for the zirconium tetrakistropolone complex with wavenumbers of 1590 cm^{-1} and 1516 cm^{-1}. The band located at 1408 cm^{-1} may be attributed to a combination of C=O, C-C and C-H functional groups in the tropolone ligand and the tropolone complex.

Raman analysis of the tropolone and zirconium tetrakistropolone complexes yielded similar results to the FTIR analysis of both the ligand and the complex. Standard correlation tables and work published by Jianlin *et al*[168] were used in assigning the Raman spectrum to possible functional groups. When comparing the Raman spectra of the free tropolone ligand to the zirconium tetrakis complex it can be seen that there is a significant shift in frequencies of the C=O and C=C functional groups. Between the wavelength range of 1000 cm^{-1} to 600 cm^{-1} a number of bands were observed which relate to vibrational modes of the ring structure, C-C, C-H *etc*. These groups show a smaller shift between the spectra of the ligand and the complex as they do not bind with the Zr metal ion to form the complex. The band at 538 cm^{-1} is unique to the complex and it is proposed that this band is due to the Zr–O interaction of the complex. This band has been reported by Jianlin *et al* [168] to be the interaction of the O of tropolone and a metal ion such as lanthanum.

3.5.5 Ethyl Maltol and Zirconium Tetrakisethyl maltol

FTIR spectra were assigned utilising work by J Burgess *et al*[169], K Thompson *et al*[170], B. S. Parajon-Casta *et al* [171, 172] and C Wagner *et al*.[173] Comparison of the spectrum of the ligand against the complex shows the broad peak around ~ 3085 cm^{-1} becomes broadened out significantly in the spectrum of the zirconium tetrakisethyl maltol complex. As is the case with oxine and tropolone this peak is due to hydrogen bonding which alters the electron cloud and in turn alters the resonance frequency of the O-H bond. As the complex does not have an O-H group that is hydrogen bonded the broad peak is distinctly reduced. The small peak relating to a O-H group is due to a small amout of moisture in the zirconium tetrakisethyl maltol complex. The bands found in the region of 2982 & 2940 cm^{-1} in the spectrum of the ligand and at a slightly higher energies in the complex at 2986 & 2943 cm^{-1} can be atributed to C-H stretching vibrations. The band located at 1556 cm^{-1} and 1557 cm^{-1} resemble the C=C vibrations in the aromatic ring in both the complex and ligand. The band located at 1606 cm^{-1} resemble the C=O vibrations in both the complex and ligand. The band located at 509 cm^{-1} & 522 cm^{-1} in the spectra of the ligand and complex may be attributed to the ring structure of tropolone.

Raman analysis ethyl maltol and zirconium tetrakisethyl maltol yielded similar results to FTIR. Standard correlation tables, work published by Panicker *et al*[174] and authors work used to assign FTIR functional groups were employed in assigning the Raman spectra to possible functional groups. When comparing the Raman spectra of the free ethyl maltol ligand to the zirconium tetrakisethyl maltol complex it can be seen that there is a shift in frequencies of the C=O and C-C functional groups. The bands at 1035 cm^{-1} in the ligand and at 1048 cm^{-1} in the complex can be attributed to symmetric C-O-C vibrations. The CH_2 wagging mode can be attributed to 1338 cm^{-1} in the free ligand and at a lower energy in the complex at 1327 cm^{-1}. The CH_2 twisting mode can be attributed to 1268 cm^{-1} in the free ligand and at a slightly lower energy in the complex at 1264 cm^{-1}. The band at 539 cm^{-1} is unique to the complex and it is proposed that this band is due to the Zr–O interaction of the complex as is the case with the tropolone complex at 538 cm^{-1}.

3.5.6 Deferiprone and Zirconium Tetrakisdeferiprone

The values obtained for the deferiprone ligand are in agreement with those that have been previously described in published work by Carla Queiros *et al*[175] and M Mohammadpour *et al.*[176] When comparing the spectrum of the deferiprone ligand against the zirconium tetrakisdeferiprone complex it is clear that the complex has a distinct lack of a broad peak around ~ 3134 cm^{-1} which is found in the spectrum of the deferiprone ligand. As is the case with oxine and tropolone this peak is due to hydrogen bonding which alters the electron cloud and in turn alters the resonance frequency of the O-H bond. As the complex does not have an O-H group that is hydrogen bonded the broad peak is distinctly reduced. The broad peak seen on the spectum of the zirconium tetrakisdeferiprone complex between 3500 cm^{-1} - 2500 cm^{-1} is proposed to be related to the 12 waters of hydration incorporated into the complex. This is in agreement with the results of CHN anlaysis of the complex. The band found at 1628 cm^{-1} can be atributed to C=O stretching in the ligand and at a slightly lower energy of 1610 cm^{-1} in the complex. Bands at 1531 cm^{-1} / 1444 cm^{-1} in the ligand and at at higher energies of 1555 cm^{-1} / 1458 cm^{-1} in the complex can possibly be assigned to the C=C group in the aromatic ring structure of deferipropne.

Raman analysis of the deferiprone ligand and zirconium tetrakisdeferiprone complex yielded similar results to the FTIR. Standard correlation tables and work published by Šebsetík *et al*[177] were used in assigning the Raman spectra to possible functional groups. The band found at 1633 cm^{-1} can be atributed to C=O stretching in the ligand and at a slightly lower energy of 1609 cm^{-1} in the complex. The bands seen at 1530 cm^{-1} in the ligand and at a slightly lower energy of 1524 cm^{-1} in the complex can be attributed to aromatic C=C stretching. The band found at 771 cm^{-1} in the spectrum of the ligand and the complex at can be atributed to C-H stretching vibrations. The band at 574 cm^{-1} is unique to the complex and it is proposed that this band is due to Zr–O interaction in the complex. This assignment was based on the work reported by Šebsetík *et al*[177] stating a bending of chelating oxygens bound to iron in the iron (III) deferiprone complex can be assigned to a wavenumber of 573 cm^{-1}.

3.6 Properties of the Zirconium Complexes

Basic properties of the each of the synthesised Zr complexes were analysed and are reported in this section of the thesis.

Melting points determination is straightforward technique that is provides characteristic information of materials. The capillary method is the standard technique for melting point determination. The melting points of the complexes were determined utilising a Stuart SMP3 melting point apparatus, full details can be found in the appendix section of this thesis. A thin glass capillary tube which contains a small amount of the complexes to be analysed was placed into the melting point apparatus the temperature of the apparatus was ramped at a constant rate until the complex in the sample tube had melted into its liquid state. Melting point temperatures were recorded.

Complex	Molecular Mass	Appearance	Melting Point
Oxine	145.16 g/mol	White Solid	70-73 ^{o}C
Zirconium Tetrakisoxine	667.82 g/mol	Dark Yellow Solid	388 ^{o}C [134]
Tropolone	122.12 g/mol	Light Yellow Solid	83-84 ^{o}C
Zirconium Tetrakistropolone	575.34 g/mol	Light Yellow Solid	>349 ^{o}C
Ethyl Maltol	104.14 g/mol	White Solid	91 – 95 ^{o}C
Zirconium Dichlorobis Ethyl Maltol	440.39 g/mol	White Solid	206 – 208 ^{o}C
Zirconium Tetrakisethyl maltol	647.74 g/mol	White Solid	186 -187 ^{o}C
Deferiprone	139.15 g/mol	White Solid	272 – 275 ^{o}C
Zirconium Tetrakisdeferiprone	751.90 g/mol	White Solid	292 – 293 ^{o}C (Decomposed)

Table 3.16: Properties of Ligands and Complexes.

3.7 Solubility

Solubility tests were be undertaken to determine the best solvent to use for each of the complexes when performing chromatographic analysis and further experimental work. For testing solubility of the complexes a concentration of 1g / 100mL was used and solubility tests were all conducted at room temperature of ~22^{o}C. Visual observations and findings are reported on page 115 of this thesis.

3.8 Solubility of Ligands and Complexes

Solubility tests were conducted at a concentration of 1 g of compound per 100 mL of solvent at a temperature of 22^{o}C at 1atm pressure. The salinity of the water used during the solubility tests was based on salt dissolved in (g/L)

Solvent	Solubility with Zirconium Tetrakisoxine	pH Pre Addition	pH Post Addition
Water (0.5g-0.30 g/L)	Suspended (Possible Low Solubility)	6.00	6.90
Water (Brine) (60 g/L)	Immiscible & Partly Suspended	5.40	6.07
Water (Purified) (<0.5 g/L)	Immiscible	6.29	N/A
Water (Saline) (30 g-50 g/L)	Immiscible & Partly Suspended	6.70	7.00

Table 3.17: Solubility of Zirconium Tetrakisoxine in Water of Various Salinities

Solvent	Solubility With Zr Tetrakisoxine	Solubility with Zr Tetrakistropolone	Solubility With Zr Tetrakisethyl maltol	Solubility With Zr Tetrakisdeferiprone
Acetone	<1g/100mL	Insoluble	Insoluble	Insoluble
Benzene	<1g/100mL	Insoluble	Insoluble	Insoluble
Chloroform	>1g/100mL	>1g/100mL	>1g/100mL	Insoluble
Dichloromethane	<1g/100mL	Insoluble	>1g/100mL	<1g/100mL
Diethyl Ether	<1g/100mL	Insoluble	Insoluble	Insoluble
Dimethyl Sulfoxide	>1g/100mL	>1g/100mL	>1g/100mL	>1g/100mL
Ethanol	<1g/100mL	<1g/100mL	<1g/100mL	>1g/100mL
Hexane	<1g/100mL	Insoluble	Insoluble	Insoluble
Methanol	<1g/100mL	<1g/100mL	>1g/100mL	>1g/100mL
Tetrahydrofuran	>1g/100mL	Insoluble	Insoluble	<1g/100mL
Water	Insoluble	Insoluble	Insoluble	>1g/100mL

Table 3.18: Solubility of Zirconium Tetrakis Complexes in a Range of Solvents

3.9 Conclusion

3.9.1 FTIR and Raman Spectroscopy

When comparing the spectra of the complexes and their related ligands it was shown that there was a difference in the fingerprint region of the spectra in all cases. In the functional group region of the spectra comparison of the complex to the ligand showed an absence of an O-H group. This is because the ligand becomes deprotonated to allow the chelation to the metal ion.

FTIR and Raman spectra of all of the ligands and their zirconium tetrakis complex forms have values that are in agreement with previously published works. All of the spectra of the ligands and zirconium tetrakis complexes have peaks that directly relate to expected functional groups. The disappearance of the OH vibrational mode when comparing the spectra of the ligands to the complexes as well as a shift in various functional groups indicates the formation of a chelated complex.

3.9.2 Melting Points and Solubility

The experiments to determine the melting points of the ligands and complexes were undertaken three times to determine precision and the average of these findings are reported in table. All of the melting points of the ligands are in agreement with the suppliers (Sigma Aldrich) material safety details sheet data. Zirconium tetrakisoxine, tropolone and ethyl maltol complexes are coloured, solid, non-hygroscopic and thermally stable. The solubility tests illustrated in table 3.18 page 115 shows that the compounds are soluble in a range of organic solvents such as chloroform, ethanol, methanol and DMSO. However, the complexes are insoluble in water. This would suggest the possibility that the complexes have strong metal ligand bonds and are non-polar and lipophilic. The zirconium tetrakisdeferiprone complex is highly water soluble, not soluble in chloroform and as such lacks lipophilic properties.

CHAPTER 4

Synthesis of Zirconium Tetrakis Complexes under Conditions Compatible with Radiopharmacy

4.1 Introduction

Chapter 4 of this thesis reports the refinement and adaption of the synthesis methods devised and reported in chapter 2. This work has been undertaken as it is necessary to synthesise the complexes under conditions that are likely to be found when dealing with radioactive Zr. Radioactive Zr is supplied in an excess of different acids depending on the form of the complex.The radioactive Zr is either supplied in the form of zirconium tetrachloride in an excess of hydrochloric acid or zirconium tetrakisoxalato in an excess of oxalic acid. Experiments have been undertaken to determine the possibility of exchanging the chloride and oxalate ligands under acidic and neutral conditions for the desired ligands reported in chapter 2 of this thesis.

Tables of equipment, equipment settings and compounds used throughout this chapter can be located in the appendix section of this thesis All compounds used can be found listed in Table A2 (p226) in the appendix section. Equipment used during this chapter can be found in appendix, section A.1.3, (p222).

4.2 Synthesis of Potassium Zirconium Tetrakisoxalato

Aim

The synthesis of potassium zirconium tetrakisoxalato was undertaken so that further experiments could be conducted that would closely resemble the circumstances in which the ^{89}Zr isotope is supplied from the manufacturer. The method was adapted from previously published work.[178]

Method

Zirconyl chloride (15 g; 0.048 mol) was dissolved in reverse osmosis water (300 mL) in a 1000 mL glass conical flask at room temperature (~20 ^{o}C). Potassium oxalate monohydrate (36 g; 0.195 mol) was dissolved in a second, separate volume of reverse osmosis water (100 mL) in a 1000 mL glass conical flask at room temperature (~20 ^{o}C). To this second solution, oxalic acid dihydrate (12 g; 0.096 mol) was added and dissolved at room temperature (~20 ^{o}C).

The zirconyl chloride solution was added carefully to the solution of potassium oxalate and oxalic acid. This was accomplished by the use of a narrow mouth bottle pipette under constant stirring utilising the magnetic stirrer function of an electric hotplate and an octagon magnetic stirrer. The solution was observed to be cloudy and opaque at this stage of the synthesis process. The solution was then heated to 100 ^{o}C and was boiled for 30 minutes. During the boiling process the solution became totally clear. The solution was then allowed to cool to room temperature (~20 ^{o}C). Once the solution was cooled the volume of the solution was increased to 400 mL with reverse osmosis water. Absolute ethanol (99.9%, 400 mL) was slowly added to the solution to precipitate out the potassium zirconium tetra oxalato. The resulting precipitate was then collected by the use of a Büchner funnel, filter paper and vacuum conical flask. The precipitate was washed with ethanol (99.7%, 50 mL). The precipitate was then dissolved in reverse osmosis water (250 mL) in a 1000 mL glass conical flask at a temperature of 70^{o} C. The solution was cooled to 30 ^{o}C and absolute ethanol (150 mL) was added.

The precipitate was then was then collected by the use of a Büchner funnel, filter paper and vacuum conical flask. The precipitate was then washed with 3 x ethanol (99.7%, 25 mL) and 2 x diethyl ether (99+%, 50 mL) The precipitate was then dried in an electric oven at a 55 ^{o}C for 1 hour, cooled and stored in a glass air tight storage container. Visual appearance of the compound was white in colour and finely crystalline.

Results and Discussion

The synthesis of potassium zirconium tetrakisoxalato was successful and confirmed *via* the use of CHN analysis. The product was successfully used in several of the experiments summarised in this section of this thesis. The zirconium tetrakisoxalate complex is soluble in water. Once the potassium zirconium tetrakisoxalato is dissolved in water, the solution remains clear at concentrations of between 1 – 200 ppm.

Carbon, hydrogen and nitrogen (CHN) analysis results for potassium zirconium tetrakisoxalate pentahydrate

Formula Weight: 689.77 g/mol

	Expected	1st Analysis	2nd Analysis
C %	13.93	14.06	14.03
H %	1.46	1.41	1.45
N %	0	0	0

Table 4.1

Theoretical Yield: 33.109g
Actual Yield: 31.509g
Percentage of Theoretical Yield: 95.2%

4.3 Synthesis of Complexes under Acidic Conditions

4.3.1 Synthesis of Zr Tetrakisoxine from Potassium Zirconium Tetrakisoxalato Reverse Osmosis Water

Aim

The ^{89}Zr isotope is supplied in the form of zirconium-89 tetrachloride in an excess of hydrochloric acid or zirconium-89 tetrakisoxalato in an excess of oxalic acid. The aim of this experiment was to ascertain if it is possible to exchange the ligands found on the zirconium tetrakisoxalato complex with 4 oxine bidentate ligands. This would result in the neutral zirconium tetrakisoxine complex. This synthesis was conducted without any of the excess acid solutions present and the reaction was under taken in reverse osmosis water.

Method

Oxine (4.330 g; 0.0298 mol) was added to reverse osmosis water (150 mL) in a 250 mL glass conical flask, heated to 70 ^{o}C and constantly stirred for 30 minutes until completely dissolved. Once the oxine was totally dissolved, the solution was cooled to room temperature (~20 ^{o}C). Potassium zirconium tetrakisoxalato (5.000 g; 0.00724 mol) was dissolved in reverse osmosis water (50 mL) in a 250 mL conical flask at room temperature. The solution of oxine was added carefully to the solution of potassium zirconium tetrakisoxalato drop wise with a narrow mouth bottle pipette. The solution was then stirred utilising the magnetic stirrer function of an electric hotplate and an octagon magnetic stirrer. The solution was stirred for 20 minutes at room temperature (~20 ^{o}C). Ammonium hydroxide, 1M (100 mL) was added to the solution and a precipitate immediately formed. The solution was then heated to 85 ^{o}C for 30 minutes to ensure the reaction was complete. The solution was then allowed to cool to room temperature (~20 ^{o}C). The solution was allowed to stand for 20 minutes and the resulting precipitate was then collected by the use of a Büchner funnel, filter paper and vacuum conical flask.

The precipitate was then dried in an electric oven at a 125 ^{o}C for 1 hour. The dried complex was then ground with a pestle and mortal to ensure homogeneity and was stored in a glass air tight storage container.

Formula weight: 667.82 g/mol

Visual appearance: Bright yellow, fine powder.

Theoretical yield: 4.835g
Actual Yield: 4.123 g
Percentage of theoretical yield: 85.3 %

Results and Discussion

The reactants and products are illustrated below;

$$K_4[Zr(oxalate)_4]^{4-} \xrightarrow[4NH_4OH]{4\ Oxine} Zr(Oxine)_4 + 4\ NH_4K(oxalate) + 4\ H_2O$$

NMR results show that the ligand exchange was successful and the Zr metal favours the oxine bidentate ligands opposed to the oxalate bidentate ligands. Reasons for this are currently unknown.

As these results showed that is possible to exchange the oxalate ligands for the required oxine ligands further experiments were undertaken to repeat this developed method under acidic conditions.

4.4 Synthesis of Zirconium Tetrakisoxalate from Zirconium Tetrakisoxine

Experiments were undertaken to ascertain if it was possible to exchange the oxine ligands of the Zr complex for oxalate ligands. NMR analysis of the resulting complexes determined that it was not possible, showing that the zirconium tetrakisoxine complex is more stable than the zirconium tetrakisoxalate complex.

4.4.1 Synthesis of Zirconium Tetrakisoxine from Zirconium Tetrachloride in 1M Hydrochloric Acid

Aim

This experiment was conducted to replicate the conditions by which the ^{89}Zr isotope is received from the supplier in the form zirconium-89 tetra chloride in 1 M of hydrochloric acid (HCl). The conditions were replicated and the oxine ligand was added in a stoichiometric ratio of 4:1 with the Zr ion. Ammonia was added to neutralise excess acid.

Method

Oxine (2.5 g; 0.01725 mol) was added to reverse osmosis water (150 mL) in a 250 mL glass conical flask, heated to 58 ^{o}C and constantly stirred for 30 minutes until completely dissolved. Once the oxine was totally dissolved, the solution was cooled to room temperature (~20 ^{o}C). Zirconium tetrachloride (1.005 g; 0.0042 mol) was dissolved in HCl (20 mL) in a 250 mL conical flask at room temperature. The pH was then raised to 7.60 by addition of 1M NH_4OH (28 mL). The solution of oxine was added carefully to the solution of zirconium tetrachloride drop wise with a narrow mouth bottle pipette under constant stirring utilising the magnetic stirrer function of an electric hotplate and an octagon magnetic stirrer. The solution was stirred for 20 minutes at room temperature (~20 ^{o}C). The solution was then heated to boiling for 30 minutes to ensure the reaction was complete and its volume was reduced by 90%. The solution was then allowed to cool to room temperature (~20 ^{o}C).

The solution was allowed to stand for a further 20 minutes and the resulting precipitate was then collected by the use of a Büchner funnel, filter paper and vacuum conical flask. The precipitate was washed with ethanol (15 mL), tetrahydrofuran (15 mL) and diethyl ether (15 mL) and then dried in an electric oven at a 100 ^{o}C for 1 hour. The dried complex was then ground with a pestle and mortar to ensure homogeneity and was stored in a glass air tight storage container.

Formula weight: 667.82 g/mol

Visual Appearance: Greenish yellow, fine powder.

Theoretical Yield: 2.805 g
Actual Yield: 2.552 g
Percentage of Theoretical yield: 90.98%

Results and Discussion

Where the zirconium ion is in a solution of HCl problems were encountered when attempting to attach the oxine to the Zr ion. This was thought to be caused by the fact that oxine will not de-protonate successfully because of the excess protons in the solution provided by the 1 M of HCl present. The addition of ammonia is thought to push the reactions to completion by neutralisation of the excess acid and allow the ligand exchange to take place. As a result of the addition of ammonia, a salt was produced between ammonia and HCl; ammonium chloride. The ammonium chloride itself may also be interfering with the reaction.

NMR analysis of the complex clearly shows that the desired complex of zirconium tetrakisoxine has been successfully synthesised (figure: 4.1, page 124). However there are a number of peaks that are currently unknown and are likely to be attributed to any remaining HCl present. The presence of the unknown contaminants is not acceptable and other methods of synthesis and purification were pursued.

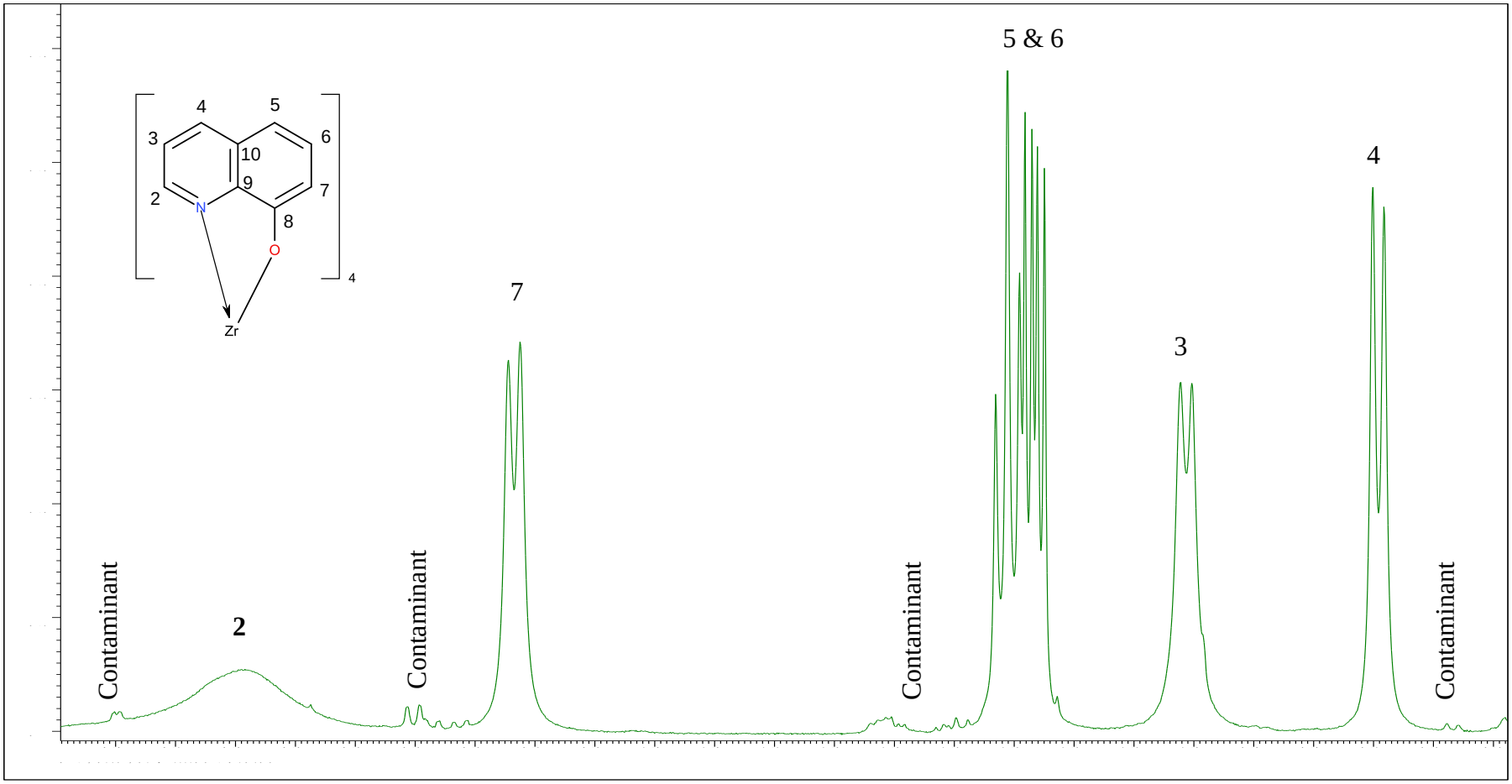

Figure 4.1: ^{1}H NMR of Zirconium Tetrakisoxine and contaminants in DMSO-*d6*

4.5 Synthesis of Zirconium Tetrakisoxine from Potassium Zirconium Tetrakisoxalato in 1 M Oxalic Acid

Aim

This experiment was conducted to replicate the conditions by which the ^{89}Zr isotope is received from the supplier in the form zirconium tetrakisoxalato in 1 M of oxalic acid. The conditions were replicated and the oxine ligand was added in a stoichiometric ratio of 4:1 with the zirconium ion. Ammonia was added to push the reaction to completion by neutralisation of the excess acid.

Method

Oxine (0.1800 g; 0.001240 mol) was added to reverse osmosis water (150 mL) in a 250 mL glass conical flask, heated to 58 ^{o}C and constantly stirred for 30 minutes until completely dissolved. Once the oxine was totally dissolved, the solution was cooled to room temperature (~20 ^{o}C). Potassium zirconium tetrakisoxalato (0.2000 g; 0.000289 mol) was dissolved in aqeous oxalic acid (50 mL; 1M) in a 250 mL conical flask at room temperature. The solution of oxine was added carefully to solution of potassium zirconium tetrakisoxalato in oxalic acid drop wise with a narrow mouth bottle pipette. The solution was then stirred utilising the magnetic stirrer function of an electric hotplate and an octagon magnetic stirrer. The solution was stirred for 20 minutes at room temperature (~20 ^{o}C). Ammonia (50 mL) was added to the solution and a precipitate immediately formed. The solution was then heated to 85 ^{o}C for 30 minutes to ensure the reaction was complete. The solution was then cooled to room temperature (~20 ^{o}C). The cooling process was accelerated by placing the 250 mL conical flask into an ice bucket. The solution was allowed to stand for 20 minutes and the resulting precipitate was then collected by the use of a Büchner funnel, filter paper and vacuum conical flask. The precipitate was then dried in an electric oven at a 100 ^{o}C for 1 hour. The dried complex was then ground with a pestle and mortar and stored in a glass air tight storage container.

Formula Weight: 667.82 g/mol

Theoretical Yield: 2.805 g
Actual Yield: 2.552 g
Percentage of Theoretical Yield: 90.98 %

Results and Discussion

Where the zirconium is in the form zirconium tetrakisoxalato in a solution of oxalic acid problems were encountered when attempting to attach the oxine to the zirconium ion. This was thought to be caused by the fact that oxine will not de-protonate successfully because of the excess protons in the solution provided by the 1 M of oxalic acid present. The addition of ammonia is thought to push the reactions to completion by neutralisation of the excess acid and and allow the ligand exchange to take place. As a result of the addition of ammonia, a salt was produced between ammonia and oxalic acid; ammonium oxalate. The ammonium oxalate itself may also be interfering with the reaction.

NMR results show that the desired zirconium tetrakisoxine complex did not form under this set of synthesis conditions. There are clear indications that the unbound oxine ligand is present along with a quantity of what is probably the salt formed between ammonia and oxalic acid (ammonium oxalate).

Further work was undertaken to rectify the problems during the attempted synthesis of zirconium tetrakisoxine from potassium tetrakisoxalato in 1 M oxalic acid involving a neutralisation step and is reported in the following section of this thesis.

4.6 Neutralisation of a 1 M HCl Acid Solution Containing Zirconium Tetrachloride and Subsequent Synthesis of Zirconium Tetrakisoxine

Aim

It was hypothesised that neutralisation of the 1 M HCl solution in which the zirconium tetrachloride is dissolved would rectify the problems with the synthesis of the desired zirconium tetrakisoxine complex previously reported in sections 4.2.3 and 4.2.4 of this thesis.

Method

Oxine (2.500 g; 0.01725 mol) was finely ground using a pestle and mortar. It was then added to reverse osmosis water (150 mL) in a 250 mL glass conical flask, heated to 58 ^{o}C and constantly stirred for 30 minutes until completely dissolved. The pH of the solution was measured and was found to be a pH of 7.11. Once the oxine was totally dissolved, the solution was cooled to room temperature (~20 ^{o}C). Zirconium tetrachloride (1.005 g; 0.00425 mol) was dissolved in HCl (20 mL) in a 250 mL conical flask at room temperature. This acidic solution (pH 0.79) was then neutralised with sodium carbonate (Na_2CO_3) in aqueous solution 1M (28 mL) (pH 12.87), The pH of the solution at this stage was measured and was found to be neutral (pH 7.60). The solution of oxine was added carefully to the solution of zirconium drop wise with a narrow mouth bottle pipette under constant stirring utilising the magnetic stirrer function of an electric hotplate and an octagon magnetic stirrer. The solution was stirred for 20 minutes at room temperature (~20 ^{o}C). The solution was then heated to 80 ^{o}C for 30 minutes to ensure the reaction was complete. To extract the compound from the solution the volume was reduced until the compound had precipitated out. At this point there was less than 10% of the original volume remaining. The solution was then cooled to room temperature (~20 ^{o}C). The cooling process was accelerated by placing the 250 mL conical flask into an ice bucket. The solution was allowed to stand for 20 minutes and the resulting precipitate was then collected by the use of a Büchner funnel, filter paper and vacuum conical flask.

The precipitate was then dried in an electric oven at a 100 ^{o}C for 10 minutes. The dried complex was then ground with a pestle and mortar to ensure homogeneity and was stored in a glass air tight storage container.

Formula weight: 667.82 g/mol

Visual Appearance: Greenish yellow, fine powder.

Theoretical Yield: 2.838g,
Actual Yield: 3.221g
Percentage of Theoretical yield: 113.50 %

Results and Discussion

NMR analysis on the complex clearly shows that the desired complex of zirconium tetrakisoxine had been successfully synthesised. However the appearance of the compound and the yield which is higher than expected suggests that the salt being formed with the neutralisation step is mixed in with the desired complex. This salt will need to be removed to ensure a purer product.

The 1 M HCl acid solution containing zirconium tetrachloride was neutralised with the required amount of sodium carbonate (Na_2CO_3) with constant stirring for the solution to obtain neutral pH of ~7.00. Products formed during neutralisation of the acid with the base was sodium chloride salt (NaCl) and water.

NMR results of the resulting product from this experiment show neutralisation of the 1 M solution containing the zirconium tetrachloride is a necessary step to ensure the successful chelation of the oxine ligand to the zirconium ion. However a further step is required to separate the desired complex from the salts formed during the synthesis process.

4.7 Neutralisation of a 1 M Oxalic Acid Solution Containing Potassium Zirconium Tetrakisoxalato and Subsequent Synthesis of Zirconium Tetrakisoxine

Aim

As is the case with the attempted synthesis of zirconium tetrakisoxine from zirconium tetra chloride in an excess of HCl it was hypothesised that neutralisation of the 1 M oxalic acid solution in which the zirconium tetrakisoxalato is dissolved, would rectify the problems with the synthesis of the desired zirconium tetrakisoxine complex previously reported in sections 4.2.3 and 4.2.4 of this thesis.

Method

Oxine (2.10 g; 0.01446 mol) was finely ground using a pestle and mortar. It was then added to reverse osmosis water (150 mL) in a 250 mL glass conical flask, heated to 58 ^{o}C and constantly stirred for 30 minutes until completely dissolved. The pH of the solution was measured and was found to be a pH of 7.11. Once the oxine was totally dissolved, the solution was cooled to room temperature (~20^{o}C). Potassium zirconium tetrakisoxalato (2.00 g; 0.002899 mol) was dissolved in oxalic acid (1 M) (20 mL) in a 250 mL conical flask at room temperature. This acidic solution (pH 1.02) was then neutralised with sodium carbonate (Na_2CO_3) (1M) (44 mL) (pH 7.80). The pH of the solution at this stage was measured and was found to be neutral (pH 7.01). The solution of oxine was added carefully to the solution of potassium zirconium tetrakisoxalato drop wise with a narrow mouth bottle pipette under constant stirring utilising the magnetic stirrer function of an electric hotplate and an octagon magnetic stirrer. The solution was stirred for 20 minutes at room temperature (~20 ^{o}C). The solution was then heated to 70 ^{o}C for 20 minutes to ensure the reaction was complete. The solution was then allowed to cool to room temperature (~20 ^{o}C). The solution was allowed to stand for a further 20 minutes and the resulting precipitate was then collected by the use of a Büchner funnel, filter paper and vacuum conical flask.

The precipitate was then dried in an electric oven at a 100 ^{o}C for 10 minutes. The dried complex was then ground with a pestle and mortar to ensure homogeneity and was stored in a glass air tight storage container.

Formula weight: 667.82

Visual Appearance: Bright yellow, fine powder.

Theoretical Yield: 1.936g
Actual Yield: 2.490g
Percentage of Theoretical yield: 128%

Results and Discussion

The 1 M oxalic acid solution containing potassium zirconium tetrakisoxalato was neutralised with the required amount of sodium carbonate (Na_2CO_3) (1M) with constant stirring for the solution to obtain a neutral pH of ~7.00. No precipitate formed during neutralisation; the salt formed due to the neutralisation of the acid with the base (sodium oxalate) remained dissolved in the solution. Carbon dioxide and water were also produced during the neutralisation process whilst the zirconium ion remained dissolved in the solution. The yield which is higher than expected suggests that the salt being formed with the neutralisation step is mixed in with the desired complex.

NMR results of the resulting product from this experiment shows that neutralisation of the 1 M solution containing the zirconium tetrakisoxalato is a necessary step to ensure the successful chelation of the oxine ligand to the zirconium ion.

It has been proven possible to exchange either the monodentate bound chloride or the bidentate bound oxalate ligands of the zirconium complex in an excess of either acid with the desired ligands. However a further step is required to separate the desired complex from the salts formed during the synthesis process to ensure a purer product.

4.8 Neutralisation of Acidic Conditions and Complex Synthesis

4.8.1 Zirconium Tetrakisoxine

Aim

The aim of this experiment is to exchange the oxalate ligands attached to the Zr ion for oxine ligands in turn producing a neutral complex and to separate the salt formed during the neutralisation step from the desired complex.

Method

Oxine was (2.10 g; 0.01446 mol) was finely ground using a pestle and mortar and then completely dissolved in chloroform (50 mL) in a 100mL glass conical flask. Potassium zirconium tetrakisoxalato (2.00 g; 0.00289 mol) was dissolved in oxalic acid (20 mL) in a 100 mL conical flask at room temperature. This acidic solution (pH 1.06) was then neutralised with sodium carbonate (Na_2CO_3) (1M) (19 mL) (pH 7.80). The pH of the solution at this stage was measured and was found to be neutral (pH 7.00). This solution was then diluted to 50 mL with reverse osmosis water. The solution of oxine was added carefully to the solution of potassium zirconium tetrakisoxalato drop wise with a narrow mouth bottle pipette under constant stirring utilising the magnetic stirrer function of an electric hotplate and an octagon magnetic stirrer. The solution was stirred for 20 minutes at room temperature (~20 ^{o}C). The solution was then transferred to a 250 mL glass separating funnel. The chloroform layer had become pale yellow in colour as the zirconium tetrakisoxine complex was extracted into the chloroform phase.

The chloroform layer was separated and heated on an electric hotplate at 60^{o}C until the zirconium tetrakisoxine complex had precipitated and the remaining chloroform had been evaporated. The complex was then stored in an air tight container. NMR analysis was then undertaken to confirm the structure of the complex and was in agreement with the findings reported in chapter two of this thesis.

Carbon, hydrogen and nitrogen (CHN) analysis results for Zirconium Tetrakisoxine.

Formula Weight: 667.82 g/mol

	Expected	1st Analysis	2nd Analysis
C %	64.75	64.59	64.66
H %	3.62	3.71	3.70
N %	8.69	8.60	8.67

Table 4.2: CHN Analysis of Zirconium Tetrakisoxine

Theoretical Yield:	1.93 0g
Actual Yield:	1.700 g
Percentage of Theoretical Yield:	88.10 %

4.8.2 Zirconium Tetrakistropolone

Aim

The aim of this experiment is to exchange the oxalate ligands attached to the Zr ion for tropolone ligands in turn producing a neutral complex and to separate the salt formed during the neutralisation step from the desired complex.

Method

Tropolone (3.600 g; 0.0298 mol) was completely dissolved in chloroform (50 mL) in a 100 mL glass conical flask. Potassium zirconium tetrakisoxalato (5.00g; 0.00725) mol was dissolved in oxalic acid (20 mL) in a 100 mL conical flask at room temperature. This acidic solution (pH 1.06) was then neutralised with sodium carbonate (Na_2CO_3) (1M) (19 mL) (pH 7.80). The pH of the solution at this stage was measured and was found to be neutral (pH 7.00). This solution was then diluted to 50 mL with reverse osmosis water. The solution of tropolone was added carefully to the solution of potassium zirconium tetrakisoxalato drop wise with a narrow mouth bottle pipette under constant stirring utilising the magnetic stirrer function of an electric hotplate and an octagon magnetic stirrer. The solution was stirred for 20 minutes at room temperature (~20 ^{o}C). The solution was then transferred to a 250 mL glass separating funnel. The chloroform layer had become pale yellow in colour as the zirconium tetrakistropolone complex was extracted into the chloroform phase.

The chloroform layer was separated and heated on an electric hotplate at 60^{o}C until the zirconium tetrakistropolone complex had precipitated. The complex was then stored in an air tight container. NMR analysis was then undertaken to confirm the structure of the complex and was in agreement with the findings reported in chapter two of this thesis.

Carbon, hydrogen and nitrogen (CHN) analysis results for Zirconium Tetrakistropolone.

Formula Weight: 658.91 g/mol

	Expected	1st Analysis	2nd Analysis
C %	53.47	53.22	53.28
H %	3.23	3.20	3.21
N %	0	0	0

Table 4.3: CHN Analysis of Zirconium Tetrakistropolone (.55 Chloroform)

Theoretical Yield:	4.780 g
Actual Yield:	4.640 g
Percentage of Theoretical Yield:	97.10 %

4.8.3 Zirconium Tetrakisethyl maltol

Aim

The aim of this experiment is to exchange the oxalate ligands attached to the Zr ion for ethyl maltol ligands in turn producing a neutral complex and to separate the salt formed during the neutralisation step from the desired complex.

Method

Ethyl maltol (4.2042g; 0.0300 mol) was completely dissolved in chloroform (50 mL) in a 100 mL glass conical flask. Potassium zirconium tetrakisoxalato (5.000 g; 0.00725 mol) was dissolved in oxalic acid (20 mL) in a 100 mL conical flask at room temperature. This acidic solution (pH 1.18) was then neutralised with sodium carbonate (Na_2CO_3) (1M) (24 mL) (pH 7.30). The pH of the solution at this stage was measured and was found to be neutral (pH 7.04). This solution was then diluted to 50 mL with reverse osmosis water.

The solution of ethyl maltol was added carefully to the solution of potassium zirconium tetrakisoxalato drop wise with a narrow mouth bottle pipette under constant stirring utilising the magnetic stirrer function of an electric hotplate and an octagon magnetic stirrer. The solution was stirred for 20 minutes at room temperature (~22 ^oC). The solution was then transferred to a 250 mL glass separating funnel. The chloroform layer had become milky/cloudy as the zirconium tetrakisethyl maltol complex was extracted into the chloroform phase.

The chloroform layer was separated and heated on an electric hotplate at 60^oC until the zirconium tetrakisethyl maltol complex had precipitated and the remaining chloroform had been evaporated. The complex was then stored in an air tight container. NMR analysis was then undertaken to confirm the structure of the complex and was in agreement with the findings reported in chapter two of this thesis.

Carbon, hydrogen and nitrogen (CHN) analysis results for Zirconium Tetrakisethyl maltol.

Formula Weight: 647.74 g/mol

	Expected	1st Analysis	2nd Analysis
C %	51.92	51.79	51.89
H %	4.36	4.33	4.43
N %	0	0	0

Table 4.4: CHN Analysis of Zirconium Tetrakisethyl maltol

Theoretical Yield:	4.701 g
Actual Yield:	4.220 g
Percentage of Theoretical Yield:	89.79 %

4.8.4 Zirconium Tetrakisdeferiprone

Aim

The aim of this experiment is to exchange the oxalate ligands attached to the zirconium ion for deferiprone ligands in turn producing a neutral complex and to separate the salt formed during the neutralisation step from the desired complex.

Method

Deferiprone (4.105g; 0.00295 mol) was completely dissolved in chloroform (50 mL) in a 100 mL glass conical flask whilst heated to 45 ^{o}C. Potassium zirconium tetrakisoxalato (5.000 g; 0.00725 mol) was dissolved in oxalic acid (20 mL) in a 100 mL conical flask at room temperature. This acidic solution (pH 1.20) was then neutralised with sodium carbonate (Na_2CO_3) (1M) (25 mL) (pH 7.30). The pH of the solution at this stage was measured and was found to be neutral (pH 7.01). This solution was then diluted to 50 mL with reverse osmosis water.

The solution of deferiprone was added carefully to the solution of potassium zirconium tetrakisoxalato drop wise with a narrow mouth bottle pipette under constant stirring utilising the magnetic stirrer function of an electric hotplate and an octagon magnetic stirrer. The solution was stirred for 20 minutes at room temperature (~22 ^{o}C). The solution was then transferred to a 250 mL glass separating funnel. The aqueous layer had become milky/cloudy indicating that the zirconium tetrakisdeferiprone complex was extracted into the aqueous phase.

Both layers were separated and heated on an electric hotplate at 60^{o}C (chloroform layer) 100^{o}C (aqueous layer) until the zirconium tetrakisdeferiprone complex had precipitated and the remaining water had been evaporated. The complex was then stored in an air tight container. NMR analysis was then undertaken to confirm the structure of the complex.

Carbon, hydrogen and nitrogen (CHN) analysis results for Zirconium Tetrakisdeferiprone.

Formula Weight: 859.99 g/mol

	Expected	1st Analysis	2nd Analysis
C %	39.02	37.31	37.39
H %	6.57	5.58	5.64
N %	6.50	6.11	6.19

Table 4.5: CHN Analysis of Zirconium Tetrakisdeferiprone

Theoretical Yield:	6.235 g
Actual Yield:	6.112 g
Percentage of Theoretical Yield:	98.03 %

4.9 Results and Discussion

The experiments reported on pages 142-149 involve the neutralisation of a 1 M oxalic acid solution containing potassium zirconium tetrakisoxalato and subsequent synthesis of zirconium tetrakis complexes. Each of the synthesis methods involves a chloroform extraction to separate the desired complex from the salt formed during the neutralisation process

The yields for all of the complexes apart from zirconium tetrakisdeferiprone are within acceptable values. The deferiprone complex has a higher than expected actual yield due to the problems separating the salt from the complex.

CHN results from zirconium tetrakisoxine, tropolone and ethyl maltol are all in agreement with the predicted and obtained values reported in chapter 2 of this thesis with the exception of the deferiprone complex. For zirconium tetrakisdeferiprone to be separated from the salt further research and method development must be undertaken.

NMR results of the resulting products from this set of experiments show that neutralisation of the 1 M solution containing the zirconium tetrakisoxalato is a necessary step to ensure the successful chelation of the oxine ligand to the zirconium ion. Furthermore the chloroform extraction step is a potential method to separate the desired complex from the salts formed during the neutralisation step in the synthesis. Zirconium tetrakisoxine, tropolone and ethyl maltol all have an affinity for the chloroform layer whereas the salt has an affinity for the aqueous layer so separation of the two is straightforward. However zirconium tetrakisdeferiprone has an affinity for the aqueous layer and as such makes the separation of the complex and the salt problematic. The CHN results for the zirconium deferiprone complex are inaccurate as it has not been possible to separate the salts formed during the synthesis from the complex itself.

Proposed Reactants and Products Formed During the Neutralisation of Zirconium Tetrakisoxalato and Subsequent Formation of Zirconium Tetrakisoxine

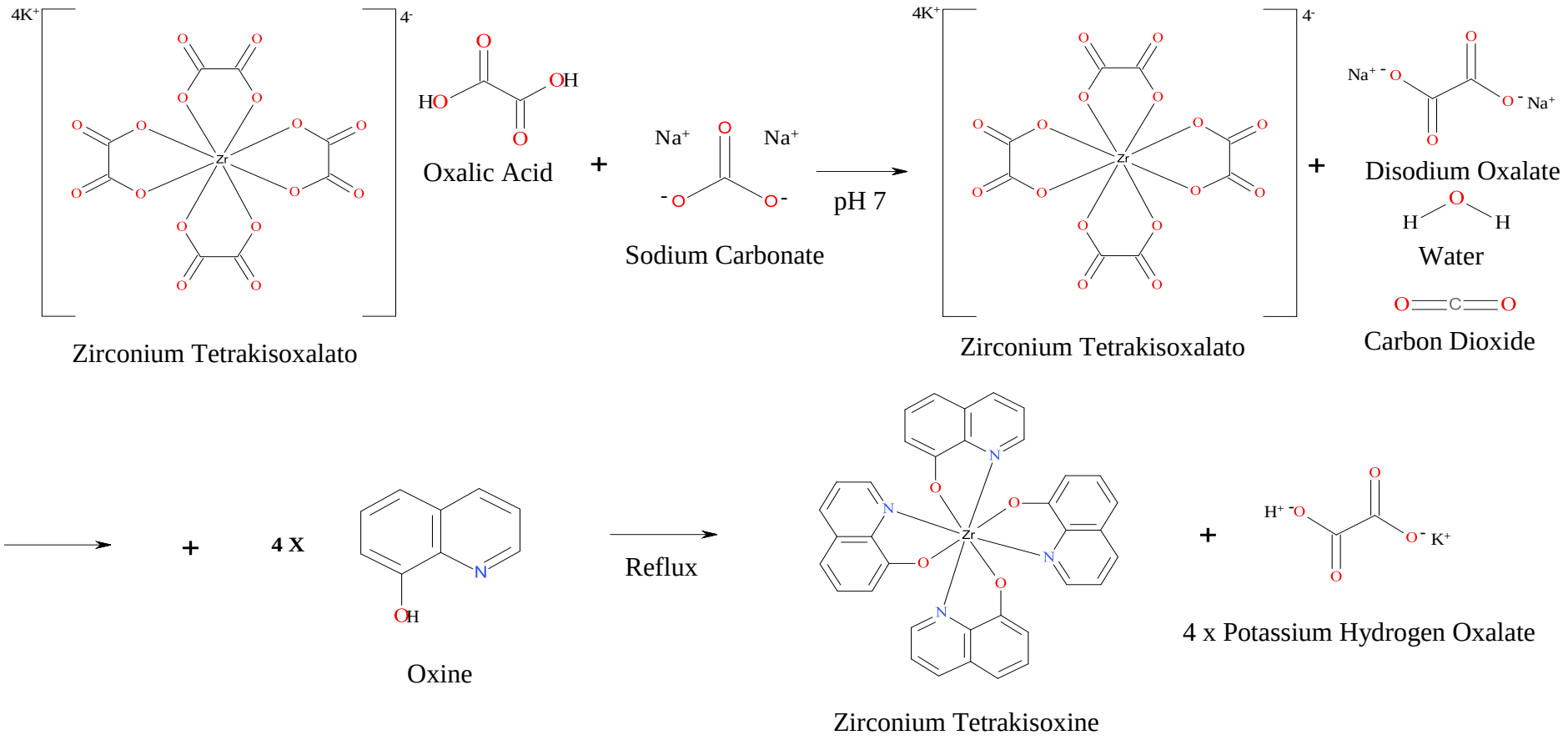

Figure 4.2: Synthesis Steps of Zirconium Tetrakioxine

4.10 Conclusions

4.10.1 Neutralisation of Acidic Solutions

A range of methods used in the attempt to synthesise the zirconium complexes from acidic solutions were unsuccessful. It was determined that a neutralisation step in the synthesis was necessary.

4.10.2 Ammonium Hydroxide

During the synthesis of the un-neutralised complexes, ammonium hydroxide was used to push the reactions to completion by neutralisation of the excess acid and consequently a salt is formed. The excess protons in the solution originate from the acidic conditions.

Generally salts of ammonia are water soluble which allows any unwanted ammonium salts to be washed away leaving the product; zirconium tetrakisoxine intact. Zirconium tetrakisoxine, tropoleone and ethyl maltol are insoluble in water and as such none of the the yield should be lost during the washing step of the synthesis. However ammonia in an aqueous solution can also be expelled by boiling which provides another option of removing any unwanted/excess ammonia from a solution. During the experiments involving the neutralisation of an excess of oxalic acid, ammonium oxalate, carbon dioxide and water are formed. During the experiments involving an excess of HCl, ammonium chloride, carbon dioxide and water are formed.

4.10.3 Sodium Carbonate

Sodium carbonate was also investigated to be utilised in the neutralisation step. As is the case with ammonium hydroxide the addition of sodium carbonate pushes the reactions to completion by neutralisation of the excess acid and consequently a salt is formed. With HCl it forms sodium chloride, carbon dioxide and water, with oxalic acid it forms sodium oxalate, carbon dioxide and water.

There does not seem to be any difference in the use of either ammonium hydroxide or sodium carbonate to neutralise either of the acidic solutions of HCl or oxalic acid. Sodium carbonate was used due to availability during the experimental process.

4.10.4 Synthesis of Complexes under Neutralised Conditions and Chloroform Extraction

Neutralisation of the acids in which the zirconium complex is supplied is essential in the process of synthesising the desired complexes. The neutralisation step results in a salt being formed which the desired compound needs to be separated from. As the complex has greater solubility in the chloroform phase and the salt has greater solubility an aqueous phase, chloroform extraction is the simplest method to separate the two.

4.10.5 CHN Analysis of the Zirconium Complexes

CHN analysis of zirconium tetrakisoxine, tropolone and ethyl maltol were all within agreement with the predicted results and the results reported in chapter 2. Zirconium tetrakisdeferiprone has been problematic when attempting to synthesise from potassium zirconium tetrakisoxalato, with or without an excess of acid in the solution. Methods to synthesis the tetrakisdeferiprone complex from potassium zirconium tetrakisoxalato have failed. CHN results vary greatly from each of the failed methods and suggest that two or three of the deferiprone ligands are attached to the zirconium ion with the remaining two ligands or single ligand being that of oxalate. It may be possible to synthesise the complex from zirconium tetra chloride in an excess of HCl, but as that is not the form in which the radioactive zirconium is currently supplied this synthesis method will not be pursued

CHAPTER 5

Ultraviolet-Visible Spectroscopy and Chromatographic Analysis of the Zirconium Compounds and their Ligands for Quality Control Purposes

5.1 Introduction

Ultraviolet-visible (UV-Vis) spectroscopy is an analytical technique that allows the determination of the concentration of solutions of transition metals ions, biological macromolecules, highly conjugated organic compounds and the rate of reactions.[179] d electrons within metal ions in solution can become excited from one electronic state to another causing the ions to be coloured. This colour is influenced by the presence of certain ligands.[180] The Beer Lambert Law is commonly used in UV-Vis analysis.

The Beer Lambert law is the linear relationship between the concentration and absorbance of an absorbing sample, usually written as $A = a(\lambda)bc$.[179] A is the measured absorbance, a (λ) relates to a wavelength dependent absorption coefficient, b is the path length and c is the sample's concentration.[179] If working in concentration units of molarity the Beer Lambert Law is written as $A = \text{Ɛ}bc$, Ɛ is the wavelength reliant molar absorptivity coefficient (units M^{-1} cm^{-1}).[180] The Beer-Lambert law was used to calculate molar absorptivity for both the ligand and the zirconium tetrakis complexes.

Each solvent used during the high performance liquid chromatography (HPLC) experiments was analysed with use of UV-Vis spectroscopy to determine whether there was any absorbance from the solvent in an area that would interfere with the detection of the ligands or the zirconium complexes. The analysis of the ligands and zirconium tetrakis complexes was also undertaken with UV-Vis spectroscopy. This analytical technique provided unique spectra which allowed identification of both the ligands and complexes. This information is essential when setting the range of the UV-Vis detector on the HPLC apparatus.

5.2 Experimental Method

Tables of equipment, equipment settings and reagents used throughout this chapter can be located in the appendix section of this thesis

Each of the precursor compounds, ligands and zirconium complexes were dissolved in an appropriate solvent into a volumetric flask. Acetonitrile for oxine and zirconium tetrakisoxine, methanol for tropolone, zirconium tetrakistropolone, ethyl maltol, zirconium tetrakisethyl maltol, millipore water for deferiprone and zirconium tetrakisdeferiprone. Serial dilutions were prepared using a range of glass pipettes in to volumetric flasks resulting in a range of concentrations. Each of the solutions were placed into a 400 µL quartz cuvette and analysed utilising a Shimadzu UV-1800 spectrometer. A reference quartz curvette containing the relevant solvent was run alongside the sample for background purposes.

Microcal Origin 5.0 was used to plot calibration curves of the ligands and complexes. Molar absorbtivity values of the compounds include a standard error of the slope value. This value was automatically calculated by the software using the following formula:

$$SE = \frac{\sqrt{\sum(y_i - \hat{y}_i)^2 / (n-2)}}{\sqrt{\sum(x_i - \bar{x})^2}}$$

5.3 Results and Discussion

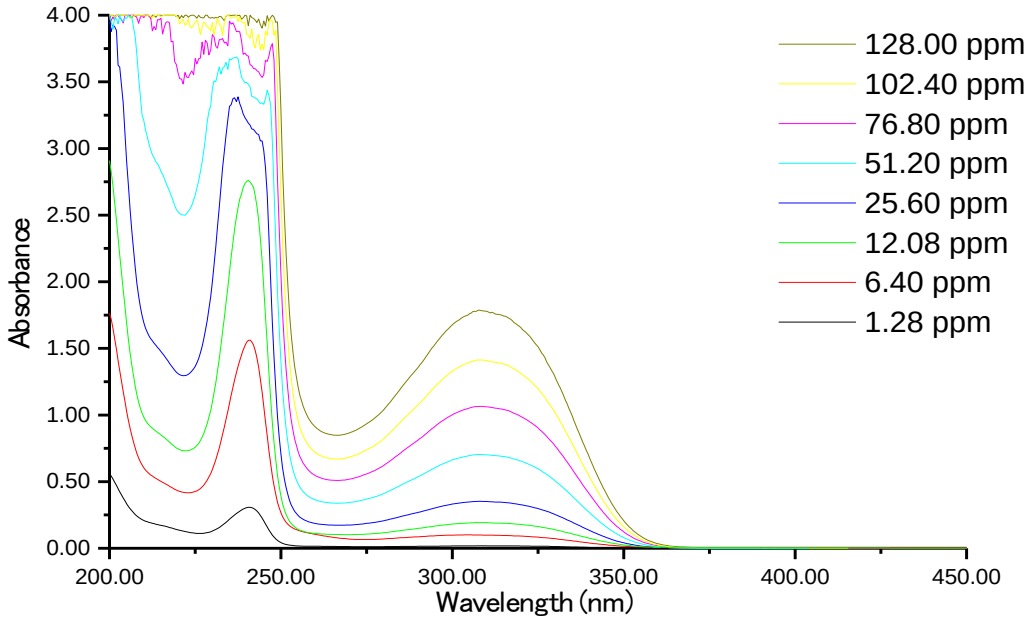

Figure 5.1: UV-Vis Stacked Spectra of Oxine

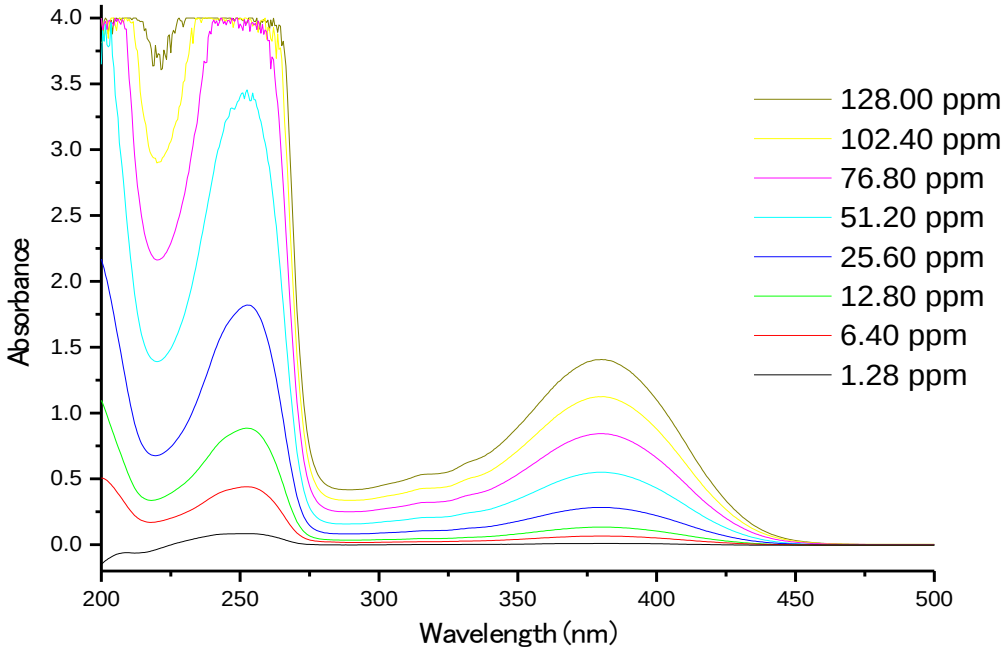

Figure 5.2: UV-Vis Stacked Spectra of Tetrakisoxine

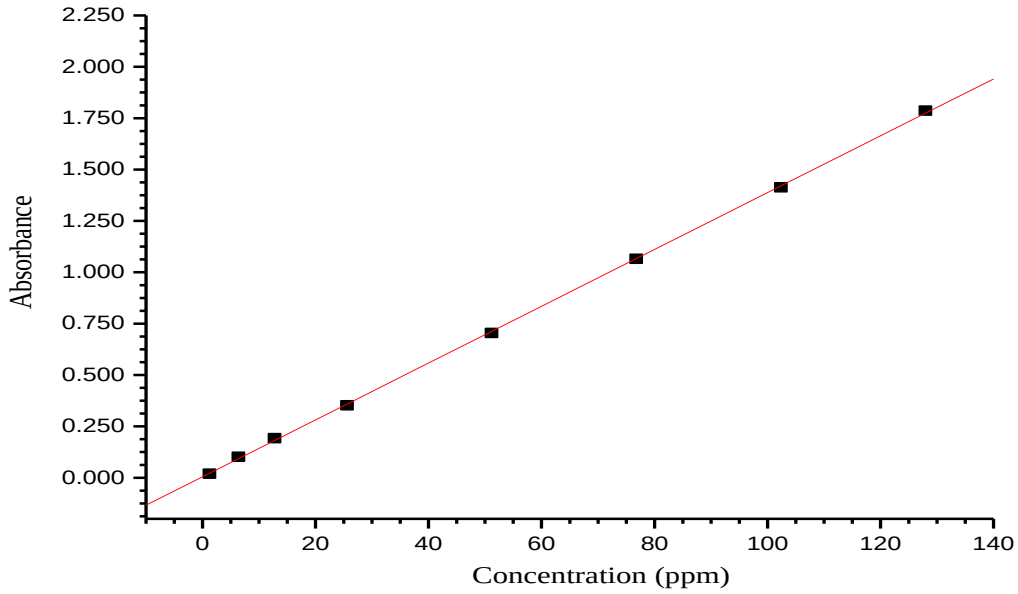

Figure 5.3: Calibration Curve of Oxine (308 nm)

y = 0.01383 x + 0.0476 R-Squared Value = 0.99997

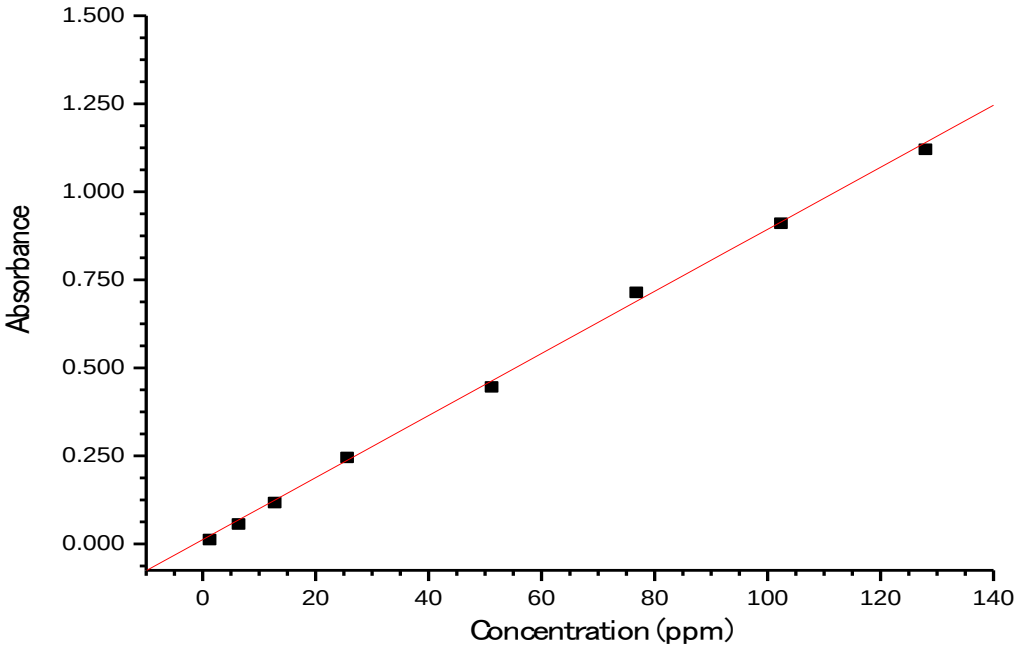

Figure 5.4: Calibration Curve of Oxine (380 nm)

y = 0.01419 x - 0.007779 R-Squared Value = 0.99936

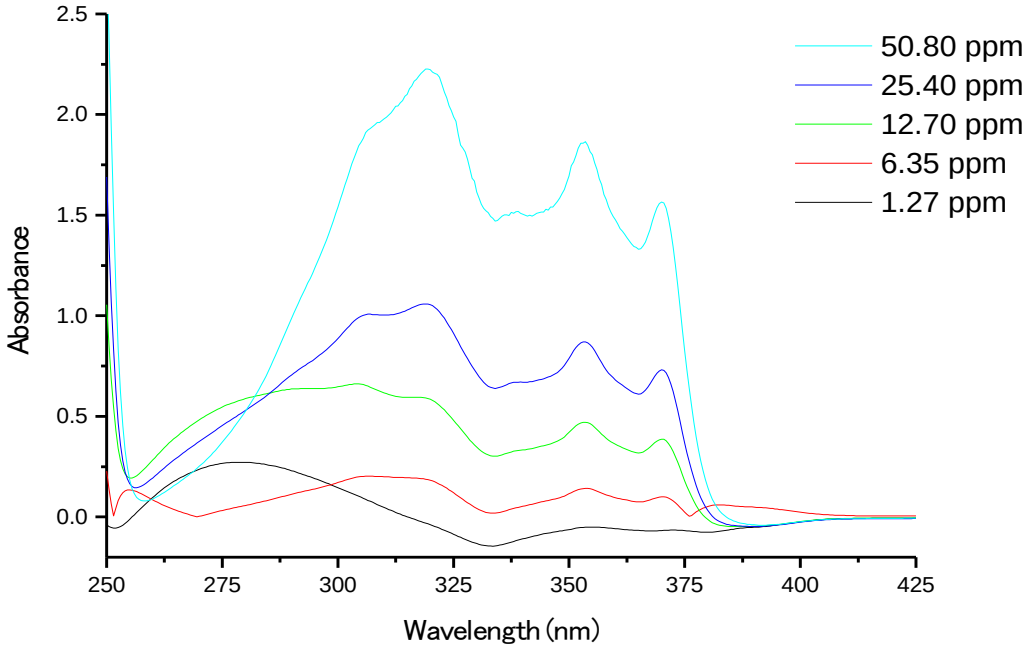

Figure 5.5: UV-Vis Stacked Spectra of Tropolone

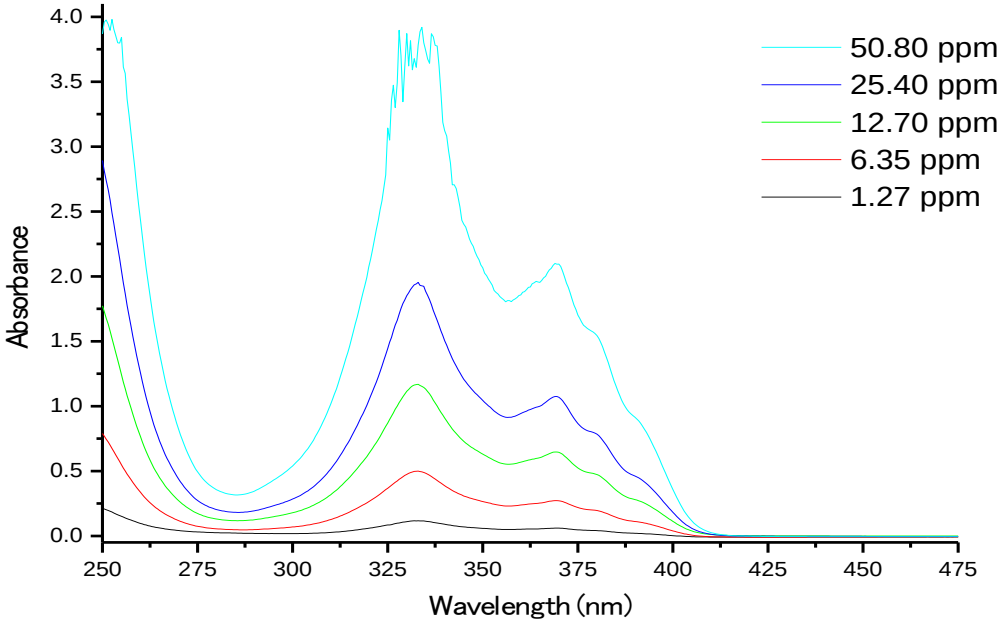

Figure 5.6: UV-Vis Stacked Spectra of Tetrakistropolone

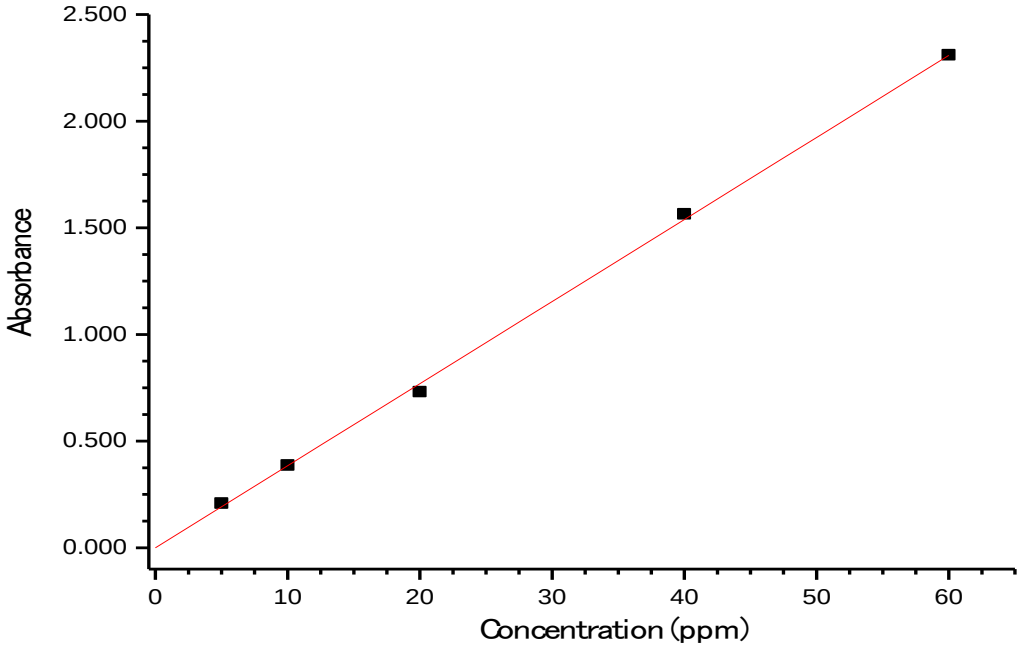

Figure 5.7: Calibration Curve of Tropolone (370 nm)

y = 0.0304 x - 0.00194 R-Squared Value = 0.99961

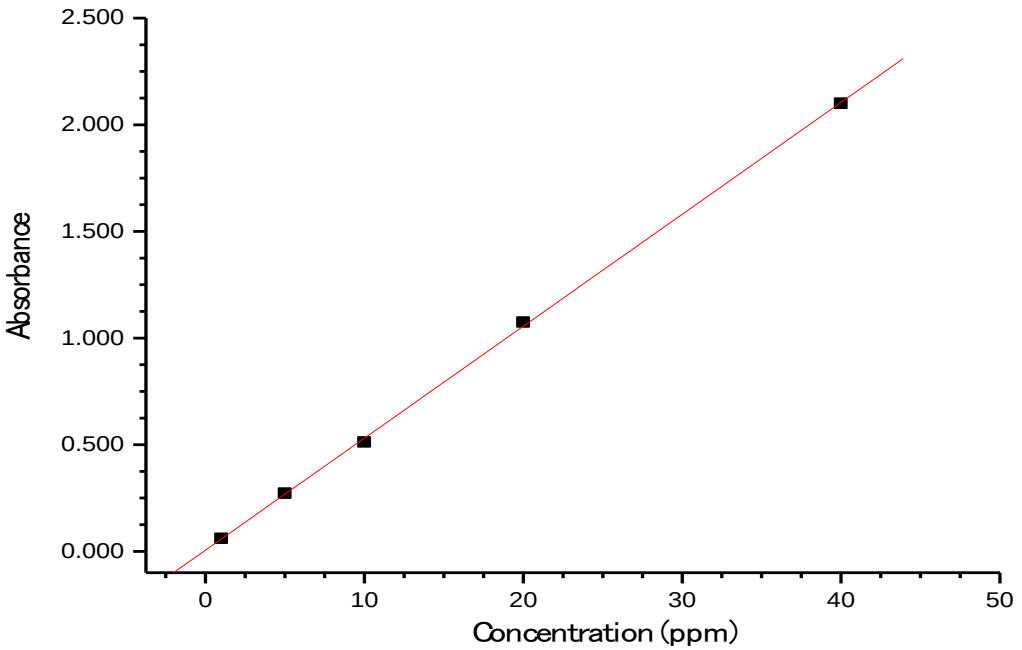

Figure 5.8: Calibration Curve of Tetrakistropolone (369 nm)

y = 0.0396 x + 0.09742 R-Squared Value = 0.99986

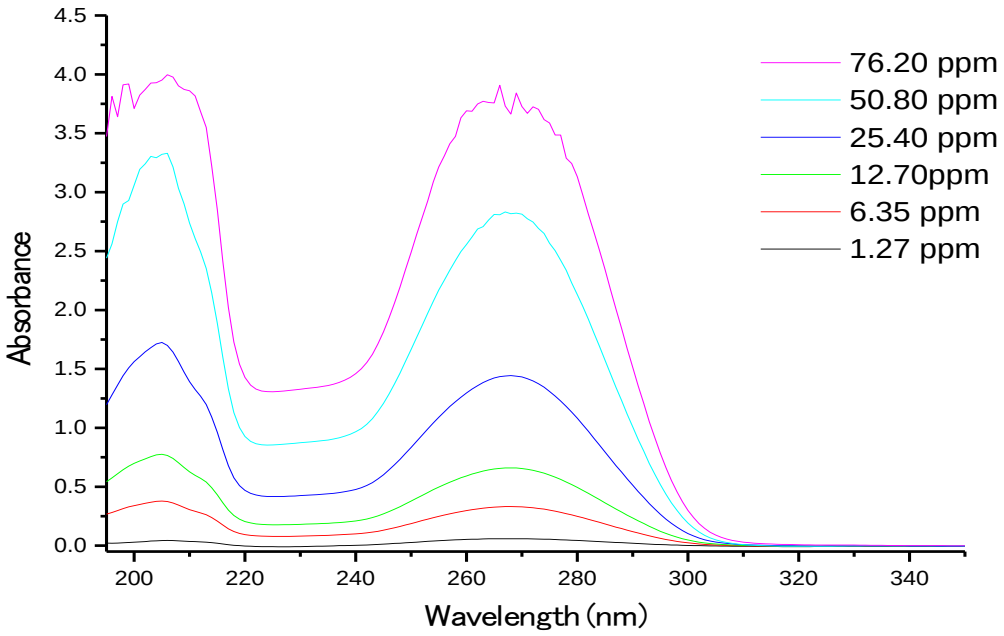

Figure 5.9: UV-Vis Stacked Spectra of Ethyl Maltol

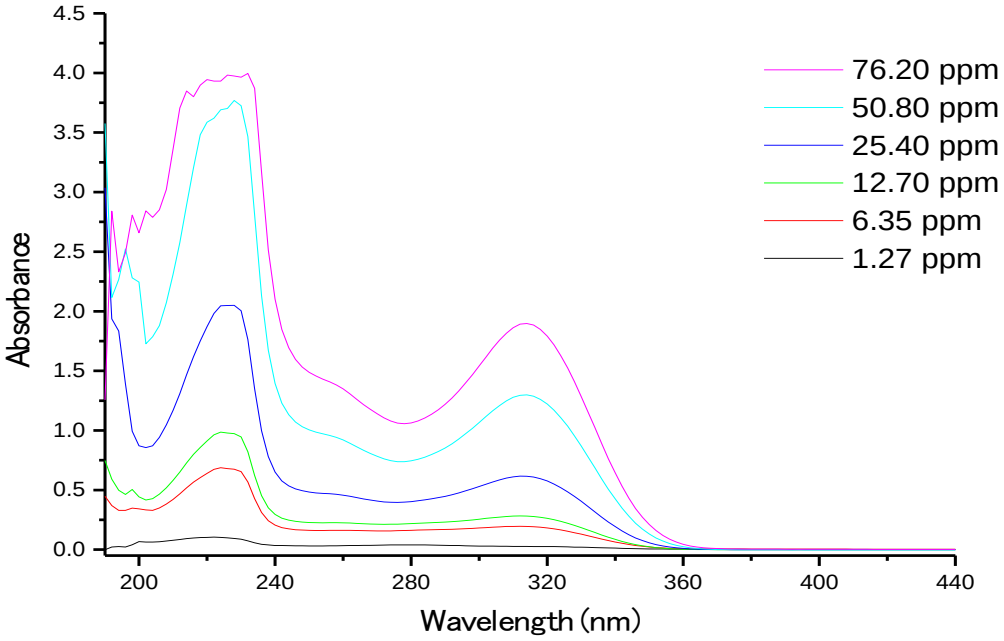

Figure 5.10: UV-Vis Stacked Spectra of Zirconium Tetrakisethyl Maltol

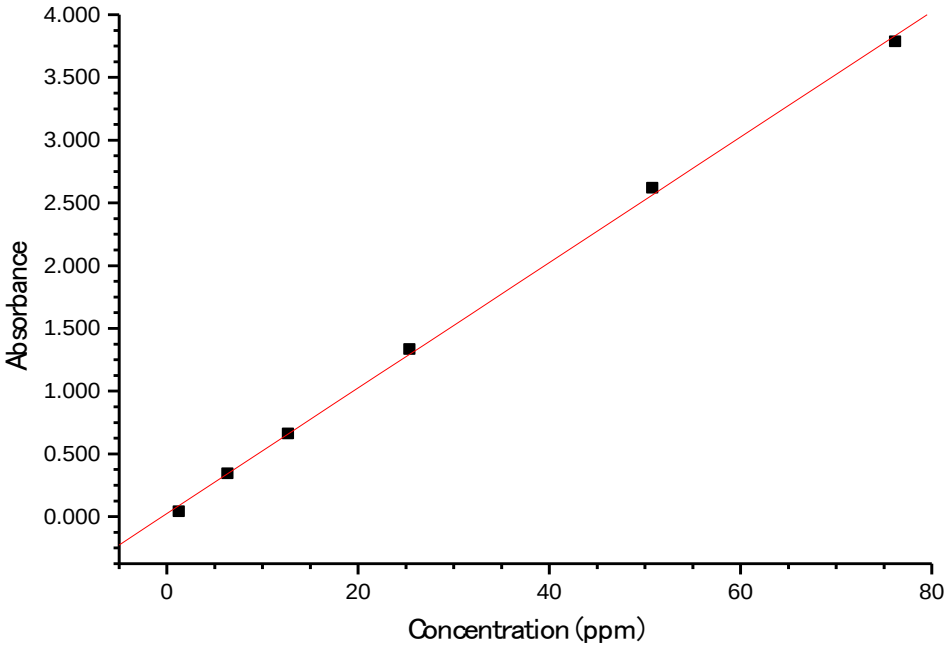

Figure 5.11: Calibration Curve of Ethyl Maltol (368 nm)

y = 0.05000 x + 0.02484 R-Squared Value = 0.99957

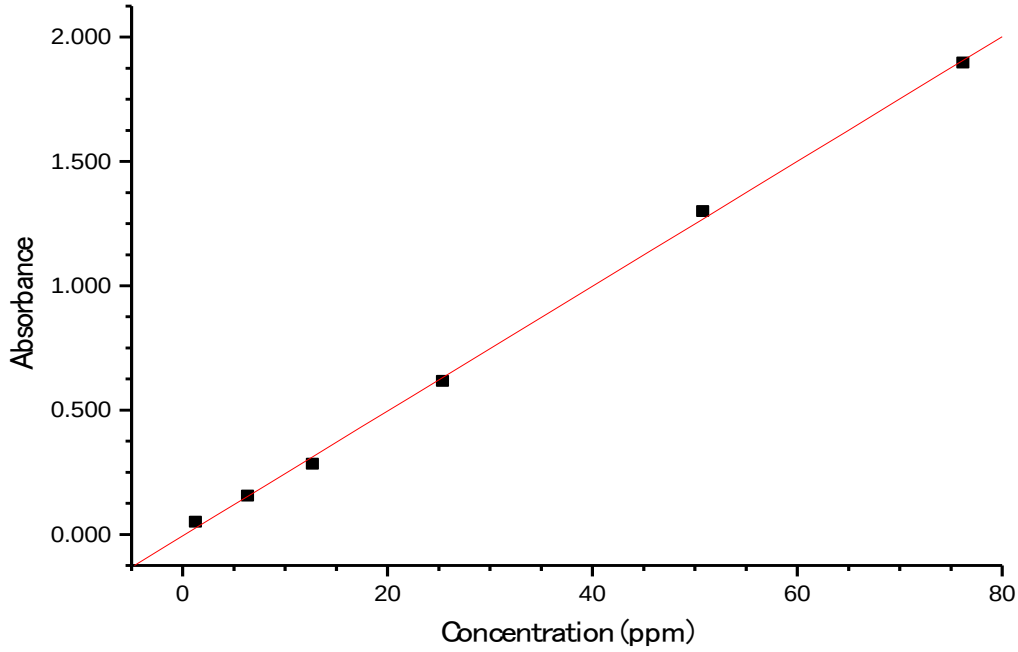

Figure 5.12: Calibration Curve of Tetrakisethyl Maltol (312 nm)

y = 0.02511 x - 0.00592 R-Squared Value = 0.99995

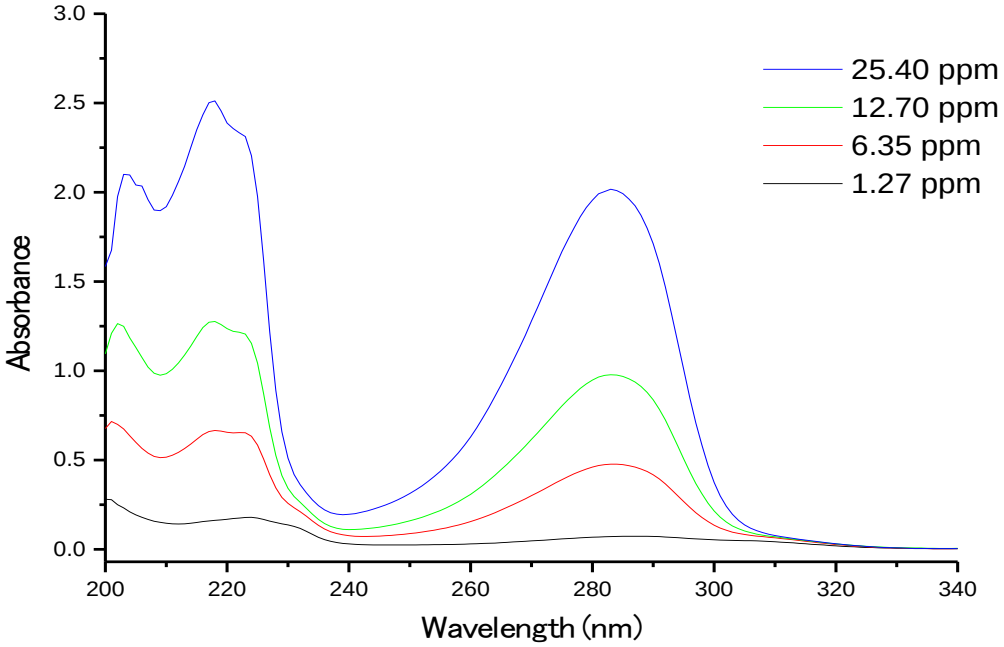

Figure 5.13: UV-Vis Stacked Spectra of Deferiprone

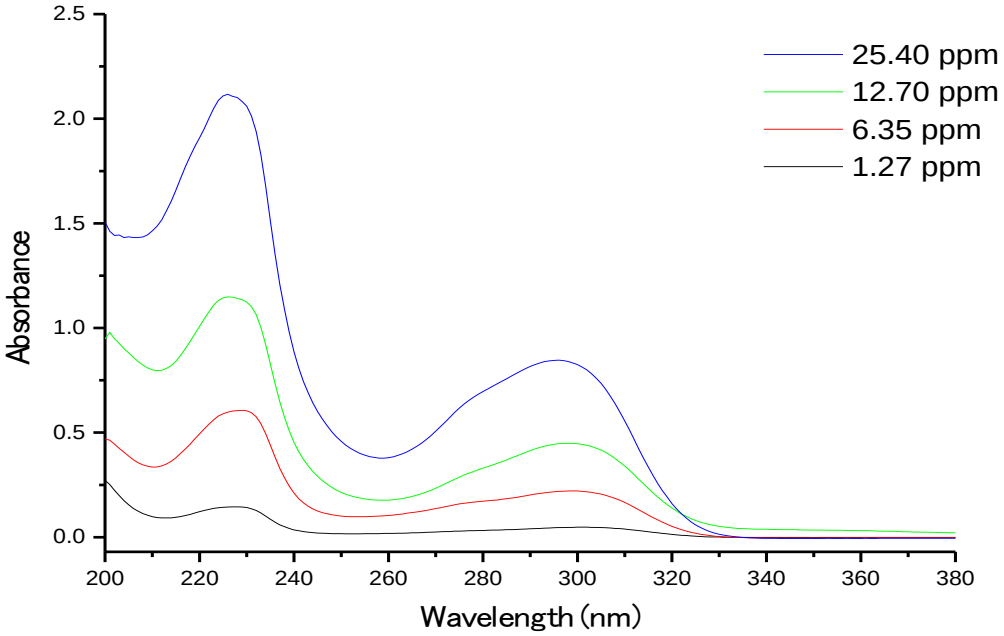

Figure 5.14: UV-Vis Stacked Spectra of Zirconium Tetrakisdeferiprone

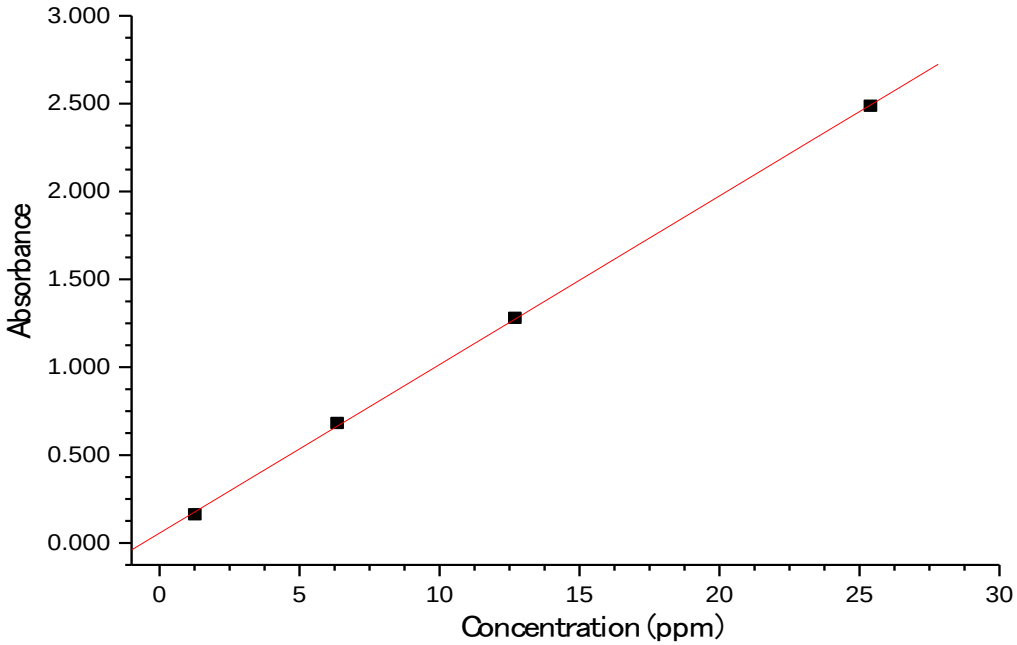

Figure 5.15: Calibration Curve of Deferiprone (217 nm)

y = 0.09596 x + 0.05576 R-Squared Value = 0.99995

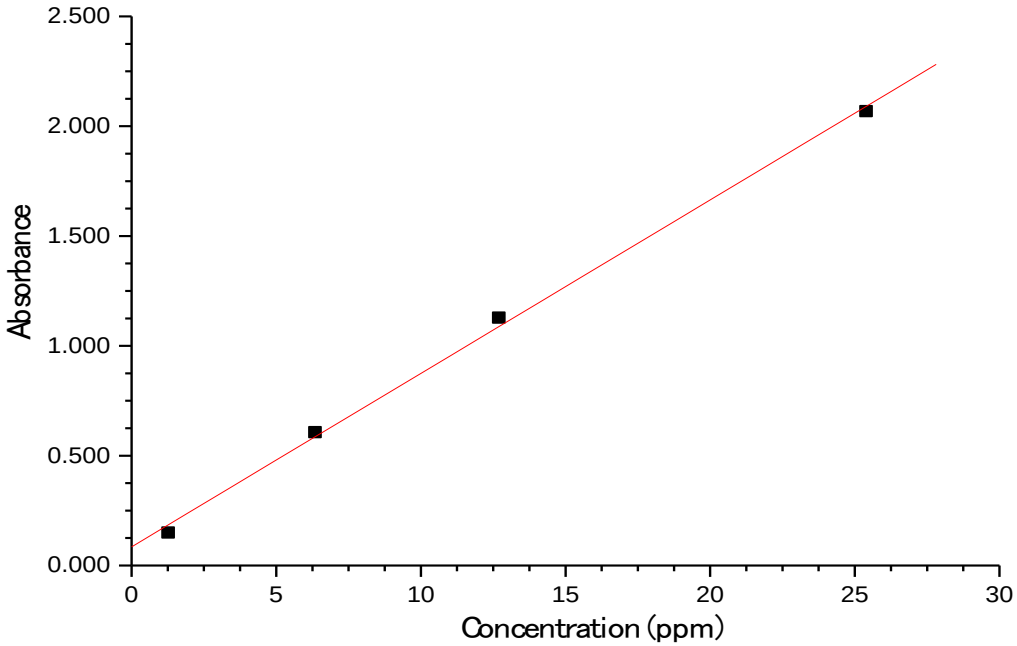

Figure 5.16: Calibration Curve of Tetrakisdeferiprone (227 nm)

y = 0.07898 x + 0.08495 R-Squared Value = 0.99907

5.3.1 UV Analysis of Oxine & Zirconium Tetrakisoxine

UV-Vis spectroscopy was used to analyse both the oxine ligand and the zirconium tetrakisoxine complex. The analysis of the ligand and complex using this technique provided unique spectra which allowed for their identification. The oxine ligand has absorption peaks at 237 nm and 308 nm. The zirconium tetrakisoxine complex has peaks at 244 nm and 380nm.

The ligand and the complex both show absorbance between a range of 200 nm – 461 nm at 256 ppm. Between 369 nm and 461 nm at 256 ppm there is an absorbance for the complex only. However this absorbance range is at the tail end of the overall absorbance for the complex and is fairly weak. When analysing the complex and ligand *via* HPLC apparatus the detector was set to a range where by both the ligand and complex have a large absorbance value and retention times were used to differentiate between the ligand and the complex.

The ligand and complex are stable in a solution of acetonitrile at concentrations of 1.28, 6.40, 12.80, 25.60, 51.20, 76.80, 102.40, 128.00 and 256.00 ppm. R-Squared value of oxine = 0.99997 and the R-Squared value of the complex = 0.99998 indicating a strong relationship between the absorbance of the ligand and complex and the concentration. The absorption spectrum of zirconium tetrakisoxine in acetonitrile has an absorption at 380 nm (previously reported in toluene at 387 nm)[134] assigned to a $\pi \rightarrow \pi^*$ transition in the ligand by comparison with related complexes.[181] Molar absorptivity of the complex at 380 nm (ε 9480 $\pm$ 30 dm^3 mol^{-1} cm^{-1}) is approximately four times that observed for the ligand at 308 nm, ε 2570 $\pm$ 10 dm^3 mol^{-1} cm^{-1} and is in accordance with the chromophore being ligand based rather than involving the Zr.

5.3.2 UV Analysis of Tropolone & Zirconium Tetrakistropolone

The analysis of both the tropolone ligand and the zirconium tetrakistropolone complex was undertaken with the use of UV-Vis spectroscopy. The analysis of the ligand and complex using this analytical technique provided unique spectra which allowed for the identification of both the ligand and the complex. The tropolone ligand has absorption peaks at 320 nm, 353 nm and 370 nm. The zirconium tetrakistropolone complex has peaks at 334 nm and 369 nm.

The ligand and the complex both show absorbance in the range of 250 nm – 403 nm at 254 ppm. Between 404 nm and 425 nm at 254 ppm there is an absorbance for the zirconium tetrakisethyl maltol complex only. This absorbance range is at the tail end of the overall absorbance for the complex and is extremely weak. This has not been able to be used to uniquely identify the compound from the ligand *via* the use of the UV-Vis detector attached to the HPLC apparatus. Hence it is not possible to uniquely identify only the ligand or the complex. When analysing the complex and ligand *via* HPLC apparatus the detector was set to a value where by both the ligand and complex have a large absorbance value and retention times were used to differentiate between the ligand and the complex.

The ligand and complex are stable in a solution of methanol at concentrations of 1.27, 6.35, 12.70, 25.40, 50.80 and 76.20 ppm. R-Squared value of tropolone = 0.99961 and the tropolone complex = 0.99926 indicating a strong relationship between the absorbance of the ligand and complex and the concentration. Electronic absorptions for free tropolone in methanol were in accord with those previously observed in DMSO[182] The absorptions are due to π-π^* transitions and analogous transitions are observed in zirconium tetrakistropolone with increased extinction coefficients attributed to the presence of four tropolone rings with enhancement by the contribution of a charge transfer transition.[182] Molar absorptivity for the complex (ε 63000 $\pm$ 5000 dm^3 mol^{-1} cm^{-1}) at 333 nm is approximately 10 times that observed for the ligand at 320 nm (ε/dm^3 mol^{-1} cm^{-1} 6500 $\pm$ 600). The complex at 369 nm has an molar absorptivity of ε 33000 $\pm$ 1000 dm^3 mol^{-1} cm^{-1} and the ligand at 354 nm an molar absorptivity of ε 5900 $\pm$ 200 dm^3 mol^{-1} cm^{-1}.

5.3.3 UV Analysis of Ethyl Maltol & Zirconium Tetrakisethyl maltol

The analysis of both the ethyl maltol ligand and the zirconium tetrakisethyl maltol complex was undertaken with the use of UV-Vis spectroscopy. The analysis of the free ligand and complex using this analytical technique provided unique spectra allowing the identification of both the free ligand and the complex. Ethyl maltol ligand absorption peaks at 205 nm and 278 nm. The complex has peaks at 224 nm, and 312 nm. The ligand and the complex both show absorbance between a range of 190 nm – 362 nm at 254 ppm. Between 319 nm and 362 nm at 254 ppm there is an absorbance for the zirconium tetrakis complex only. However this absorbance range is at the tail end of the overall absorbance for the complex and is extremely weak. This has not been able to be used to uniquely identify the compound from the ligand *via* the use of the UV-Vis detector attached to the HPLC apparatus at UKC. As this is the case it is not possible to set the UV-Vis detector attached to the HPLC apparatus to a unique range to identify only the ligand or the complex. When analysing the complex and ligand *via* HPLC apparatus the detector was set to a range where by both the ligand and complex have a large absorbance value.

The ligand and complex are stable in a solution of acetonitrile at concentrations of 1.27, 6.35, 12.70, 25.40, and 50.80 ppm. R-Squared value of ethyl maltol = 0.99957 R-Squared value of the ethyl maltol complex = 0.99995 indicating a strong relationship between the absorbance of the ligand/complex and the concentration.An electronic absorption for ethyl maltol in methanol was recorded as 268 nm, observed previously in toluene at 286 nm and interpreted as a π-π^* transitions of the α, β unsaturated enone.[138] In the complex this band disappears due to the loss of conjugation of the enone, demonstrating complexation by the carbonyl group. Absorption bands appear in UV spectrum at 224 and 312 nm, the latter may be attributed to a ligand-to-metal charge transfer from a π ligand orbital to the d^0 orbital of the zirconium. Molar absorptivity for the complex is (ε 64000 $\pm$ 5000 dm^3 mol^{-1} cm^{-1}) at 224 nm and at 312 nm (ε/dm^3 mol^{-1} cm^{-1} 21000 $\pm$ 1000). The ligand at 268 nm has a molar absorptivity of ε 10200 $\pm$ 300 dm^3 mol^{-1} cm^{-1}.

5.3.4 UV Analysis of Deferiprone & Zirconium Tetrakisdeferiprone

The analysis of both the deferiprone ligand and the zirconium tetrakisdeferiprone complex was undertaken with the use of UV-Vis spectroscopy. The analysis of the free ligand and complex using this analytical technique provided unique spectra which allowed for the identification of both the free ligand and the complex. The deferiprone ligand has absorption peaks at 217 nm and 283 nm. The zirconium tetrakisdeferiprone complex has peaks at 227 nm and 296 nm.

The ligand and the complex both show absorbance between a range of 200 nm – 344 nm at 254 ppm. Between 328 nm and 344 nm at 254 ppm there is an absorbance for the zirconium tetrakisdeferiprone complex only. This absorbance range is at the tail end of the overall absorbance for the complex and is fairly weak. This has not been able to be used to uniquely identify the compound from the ligand *via* the use of the UV-Vis detector attached to the HPLC apparatus at UKC. As this is the case it is not possible to set the UV-Vis detector attached to the HPLC apparatus to a unique range to identify only the ligand or the complex. When analysing the complex and ligand *via* HPLC apparatus the detector was set to a range where by both the ligand and complex have a large absorbance value.

The ligand and complex are stable in a solution at concentrations of 1.27, 6.35, 12.70 and 25.40 ppm. At concentrations of above 25.40 ppm the absorbance for the ligand becomes greater than the upper detection limit of 4.00 absorbance units for the apparatus. The deferiprone complex can be detected up to a concentration of 25.40 ppm as is the case of the deferiprone ligand. R-Squared value of deferiprone = 0.99995 and the R-Squared value of the complex = 0.99907 indicating a strong relationship between the absorbance of the ligand and complex and the concentration. The intense absorptions in the 280-300 nm region of the UV spectrum can be assigned to both hydroxyl and carbonyl Zr(IV) ligand to metal charge transfer (MLCT).[144] Molar absorptivity for the complex is (ε 78000 $\pm$ 6000 dm^3 mol^{-1} cm^{-1}) at 227 nm and at 296 nm, ε 32000 $\pm$ 1000 dm^3 mol^{-1} cm^{-1} The ligand at 283 nm has a molar absorptivity of ε 14240 $\pm$ 90 dm^3 mol^{-1} cm^{-1}.

5.4 Conclusion

5.4.1 UV-Vis Analysis of Zirconium Tetra Chloride & Potassium Zirconium Tetrakisoxalate

The analysis of zirconium tetra chloride and potassium zirconium tetrakisoxalate was under taken with a UV-Vis spectrometer at a range of concentrations. It was found that there was not any noticeable absorbance within the range of 200 to 900 nm. These results are clearly problematic when developing a HPLC method at UKC as the HPLC apparatus in the research lab is fitted with a UV-Vis detector and as such it will not be possible to detect these complexes.

5.4.2 Spectra

Unique UV-Vis spectra were obtained for both the ligands and the zirconium tetrakis complexes. In each case the complex had a greater wavelength range with the same beginning wavelength value as the ligand. This absorbance range is at the tail end of the overall absorbance for the complex and was consistently weak

5.4.3 Calibration Curves

The ligand and complex were shown to be stable at range of concentrations. Calibration curves were plotted and indicate a strong relationship between the absorbance and the concentration of the ligand and zirconium tetrakis complexes.

5.4.4 Absorbance

It was found that there was always an increase in the molar absorptivity of the zirconium complex when compared to its related ligand. However it was seen that this increase is not always simply four times the molar absorptivity of the ligand.

5.5 High Performance Liquid Chromatography Analysis

HPLC is used in the fields of chemistry and biochemistry to assist devising methods to synthesise chemical compounds, for purification purposes, analysing and separating mixtures, isolating natural products and predicting physical properties of compounds.[183] HPLC can also be used in quality control processes such as ensuring the purity of raw materials and synthesised compounds, determining the stability and monitoring the dissociation of compounds and quantifying the amount of synthesised compounds.[183]

The HPLC analysis of analytes involves the injection of a minute amount of sample in solution into a moving stream of liquid known as the mobile phase. The mobile phase passes through a column that is packed with particles of a stationary phase such as silica. The separation of a mixture into its constituent components depends on the different levels of retention of each component in the column.[184] The partitioning of a component between the stationary phase and the mobile phase determines its retention in the column.[183] The stationary/solute phase and mobile solute/phase interactions directly affect the partitioning between the two. Even minute changes in the composition of mobile phases will cause an exceptional effect on the separation of analytes. The components of the analytes will have in the majority of cases different rates of mobility. Because of this different components should exit the column at different times so that they will have different retention times.[184] Detectors sense anything that is not considered part of the mobile phase and transforms this information into an electrical signal, this is in turn is converted into a chromatogram *via* the use of integrated system software.

Radiochemical analysis and quality control for research in nuclear medicine and PET is extremely important. Radiochemical purity can be defined as a fraction of the total amount of activity in the desired chemical form contained within a sample. It is important that impurities are identified as they can cause altered bio distribution.[185] HPLC can be used to identify and quantify the components of a sample by both detecting and counting the amount of radiation in each separated fragment of the sample or by identifying the amount of absorbance by a UV detector.[185]

5.6 Experimental Method

5.6.1 Sample Preparation

A range of solutions were prepared at various concentrations in parts per million of both the ligands (oxine, tropolone, ethyl maltol and deferiprone) and the zirconium tetrakis complexes from each of the ligands. These were obtained by dissolving the appropriate weight of each of the compounds separately into either 250 mL of acetonitrile, water or methanol depending on solubility of the complex or the ligand. 2 mL of each of the solutions was separately filtered using a single use filter and the resulting filtrate was placed into 2 mL screw cap glass vials.

5.6.2 HPLC Instrument Preparation

Firstly the instrument and PC were been switched on and the appropriate software was loaded (Chromeleon 7.1.0.898). Utilising the Chromeleon software the pump and UV-Vis lamps were switched on and parameters such as the flow rate, wavelength and attenuation was set to the required values. The instrument was allowed to warm up for a period of 30 minutes. The stability of the base line was checked and observations were made for any large changes in the absorbance values. Mobile phase solvents degassed automatically *via* the HPLC apparatus to ensure that there is not a build-up of gas in the system that will affect the retention times of the analytes.

5.6.3 HPLC Analysis of Zirconium Tetrachloride & Potassium Zirconium Tetrakisoxalate

The UV-Vis spectrometer analysis of zirconium tetra chloride and potassium zirconium tetrakisoxalate was as expected, there was not any noticeable absorbance within the range of 200 nm to 900 nm. Unfortunately the HPLC spectrometer at the University of Kent at Canterbury is only equipped with a UV-Vis detector and analysis of these compounds is not possible with the current apparatus.

5.7 Method Development

5.7.1 Oxine and Zironium Tetrakisoxine

Methods adapted to fit the available equipment and to identify oxine and zirconium tetrakisoxine include the identification of aluminium chelates of oxine utilising HPLC, Hambali *et al*[186], Fluorescence properties of metal-complexes of 8-hydroxyquinoline-5-sulfonic acid and chromatographic applications, Krystyna Sorok *et al*[187], Extraction with toluene and HPLC determination of aluminium in the form of an 8-hydroxyquinoline derivative, Hongzhen Lian *et al*[188] and Reverse-phase high-performance liquid chromatographic determination of halogenated 8-hydroxyquinoline compounds in pharmaceuticals and bulk drugs, Wojtowicz *et al*.[189]

5.7.2 Tropolone and Zirconium Tetrakistropolone

There are currently no published papers reporting a HPLC protocol for the identification of zirconium tetrakistropolone. The method developed to separate and identify tropolone and zirconium tetrakistropolone was based on the methods used to analyse oxine and zirconium tetrakisoxine.

5.7.3 Ethyl Maltol and Zirconium Tetrakisethyl maltol

There are currently no published papers reporting a HPLC protocol for the identification of zirconium tetrakisethyl maltol. The method to separate vanilla compounds reported by Jean-Paul Larcinese[190] was adapted to fit the equipment available and subsequently identify ethyl maltol.

5.7.4 Deferiprone and Zirconium Tetrakisdeferiprone

There are no published papers reporting a HPLC method to identify zirconium tetrakisdeferiprone. The method to identify deferiprone was adapted from work reported by Mateen Abbasto *et al*[191] to study deferiprone in human plasma and adapted to fit the equipment available.

5.8 Results and Discussion for HPLC Analysis with a Mobile Phase of Acetonitrile and Water and a Eclipse XDB-C8 Column

5.8.1 Oxine

Oxine was dissolved in acetonitrile and HPLC conditions for the identification of oxine at a concentration of 12.8 ppm with the use of a XDB-C8 Eclipse column and a mobile phase of acetonitrile and water are as follows;

Column:	Eclipse XDB-C8	**Mobile Phase:**	75/25 Acetonitrile/Water
Column Pressure:	125 bar	**Wavelength:**	380 nm
Flow Rate:	1 mL min^{-1}	**Concentration:**	12.8 ppm.
Injection Volume:	10 µL	**Temperature:**	22^{o}C

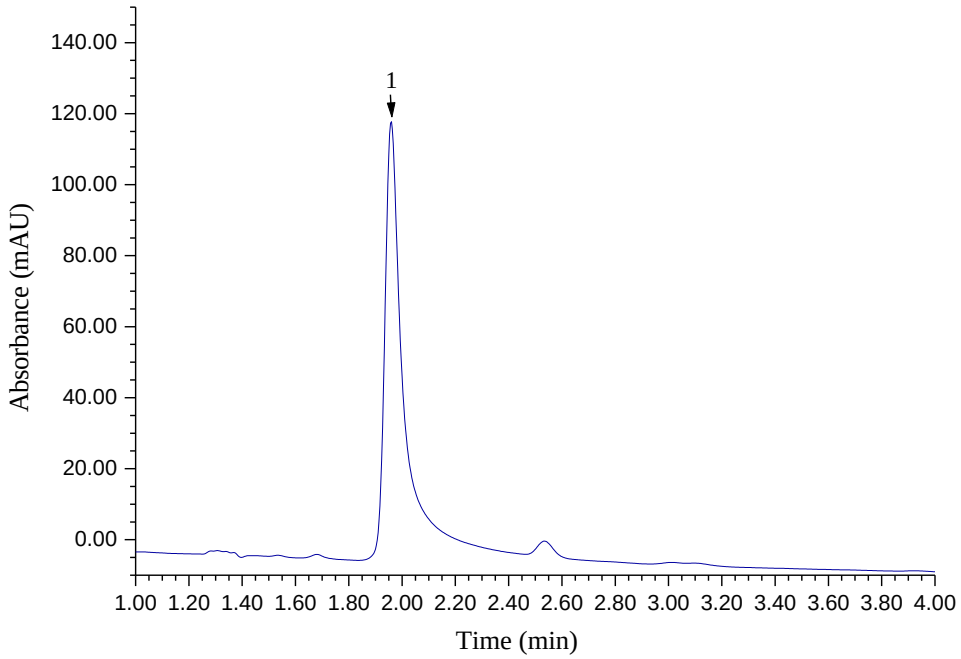

Figure 5.17: HPLC Chromotogram of Oxine (Acetonitrile/Water)

No	**Retention Time (min)**	**Area mAU* min**	**Height mAU**	**Relative Area %**	**Identification**
1	1.960	11.31	123.73	86.16	Oxine

5.8.2 Zirconium Tetrakisoxine

Zirconium tetrakisoxine was dissolved in acetonitrile and HPLC conditions for attempted identification of the zirconium tetrakisoxine with the use of a XDB-C8 Eclipse column and a mobile phase of acetonitrile and water are as follows;

Column:	Eclipse XDB-C8	**Mobile Phase:**	75/25 Acetonitrile/Water
Column Pressure:	125 bar	**Wavelength:**	380 nm
Flow Rate:	1 mL min^{-1}	**Concentration:**	12.8 ppm.
Injection Volume:	10 µL	**Temperature:**	22°C

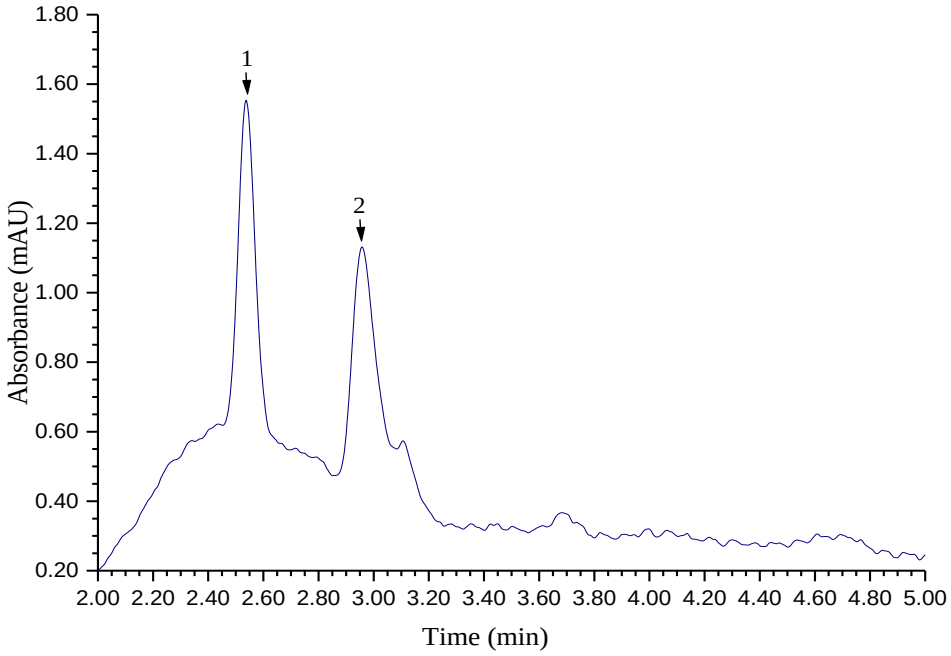

Figure 5.18: HPLC Chromotogram of Zirconium Tetrakisoxine (Acetonitrile/Water)

No	**Retention Time (min)**	**Area mAU* min**	**Height mAU**	**Relative Area %**	**Identification**
1	2.501	0.37	0.85	87.64	Unknown
2	2.943	0.06	0.34	2.75	Unknown

5.8.3 Zirconium Tetrakisoxine with Excess Ligand

Zirconium tetrakisoxine was dissolved in acetonitrile and HPLC conditions for the identification of zirconium tetrakisoxine (12.8 ppm) with the use of a XDB-C8 Eclipse column and excess ligand (concentration 1000 ppm) in the mobile phase of acetonitrile and water are as follows;

Column:	Eclipse XDB-C8	**Mobile Phase:**	75/25 Acetonitrile/Water
Column Pressure:	125 bar	**Wavelength:**	380 nm
Flow Rate:	1 mL min^{-1}	**Concentration:**	12.8 ppm.
Injection Volume:	10 µL	**Temperature:**	22^{o}C

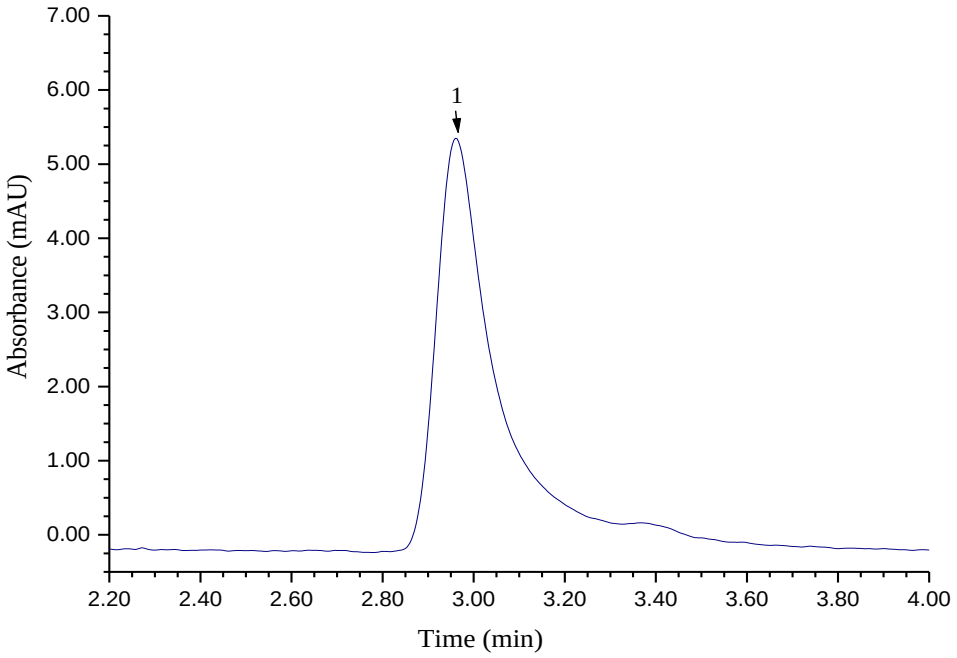

Figure 5.19: HPLC Chromotogram of Zirconium Tetrakisoxine 12.8ppm (Acetonitrile/Water + Excess Ligand)

No	**Retention Time (min)**	**Area mAU* min**	**Height mAU**	**Relative Area %**	**Identification**
1	2.960	1.55	7.06	94.20	Zirconium Tetrakisoxine

5.8.4 Zirconium Tetrakisoxine with Excess Ligand

Zirconium tetrakisoxine was dissolved in acetonitrile and HPLC conditions for the identification of zirconium tetrakisoxine (128 ppm) with the use of a XDB-C8 Eclipse column and excess ligand (concentration 1000 ppm) in the mobile phase of acetonitrile and water are as follows;

Column:	Eclipse XDB-C8	**Mobile Phase:**	75/25 Acetonitrile/Water
Column Pressure:	125 bar	**Wavelength:**	380 nm
Flow Rate:	1 mL min^{-1}	**Concentration:**	128 ppm.
Injection Volume:	10 µL	**Temperature:**	22^{o}C

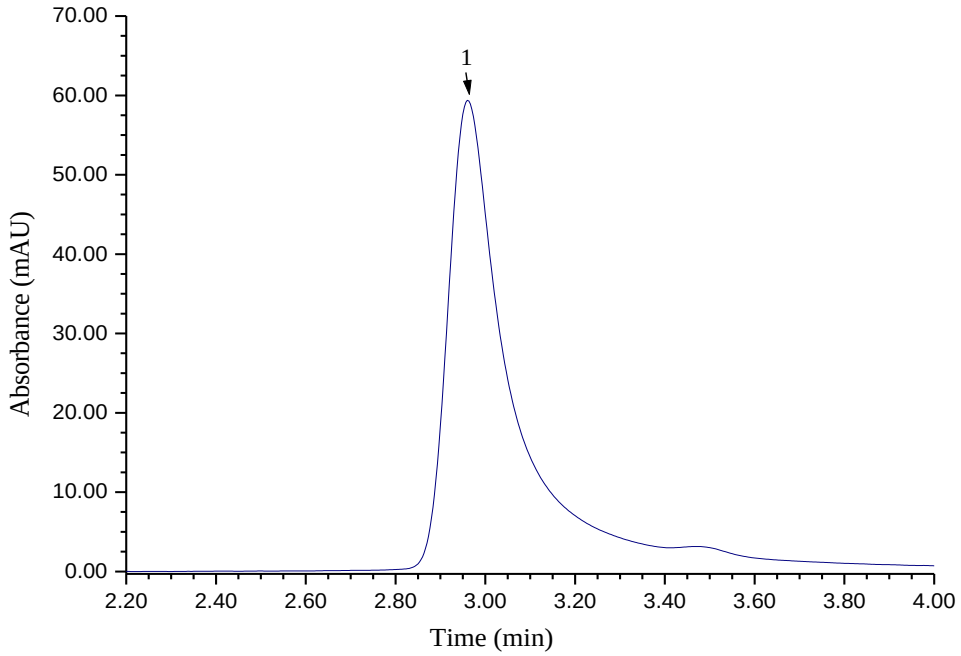

Figure 5.20: HPLC Chromotogram of Zirconium Tetrakisoxine 128ppm (Acetonitrile/Water + Excess Ligand)

No	**Retention Time (min)**	**Area mAU* min**	**Height mAU**	**Relative Area %**	**Identification**
1	2.960	10.52	60.82	84.45	Zirconium Tetrakisoxine

5.8.5 Oxine

It was possible to identify the oxine ligand utilising the Eclipse XDB-C8 HPLC column and a mobile phase of acetonitrile and water. The most efficient ratio of the mobile phase was found to be 75 % acetonitrile and 25 % water. An increase or decrease of acetonitrile caused the complex peak to become less pronounced.

5.8.6 Zirconium Tetrakisoxine

The resulting chromatogram at a wavelength of 380 nm for the Eclipse HPLC column showed two major peaks which would suggest that the complex is dissociating in to its constituent parts. As such the column is not suitable to analyse the zirconium tetrakisoxine complex with a mobile phase of acetonitrile and water.

5.8.7 Zirconium Tetrakisoxine at 12.8 ppm and 128 ppm with Excess Ligand

An excess of ligand in the mobile phase (concentration 1000 ppm) was added in the attempt to stabilise the Zr complex during the HPLC analysis with success. Concentrations of 12.8 ppm and 128 ppm of the complexes were run to ensure an increase in area and peak height to confirm the presence of the Zr complex. However an excess of ligand in the mobile phase would result in problems when trying to quantify the complex and any remaining unbound ligand for quality control purposes and as such further methods that have been undertaken are reported.

5.8.8 A Mixture of Oxine and Zirconium Tetrakisoxine

Separation of the oxine ligand and zirconium tetrakisoxine complex was not possible with the Eclipse HPLC column and a mobile phase of acetonitrile and water. Methanol was exchanged for acetonitrile in the following experiments in the attempt to separate the two analytes of interest.

5.9 HPLC Analysis with a Mobile Phase of Methanol and Water and a Eclipse XDB-C8 Column

5.9.1 Oxine

Oxine was dissolved in acetonitrile and HPLC conditions for the identification of oxine with the use of a XDB-C8 Eclipse column and a mobile phase of methanol and water are as follows;

Column:	Eclipse XDB-C8	**Mobile Phase:**	75/25 Methanol/Water
Column Pressure:	125 bar	**Wavelength:**	308 nm
Flow Rate:	1 mL min^{-1}	**Concentration:**	12.8 ppm.
Injection Volume:	10 µL	**Temperature:**	22^{o}C

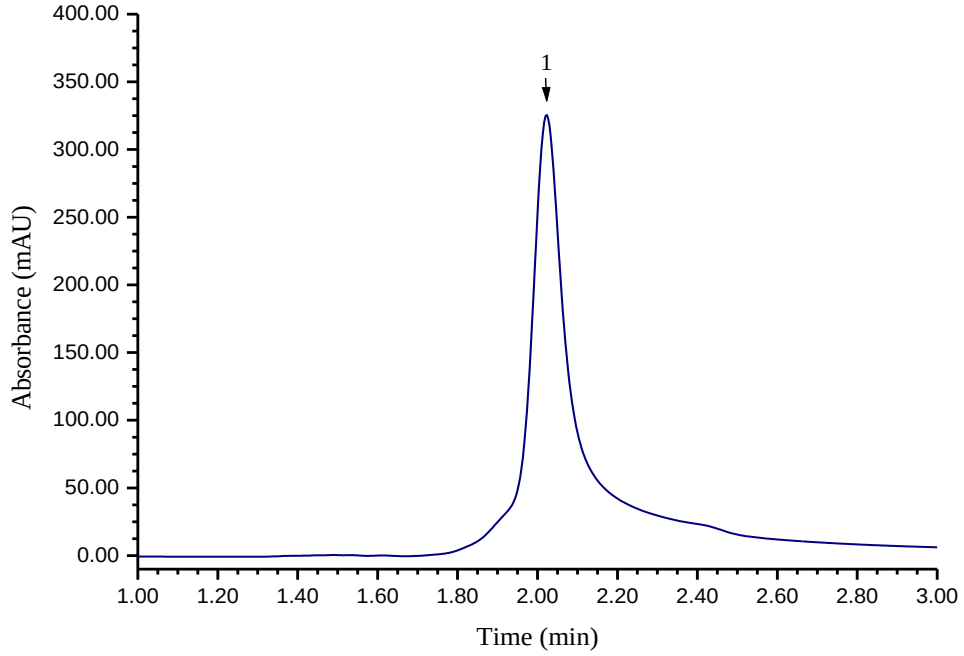

Figure 5.21: HPLC Chromotogram of Oxine (Methanol/Water)

No	**Retention Time (min)**	**Area mAU* min**	**Height mAU**	**Relative Area %**	**Identification**
1	2.023	41.60	326.69	96.50	Oxine

5.9.2 Zirconium Tetrakisoxine

Zirconium tetrakisoxine was dissolved in acetonitrile and HPLC conditions for the identification of the zirconium tetrakisoxine with the use of a Luna 3 column and a mobile phase of methanol and water is as follows;

Column:	Lunar 3 Silica	**Mobile Phase:**	75/25 Methanol/Water
Column Pressure:	125 bar	**Wavelength:**	380 nm
Flow Rate:	1 mL min^{-1}	**Concentration:**	12.8 ppm.
Injection Volume:	10 µL	**Temperature:**	22^{o}C

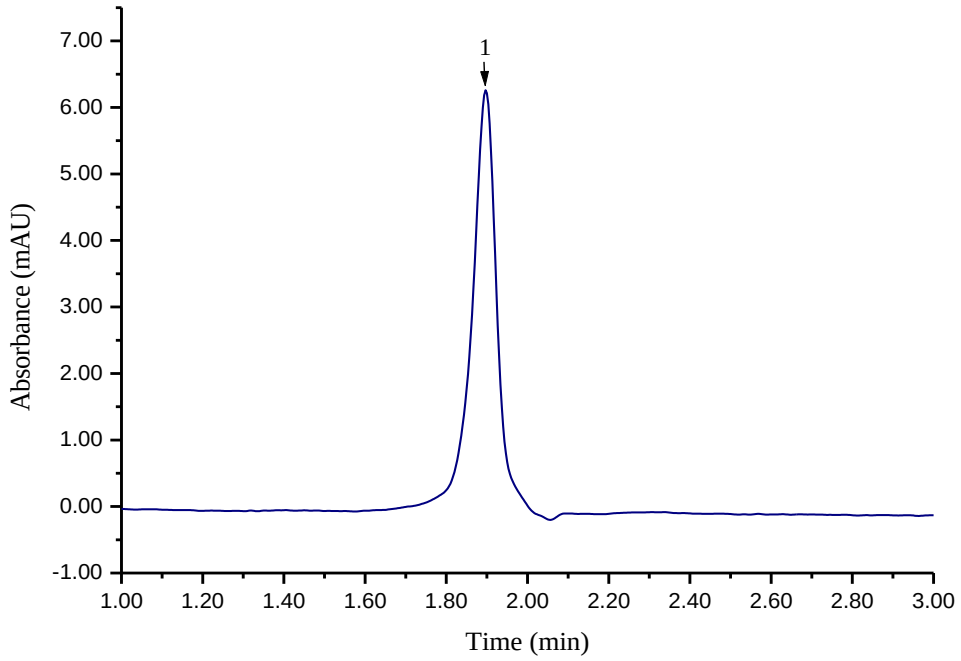

Figure 5.22: HPLC Chromotogram of Zirconium Tetrakisoxine (Methanol/Water)

No	**Retention Time (min)**	**Area mAU* min**	**Height mAU**	**Relative Area %**	**Identification**
1	1.897	0.51	6.39	91.12	Zirconium Tetrakisoxine

5.9.3 Zirconium Tetrakisoxine (Excess Ligand)

Zirconium tetrakisoxine was dissolved in acetonitrile. HPLC conditions for the identification of zirconium tetrakisoxine with a Luna 3 column and excess ligand (concentration 1000ppm) in the mobile phase of methanol and water is as follows;

Column:	Eclipse XDB-C8	**Mobile Phase:**	75/25 Methanol/Water
Column Pressure:	143 bar	**Wavelength:**	380 nm
Flow Rate:	1 mL min^{-1}	**Concentration:**	12.8 ppm.
Injection Volume:	10 µL	**Temperature:**	22°C

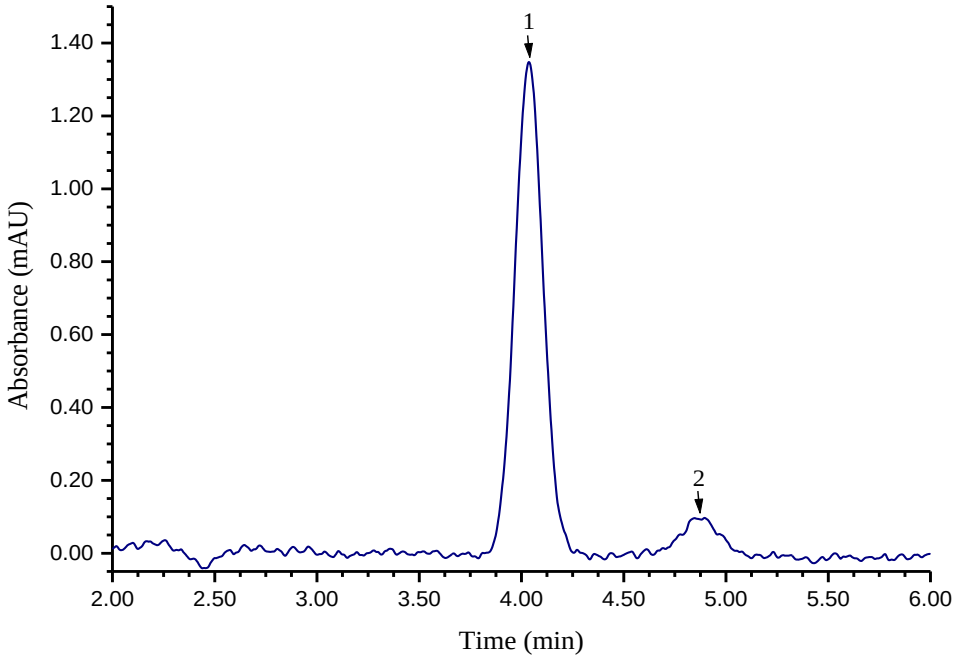

Figure 5.23: HPLC Chromotogram of Zirconium Tetrakisoxine (Methanol/Water + Excess Ligand)

No	**Retention Time (min)**	**Area mAU* min**	**Height mAU**	**Relative Area %**	**Identification**
1	4.037	0.28	1.46	88.91	Zirconium Tetrakisoxine
2	4.897	0.79	0.07	0.002	Unknown

5.9.4 Oxine

A range of columns were tested with the oxine ligand and it was found that the Eclipse XDB-C8 column and a mobile phase of methanol and water could be used to identify the oxine ligand. A Luna 3 silica column was also tested under the same conditions with the zirconium tetrakisoxine complex unsuccessfully.

5.9.5 Zr Tetrakisoxine

It was not possible to analyse the zirconium tetrakisoxine complex with the Eclipse XDB-C8 column with a mobile phase of methanol and water as the complex dissociates under these conditions. It was however possible to identify the oxine ligand utilising a Luna 3 silica without an excess of ligand in the mobile phase.

It was not possible to use this column to separate and identify the zirconium tetrakis complex and any remaining unbound ligand as the ligand itself breaks apart using this column. This column would have been ideal to separate a mixture of both the ligand and complex, as the complex does not dissociate with the Luna 3 silica column and does not require an excess of ligand in the mobile phase.

5.9.6 Zirconium Tetrakisoxine with Excess Ligand

Utilising the Eclipse XDB-C8 column and an excess of ligand in the mobile phase (concentration 1000 ppm) it was possible to stabilise the zirconium complex during the HPLC analysis. An excess of ligand in the mobile phase results in problems when trying to quantify the complex and any remaining unbound ligand for quality control purposes and as such further methods that have been undertaken are reported.

The following experiments were conducted to use a single HPLC column to separate the free oxine ligand and complex without an excess of ligand in the mobile phase.

5.10 HPLC Analysis with a Mobile Phase of Acetonitrile and Water anda Alima C18 Micron Column

5.10.1 Oxine

Oxine was dissolved in acetonitrile and HPLC conditions for the identification of oxine with the use of an Altima C18 column and a mobile of water + 0.1% formic acid and acetonitrile is as follows;

Column:	Altima C18 Micron	**Mobile Phase:**	50/50 Acetonitrile/Water
Column Pressure:	120 bar	**Wavelength:**	245 nm
Flow Rate:	2 mL min^{-1}	**Concentration:**	128 ppm.
Injection Volume:	10 µL	**Temperature:**	23^{o}C

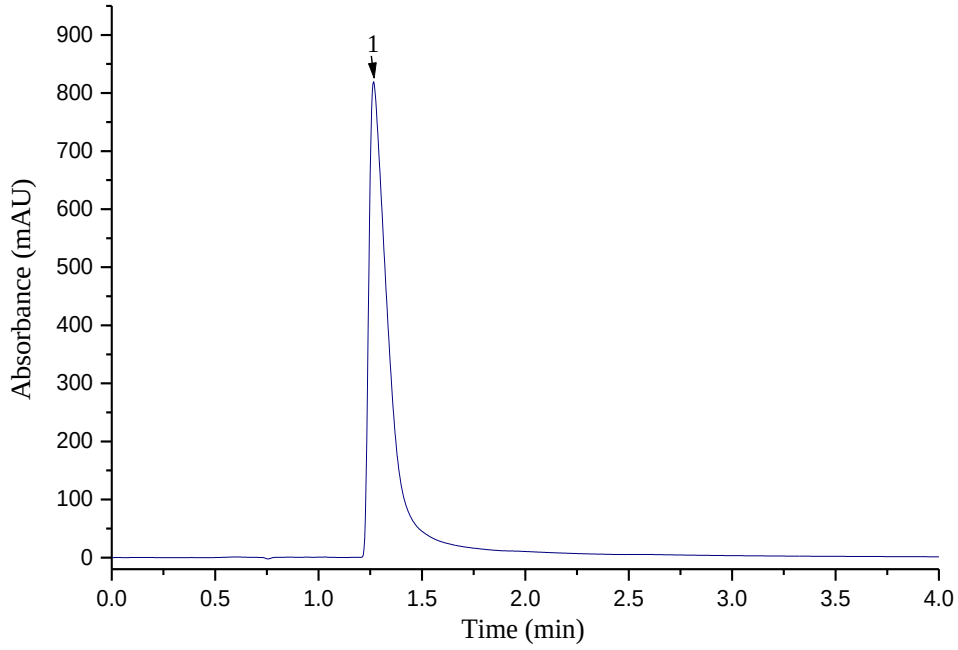

Figure 5.24: HPLC Chromotogram of Oxine (Acetonitrile/Water, Altima C18 Column)

No	Retention Time (min)	Area mAU* min	Height mAU	Relative Area %	Identification
1	1.267	0.25	816.290	93.51	Oxine

5.10.2 Zirconium Tetrakisoxine

Zirconium tetrakisoxine was dissolved in acetonitrile and HPLC conditions for the identification of zirconium tetrakisoxine with the use of an Altima C18 column and a mobile of water + 0.1% formic acid and acetonitrile is as follows;

Column:	Altima C18 Micron	**Mobile Phase:**	50/50 Acetonitrile/Water
Column Pressure:	124 bar	**Wavelength:**	245 nm
Flow Rate:	2 mL min^{-1}	**Concentration:**	128 ppm.
Injection Volume:	10 µL	**Temperature:**	23^{o}C

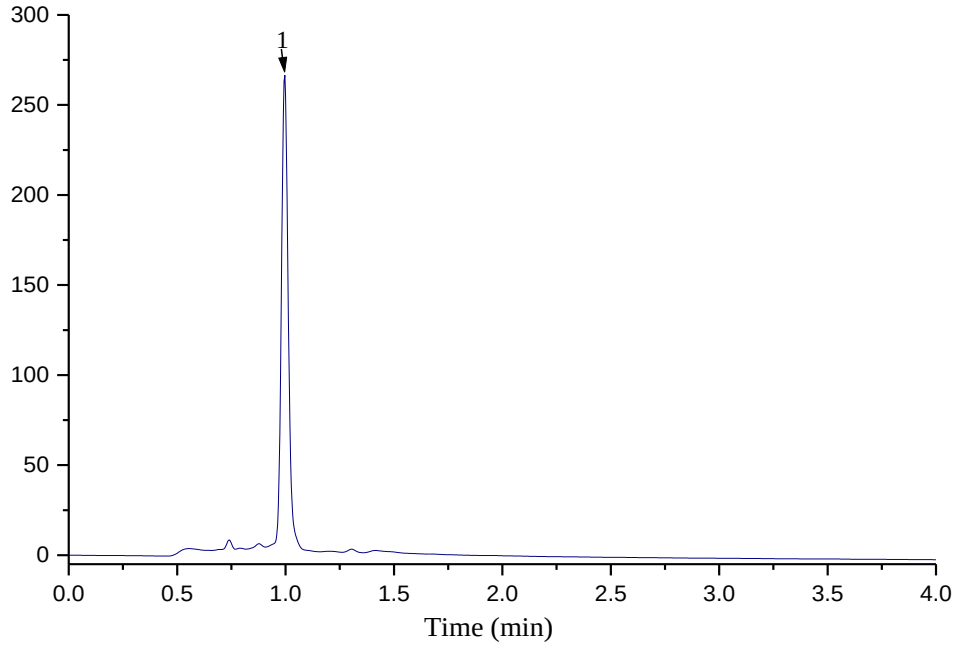

Figure 5.25: HPLC Chromotogram of Zirconium Tetrakisoxine (Acetonitrilel/Water + Altima C18 Column)

No	**Retention Time (min)**	**Area mAU* min**	**Height mAU**	**Relative Area %**	**Identification**
1	0.997	1.12	267.50	100.00	Zirconium Tetrakisoxine

5.10.3 Oxine and Zirconium Tetrakisoxine (Mixture)

Oxine and zirconium tetrakisoxine was dissolved in acetonitrile and HPLC conditions for the separation and identification of oxine and zirconium tetrakisoxine with the use of an Altima C18 column and a mobile phase of acetonitrile and water is as follows;

Column:	Altima C18 Micron	**Mobile Phase:**	50/50 Acetonitrile/Water
Column Pressure:	124 bar	**Wavelength:**	245 nm
Flow Rate:	2 mL min^{-1}	**Concentration:**	64 ppm.
Injection Volume:	10 µL	**Temperature:**	23^{o}C

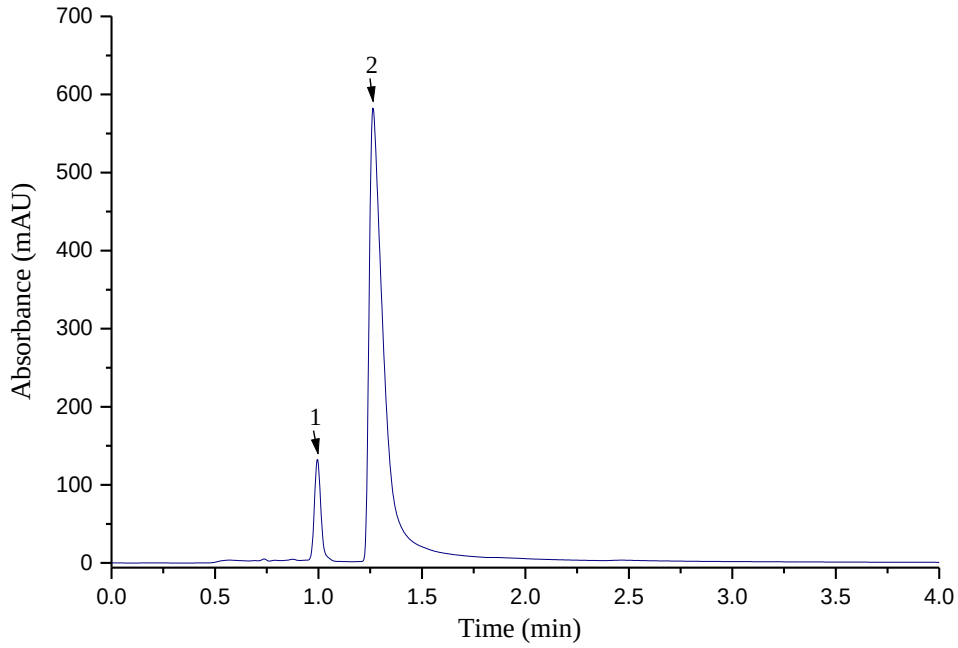

Figure 5.26: HPLC Chromotogram of Oxine and Zirconoum Tetrakisoxine (Mixture) (Acetonitrile/Water + Altima C18 Column)

No	Retention Time (min)	Area mAU* min	Height mAU	Relative Area %	Identification
1	0.997	0.0226	128.077	16.06	Zirconium Tetrakisoxine
2	1.267	0.1183	585.400	83.94	Oxine

5.10.4 Formic Acid

Formic acid has been added to the mobile phase in several experements to alter the pH of the water portion of the mobile phase to ~3.5. This greatly reduces interactions between the ligand and the complex which results in reduced peak tailing.

5.10.5 Oxine

It was possible to identify the oxine ligand utilising the Altima C18 Micron HPLC column and a mobile phase of acetonitrile and water. The most efficient ratio of the mobile phase was found to be 50 % acetonitrile and 50 % water. An increase or decrease of acetonitrile caused the complex peak to become less pronounced.

5.10.6 Zirconium Tetrakisoxine

It was possible to separate and identify both the zirconium tetrakisoxine complex and the oxine ligand utilising the Altima C18 Micron HPLC column and a mobile phase of acetonitrile and water. The most efficient ratio of the mobile phase was found to be 50 % acetonitrile and 50 % water. The complex is stable with a mobile phase of acetonitrile and water with an Altima C18 Micron HPLC column so it was not been necessary to add an excess of the oxine ligand into the mobile phase. This in turn will allow the separation, identification and quantification of the ligand and complex for quality control purposes.

5.10.7 A Mixture of Oxine and Zirconium Tetrakisoxine

A mixture of oxine and zirconium tetrakisoxine was successfully separated using the Altima C18 Micron HPLC column and a 50:50 ratio of water and acetonitrile mobile phase. As such this column and mobile phase can be used to separate the oxine ligand and zirconium tetrakisoxine complex. The HPLC UV-Vis detector was set to a wavelength of 245 nm for the analysis of the oxine ligand, zirconium tetrakisoxine complex and a mixture of the two. This wavelength encompasses both the ligand and the complex and as such this single wavelength can be used to identify both.

5.11 Oxine and Zirconium Tetrakisoxine Discussion

5.11.1 Oxine

Detection of the ligand can be conducted under a variety of conditions with excellent results. The majority of the columns used throughout these experiments could be used to identify the ligand with peaks that show the complex in a stable condition. The main column that caused problems with the analysis of the ligand was a Phenomenex Luna 3 silica. The XDB C8 and Altima C18 columns are the best choice for the analysis of the ligand, and the UV-Vis detector shows the best responses at settings of 308 nm for oxine and 245 or 380 nm for zirconium tetrakisoxine.

5.11.2 Zirconium Tetrakisoxine

The Phenomenex Luna 3 silica and Altima C18 column are the best choices for the analysis on the complex without any excess ligand in the mobile phase. The UV-Vis detector shows the best response at a setting of 380 nm. The wavelengths were chosen for the identification of the complex without excess ligand as they provided the clearest chromatogram of the complex at various concentrations. To ensure that the ligand was not being detected a range of experiments were conducted under the same conditions with only the free ligand. The resulting chromatograms were different in both retention times and smoothness of the peaks. It would appear that the free ligand has problems passing through the Luna 3 silica column perhaps due to the nature of it being un-bound. The chromatogram using an Altima C18 column shows one peak indicating the complex is stable with this column. In the majority of the experiments conducted without excess ligand, with a variety of columns and conditions it was found that the complex itself was prone to dissociate. A number of peaks indicated a result of the complex breaking apart into its constituent ligands.

However this was rectified with addition of excess ligand to the mobile phase or the use of an Altima C18 column. The excess ligand stabilises the complex so accurate and reproducible retention times can be determined using the DBX C8 column.

5.11.3 Zirconium Tetrakisoxine (Excess Ligand in Mobile Phase)

The addition of excess ligand in the mobile phase proved to be very problematic. Problems such as inconstant baselines and problems running blanks occurred. (Baseline problems are common when using inconsistent or contaminated solvents). The ligand constantly passing through the detector caused problems when setting the base line or running a blank due to inconsistent detection parameters.

Variables were altered to take into consideration the excess of ligand in the mobile phase. A blank was run in-between every attempted analysis of the zirconium tetrakisoxine with excess ligand to try and reduce detection problems. In many cases this resulted in peaks which were unexpected.

These unexpected peaks suggest that the zirconium ion and ligand have an affinity for a variety of columns and as such it is imperative that each of the columns is thoroughly flushed with a strong solvent between runs. It is suggested that approximately 10 columns worth will ensure the column has had any unwanted analytes removed.

When analysing the zirconium tetrakisoxine with an excess of ligand in mobile phase (x10 concentration of complex) it was found that the best column for analysis was the DBX C8. The optimum wavelength for analysis of the complex with excess of ligand was 380 nm once a number of blanks had been run.

Retention times for the ligand and the complex (with excess ligand in the mobile phase) differed with the ligand having a retention time of 1.960 minutes and the complex having a retention time of 2.960 minutes when utilising the following conditions; DBX C8 HPLC column, 75/25 acetonitrile/water, 22^{o}C, and a flow rate of 1mL per minute. However as there was an excess of ligand in the mobile phase it was not possible to separate and quantify the amount of ligand and complex in a sample hence another method was found to rectify this problem.

5.11.4 Mixture of Oxine and Zirconium Tetrakisoxine

It was not possible to separate the oxine ligand and zirconium tetrakisoxine complex with the Eclipse HPLC column and a mobile phase of acetonitrile and water. It was also not possible to separate these two analytes utilizing the Luna 3 silica column.

Using an Altima C18 column with the addition of a buffer (formic acid 0.1%), altering the pH of the water portion of the mobile phase to ~3.5 greatly reduced interactions between the ligand and the complex resulting in reduced peak tailing. This method also allowed the separation of both the ligand and complex without the addition of excess ligand in the mobile phase illustrated in figure 5.2.10.

5.11.5 Column Types

A number of HPLC columns were tested against the oxine ligand and the zirconium tetrakisoxine complex. The Eclipse XDB-C8 HPLC column has a solid support of fully porous silica and a stationary phase of C8.[192] It was not possible to analyse the complex with this column without an excess of ligand in the mobile phase but it was possible to analyse the ligand. This is possibly due to the Zr being stripped from the ligands as there seems to be an affinity with Zr and this column.

The Luna 3 Silica HPLC column has a solid support of fully porous silica and stationary phase of ultra-pure unbonded silica[193] with high column bed stability which is enhanced by partial shape uniformity.[194] Used in the separation of polar compounds it would be expected that the analysis of the ligand would be possible with this column as it is polar and the complex which is not polar would be problematic. However the reverse is true and at this time is not fully understood.

The Altima C18, 5u Micron HPLC column uses a pH stable silica of high purity and low metal and is ideal for analysis of complex hydrophobic mixtures.[195] The Altima HPLC column was manufactured to eliminate activated silanols that cause peak tailing on silica-based columns.[196] The elimination of the activate silanols may prevent the Zr complex from breaking apart into its substituents.

5.12 Results: Tropolone and Zirconium Tetrakistropolone

5.12.1 Tropolone

Tropolone was dissolved in methanol and HPLC conditions for attempted identification of tropolone with the use of a Luna 3 Silica column and a mobile phase of acetonitrile and water are as follows:

Column:	Luna 3 Silica	**Mobile Phase:**	90/10 Acetonitrile/Water
Column Pressure:	125 bar	**Wavelength:**	333 nm
Flow Rate:	1 mL min^{-1}	**Concentration:**	12.7 ppm.
Injection Volume:	10 µL	**Temperature:**	22^{o}C

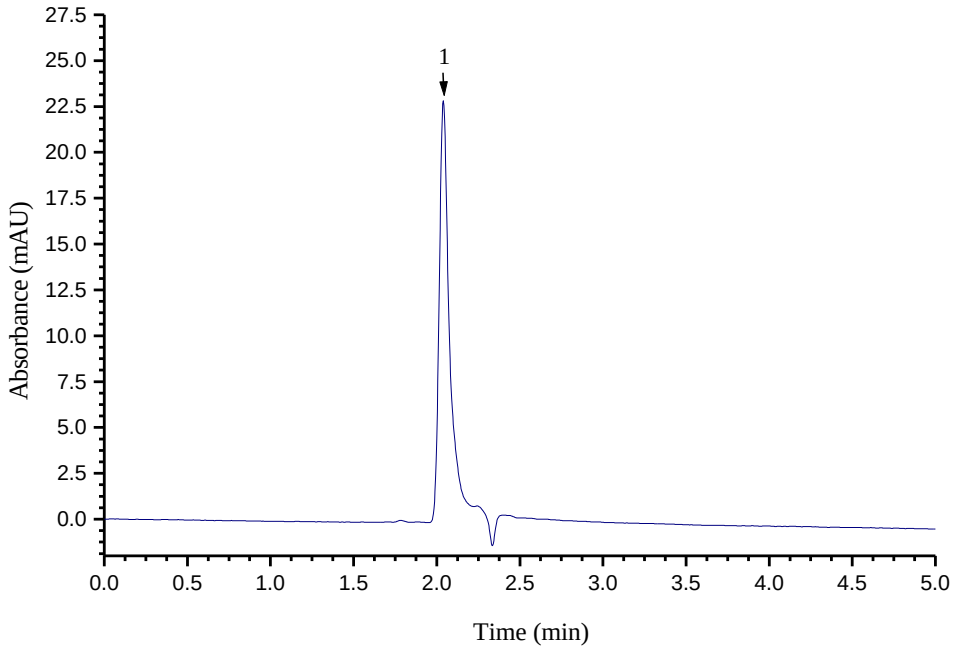

Figure 5.27: HPLC Chromotogram of Tropolone (Acetonitrile/Water)

No	**Retention Time (min)**	**Area mAU* min**	**Height mAU**	**Relative Area %**	**Identification**
1	2.040	1.967	24.077	95.51	Tropolone

5.12.2 Zirconium Tetrakistropolone

Zirconium tetrakistropolone was dissolved in methanol and HPLC conditions for attempted identification of the Zr tetrakistropolone with the use of a Luna 3 Silica column and a mobile phase of acetonitrile and water are as follows:

Column:	Luna 3 Silica	**Mobile Phase:**	90/10 Acetonitrile/Water
Column Pressure:	125 bar	**Wavelength:**	333 nm
Flow Rate:	1 mL min^{-1}	**Concentration:**	12.7 ppm.
Injection Volume:	10 µL	**Temperature:**	22^{o}C

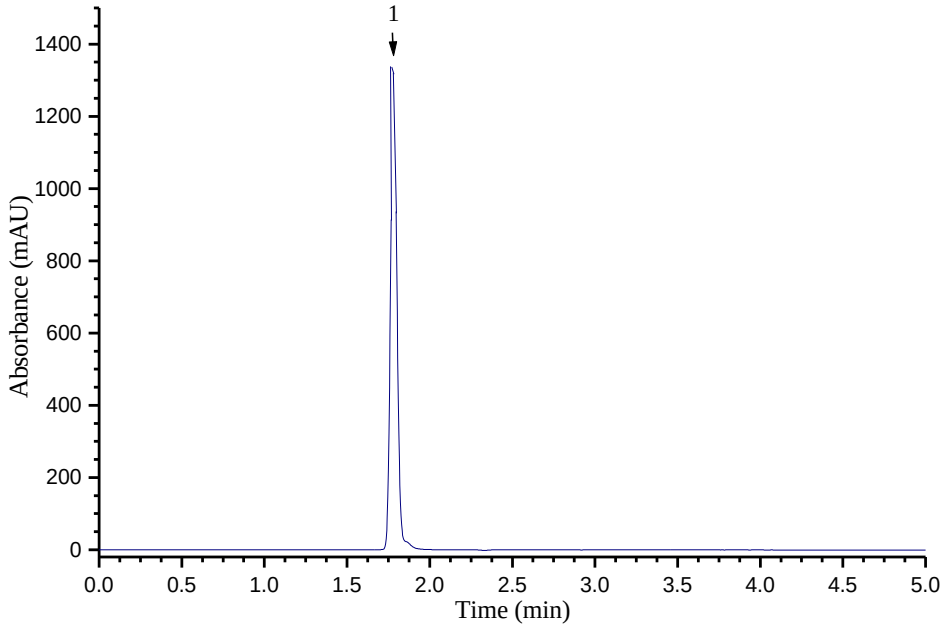

Figure 5.28: HPLC Chromotogram of Zirconium Tetrakistropolone (Acetonitrile/Water)

No	**Retention Time (min)**	**Area mAU* min**	**Height mAU**	**Relative Area %**	**Identification**
1	1.780	59.835	1339.00	99.26	Zirconium Tetrakistropolone

5.12.3 Mixture of Tropolone and Zirconium Tetrakistropolone

Tropolone and zirconium tetrakistropolone was dissolved in methanol and HPLC conditions for the separation and identification of tropolone and zirconium tetrakistropolone from a mixture using a Luna 3 Silica column and a mobile phase of water and acetonitrile are as follows;

Column:	Luna 3 Silica	**Mobile Phase:**	90/10 Acetonitrile/Water
Column Pressure:	125 bar	**Wavelength:**	333 nm
Flow Rate:	1 mL min^{-1}	**Concentration:**	6.35 ppm.
Injection Volume:	10 µL	**Temperature:**	22^{o}C

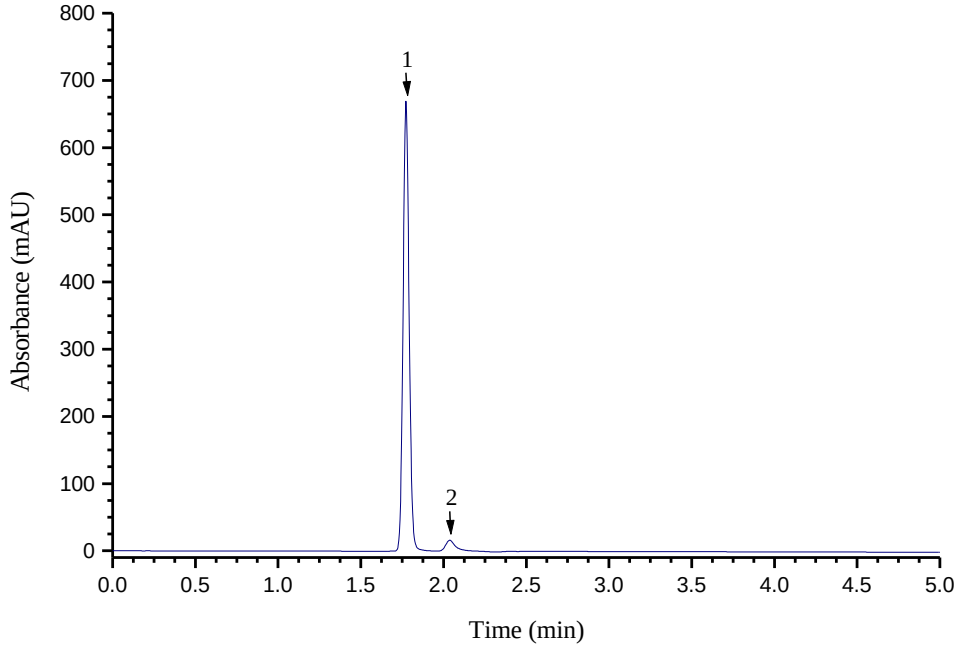

Figure 5.29: HPLC Chromotogram of Tropolone and Zirconium Tetrakistropolone (Mixture), (Acetonitrile/Water)

No	**Retention Time (min)**	**Area mAU* min**	**Height mAU**	**Relative Area %**	**Identification**
1	1.773	28.644	670.361	90.63	Zirconium Tetrakistropolone
2	2.037	1.389	17.395	4.39	Tropolone

5.13 Discussion of Results

5.13.1 Tropolone

The majority of the columns used throughout these experiments could be used to identify the ligand. The Luna 3 silica HPLC-RP column is the best choice for the analysis of tropolone. Optimum conditions to obtain a retention time of 1.967 minutes were obtained with a flow rate of 1mL a minute, 22^{o}C column temperature, 10% Water and 90% Acetonitrile. In the chromatogram under these conditions a negative peak can bee seen just after the peak of tropolone. This is because the less absorbing solvent has passed the detector in which the tropolone has been dissolved.

5.13.2 Zirconium Tetrakistropolone

The HPLC analysis of zirconium tetrakistropolone was undertaken and was found to be problematic. Results show that various HPLC columns strip the ligand from the Zr metal. For example a commonly used HPLC column such as the Eclipse XDB-C8 will strip the ligand from the Zr metal resulting in a retention time of only the free ligand. This is under a variety of temperatures, flow rates, pressures and mobile phase constituents. Various HPLC columns were used to resolve the stripping of the ligand from the complex. The optimum column for the analysis of the zirconium tetrakistropolone was found to be a Phenomenex Luna 3 SILICA (2), 150 X 4.60 mm, 3 MICRON, 00F-4162-E0 with a retention time of 1.780 minutes, flow rate of 1mL a minute, 22^{o}C column temperature, 90% Water and 10% Acetonitrile.

5.13.3 Mixture of Tropolone and Zirconium Tetrakistropolone

Utilising the Phenomenex Luna 3 SILICA (2), 150 X 4.60 mm, 3 MICRON, 00F-4162-E0 HPLC-RP column it is possible to separate the tropolone ligand and the zirconium tetrakistropolone complex. A retention time of 1.773 minutes was achieved for the zirconium tetrakis complex and 2.037 minutes for the tropolone ligand. Figure 5.2.13 indicates a clear separation of both the ligand and the complex when in a mixture. Conditions for this separation are a flow rate of 1mL a minute, 22^{o}C column temperature, 90% Water and 10% Acetonitrile.

5.14 Results Ethyl Maltol and Zirconium Tetrakisethyl Maltol

5.14.1 Ethyl Maltol

Ethyl maltol was dissolved in acetonitrile and HPLC conditions for the identification of ethyl maltol with the use of an Altima C18 5 micron column and a mobile phase of water with 0.1% formic acid buffer and acetonitrile are as follows.

Column:	Altima C18 Micron	**Mobile Phase:**	80/20 Water/Acetonitrile
Column Pressure:	118 Bar	**Wavelength:**	278 nm
Flow Rate:	2 mL min^{-1}	**Concentration:**	12.7 ppm.
Injection Volume:	10 µL	**Temperature:**	35°C

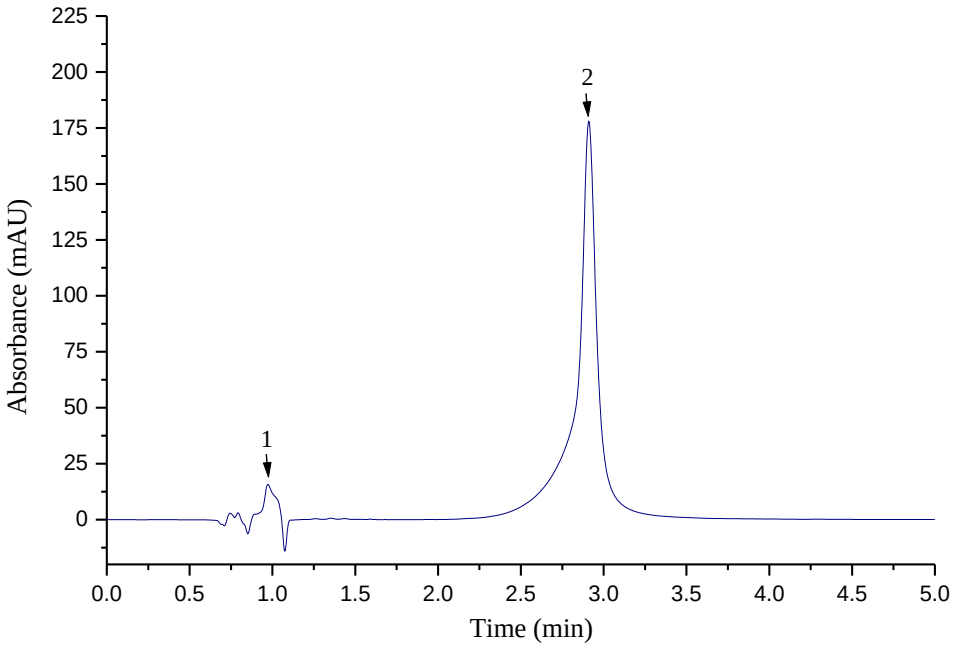

Figure 5.30: HPLC Chromotogram of Ethly Maltol (Acetonitrile/Water)

No	Retention Time (min)	Area mAU* min	Height mAU	Relative Area %	Identification
1	0.967	1.70	28.97	1.48	Unknown
2	2.887	92.90	177.16	80.99	Ethyl Maltol

.

5.14.2 Zirconium Tetrakisethyl Maltol

Zirconium tetrakisethyl maltol was dissolved in acetonitrile and HPLC conditions for the identification of the zirconium tetrakisethyl maltol with the use of an Altima C18 5 micron column and a mobile phase of water with 0.1% formic acid buffer and acetonitrile are as follows;

Column:	Altima C18 Micron	**Mobile Phase:**	80/20 Water/Acetonitrile
Column Pressure:	118 bar	**Wavelength:**	278 nm
Flow Rate:	2 mL min^{-1}	**Concentration:**	127 ppm.
Injection Volume:	10 µL	**Temperature:**	35^{o}C

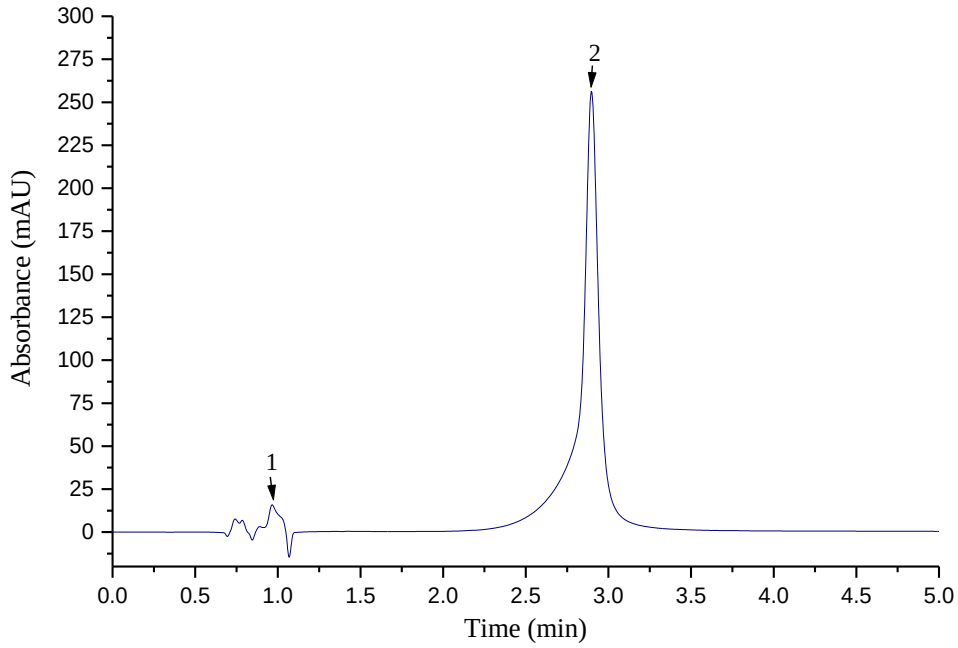

Figure 5.31: HPLC Chromotogram of Zirconium Tetrakisethyl Maltol (Acetonitrile/Water)

No	**Retention Time (min)**	**Area mAU* min**	**Height mAU**	**Relative Area %**	**Identification**
1	0.973	1.69	13.79	0.58	Unknown
2	2.910	49.08	254.32	89.28	Zirconium Tetrakisethyl maltol

5.14.3 Mixture of Ethylmaltol and Zirconium Tetrakisethyl Maltol

Ethyl maltol and zirconium tetrakisethyl maltol was dissolved in acetonitrile and HPLC conditions for the attempted separation and identification of ethyl maltol and zirconium tetrakisethyl maltol from a mixture using an Altima C18 5 micron column and a mobile phase of water and acetonitrile are as follows;

Column:	Altima C18 Micron	**Mobile Phase:**	80/20 Water/Acetonitrile
Column Pressure:	118 bar	**Wavelength:**	278 nm
Flow Rate:	2 mL min^{-1}	**Concentration:**	127 ppm.
Injection Volume:	10 µL	**Temperature:**	35°C

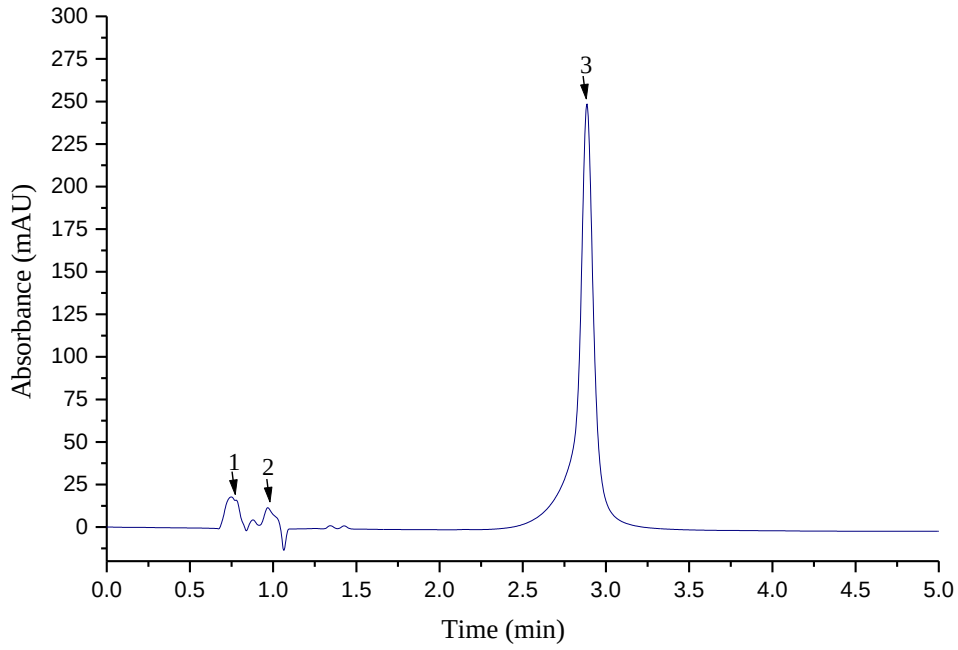

Figure 5.32: HPLC Chromotogram of Ethylmaltol and Zirconium Tetrakisethyl Maltol (Mixture), (Acetonitrile/Water)

No	**Retention Time (min)**	**Area mAU* min**	**Height mAU**	**Relative Area %**	**Identification**
1	0.750	4.03	27.38	4.48	Unknown
2	0.967	1.51	23.82	1.68	Unknown
3	2.887	67.28	259.75	74.72	Mixture

5.15 Discussion of Results

5.15.1 Ethyl Maltol

When analysing ethyl maltol an addition of a buffer (formic acid 0.1 %) is required to ensure its stability. The majority of the columns used throughout these experiments could not be used to identify the ligand with peaks indicating that the complex had broken apart. The Altima C18 5 Micron HPLC-RP column is the best choice for the analysis of the ethyl maltol ligand. Optimum conditions to obtain a retention time of 2.877 minutes was obtained with a flow rate of 2mL a minute, 35^{o}C column temperature, 80% water + 0.1% formic acid and 20% acetonitrile.

5.15.2 Zirconium Tetrakisethyl maltol

Results show that the retention time for the supposed zirconium tetrakisethyl maltol complex 2.910. This retention time is extremely close to the retention time of the ethyl maltol ligand and as such it is not possible to identify the complex using a UV detector. A variety of columns, temperatures, flow rates, pressures and mobile phase constituents were screened in an attempt to increase the differences in the retention times of both the ligand and the complex without success. It is possible that the ligands are being stripped from the Zr metal resulting in the detection of just the ligands. With a HPLC mass spectrometer system it may be possible to determine whether the retention time of 2.910 relates to the complex or the ligand. The optimum column for the possible identification of the complex is Altima C18 5 Micron with a retention time of 2.910 minutes, flow rate of 2mL a minute, 35^{o}C column temperature, 80% water + 0.1% formic acid and 20% acetonitrile.

5.15.3 Mixture of Ethylmaltol and Zirconium Tetrakisethyl maltol

It has not been possible to separate the two with the equipment that is currently available. Other HPLC columns with different types of stationary phase and different size of partials may rectify this problem and allow the separation of the two analytes. A column that may rectify this problem is a Cadenza CW-C18, specifically used in the food industry for analysis of maltol and ethyl maltol.[197]

5.16 Results: Deferiprone and Zirconium Tetrakisdeferiprone

5.16.1 Deferiprone

Deferiprone was dissolved in water and HPLC conditions for the identification of deferiprone using an Altima C18 column and a mobile phase of water with 0.1% formic acid buffer and acetonitrile are as follows;

Column:	Altima C18 Micron	**Mobile Phase:**	50/50 Acetonitrile/Water
Column Pressure:	124 bar	**Wavelength:**	282 nm
Flow Rate:	2 mL min^{-1}	**Concentration:**	127 ppm.
Injection Volume:	10 µL	**Temperature:**	23.5°C

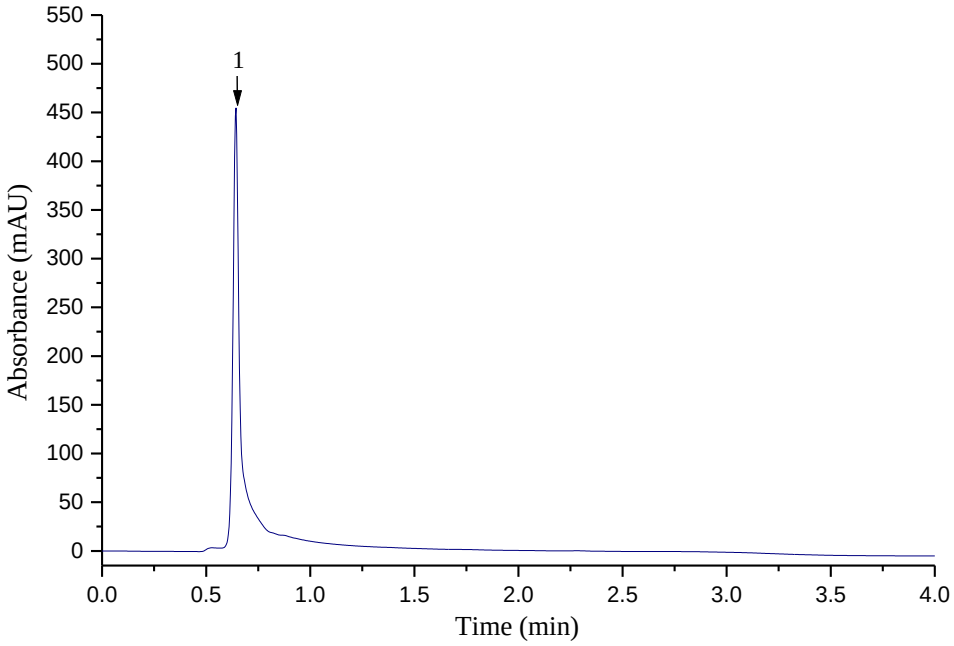

Figure 5.33: HPLC Chromotogram of Deferiprone (Acetonitrile/Water)

No	**Retention Time (min)**	**Area mAU* min**	**Height mAU**	**Relative Area %**	**Identification**
1	0.630	20.96	463.93	99.08	Deferiprone

5.16.2 Zirconium Tetrakisdeferiprone

Zirconium tetrakisdeferiprone was dissolved in water and HPLC conditions for the identification of zirconium tetrakisdeferiprone using an Altima C18 column and a mobile phase of water with 0.1% formic acid buffer and acetonitrile are as follows;

Column:	Altima C18 Micron	**Mobile Phase:**	50/50 Acetonitrile/Water
Column Pressure:	123 bar	**Wavelength:**	282 nm
Flow Rate:	2 mL min^{-1}	**Concentration:**	127 ppm.
Injection Volume:	10 µL	**Temperature:**	23.5^{o}C

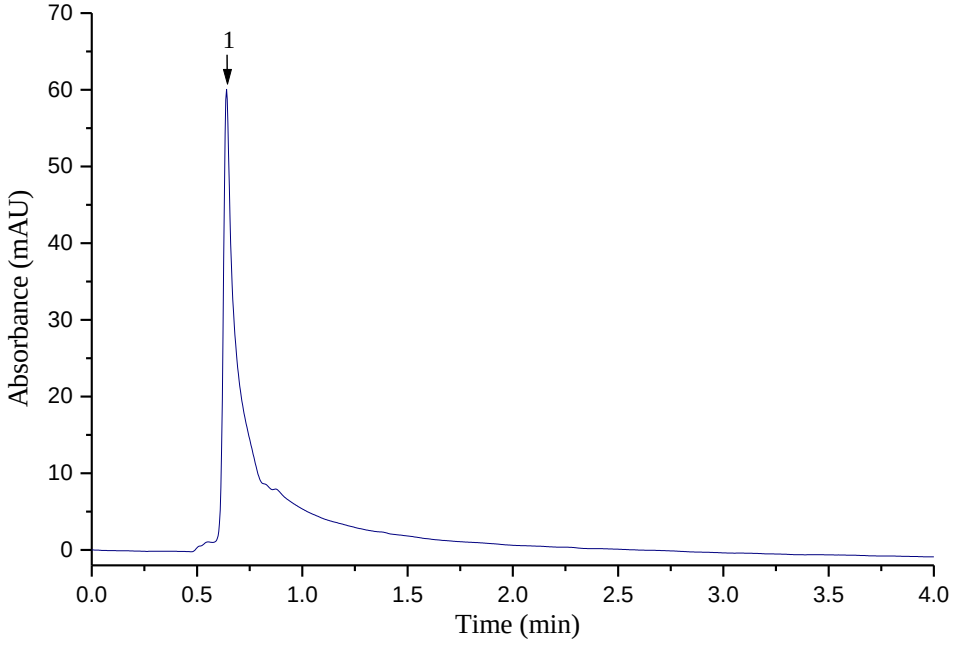

Figure 5.34: HPLC Chromotogram of Zirconium Tetrakisdeferiprone (Acetonitrile/Water)

No	**Retention Time (min)**	**Area mAU* min**	**Height mAU**	**Relative Area %**	**Identification**
1	0.649	7.55	60.31	95.86	Zirconium Tetrakisdeferiprone

5.16.3 Mixture of Deferiprone and Zirconium Tetrakisdeferiprone

Deferiprone and zirconium tetrakisdeferiprone was dissolved in water and HPLC conditions for the attempted separation and identification of deferiprone and zirconium tetrakisdeferiprone from a mixture using an Altima C18 column and a mobile phase of water with 0.1% formic acid buffer and acetonitrile are as follows;

Column:	Altima C18 Micron	**Mobile Phase:**	50/50 Acetonitrile/Water
Column Pressure:	123 bar	**Wavelength:**	282 nm
Flow Rate:	2 mL min^{-1}	**Concentration:**	63.5 ppm.
Injection Volume:	10 µL	**Temperature:**	23.5^{o}C

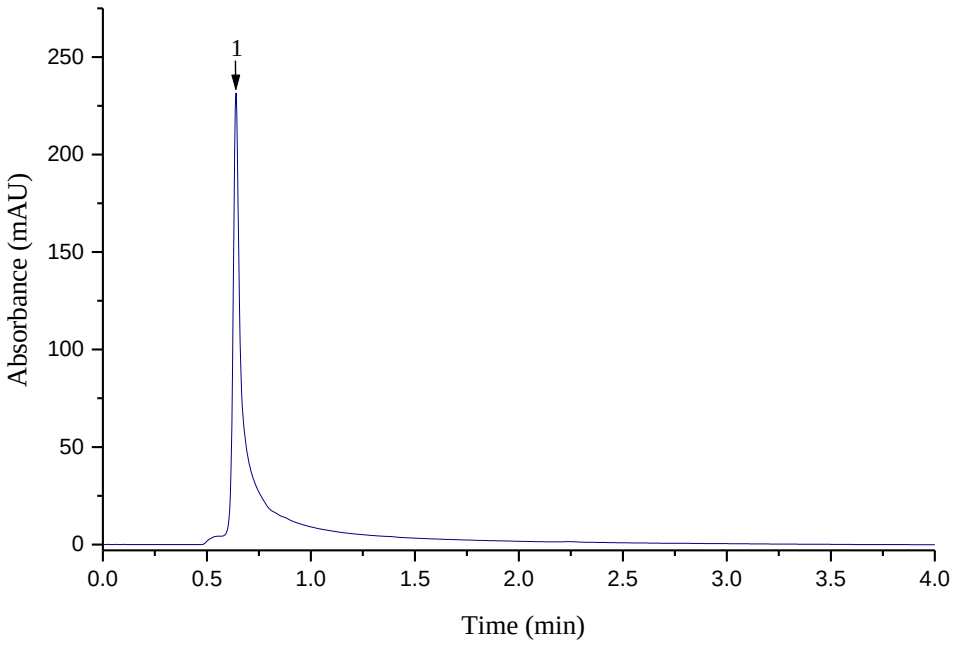

Figure 5.35: HPLC Chromotogram of Deferiprone and Zirconium Tetrakisdeferiprone (Mixture), (Acetonitrile/Water)

No	**Retention Time (min)**	**Area mAU* min**	**Height mAU**	**Relative Area %**	**Identification**
1	0.640	13.11	235.87	95.57	Mixture

5.17 Discussion of Results

5.17.1 Deferiprone

Analysis of deferiprone requires the addition of formic acid at a concentration of 0.1% into the water component of the mobile phase to ensure its stability. The Altima C18 5 Micron HPLC-RP column is the best choice for the analysis of the deferiprone ligand. Optimum conditions to obtain a retention time of 0.630 minutes was obtained with a flow rate of 2mL a minute, 23.5^{o}C column temperature, 50% Water + 0.1% formic acid and 50% Acetonitrile.

5.17.2 Zirconium Tetrakisdeferiprone

The retention time for the supposed zirconium tetrakisdeferiprone complex is 0.649 minutes. This retention time is extremely close to the retention time of the deferiprone ligand and hence it is not possible to confidently identify the complex using a UV detector. There is a greater amount of tailing, comparing the ligand to the complex which suggests different compounds. Various columns, temperatures, flow rates, pressures and mobile phase constituents were used in an attempt to increase the differences in the retention times of both the ligand and the complex without success. By using a HPLC mass spectrometer system it may be possible to confirm that it is the complex that is exiting the HPLC column at 0.649 and not the ligand. The optimum column for the possible identification of the complex is an Altima C18 5 Micron with a flow rate of 2mL a minute, 23.5^{o}C column temperature, 50% Water + 0.1% formic acid and 50% Acetonitrile.

5.17.3 Deferiprone and Zirconium Tetrakisdeferiprone

The relatively short retention times of the analytes suggests that there is minimal interaction of both the ligand and complex with the stationary phase in the column. As the retention times of the ligand and the supposed complex are very similar it has not been possible to separate the two with the equipment that is currently available. Utilising other HPLC columns with different types of stationary phase and different size of partials may rectify this problem and allow the separation of the two analytes.

5.18 HPLC Variables

A range of variables were investigated to provide a means of identifying each of the ligands and their respective zirconium tetrakis complexes. Variables were altered in the process of determining the best protocol for identifying the ligand, complex and complex with excess ligand (if necessary). Column type, mobile phase, temperature, flow rate, concentrations and injection volumes were all investigated. These are standard variables for HPLC method development.

5.18.1 Column Type

A range of columns were tested against the complexes during the experiments and the following columns yielded the best results; Alltech Nucleosil C18 5 Micron, Agilent Eclipse XDB-C8, Altima C18 5u, Phenomenex Luna 3 Silica, and Phenomenex Luna 5u Phenyl-Hexyl.

5.18.2 Mobile Phase

It is preferable to use a solvent to dissolve the compounds which will be used as a mobile phase during the HPLC analysis.[198] This will reduce interference and unwanted peaks during the analysis. Acetonitrile, methanol and water were the optimum mobile phases used during the experiments. Tetrahydrofuran was tested as a mobile phase with the oxine ligand and complex unsuccessfully.

5.18.3 Temperature

Increasing the temperature will decrease the retention time of a solute (k). In the majority of systems a decrease in retention time will not be greater than 50% of the analytes reduced retention time at ambient temperature.[198] It was seen with the ligands and Zr tetrakis complexes that once the column had been stabilized under an elevated temperature stabilization of retention times occurred. Controlled temperatures resulted in the improvement of peak shapes and faster experimental run times without impacting the efficiency of the experiments conducted.

5.18.4 Flow rate

Increasing the flow rate of the mobile phase decreases the time taken for analytes to pass through the HPLC apparatus resulting in sharper improved peaks. However when analysing a ligand and suspected complex the flow rate was decreased to the minimum possible in an attempt to separate the retention times between the two.

5.18.5 Concentrations

Increasing the concentrations of the ligand and complex resulted in an increase in peak height and area with the same retention time being upheld. By using a range of concentrations it was confirmed that it was the ligand and complex being identified

5.18.6 Buffers and pH

An addition of formic acid at a concentration of 0.1% into the water portion of the mobile phase resulted in greater stability of the complexes but had little effect on the analysis of the ligands. The buffer reduces the interaction of the complex with any residual silanol groups/active sites on the stationary phase of the HPLC column.

5.18.7 Injection Volumes

When the injection volume was increased from 10 µl to 20 µl the peak-width increased greatly and a significant increase in tailing occurred indicating interactions with the analytes and stationary phase of the HPLC column. To reduce this interaction it was decided to analyse all analytes with an injection volume of 10 µl.

5.18.8 UV-Vis Detector Settings

By using the UV-Vis data of the ligand and the complex reported in section 5.1 it was possible to set the detector at the optimum wavelengths to identify the ligands and complexes. The baseline was observed before the injection and following it to monitor the quality of the mobile phase and the condition of the column.

5.18.9 Ligand and Complex Peak Identification

It was determined that the optimum method of proving the peak was actually the complex and not an anomaly was to run a serial dilution of the complex through the HPLC apparatus. An increase in the concentration of complex will result in an increase in peak height and area with the same retention time being upheld. It was decided to run a range of concentrations of both the ligands and the complex. The results from this experiment allowed the ligand and complex peak to be identified and verified. From the positive results from the serial dilution experiments it was possible to identify the most useful wavelengths in partnership with the UV-Vis data and to identify the ligand and complex depending on the mobile phase and column used as well when there is an excess of ligand in the mobile phase as is required when analysing Zr tetrakisoxine.

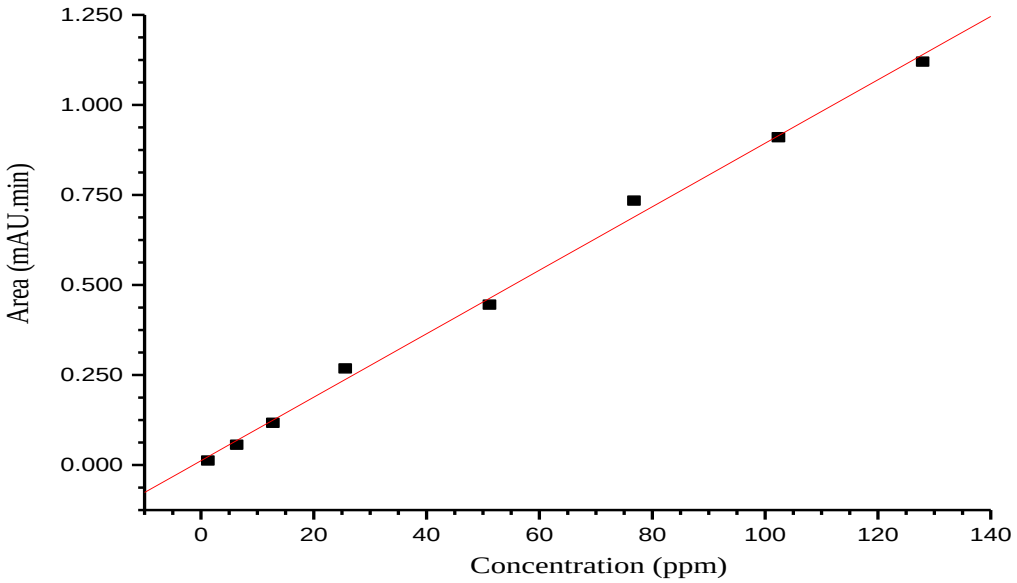

Figure 5.36: Concentration *vs* Peak Area of Zirconium Tetrakisoxine

y=0.00881x0.01207 R-Squared Value = 0.99835

5.19 Conclusion

5.19.1 Oxine & Zirconium Tetrakisoxine

The optimal column for the analysis of both oxine and zirconium tetrakisoxine was found to be an Altima C18 HPLC-RP column. Using this column it was possible to separate both the ligand and complex. When analysis of the zcomplex was undertaken with a range of other columns it was essential to have an excess of ligand in the mobile phase. There are currently no published papers reporting a HPLC protocol for the identification of zirconium tetrakisoxine.

5.19.2 Tropolone & Zirconium Tetrakistropolone

The optimal column for the analysis of both tropolone and zirconium tetrakistropolone was found to be a Luna 3 Silica column. Using this column it was possible to separate both the ligand and complex from each other. When analysis of the tropolone ligand or the zirconium tetrakistropolone complex was undertaken with a range of other columns the stability of the complex was not consistent.

5.19.3 Ethyl Maltol

It was not possible to identify the complex or separate it from the ligand in a mixture of the two using the currently available equipment. This may be rectified using a HPLC system connected to a mass spectrometer. It may be possible to use a gamma counter to ascertain whether it is the complex that exits the column at a retention time of 2.910 minutes when analysing the zirconium-89 tetrakisethyl maltol complex.

5.19.4 Deferiprone

It was not possible to successfully identify the complex or separate it from an amount of ligand in a mixture of the two using the currently available equipment. It may be possible to rectify this using a HPLC system connected to a mass spectrometer. It may also be possible to use a gamma counter detector to ascertain whether it is the complex that exits the column.

5.20 Instant Thin Layer Chromatography

5.20.1 Introduction

In the field of nuclear medicine it is standard practise to synthesise the majority of complexes close to the time of being dispensed. Each complex must be tested before any dose is administered. The use of instant thin layer chromatography (ITLC) can ensure a quick and accurate test that provides information about the radiochemical composition of the kit that was prepared.[199] Once the radiochemical purity of the complex has been established it can then be safely administered to patients.

In the case of any complexes that are being synthesised there is a need to ensure that certain impurities have been removed from the solution containing the radiopharmaceutical before it can be administered to the patient.[199] The impurity that is a concern with the Zr complexes is any remaining free ^{89}Zr. This free ^{89}Zr can either be in the form of zirconium-89 tetrakisoxalato or zirconium-89 tetra chloride. Any unbound Zr may be harmful to the patient. A range of stains, visualisation methods and mobile phases were investigated for the use in ITLC analysis.

ITLC analysis involves a small amount of the compound to be analysed, spotted onto an ITLC strip.[200] The ITLC strips are comprised of glass fibre impregnated with either silica gel (SG) or polysilicic acid (SA). Chromatography is undertaken by placing the spotted ITLC strip into a suitable solvent contained in a chamber. The solvent travels up the ITLC strip and during this process there is a spreading of the different constituents of the analyte of interest. The different constituents are distributed between the absorbent stationary phase (SG) and the solvent mobile phase, which is dependent on their individual distribution coefficients.[200] The electrostatic forces of the stationary phase normally slow down various components whilst the mobile phase transports them along. This along with the polarity of the solvent mobile phase affects the amount of distance each of the components on the analyte travels along the ITLC strip.[201] Each of the components is then allocated an R*f* value, defined as the distance travelled by the component divided by the distance travelled by the solvent.[200]

5.20.2 Experimental Method

A 20 mM citrate solution (pH 4.0) was made by the addition of 0.262 g of citric acid and 0.193 g of tri sodium citrate to 100 mL of millipore water. An amount of this solution was added to a glass 250 mL beaker to a depth of 0.5 cm. A filter paper was then folded and added so that it lined the walls and was immersed in the citrate solution. The beaker was then sealed and left for ~20 minutes to allow the atmosphere in the beaker to become saturated with solvent. The compounds to be tested were dissolved into a solvent at a concentration of 1mg/mL. The ITLC-SG plates were then marked with a pencil and a drawn out capillary tube was used to spot the samples of complexes on to the ITLC-SG plates. The plates were placed in to the development chamber and the solvent was allowed to travel to within 1 cm of the top of the plate which was then removed and allowed to dry at ambient temperature. A UV lamp was used to visualise the compounds and images were taken using a Foster and Freeman video spectral comparator and document imaging software (suite V 1.3), R_f values were then calculated for each of the compounds.

5.21 Results and Discussion

Reagent indicators were obtained to match the functional groups of the compounds being investigated.

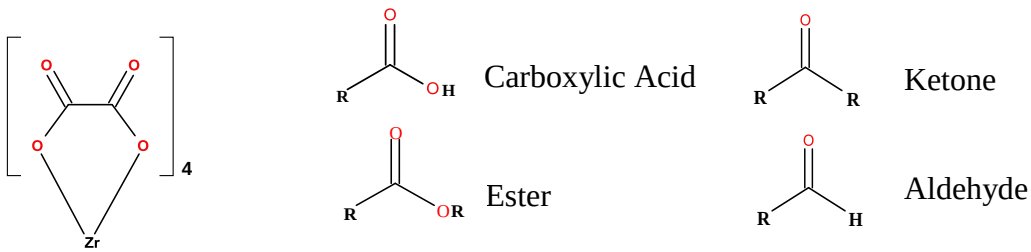

Figure 5.37: Zirconium Tetrakisoxalate & Similar Functional Groups

The following reagent indicators were tested against the complex with poor or absent indication/visualisation of the potassium zirconium tetrakisoxalate complex;

Indicator	Group/s Detected	Observation
Ferric Chloride	Phenols	Very Faint Outline of Complex
Iodine	Range of Organic Compounds	None Detectable
Potassium Permanganate	Oxidisable Functional Groups	None Detectable
Bromocresol Green	Carboxylic Acids	Complex observable for a few seconds

Table 5.3.1: ITLC Indicators

5.21.1 Developing ITLC Quality Control Protocol without Visualising Free ^{89}Zr

The process of developing a quality control protocol to detect unbound ^{89}Zr in the form of zirconium tetrakisoxalato as a cold chemistry experiment has proven problematic. This is due to the lack of ability to visualise the complex reliably as reported above. In order to develop an ITLC quality control method for both the zirconium tetrakisoxine and tetrakistropolone complexes it was necessary to conduct the experiments without the ability to visualise free ^{89}Zr in the form of zirconium-89 tetrakisoxalate. To do this successfully research was undertaken to establish the Rf value of zirconium-89 tetrakisoxalate under certain mobile phase conditions.

A range of mobile phases were investigated and it was found that the optimum mobile phase composition to be used to identify the Zr complexes was a 20mM sodium citrate solution or alternatively ethyl acetate can be used as the mobile phase. The mobile phase of sodium citrate has been previously reported to identify the R*f* value of the unbound zirconium-89 tetrakisoxalate complex by radio ITLC. It has not been possible to visualise the zirconium oxalate complex *via* stains/light sources so this information is essential in developing a quality control protocol. The image below is an ITLC-SG chromatogram (counts per second) of the zirconium-89 tetrakisoxalate complex which is a result of the work undertaken by David J. Berry: King's College London. Division of Imaging Sciences and Biomedical Engineering, The Rayne Institute, St Thomas' Hospital, London.

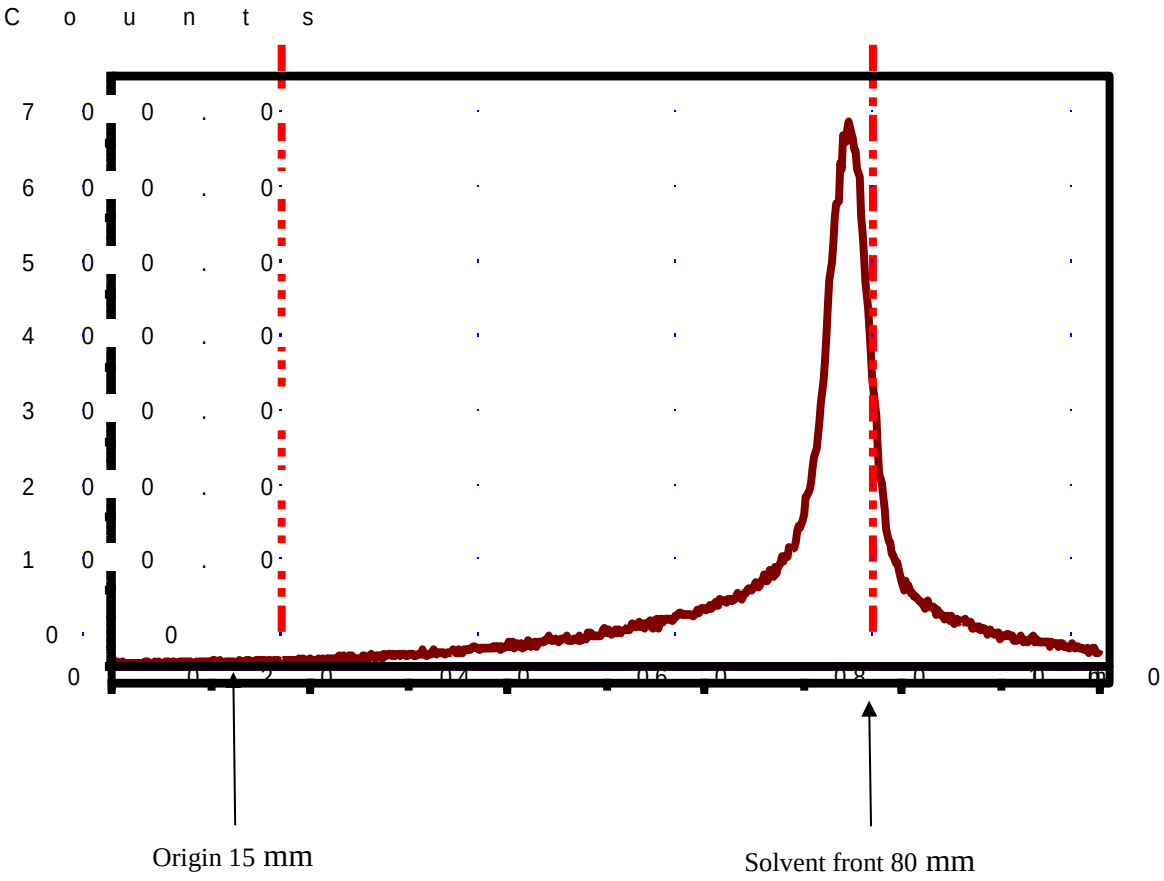

Figure 5.38: Radio ITLC-SG Scan of Zirconium-89 Tetrakisoxalate
Mobile phase 20 mM citrate: R*f* Value: 0.90

Compound	Ref	Solvent System	Visualization	Experimental Observation	Rf Value
Zirconium Tetra Chloride	A	20 mM Sodium Citrate	$AgNO_3$	Travels with the solvent front.	1.0
Zirconium Tetrakisoxalate	N/A	20 mM Sodium Citrate	^{89}Zr	Travels close to the solvent front.	0.9
Zirconium Tetrakisoxalate	N/A	Ethyl Acetate	^{89}Zr	Complex remains at origin	0.0
Oxine	B	20 mM Sodium Citrate	UV 254 nm	Streaking of free ligand.	0.8
Zirconium Tetrakisoxine	C	20 mM Sodium Citrate	UV 254 nm	Complex remains at origin.	0.0
Oxine	N/A	Ethyl Acetate	UV 254 nm	Ligand streaks slightly.	0.2
Zirconium Tetrakisoxine	N/A	Ethyl Acetate	UV 254 nm/^{89}Zr	Travels close to the solvent front.	0.9
Tropolone	D	20 mM Sodium Citrate	UV 254 nm	Ligand travels with the solvent front.	1.0
Zirconium Tetrakistropolone	E	20 mM Sodium Citrate	UV 254 nm	Complex remains at origin.	0.0

Table 2: ITLC Protocols and Results

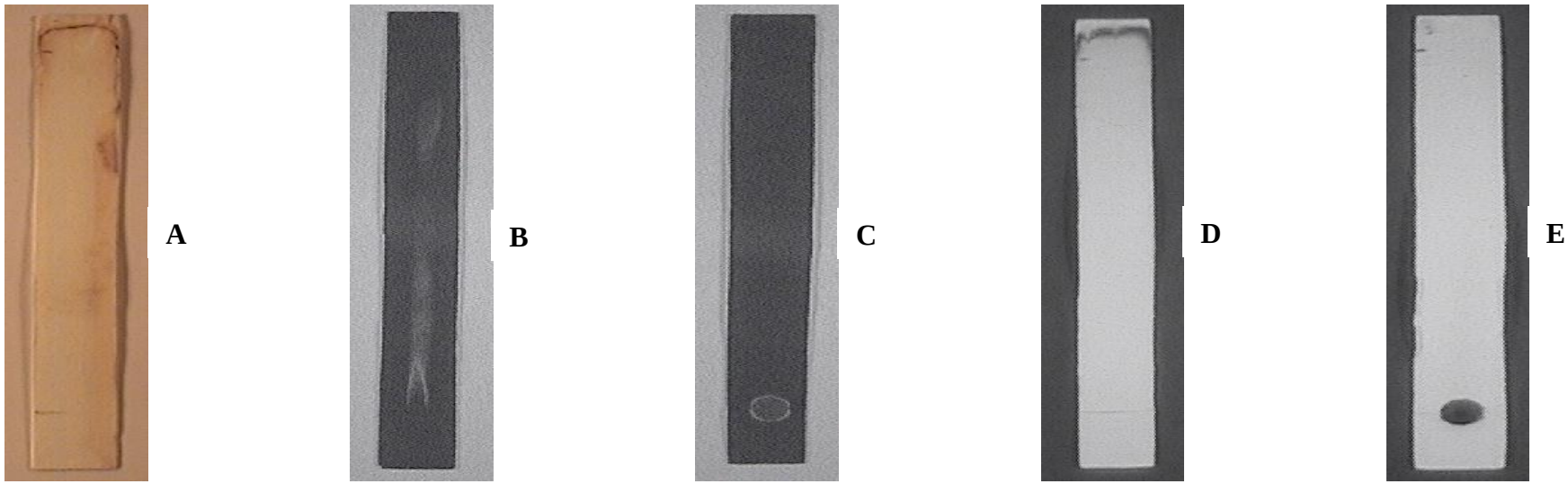

Figure 5.39: ITLC-SG Results

5.22 Conclusion

5.22.1 Visualisation and Staining

The most common method for visualisation of compounds analysed on TLC plates is the use of visible or UV light. However the precursor complexes; zirconium tetra chloride and potassium zirconium tetrakisoxalate are not visible with these light sources. A range of stains were investigated based on their ability to react with the complexes and provide a coloured indicator of their location and subsequently Rf values could be obtained. The visualisation methods that have been tested to identify the precursor complexes and the compounds will not be used to analyse the complexes when using the radioactive ^{89}Zr isotope. Instead radio ITLC methods will be used as the standard method for quality control purposes.

5.22.2 Zirconium Tetrachloride

A range of possible stains to visualise zirconium tetrachloride were tested unsuccessfully such as potassium permanganate solution and iodine vapour. It was determined that the reagent silver nitrate indicates the presence of zirconium tetrachloride. It has a reported detection limit range of between 20 and 100 ng per zone of complexes containing either chlorine or bromine. For rapid visualisation of the zirconium tetrachloride complex the plate should be illuminated with UV light at 256 nm immediately after being dipped in the silver nitrate reagent or after drying.

5.22.3 Zirconium Tetrakisoxalate

A range of indicator reagents were tested against the zirconium tetrakisoxalate complex, chosen on their ability to indicate various functional groups which were either present in the complex or were of a similar nature. It was not possible to visualise this complex with any UV light at a frequency of 256 nm or 365 nm or any of the staining methods. It is known that the zirconium tetrakisoxalate complex has an R*f* value of 0.90 with a mobile phase of sodium citrate solution hence the location of this complex without visualisation can be known. Alternatively eluting zirconium-89 tetrakisoxalate with a mobile phase of ethyl acetate results in an R*f* value of 0.

5.22.4 Oxine and Zirconium Tetrakisoxine

The visualisation of both oxine and zirconium tetrakisoxine is possible with the use of a UV lamp. Visualisation is clearest at a short wavelength of 254 nm but the compounds are also visible at a wavelength of 365 nm. The oxine ligand has an R*f* value 0.80 and results show streaking along the ITLC strip. Using a mobile phase of sodium citrate the zirconium tetrakisoxine complex does not move from the point of spotting and has an R*f* value of 0. Radio ITLC results of unbound zirconium tetrakisoxalate complex show an R*f* value of 0.9 and as such it will be possible to separate and analyse these three components using ITLC-SG. Alternatively eluting with a mobile phase of ethyl acetate results in an R*f* value of 0.2 for the oxine ligand. An R*f* 0.9 for the zirconium tetrakisoxine complex is obtained for both zirconium tetrakisoxine and zirconium-89 tetrakisoxine.

5.22.5 Tropolone and Zirconium Tetrakistropolone

The visualisation of both tropolone and zirconium tetrakistropolone is possible with the use of a UV lamp. As is the case with oxine and zirconium tetrakisoxine visualisation is clearest at a short wavelength of 254 nm but the compounds are also visible at a wavelength of 365 nm. The tropolone ligand has an R*f* value 1.00 traveling with the solvent front. The complex itself does not move from the point of spotting and has a R*f* value of 0.0. Radio ITLC results of unbound zirconium tetrakisoxalate complex show an R*f* value of 0.90 and as such it will be possible to separate and analyse these three components using ITLC-SG.

5.22.6 Ethyl Maltol and Zirconium Tetrakisethyl maltol

The visualisation of ethyl maltol and zirconium tetrakisethyl maltol was not possible with the use of a UV lamp. Stains to visualise these complexes such as potassium permanganate solution, ferric chloride, bromocresole green and iodine vapour were unsuccessful. It may be possible to use vanillin to stain these compounds.

5.22.7 Deferiprone and Zirconium Tetrakisdeferiprone

The visualisation of both deferiprone and zirconium tetrakisdeferiprone was not possible with the use of a UV lamp. Stains to visualise these complexes such as potassium permanganate solution and iodine vapour were unsuccessful.

CHAPTER 6

The *In Vitro* and *In Vivo* Analysis of Zirconium Compounds

6.1. Introduction

Chapter six of this thesis is concerned with the *in vitro* analysis of zirconium tetrakisoxine, tropolone and ethyl maltol and *in vivo* analysis of zirconium tetrakisoxine. The zirconium deferiprone complex is not a suitable candidate for pursuing in cell labelling experiments at this time. This is due to the fact that it is not possible to synthesise the complex successfully from potassium zirconium tetrakisoxalato reported in chapter 4. Tables of equipment, equipment settings and reagents used throughout this chapter can be located in the appendix section of this thesis

6.1.1 In Vitro

In Vitro (Latin: within the glass) experiments do not involve the use of live animals but involve reactions or processes taking place outside or isolated from a living organism[26]. Experiments using the components of the living organism can be conducted within culture dishes, test tubes or anywhere else outside of an organism.[26]

The findings of cell labelling experiments of the Zr tetrakisoxine, tropolone and ethyl maltol complexes will be reported in this chapter. The following cell lines were used throughout these experiments; HCT116: Colon Cancer, J774: Mouse Macrophage and MDA-MB-231: Breast Cancer.

6.1.2 In Vivo

In Vivo (Latin within the living) experiments involve the utilisation of a living animal where a clinical condition has been induced which in turn can be studied with pharmaceuticals/ radiopharmaceuticals undergoing development.[26] In these experiments zirconium tetrakisoxine was tested *in vitro* with white blood cells and GFP-5T33: Mouse Myeloma cells.

6.2 *In Vitro* Experimental Method

The following experimental work was conducted primarily by Putthiporn Charoenphun, Kings College London. Work undertaken by the author was undertaken alongside Putthiporn Charoenphun. Further details of experimental work and subsequent work following this research can be found in [^{89}Zr]-Zr(oxinate)$_4$ for *in vivo* cell tracking by positron emission tomography.

6.3 Synthesis of ^{89}Zr Tetrakis Complexes

The synthesis of the ^{89}Zr tetrakis complexes was undertaken utilising the chloroform extraction method reported in chapter 4 of this thesis. Sodium carbonate (0.1 M) was used to neutralise 20 – 90 MBq (1.36×10^{-11} – 6.12×10^{-11} moles) of ^{89}Zr tetrakisoxalate in oxalic acid (1M). The pH at this stage was measured to be at a value of ~7. The solution was then diluted with millipore water to a total volume of 500 µL. Oxine, ethyl maltol or tropolone (500 µg) was dissolved in chloroform (500 µL) and this solution was mixed together utilising a centrifuge (1000 RPM) with the neutralised solution containing ^{89}Zr in a new unused clean glass vial with a glass pasteur pipette for 15 minutes. The two phases were then allowed to separate. The chloroform phase containing the ^{89}Zr tetrakis complex was transferred into a new, unused glass vial. The chloroform was removed by slow evaporation utilising a heating block at a temperature of ~50^{o}C to 60^{o}C. The now dried ^{89}Zr complex was re-dissolved in DMSO (10-20 µL) and was ready for the cell uptake and efflux experiments. The radiochemical purity was determined by utilising the chloroform extraction method. The zirconium tetrakis complexes are found in the chloroform layer whereas the free ^{89}Zr is found the aqueous layer.

6.4 Cell Cultures

To determine the percentage uptake and efflux of zirconium tetrakisoxine, tropolone and ethyl maltol the following cell lines were used; HCT116: colon cancer, J774: mouse macrophage and MDA-MB-231: breast cancer. Cell lines were cultured as adhesion cells at 37^{o}C with CO_2 at 5 % under a humidified atmosphere.

6.5 Uptake Experiments

^{89}Zr tetrakis; oxine, tropolone or ethyl maltol was diluted to an activity of 0.05 MBq in 50 µL of a serum free medium. This was then added to glass test tubes containing the cell line under investigation (~1 x 10^6 cells) in 500 µL of a serum free medium. The percentage of uptake was determined in triplicate at 1, 15, 30, 45 and 60 minutes after adding the ^{89}Zr tetrakis tracer to the cell line under investigation. Percentage uptake was determined at each of the time points by centrifuging the sample for 5 minutes at 2500 RPM. This separated the solution into a supernatant and cell pellet. 450 µL of supernatant was collected using a micro pipette and placed into a clean glass vial. The (cpm) of supernatant (S) and cell pellet (C) were placed separately into a gamma counter to calculate the percentage of radioactivity in the labelled cells in cpm (Activity in the cell pellet corrected for residual 50 µL of supernatant). This was calculated by the equation; (C / (C + S)) x 100. Controls included uptake of neutralised ^{89}Zr in sodium carbonate into the cells and the determination of the degree of binding of the tracers to the glass test tubes.

6.6 Efflux Experiments

Following the method reported above the ^{89}Zr tracers were allowed 30 minutes for uptake to occur in the respective cell lines. Efflux was measured at time points of 1, 2, 3, 20 and 24 hrs depending on the tracer. Samples were centrifuged at ~ 2000 RPM for 5 minutes. 450 µL of supernatant was then removed from the glass reaction vial. Cell pellets were washed with phosphate buffered saline (PBS) 500 µL x 2 to remove any excess tracer. Fresh media (with serum, 500 µL) was added to each reaction vial. Samples were incubated at 37^{o}C until the required time point. At the required time point the sample was centrifuged at 3000 rpm for 5 minutes to obtain a cell pellet. Supernatant (~400-500 µL) from each reaction vial was placed into a new vial and matched to its cell pellet and both were analysed for radioactivity utilising a gamma counter. The calculations used in the uptake experiments were used to determine the percentage of efflux of the various tracers. Percentage of retention of the tracers in the labelled cells was calculated by the comparison of the total activity in the cells and the supernatant.

6.7 *In Vitro* Results and Discussion

6.7.1 Zirconium-89 Tetrakisoxine & MDA-MB-231 Breast Cancer

Radioactive zirconium arrives from the supplier in the form zirconium-89 tetrakisoxalate, a non-neutral complex was tested alongside the neutral oxine complex.

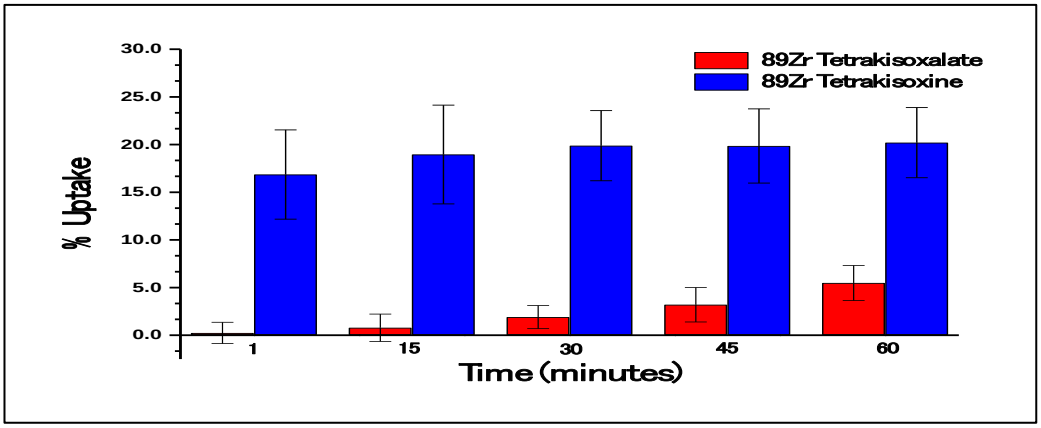

Figure 6.1: MDA-MB-231 Uptake of Zirconium-89 Tetrakisoxine

Uptake of zirconium-89 tetrakisoxalate into breast cancer cell line; MDA-MB-231 was 5.5 % over a period of 60 minutes. The uptake of zirconium-89 tetrakisoxine in to the cells was found to be between 16.5% to 23.9% for the breast cancer cell line.

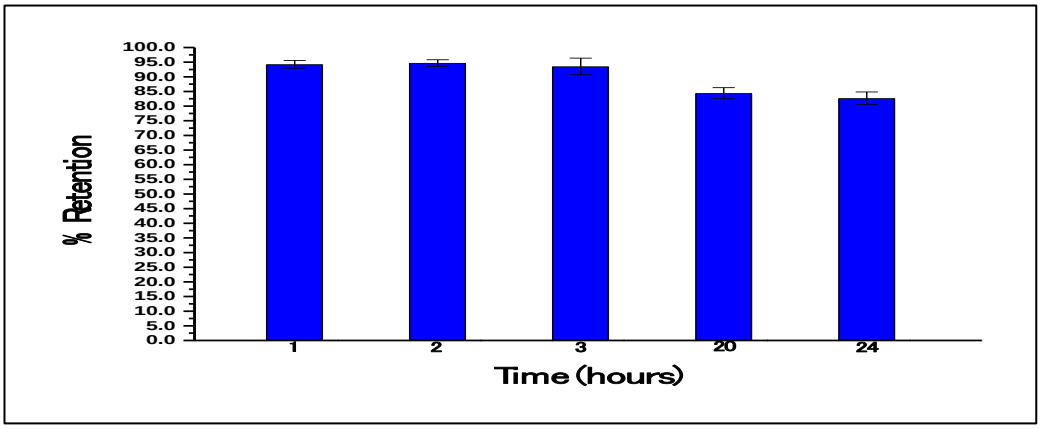

Figure 6.2: MDA-MB0231 Retention of Zirconium-89 Tetrakisoxine

The retention percentage of the zirconium-89 tetrakisoxine complex in cell line MDA-MB-231 was found to be high with 84.0 % and 82.0 % over 20 and 24 hours respectively.

6.7.2 Zirconium-89 Tetrakisoxine & J447 Mouse Macrophage

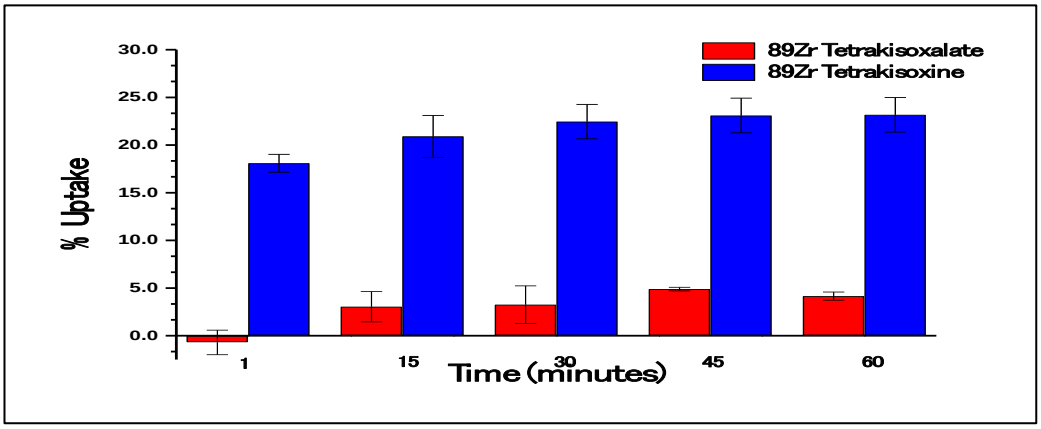

Figure 6.3: J447 Mouse Macrophage Cell Uptake of Zirconium-89 Tetrakisoxine

Uptake of zirconium-89 tetrakisoxalate was less than 4.9% % over 60 a period of minutes. The uptake of zirconium-89 tetrakisoxine in to the cells was between and 21.3% to 24.0% for mouse macrophage cells; J447 over a period of 60 minutes. Both MDA-MB-231 and J774 the non-neutral complex zirconium-89 tetrakisoxalate have an uptake less than that of zirconium-89 tetrakisoxine.

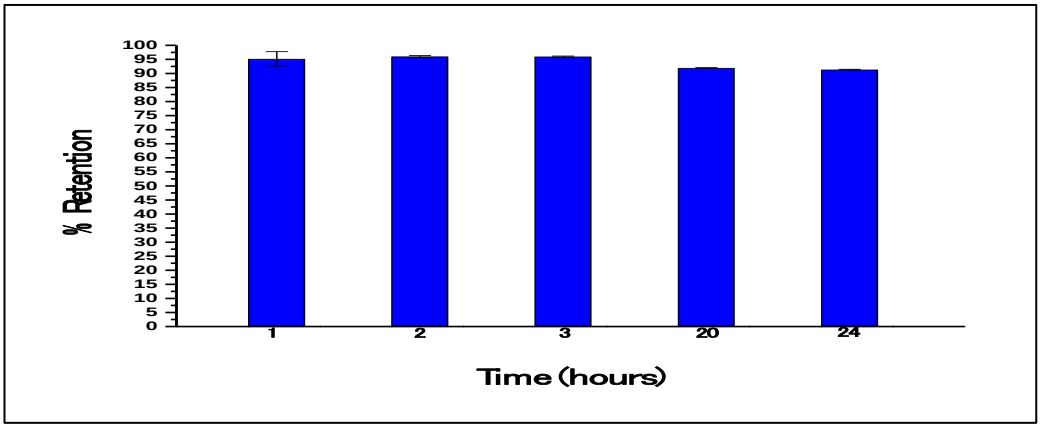

Figure 6.4: J447 Mouse Macrophage Retention of Zirconium-89 Tetrakisoxine

The retention percentage of the zirconium-89 tetrakisoxine complex in cell line J774 was found to be high at 92.0 % and 91.0 % over 20 and 24 hours respectively. This is the highest retention percentages out of both of the cell lines tested with the zirconium-89 tetrakisoxine complex. As such the zirconium-89 tetrakisoxine complex is a plausible candidate for *in vivo* studies of J447.

6.7.3 Zirconium-89 Tetrakistropolone & J447-Mouse Macrophage

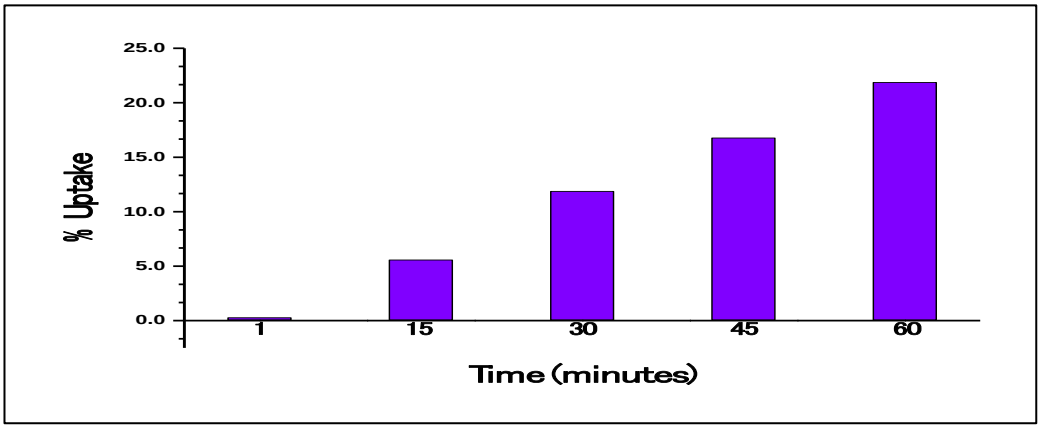

Figure 6.5: J447 Mouse Macrophage Cell Uptake of Zirconium-89 Tetrakistropolone

The uptake of zirconium-89 tetrakistropolone in to J447; mouse macrophage cells was found to be 21.9% over a period of 60 minutes. This uptake percentage is similar to that of zirconium-89 tetrakisoxine in the same cell line over the same period of time.

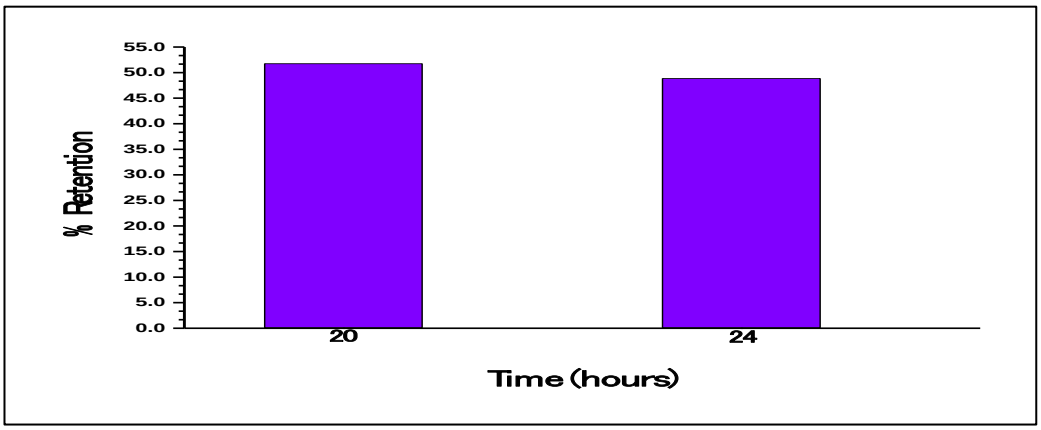

Figure 6.6: J447 Mouse Macrophage Retention of Zirconium-89 Tetrakistropolone

The retention percentage of the zirconium-89 tetrakistropolone complex in cell line J447 was found to be 51.2% and 48.9% over 20 and 24 hours respectively. Whereas the uptake of this tracer is similar to zirconium-89 oxine its retention in the cells is significantly less. In comparison the retention rate of the zirconium-89 tetrakisoxine complex in cell line J774 is 40.8% percent greater over 20 hours and 42.1 % greater over 24 hours.

6.7.4 Zirconium-89 Tetrakisethyl maltol & HTC-116 Colon Cancer

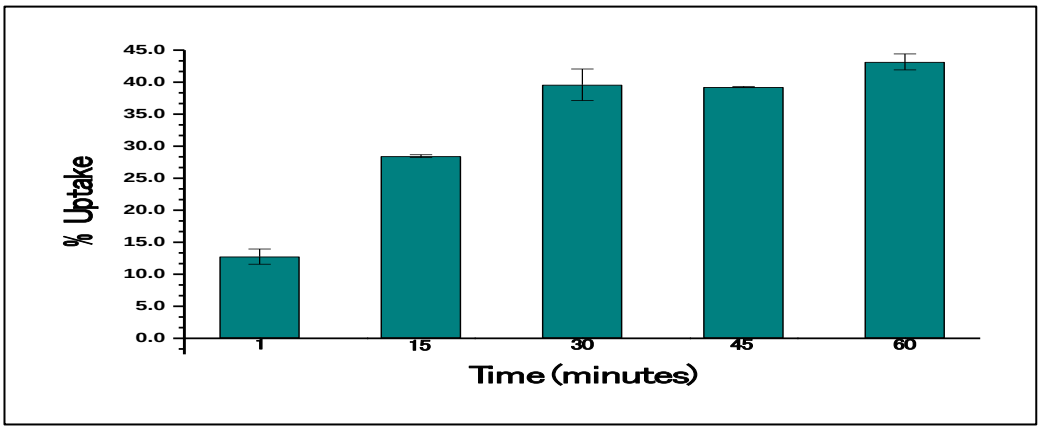

Figure 6.7: HCT-116 Cell Uptake of Zirconium-89 Tetrakisethyl Maltol

The uptake of zirconium-89 tetrakisethyl maltol was found to be 43.2% after one hour for HTC-116; colon cancer cells. This is an excellent uptake of the tracer however it cannot be compared to the other tracers because they were tested against different cell lines.

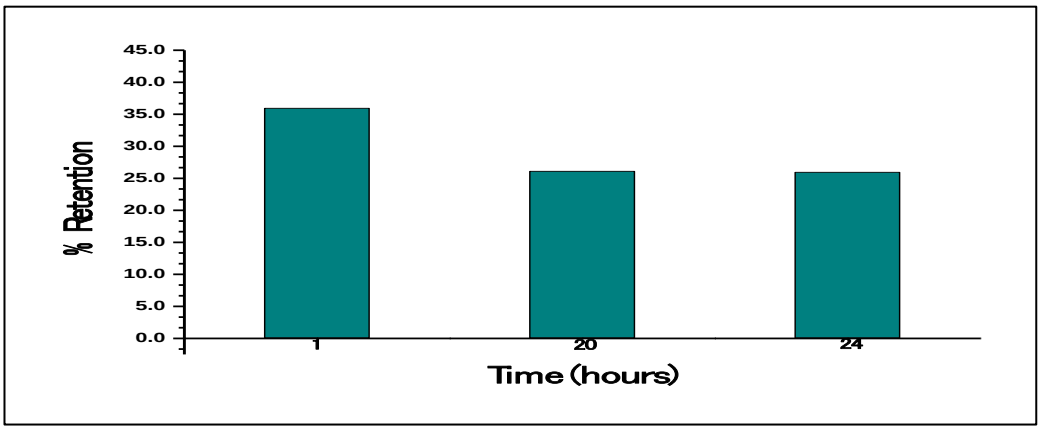

Figure 6.8: HCT-116 Retention of Zirconium-89 Tetrakisethyl Maltol

The retention percentage of the zirconium-89 tetrakisethyl maltol complex in cell line HTC-116 colon cancer was found to be 36.0 %, 26.2 % and 26.2 % over 1, 20 and 24 hours respectably. These results show that the tracer is quickly being removed from the cells and as such it is not a suitable candidate for further studies in *in vivo* experimental work.

6.7.5 Radiochemical Purity

The radiochemical purity of a radiopharmaceutical synthesis is the percentage of the radionuclide present in its desired chemical form. In this case this is the amount of radionuclide percentage present in the desired tetrakis complex. Radiochemical purity of all the tetrakis complexes was greater than 95% .This was determined from solvent extractions in the case of zirconium-89 tetrakisoxine, tropolone and ethyl maltol. The radiochemical purity of the zirconium-89 tetrakisoxine complex was also determined by radiochromatography.

6.7.6 Retention of Tracers on Glass Reaction Vials

As a control the amount of the zirconium-89 tetrakis complexes binding to the glass reaction vials without cells was determined.

Time (Minutes)	Zirconium-89 Tetrakisoxine (%)	Zirconium-89 Tetrakistropolone (%)	Zirconium-89 Tetrakisethyl maltol (%)
1	**0.13 ± 0.04**	**0.16 ± 0.00**	**3.70 ± 0.31**
15	**0.38 ± 0.19**	**0.24 ± 0.03**	**10.63 ± 0.48**
30	**0.24 ± 0.14**	**0.14 ± 0.04**	**18.54 ± 0.13**
45	**0.25 ± 0.11**	**0.17 ± 0.07**	**26.12 ± 3.88**
60	**0.29 ± 0.09**	**0.12 ± 0.08**	**30.61 ± 1.44**

Table: 6.2.1: Percentage of Activity Found to be Bound to Reaction Vials

In the case of zirconium-89 tetrakisoxine less than 0.57% of activity was found to be attached to the glass reaction vials. The tracer zirconium-89 tetrakistropolone has less than 0.27% of activity attached to the glass reaction vials. In both of these tracers it can be seen that there is a low affinity of the tracer for the glass reaction vial. Unfortunately the zirconium-89 ethyl maltol tracer has a high affinity for the glass reaction vial with nearly 33% of activity being detected on the glass vial after a period of 60 minutes. The activity that has been found to be attached to the reaction vials and not the cells themselves has been deducted from overall cell labelling uptake percentages as in figure 6.2.7.

6.8 *In Vivo* Experimental Method

The following experimental work was conducted by Levente Meszaros, Kings College London utilising synthesis methods developed by the author. Work involving 5T33 Murine Multiple Myeloma cells in the following paper; [^{89}Zr]-Zr(oxinate)$_4$ for *in vivo* cell tracking by positron emission tomography.

6.8.1 Zirconium-89 Tetrakisoxine and Labelled White Blood Cells

Male Lewis rats were injected in the left back ankle subcutaneously with 35 µg of lipopolysaccharide in 40 µL of saline solution. The injections took place 4 hours before images were taken. For a control 40 µL of saline solution was injected into each of the Lewis rat's right back ankle. The rats were then injected intravenously with zirconium-89 tetrakisoxine (activity; 4 MBq) labelled white blood cells. Images were then taken at 2, 24 and 44 hours post injection.

6.8.2 Zirconium-89 Tetrakisoxine and GFP-5T33 Murine Multiple Myeloma Model

The following animal experiments were undertaken in full compliance with the Animal Scientific Procedures ACT (1986) and Home Office (UK) guidelines. Male C57BL/KaLwRij mice were inoculated with 1.7 MBq (In111 tris oxine) or 0.6 – 0.8 MBq (zirconium-89 tetrakisoxine) radiolabelled cells (~ 10^7 cells) and imaged for 7 days in preclinical SPECT/CT and PET/CT scanners. The mice were inoculated with 0.5 MBq ^{111}In tris oxine or zirconium-89 tetrakisoxine labelled 5T33 cells for ex vivo tissue counting and culled 7 days post inoculation.

PET/CT images were acquired in a nanoScan PC *in vivo* pre-clinical PET/CT imager (Mediso Hungary). SPECT images were acquired in a nanoSPECT/CT Plus system (Mediso Hungary) equipped with four 1 mm high resolution pinhole collimators. Mice were anesthetised, cannulated and injected *via* the cannula with the radiolabelled cells as described above.

6.9 *In Vivo* Results and Discussion

6.9.1 Zirconium-89 Tetrakisoxine & Labelled White Blood Cells

PET images below of Lewis rats with zirconium-89 tetrakisoxine labelled white blood cells, imaged at 2 (fig 6.9), 24 (fig 6.10) and 48 (fig 6.11) hrs.

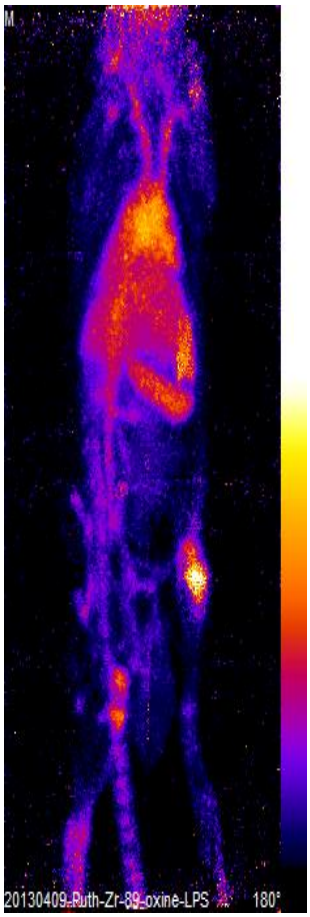

Figure 6.9: 2 Hrs Post Inoculation ^{89}Zr

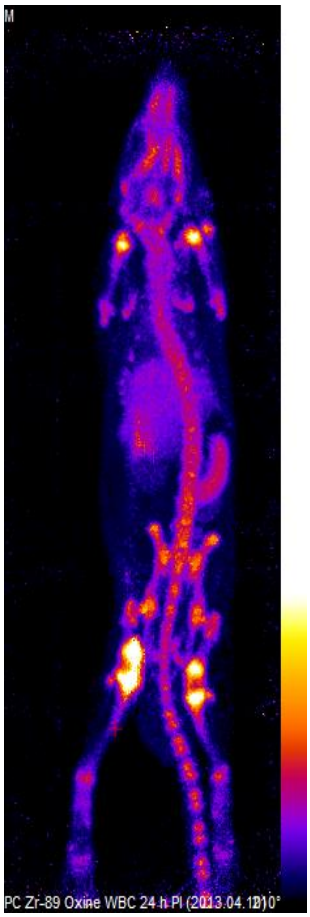

Figure 6.10: 24 Hrs Post Inoculation ^{89}Zr

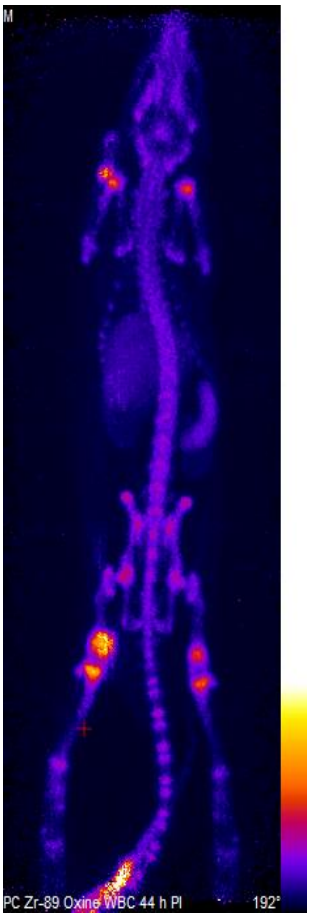

Figure 6.11: 48 Hrs Post Inoculation ^{89}Zr

There is a good accumulation of the zirconium-89 oxine tracer at the 2 hr time point in the left back ankle. This is reduced greatly over time, seen in the PET image at 24 hrs. In the PET image taken at 48 hrs the skeleton of the Lewis rat can be seen indicating that there is mostly skeletal uptake of zirconium-89 tetrakisoxine. This indicates that the tracer has left the cells and fallen apart. Unfortunately the quantity of white blood cells obtained from one rat is small compared to the required amount, hence it is not an easy or particular viable experiment.

6.9.2 Zirconium-89 Tetrakisoxine and 5T33 Murine Multiple Myeloma Model

The SPECT image (figure: 6.12) below is indium-111 tris oxine acquired 7 days post inoculation. PET images below are zirconium-89 tetrakisoxine 7 days (figure 6.13) and 14 days (figure 6.14) post inoculation.

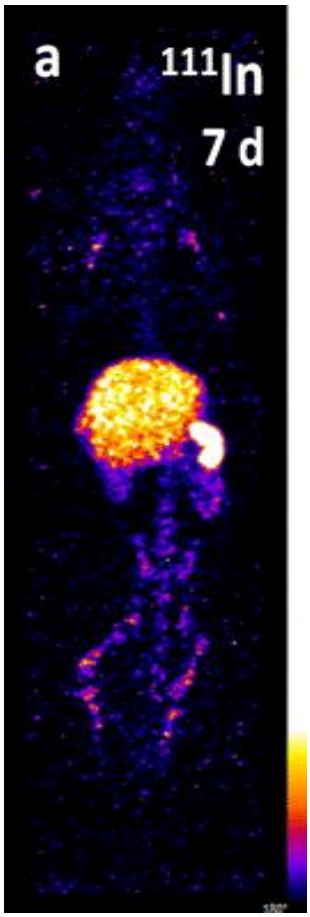

Figure 6.12: <u>7 Days</u> Post Inoculation ^{111}In

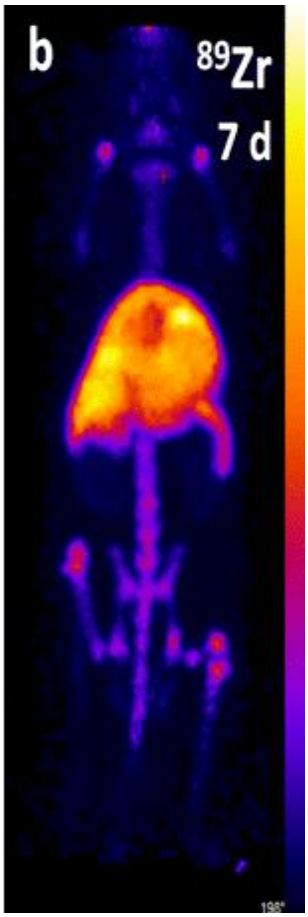

Figure 6.13: <u>7 Days</u> Post Inoculation ^{89}Zr

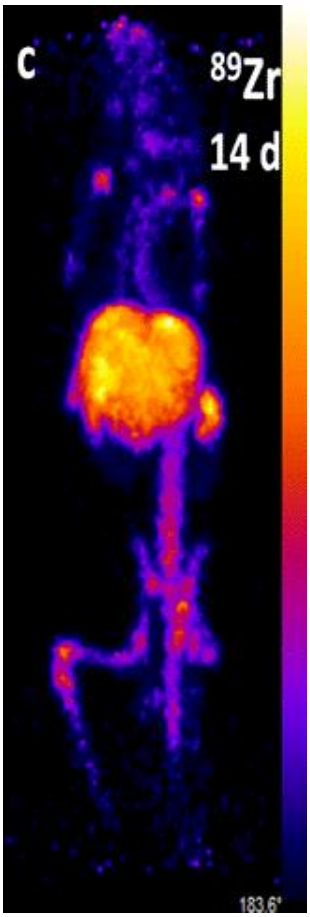

Figure 6.14: <u>14 Days</u> Post Inoculation ^{89}Zr

The imaging results of indium-111 oxine and zirconium-89 oxine labelled 5T33 cells at 30 mins – 2 hrs showed an initial accumulation in the lungs. The labelled myeloma cells rapidly migrated to the liver, spleen and skeleton of the C57Bl/KaLwRij mice as illustrated above. The tissue distribution of indium-111 oxine and zirconium-89 oxine labelled cells was found to be very similar in turn suggesting that zirconium-89 oxine is a suitable substitute for indium-111 oxine. The *ex vivo* results confirmed that the tissue distribution of radiolabelled GFP-5T33 cells was not affected by the tracers that they carried.

6.10 Conclusion

6.11 *In Vitro*

6.11.1 Neutralised Zirconium-89

Neutralised zirconium-89 in sodium carbonate was used as a control for the zirconium-89 uptake into the cell lines. Neutralised zirconium-89 was shown to have the lowest uptake of all of the zirconium-89 complexes at 4.9 % for J774; mouse macrophage cells and 5.5 % for MDA-MB-231; breast cancer cells.

6.11.2 Zirconium-89 Tetrakisoxine

Results of the uptake and retention experiments for the zirconium-89 tetrakisoxine complex were promising. There was a good level of uptake of the complex into the breast cancer cell line MDA-MB-231 and mouse macrophage cell line J447. Retention % of the zirconium-89 tetrakisoxine complex over a period of 24 hours was very high at 91% in cell line J774 and 82% in cell line MDA-MB-231. As the zirconium-89 tetrakisoxine complex had the highest retention % in the *in vitro* experiments its potential as a new radiotracer will be established in a range of *in vivo* experiments.

6.11.3 Zirconium-89 Tetrakistropolone

The uptake of this tracer was similar to zirconium-89 tetrakisoxine in cell line J447 with 21.9 %. However its retention in these cells was significantly less, therefore zirconium-89 tetrakisoxine is the most suitable candidate out of the two for further studies *in vivo*.

6.11.4 Zirconium-89 Tetrakisethyl maltol

The uptake percentage of zirconium-89 tetrakisethyl maltol was the highest out of all of the tested tracers, however direct comparison cannot be undertaken as different cell lines were used due to availability. The retention rate of this tracer was low and as such it is not a suitable candidate for further studies in *in vivo* experimental work.

6.12 In Vivo

6.12.1 Zirconium-89 Tetrakisoxine & Labelled White Blood Cells

There is an accumulation of zirconium-89 tetrakisoxine labelled white blood cells in the lesion of the Lewis rat. This is seen in the bottom left of the PET image at 2 hrs (figure 6.3.1). At 24 hrs (figure 6.3.2) there is still a small amount of accumulation of the zirconium-89 tetrakisoxine labelled white blood cells but as can be seen in the image there is mostly skeletal uptake at this time point. At 48 hrs (figure 6.3.3) there is minimal accumulation of the zirconium-89 tetrakisoxine labelled white blood cells and there is a high skeletal uptake. This indicates that the tracer has not stayed within the cell for reasons unknown and is possible that the labelled cells have denatured releasing the zirconium-89 which accumulated in the bones of the Lewis rat.

6.12.2 Zirconium-89 Tetrakisoxine & GFP-5T33 Murine Multiple Myeloma Model

Once intravenously administered in animal models, GFP-5T33 cells are known to home exclusively in the spleen, liver and skeleton. The zirconium-89 labelled cells showed a high *in vivo* stability and they also have a very similar biodistribution pattern to indium-111 oxine labelled GFP-5T33. After inoculation of GFP-533 myeloma cells PET imaging showed accumulation of the cells in the lungs after 30 mins, followed by cell migrating and accumulating in the spleen and bone marrow after a period of 24hrs. *Ex vivo* tissue sampling confirmed that the location of radioactivity was largely in the liver, spleen and bone marrow.

The high renal uptake that can be seen in figure: 6.3.4 is of indium-111 oxine labelled cells is probably due to dead cells releasing protein bound indium-111. The images of the kidneys in figures: 6.3.5 and 6.3.6 show a lower uptake of the zirconium-89 tracer in to the kidneys suggesting that zirconium-89 is being retained in the cells more efficiently.

Radiobiological effects of indium-111 and zirconium-89 on labelled GFP-5T33 cells needs to be determined. Indium-111 emits Auger electrons which can be deadly to cells whereas zirconium-89 emits 900 KeV positrons that possibly go past the nucleus resulting in zirconium-89 being less toxic to the cells. Clonogenic assay studies need to be undertaken to compare and confirm that indium-111 is more toxic to cells than zirconium-89.

In conclusion within the GFP-5T33 murine multiple myeloma model the zirconium-89 oxine labelled cells showed a higher *in vivo* stability than those labelled with indium-111 oxine. The new zirconium-89 oxine complex is lipophilic and can be used to radiolabel a range of cell types. It may be a replacement for indium-111 to be used to image cell migration. Advantages would include improved quantification, resolution and sensitivity using PET instead of scintigraphy or SPECT.

CHAPTER 7

Future Work and Conclusion

7.1 Future Work

7.1.1 Synthesis of Zirconium Tetrakisdeferiprone

The synthesis of zirconium tetrakisdeferiprone was problematic when attempting synthesis from potassium zirconium tetrakisoxalato, with or without an excess of acid in the solution. As it has been possible to synthesise zirconium tetrakisdeferiprone from zirconium tetrachloride it may be possible to synthesise this complex with an excess of acid in solution, by simply neutralising the acid. It is possible to obtain ^{89}Zr in the form zirconium-89 tetrachloride in an excess of HCl and as such the synthesis of this complex is probable.

7.1.2 ITLC and HPLC methods for Zirconium Tetrakisethyl maltol and Deferiprone

The development of ITLC and HPLC methods for quality control purposes is very important. It is necessary to ensure a compound is pure so that once administered it is effective and does not deliver unnecessary radiation exposure to a patient. ITLC methods to identify the two complexes will require the further investigation of staining or radio techniques. Development of HPLC protocols for the two complexes will require the investigation and utilisation of more suitable HPLC columns.

7.1.3 In Vitro Analysis of Deferiprone and In Vivo Analysis of Complexes

If the difficulties in synthesising the zirconium tetrakisdeferiprone complex from potassium tetrakisoxalate or zirconium tetra chloride are overcome, *in vitro* and *in vivo* analysis of this complex would be of interest. The complex would fulfil some criteria required in the development of new ^{89}Zr radiopharmaceuticals such as it being neutral, but it lacks lipophilic properties. Determining affinity of deferiprone for Zr against other metals is important. It has been reported that iron has the greatest affinity for deferiprone against other metals such as copper. It is important to determine whether deferiprone would release Zr in preference to other metals.

7.1.4 Diethyldithiocarbamate

Diethyldithiocarbamate would be a suitable ligand to chelate to Zr and investigate for use in PET. The ligand would attach to the Zr ion in a manner similar to the Zr complexes reported in this thesis. Bonding would occur through the sulfur atoms of this ligand to the Zr ion and a neutral complex would be formed. If this complex is successfully synthesized it would provide a wide range of tetrakis complexes that could be tested *in vitro/vivo* as the ethyl groups of the ligand could be exchanged.

Sodium diethyldithiocarbamate is an organosulfur complex, formula; $NaS_2CN(C_2H_5)_2$ and it has been previously used in a variety of medical applications. It has been used to treat acute nickel carbonyl poisoning in various cases with success.[202] In the treatment of cancer the compound chelates to zinc. This resulting zinc diethyldithiocarbamate complex inhibits metalloproteinases. This prevents the breakdown of the extracellular matrix which is the first step in cancer metastasis and angiogenesis.[184] In nuclear medicine the ligand has been used in several research areas. The properties of technetium-99m diethyldithiocarbamate (^{99m}Tc-DDC) were compared (both *in vitro* and *in vivo*) with those of thallium-201 diethyldithiocarbamate (^{201}Tl-DDC) which is a compound used in cerebral perfusion imaging (CPI). Results of the research in rabbits showed that ^{99m}Tc-DDC does in fact enter the brain but is not retained as much as the ^{201}Tl-DDC compound.[203] ^{201}Tl-DDC has also been investigated as an alternative to iodine-123-*N*-isopropyl-p-iodoamphetamine [(^{123}I) IMP] which is used to monitor cerebral blood flow in SPECT. The lipophilic radiopharmaceutical ^{201}Tl-DDC is cheaper to produce than [(^{123}I) IMP] and studies have concluded that the two radiopharmaceuticals in comparison are equivalent when studying the blood flow in rabbit brains.[204] Human tomographic experiments were under taken with two healthy subjects and the results obtained with ^{201}Tl-DDC show that it may be possible to for the radiopharmaceutical to be used in combination with SPECT for clinical applications.[204] Diethyldithiocarbamate complexes are established and as such warrant investigation for possible chelation with Zr and subsequent use in PET.

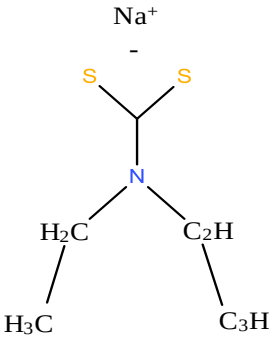

Figure: 7.1: Sodium Diethyldithiocarbamate

7.2 Summary of Complexes

7.2.1 Zirconium Tetrakisoxine

Zirconium tetrakisoxine was synthesised from zirconium tetrachloride by the reaction of four molar equivalents of oxine. The resulting complex was characterised utilising FTIR and Raman spectroscopy. Assignment of functional groups was undertaken utilising published work by T. Gavrilko *et al*[163], A Patel *et al*[164], *M Sekkina et al* and [165] Wagner *et al*.[166] Both the ^{1}H and ^{13}C NMR spectroscopic data and CHN elemental analysis were in accord with the formation of the desired zirconium tetrakisoxine compound. UV-Vis analysis showed that the molar absorptivity of the complex is approximately four times that observed for the ligand in accord with the chromophore being ligand based rather than involving the Zr. ITLC and HPLC protocols were developed for quality control purposes. Uptake and retention of the complex in to cell lines was promising and the complex progressed to *in vivo* testing. *In vivo* testing with the 5T33 model showed that the zirconium-89 oxine labelled cells show a higher *in vivo* stability than cells labelled with indium-111 oxine. The complex was synthesised from potassium zirconium tetrakisoxalate in 0.1M and 1M oxalic acid if the acidic solutions were first neutralised.

7.2.2 Zirconium Tetrakistropolone

Zirconium tetrakistropolone was synthesised adapting the published method of synthesis of zirconium tetrakis isopropyltropolone[143] ^{1}H and ^{13}C NMR spectra were in accord with the proposed product showing ligand resonances perturbed from their positions in tropolone. ^{1}H NMR spectroscopy and elemental analysis data suggest inclusion of $CHCl_3$. FTIR and Raman spectra were assigned by comparison with work by Yusaku Ikegami[167] and Jianlin *et al*.[168]. Electronic absorptions for tropolone in methanol were in accord with those observed in DMSO.[182] Absorptions observed in zirconium tetrakistropolone have increased extinction coefficients attributed to the presence of four tropolone rings with enhancement by the contribution of a charge transfer transition.[182] The complex was synthesised from potassium zirconium tetrakisoxalate in 0.1 M and 1M oxalic acid if the acid is first neutralised.

7.2.3 Zirconium Tetrakisethyl maltol

Zirconium tetrakisethyl maltol was synthesised by the reaction of four equivalents of ethyl maltol with $ZrCl_4$ in tetrahydrofuran. CHN Elemental analysis data was in accord with the desired complex. The ^1H NMR spectrum shows no resonance due to free ligand OH in the region of 8.8 ppm and the shift of the H_a and H_b protons to lower frequencies in relation to the ligand demonstrates the loss of aromaticity due to the donation of electron density to the metal. FTIR and Raman spectra were assigned by comparing work by J Burges *et al*[169], B S Parajon- Costa *et al* [171, 172], C Y Panicker *et al*[174], K Thompson *et al*[170] and C Wagner *et al*.[173] An electronic absorption for tropolone in methanol was recorded as 268 nm having been observed previously in toluene at 286 nm.[138] In the zirconium tetrakisethyl maltol complex this band due to the loss of conjugation of the enone, demonstrating the complexation by the carbonyl group. Zirconium tetrakisethyl maltol was also synthesised from potassium zirconium tetrakisoxalate in 0.1M and 1M oxalic acid once the acidic solution was neutralised.

7.2.4 Zirconium Tetrakisdeferiprone

Zirconium tetrakisdeferiprone dodeca hydrate was synthesised by the reaction of four equivalents of deferiprone with zirconium tetrachloride in methanol. Elemental analysis data fits with the inclusion of twelve molecules of water. In contrast to the other zirconium tetrakis complexes zirconium tetrakisdeferiprone is soluble in water and insoluble in chloroform suggesting a lack of lipophilicity. ^1H NMR spectroscopy revealed a shift of the alkenic protons to lower frequency in relation to the ligand as expected due to electron density donation to the metal. IR and Raman spectra were assigned by comparison with Chromium tris deferiprone dodeca hydrate[144] and iron tris deferiprone.[177] The FTIR spectrum displays a broad band is due to the waters of crystallisation and four strong bands in the region 1600-1400 cm^{-1} characteristic of coordinated 3-hydroxy-4-pyridinones. The intense absorptions in the 280-300 nm region of the UV spectrum can be assigned to both hydroxyl and carbonyl Zr(IV) ligand to metal charge transfer.[144] Numerous attempts to prepare the complex from neutralised acidic solutions failed.

7.3 Overall Conclusion

The aim of this PhD research was to produce a range of Zr complexes of the general form ZrL_4 where L is a bidentate uninegative ligand. These Zr complexes needed to be neutral and able to diffuse into cells and dissociate easily. Determining the usefulness of these Zr complexes in PET medical imaging applications was the final goal of this research. All of these aims were fulfilled and are reported in this thesis.

Methods to synthesise the neutral complexes; zirconium tetrakis; oxine, tropolone, ethyl maltol and deferiprone under a range of conditions were developed. Characterisation of the zirconium tetrakis complexes was undertaken with ^{1}H and ^{13}C NMR, FTIR, Raman spectroscopy, UV-Vis spectroscopy and CHN elemental analysis. HPLC and ITLC methods to analyse the zirconium tetrakisoxine and zirconium tetrakistropolone complex were developed. These methods can be used for quality control purposes in the process of radiolabeling to determine radiochemical purity.

Cell uptake and efflux studies showed that zirconium tetrakis; oxine, tropolone and ethyl maltol complexes are able to diffuse into cells with varying levels of uptake with zirconium-89 tetrakisoxine having the highest retention percentage in J774; mouse macrophage cells. The *in vitro* evaluation of the three potential radiotracers resulted in zirconium tetrakisoxine being investigated as a lead compound to be used in *in vivo* studies.In the GFP-5T33 murine multiple myeloma animal model zirconium-89 tetrakisoxine labelled cells demonstrated a higher level of *in vivo* stability than those labelled with indium-111 tetrakisoxine. However radiobiological effects still need to be determined.

The use of ^{89}Zr complexes in PET have the benefits of longer time periods for studies and no known biological interactions with ^{89}Zr becoming increasingly available. Zirconium-89 tetrakisoxine labelled cells have shown high *in vivo* stability with a bio distribution pattern that is similar to that of indium-111 tetrakisoxine. The developed complexes and especially zirconium-89 tetrakisoxine have the potential to become effective PET imaging agents.

Appendix

A.1 Equipment and Materials

A.1.1 Chapter 2, Synthesis Methods of Zr Complexes.

The following equipment and materials were used throughout the synthesis of all of the zirconium based complexes reported in chapter 2 of this thesis.

- 100 mL glass volumetric flask with plastic stopper ± 0.10 mL, manufacturer: Volac.
- 150, 250 mL glass conical flasks, manufacturer: Pyrex.
- 50 mL glass measuring cylinder, Class B, ± 0.5 mL, manufacturer: Fisherbrand.
- Air tight glass bottles with plastic lids, sizes: 100 mL, 50 mL, 25 mL, manufacturer; Simax.
- Buchi B465 water bath with power cord; 240 Volt 50-60 Hz 11 Amps 1200 watts.
- Buchi Rotovapor R-114 rotary evaporator; 240 Volt 50-60 Hz 35 Watt.
- Büchner funnel and vacuum conical flask.
- Electric hot plate with magnetic stirrer function; 250V, 750 watts, manufacturer Bibby Stuart.
- Electric oven, 100 watts, 3.5 amps, 220/240 volts, 50/60Hz, model: GP/40CLAV/250/HYD, manufacturer: Scientific Laboratory Supplies.
- Electromantle MA Solid State Stirrer; EMA025/CE MK5, 230 V, 170 W.
- Filter paper, 6 cm diameter, for crystalline precipitates, maximum ash per circle .000036 grams, No 43, manufacturer WHATMAN.
- Fisherbrand; Immersion thermometer general purpose/stirring 76 mm immersion red spirit filled amber graduations white backed -10°C to 110°C x 1°C 305mm.
- Glass spatula, spoon and paddle ends, dimensions; 7 mm x 200 mm.
- Glass stirring rod 25 cm in length.
- Grant water bath; Grant Instruments (Cambridge) Ltd, JB2, 3,3A/220-240V/50-60 Hz. Serial No: 9826.

- HI 98103 pH meter (Checker®) with HI 1270 electrode. Manufacturer: HANNA instruments. Specifications: range; 0.00 to 14 pH, resolution 0.01 pH, accuracy ±0.2 pH, environment; 0 to 50°C (32 to 122°F); RH max 95%.
- Metal spatula, nickel stainless steel rod, dimensions; 4mm x 200mm.
- Nalgene 180 PVC Metric tubing; Various Lengths.
- Narrow range pH indicator paper (pH 7-9), manufacturer: WHATMAN-BHD.
- Octagon Magnetic Stirrer; 20 mm x 8 mm.
- Pestle and Mortar; capacity 30 mL.
- Plastic disposable narrow mouth bottle pipettes, manufacturer: Nalgene.
- Purified water obtained by reverse osmosis at the School of Physical Sciences, University of Kent.
- PVC Metric tubing, various lengths and diameters.
- Quickfit; glass cooling column, 19/26, 19/26, 153 cm length.
- Quickfit; glass round bottomed flask, 250 mL capacity, 24/29.
- Quickfit; glass size adapter, B19/26, B34/35, DA 25.
- Quickfit; glass stopper 19/26.
- Quickfit; soxhlet extractor, 60 mL borosilicate glass 34/35 socket 24/29 cone.
- Whatman cellulose extraction thimbles. Internal diameter x external length 30 mm x 100 mm, external diameter x external length 32 mm x 100 mm.

A.1.2 Chapter 2, Nuclear Magnetic Resonance Spectroscopy.

- Dimethyl Sulfoxide-D6 (D, 99.9%), Cambridge Isotope Laboratories, Inc.
- Deuterium Oxide (>99.8%), Fluka Chemika.
- Plastipak, 2 mL sterile syringe (PP), Becton Dickson Ireland.
- 7 mL clear neutral squat form vial, Kent University stores.
- Minisart, single use filter unit, Sterile, 0.45µm, Sartorius stedim biotech.
- BD Sterile microlance 3, 25G 0.5 X 16mm, BD Drogheda, Ireland.
- Economy NMR Tube, thin walled, O.D: 5mm, Length 20 cm, ASTM Type 1 Class B Borosilicate Glass (N51), Goss Scientific Instruments Limited.

A.1.3 *Chapter 4, Synthesis of Zirconium Tetrakis Complexes under Conditions Compatible with Radiopharmacy.*

- Borosilicate glass funnel, 100 mm diameter; Pyrex®
- Safety control,hot plate magnetic stirrer, 1100 rpm; IKA® RTC IKAMAG™
- Temperature controller electronic contact thermometer with 3 operating modes, stainless steel, 1/cs; IKA® ETS-D5.
- Laboratory stand and clamp, chemistry retort stand; Griffin & George.
- 500 mL capacity borosilicate glass separating funnel conical, with plain glass key and 24/29 glass stopper; Pyrex®.

A.1.4 *Chapter 5, Ultraviolet-Visible Spectroscopy.*

- 1 mL and 10 mL Glass Pipettes; VOLAC®
- 500 mL, 100 mL & 10 mL Volumetric Flasks (Boro) Fisherbrand
- Acetonitrile: HPLC Gradient Grade, Fisher Chemical
- Methanol: HPLC Gradient Grade, Fisher Chemical
- Millipore Water (Prepared utilising Thermo Scientific Easy Pure II)
- Quartz Absorption Cuvettes, 400 µL, Pathlength 10mm, 25 x 12.5 x 12.5; Sciensco

A.1.5 *Chapter 5, High Performance Liquid Chromatography Analysis.*

- Sterile Syringe (PP), 2 mL, Plastipak, Becton Dickson.
- Ministart, Single use filter unit, non-pyrogenic, Sartiorius stedim biotech.
- Sample Vials: 2 mL screw top clear glass vial with PTFE/silicone pre-slit grey cap closure, 12 x 13 mm, Perkin Elmer.
- Methanol: HPLC Grade, Fisher Chemical.
- Acetonitrile: HPLC Grade, Fisher Chemical.
- Millipore Water (Prepared utilising Thermo Scientific Easy Pure II).

A.1.6 *Chapter 5, 1 Instant Thin Layer Chromatography*

- 250 mL beaker, Fisher Brand
- Bromocresol Green Indicator; Fisions
- Micro Capillary Tubes, L = 75 $\pm$ 1.00 mm x D = 1.15 $\pm$ 1.00 mm; GMBH
- Checker Pocket Sized pH Meter, Range: 0-14 pH, Hanna instruments
- Citric Acid > 99.5 %; Sigma Aldrich
- Ferric Chloride Hexahydrate 97%, Aldrich Chemicals
- Filter Paper, 1 Qualitative Circles 70mm, Whatman
- Handheld UV Lamp, LW/SW, 6W, UVGL-58, 254/365 nm
- Instant Thin Layer Chromatography Silica Gel (ITLC-SG) Plates; Varian
- Iodine, 99.8% ACS Reagent; Sigma - Aldrich
- Millipore Water (Prepared utilising Thermo Scientific Easy Pure II)
- Potassium Permanganate, $\geq$ 99.0%; Sigma-Aldrich
- Tri Sodium Citrate, 99.5%; Fisons Analytical
- Video Spectral Comparator, VSC4CX; Foster and Freeman

A.1.7 *Chapter6, The In Vitro and In Vivo Analysis of Zirconium Compounds.*

- Auto Pipette, Volume 0.1 - 2 µL & 100 – 1000; Star Labs
- Automated Cell Counter, Countess™ & Trypan Blue Solution; Sigma Aldrich
- Centrifuge, FB15024; Fisher Scientific &, Rotina 380R; Hettich Zentrafugen
- Chloroform (99.8+ %); Fisher Scientific
- CRC ® -25R Dose Calibrator; Capintech
- Dimethyl Sulfoxide ≥99.7 %; Fisher Scientific
- Falcon Tubes, 15 mL; BD Biosciences
- Fix Test pH Strips 0 - 14, 100 colour fixed; Macherey-Nagel
- Gamma Counter Personal Computer & Eden Term v1.21 Software
- Gamma Counter, Compugamma model, 1282; LKB Wallac
- Glass Sample Bottle and Screw Cap Septum 5 mL; Sigma Aldrich
- Glass Test Tubes, Glass Borosilicate 12 mm x 50 mm, Pyrex

- Graduated Filter Tips, 2 µL & 1000 µl; Star Labs
- Hanks Balanced Salt Solution (HBBS), (with/without phenol red); Sigma Aldrich
- Interlocking Lead Brick Shielding 40 mm; Britec
- LB 124 SCINT monitor for α- and β-γ-measurements; Berthold Technologies
- Lead Cylinder Sample Container
- Microcentrifudge Tube 1.5 mL Blue; Cliklok
- Standard Viewing Barrier Pb Glass 30 mm Lead Equivalence; Britec

Cells

HCT116: Colon Cancer Cells.
MDA-MB-231: Breast Cancer Cells.
GFP-5T33: Mouse-Myeloma Cells.
J774: Mouse Macrophage Cells.
White Blood Cells.

89Zr

89Zr in 1 M oxalic acid. Radioactive concentration between 740 – 1850 MBq/ mL (20 – 50 mCi/ mL), Radionuclide purity >99.9% 89Zr at calibration. Supplier; iba Molecular, Belgium or supplied from Perkin-Elmer in 0.1 M in oxalic acid

Table A1 below contains information regarding the range of compounds used in all of the experiments reported in chapter 2 of this thesis. Each compound has a full description, its chemical formula and supplier details.

Compound	IUPAC Name	Chemical Formula	Supplier
1,4-Dioxane	1,4-dioxacyclohexane	$C_4H_8O_2$	Sigma Aldrich
Oxine	Quinolin-8-ol	C_7H_9NO	Sigma Aldrich
Chloroform (99.8+ %)	Chloroform	$CHCl_3$	Fisher Scientific
Deferiprone (98%)	3-hydroxy-1,2-dimethyl-4(1H)-pyridon	$C_7H_9NO_2$	Aldrich
Diethyl ether (99+ %)	Ethoxyethane	$C_4H_{10}O$	Fisher Scientific
Ethanol (99.8%)	Ethanol	C_2H_6O	Fisher Scientific
Ethyl maltol (99%)	2-ethyl-3-hydroxy-4-pyranone	$C_7H_8O_3$	SAFC
Hexane	Hexane	C_6H_{14}	Fisher Scientific
Piperidine	Piperidine	$C_5H_{11}N$	GPR
Tetrahydrofuran (99.6%)	Oxolane	$C_4H_8O_2$	Fisher Scientific
Tropolone (98%)	2-hydroxy-2,4,6-cycloheptatrien-1-one	$C_7H_6O_2$	Aldrich
Zirconium (IV) chloride	Zirconium tetrachloride	$ZrCl_4$	Aldrich

Table A1

.

Table A2 below contains information regarding the range of compounds used in all of the experiments reported in chapter 4 of this thesis. Each compound has a full description, its chemical formula and supplier details.

Compound	IUPAC Name	Chemical Formula	Supplier
Absolute ethanol (99.9%)	Ethanol	C_2H_6O	Fisher Chemical
Ammonia (35%)	Azane	$NH_3.H_2O$	Fisher Chemical
Chloroform (99.8+ %)	Chloroform	$CHCl_3$	Fisher Scientific
Deferiprone	3-hydroxy-1,2-dimethyl-4(1H)-pyridon	$C_7H_9NO_2$	Aldrich
Diethyl ether (99+%)	Ethoxyethane	$(C_2H_5)_2O$	Fisher Chemical
Ethanol (99.7%)	Ethanol	C_2H_5OH	BHD
Ethyl Maltol	2-ethyl-3-hydroxy-4-pyranone	$C_7H_8O_3$	SAFC
Hydrochloric acid	Chlorane, Hydrogen chloride	HCl	Sigma Aldrich
Oxalic acid	Ethanedioic acid	$H_2C_2O_4$	Sigma Aldrich
Oxalic acid dihydrate	Ethanedioic acid dihydrate	$C_2H_2O_4.2H_2O$	Sigma Aldrich
Oxine	Quinolin-8-ol	C_9H_7NO	Sigma Aldrich
Potassium oxalate monohydrate	Dipotassium oxalate hydrate	$C_2K_2O_4.H_2O$	Sigma Aldrich
Potassium zirconium tetrakisoxalato	Potassiumoxalatozirconate(IV)	$K_4(C_2O_4)_4.5H_2O$	Synthesised at UKC
Sodium hydrogen carbonate	Sodium hydrogen carbonate	$NaHCO_3$	Sigma Aldrich
Sodium hydroxide	Sodium hydroxide	NaOH	Fisons
Tropolone (98%)	2-hydroxy-2, 4, 6-cycloheptatrien-1-one	$C_7H_6O_2$	Aldrich
Zirconium (IV) chloride	Zirconium tetrachloride	Cl_4Zr	Sigma Aldrich
Zirconyl chloride octahydrate	Zirconyl chloride octahydrate	$Cl_2OZr.8H_2O$	Sigma Aldrich

Table A2

A.2 Settings and Specifications

A.2.1 NMR Settings

ECS 400 NMR Spectrometer

Observation nuclei 1H/19F, 31P to 15N, 39K to 109Ag
Observation frequency 1H: 400 MHz, 13C: 100 MHz
Sensitivity for 13C _190 (ASTM)
Sensitivity for 1H _280 (0.1% ethyl benzene)
Variable temperature range _100 to 180° C (dependant on probe)

Hardware Configuration

Alternate HF receiver gain limit:	80 [dB]
Alternate HF receiver gain point:	200000 [Hz]
Alternate LF receiver gain limit:	60 [dB]
Alternate LF receiver gain point:	150000 [Hz]
IRM crossover point:	490000000 [Hz]
90 [deg] Pulse attenuation default:	79[dB]
90 [deg] Pulse width default:	1[us]
Auto shim delay:	3600 [s]
Lock settle point:	4096
Optimum lock phase width:	60 [deg]
Shim drift correction interval:	60 [sec]
Shim system type:	DM

Dell Personal Computer

Operating System:	Windows 7 Professional
Processor:	Intel® Core ™ i3-2120 CPU @ 3.30 GHz
Installed Memory:	4.00 GB (3.24 usable)
System Type:	32-bit Operating System

A.2.2 FTIR Settings and Specifications

Shimadzu IRAffinity-1 Fourier Transform Infrared Spectrophotometer

Michelson interferometer (30º incident angle)
Equipped with dynamic alignment system (JPN patent No.2115670, 3613171)
Sealed interferometer with auto dryer (JPN registration of utility model No.3116465)

Wave number range:	7,800 to 350 cm-1
Resolution:	0.5, 1, 2, 4, 8, or 16 cm-1
S/N ratio:	30,000:1 or higher (peak-to-peak, 4 cm-1 resolution, in a neighbourhood of 2,100 cm-1, 1-minute accumulation)
Dimensions:	514(W) X 606(D) X 273(H) mm
Weight:	35 kg

Standard Specac Golden Gate ATR Single reflection diamond ATR accessory

ATR Crystal Diamond: Type IIIa Diamond 45° 2 mm x 2 mm
Germanium: Ge 45° 4 mm x 4 mm
Accessory Transmission Range: 6500 -600 cm-1 (with ZnSe lenses), 6500 - 400cm-1 (with KRS-5 lenses), 5200 – 650 cm-1 (with ZnSe lenses or KRS-5 lenses)
Refractive Index at 1000 cm^{-1}: 2.4 4.0
ATR Plate: Diamond brazed into Tungsten Carbide Disc Germanium Sampling Area: (50% of Transmitted Energy): 0.8 mm diameter 0.8 mm diameter
Maximum Applied Force: 100 cNm (torque) 160 lbs or 128 lbs, 0.36 KBar.
Depth of Penetration 2.0μm (For sample of Refractive Index 1.5 @1000 cm-1)
0.7μm (For sample of Refractive Index 1.5 @1000 cm-1)

Viglen Personal Computer

Operating System:	Windows 7 Professional
Processor:	Intel® Core ™ 2 Duo CPU E7600 @ 3.06 GHz
Installed Memory:	4.00 GB (3.18 usable)
System Type:	32-bit Operating System

A.2.3 Raman Settings and Specifications

LabRAM HR UV-VIS-NIR Raman Spectrometer

Detector (s):	LN2 cooled CCD detectors
Measurement mode (s):	Raman, photoluminescence
Laser source:	224, 247 and 325 nm (Opt 532, 633, 785 nm)
Focal length:	800 nm

Hardware Configuration

Acquisition time (s):	2
Accumulation:	10
Range (cm-1):	100-2000
Windows:	3
Delay time (s):	0
ICS correction:	On
Detector:	Synapse
Objective:	x 50 LWD NIR
Grating:	600
ND filter:	25 %
Laser:	784.14
Slit:	100.021
Hole:	799.986
Stage XY:	Märzhäuser
Stage Z:	Märzhäuser

Dell Personal Computer

Operating System:	Microsoft XP: Professional Service Pack 3, Version 2002
Processor:	Pentium® Dual Core E5800 Dual Core CPU @ 3.20 GHz
Installed Memory:	4.00 GB (3.46 usable)
System Type:	32-bit Operating System

A.2.4 HPLC Settings and Specification

UltiMate® 3000 Standard LC systems with UltiMate® 3000 Solvent Rack SR-3000

Hardware Configuration

UltiMate® 3000 Quaternary Analytical Pump LPG-3400SD

Operating flow rate range:	200 µL min – 10 mL min
Operating pressures:	Maximum, 620 bar (9000 psi)
Pump module pressure lower limit:	10 bar
Pump module pressure upper limit:	350 bar
Pump module pump flow nominal:	1.000 mL min

Pump module pressure maximum flow ramp up 6.000 mL/min^2

Pump module pressure maximum flow ramp up 6.000 mL/min^2

UltiMate® 3000 Autosampler Column Compartment ACC-3000

Pulled-loop injection:	Full & partial-loop injections
Injection volume ranges:	1–10 mL, partial-loop, 20 µL full-loop.
Wash speed:	50.000 µL / s
Wash volume:	150.000 µL
Sample height:	2.000 mm
Waste speed:	50.000 µL / s
Dispense delay:	0.000 s
Dispense speed:	20.000 µL / s
Draw speed:	5.000 µL /
Flush Volume:	80.000 µL
Column oven ready temp:	1.0 ^{o}C

UltiMate® 3000 RS Diode Array Detector DAD-3000RS

Noise:	<±7 µAU
Drift:	<0.5 mAU/h
UV 3D Field Min Wavelength:	190.0 nm
UV 3D Field Max Wavelength:	800.0 nm
UV Response Time:	1.000 (s)
UV Data Collection Rate:	5.0 [Hz]
UV Vis 1 Wavelength:	Variable
UV Vis 1 Bandwidth:	4 [nm]
UV Vis 1 Ref Wavelength:	Off
UV Vis 2 Wavelength:	Variable
UV Vis 2 Bandwidth:	4 [nm]
UV Vis 2 Ref Wavelength:	Off
UV Vis 3 Wavelength:	Variable
UV Vis 3 Bandwidth:	4 [nm]
UV Vis 3 Ref Wavelength:	Off
UV Vis 4 Wavelength:	Variable
UV Vis 4 Bandwidth:	4 [nm]
UV Vis 4 Ref Wavelength:	Off

Dell Personal Computer

Operating System:	Windows 7 Professional
Processor:	Intel® Core ™ Duo CPU E7600 @ 3.06 GHz 3.06 GHz
Installed Memory:	4.00 GB (3.18 usable)
System Type:	32-bit Operating System

A.2.5 UV-Vis Settings and Specifications

Shimadzu UV-1800

Resolution:	1 nm

Hardware Configuration

Wavelength Range (nm):	190-1100
Scan Speed:	Fast
Sampling Interval (nm):	0.5
Scan Mode:	Single
Repetitions:	2
Measuring Mode:	Absorbance
Slit Width (nm):	1.0 Fixed
Light Source Change Wavelength:	340nm
S/R Exchange:	Normal
Attachments:	None

Dell Personal Computer

Operating System:	Windows 7 Enterprise
Processor:	Intel® Core ™ i5-3470 CPU @ 3.20 GHz
Installed Memory:	4.00 GB (3.41 usable)
System Type:	32-bit Operating System

A.2.6 Melting Point Apparatus Specifications

Stuart SMP3 Melting Point Apparatus

Dimensions:	L 180 mm, H 259 mm, W 300 mm
Maximum Temperature:	360°C
Memory Storage:	8 x temperature readings per sample tube tested
Number of Samples:	3
Temperature range:	0.1°C
Temperature resolution:	Ambient to 360°C
Ramp rate:	0.5° to 10°C minute
Net weight:	8 lbs
Sensor:	PT100

REFERENCES

1.) M. Chen, T. Pope and D. Ott, Basic Radiology, McGraw-Hill Companies, Incorporated, 2010, ISBN: 9780071627085.

2.) R. Hoskins and A. Thrush, Diagnostic Ultrasound: Physics and Equipment, Greenwich Medical Media, 2010, ISBC: 9781841100425.

3.) G. B. Saha, Fundamentals of Nuclear Pharmacy, Springer, 2010, ISBN: 9781441958600.

4.) Medical X-rays, http://www.fda.gov/Radiation-EmittingProducts/RadiationEmittingProductsandProcedures/MedicalImaging/MedicalX-Rays/defult.htm. (Last Accessed March 2015).

5.) J. T. Bushberg, J. A. Seibert, E. M. Leidholdt and J. M. Boone, The Essential Physics of Medical Imaging, 2011, ISBN: 9780781780575.

6.) J. A. Pope, Medical Physics: Imaging, Heinemann Advanced Science Series, 1999, ISBN: 9780435570941.

7.) Contrast Radiology, Hillcrest Hospital Cushing, http://hillcrestcushing.com/contrast-radiology. (Last Accessed March 2015).

8.) C. J. Powell, M. Dobrota, E. Holtz and H. Vik, *Eur Radiol*,1995, **2**, 176-180.

9.) O. Pert, Mammography and Breast Imaging: Just The Facts, McGraw-Hill Companies,Incorporated, 2005, ISBN: 9780071431200.

10.) S. Vallabhajosula, Molecular Imaging: Radiopharmaceuticals for PET and SPECT, Springer, 2009, ISBN: 9783540767350.

11.) AngioCalc, Cerebral and Peripheral Aneurysm Calculator, http://www.angiocalc.com/ed_sample_case.php, (Last Accessed March 2015).

12.) K. K. Shung, Diagnostic Ultrasound: Imaging and Blood Flow Measurements, Taylor & Francis, 2005, ISBN: 9780849338922.

13.) B. A. Schueler, *Radiographics*, 2000, **20**, 1115-26.

14.) P. V. Prasad, Magnetic Resonance Imaging: Methods and Biologic Applications, Humana Press, 2006, ISBN: 9781597450102.

15.) P. Blower, *Dalton Trans*, 2006, 1705-1711.

16.) A. H. Elgazzar, A Concise Guide to Nuclear Medicine, Springer Berlin Heidelberg, 2011, ISBN: 9783642194269.

17.) M. P. Sandler, Diagnostic Nuclear Medicine, Lippincott Williams & Wilkins, 2003, ISBN: 9780781732529.

18.) J. M. McAlister, Radionuclide Techniques in Medicine, Cambridge University Press,1979, ISBN: 9780521294744.

19.) H. J. Arnikar, Essentials of Nuclear Chemistry, New Age International Publishers, 1995, ISBN: 9788122407129.

20.) Radiopharmaceuticals, http://www.ife.no/en/ife/main_subjects_new/nukleaerteknologi-og-helse/radiofarmaka-en. (Last Accessed March 2015).

21.) E. D. Agdeppa and M. E. Spilker, *APPS J*, 2009, **11**, 286-299.

22.) R. Zimmerman, Nuclear Medicine: Radioactivity for Diagnosis and Therapy, EDP Sciences, 2007, ISBN: 9782868839626.

23.) J. R. Turner, New Drug Development: Design, Methodology, and Analysis, Wiley, 2007, ISBN: 9780470073735.

24.) M. J. Welch, M. L. Thakur, R. E. Coleman, M. Patel, B. A. Siegel, and M. M. Terpogossian, *J. Nucl. Med*, 1977, **18**, 558-562.

25.) P. Charoenphun, R. Paul, A. Weeks, D. Berry, K. Shaw, G. Mullen, J. Ballinger and P. J. Blower, *EJNMMI*, 2011, **38**, S294.

26.) G. L. Patrick, An Introduction To Medicinal Chemistry, Oxford University Press, Incorporated, 2005, ISBN: 9780199275007.

27.) L. K. Steinmetz and E. G. Spack, *BMC Neurol*, 2009, **9**, (Suppl 1): S2

28.) Phases of Development, Pfizer: the world's largest research-based pharmaceutical company, http://www.pfizer.com/research/clinical_trials/phases_of_development, (Last Accessed March 2015).

29.) E. Havas, T. Parvianen, J Vuorela, J. Toivanen, T. Nikula and V. Vihko, *J. Physiol*., 1997, **507**, 233-239.

30.) R. J. Gibbons, *Heart*, 2000, **83**, 355-360.

31.) J. Li, M. M. Cona, F. Chen, Y. Feng, L. Zhou, J. Yu, J. Nuyts, P. de Witte, J. Zhang, U. Himmelreich, A. Verbruggen and Y. Ni, *Theranostics*, 2012, **10**, 1010-1019.

32.) F. Joliot and I Curie, *Nature*, 1934, **3354**, 201-202.

33.) C. Aktolun and S. Goldsmith, Nuclear Medicine Therapy: Principles and Clinical Applications, Springer 2010, ISBN: 9781461440208.

34.) H. Lundqvist, M. Lubberink and V. Tolmachev, *Eur J Phys*, 1988, **19**, 537.

35.) Positron Emmision Tomography, http://www.rah.sa.gov.au/nucmed/PET/pet_info.htm#PEThistory. (Last Accessed March 2015)

36.) D. L. Baily, T. W. Townsend, P. E. Valk and M. N. Maisey, Positron Emission Tomography: Basic Sciences, Springer, 2005, ISBN: 1852337982

37.) G. L. Lenzi, T. Jones, C. G. Mckenzi and S. Moss, *J Neurol Neurosurg Psychiatry*, 1978, **41**, 11-7.

38.) P. Herrero and S. Bergmann, *Developments in Cardiovascular Medicine*, 1992, **133**, 157-164.

39.) L. L. Demer, K. L. Gould, R. A. Goldstein, R. L. Kirkeeide, N. A. Mullani, R. W. Smalling, A. A. Nishikwa and M. E. Merhige, *Circulation*, 1989, **79**, 825-835.

40.) K. L. Gould, *Am. J. Cardiol*, 1990, **66**, 51-58.

41.) S. Leskinenkallio, K. Nagren, P. Lehikoinen, U. Ruotsalaien, M. Teras and H. Joensuu, *J. Nucl. Med*, 1992, **33**, 691-695.

42.) H. Zhang, K. Yoshikawa, K. Tamura, K. Sagou, M. Tian, T. Suhara, S. Kandatsu, K. Suzuki, S. Tanada and H. Tsujii, *Skeletal Radiol*, 2004, **33**, 524-530.

43.) C. Anagnostopoulos, A. Georgakopoulos, N. Pianou, and S. G. Nekolla, *Int J Cardiol*, 2013, **167**, 1737.

44.) W. F. Walsh, H. R. Fill and P. V. Harper, *Semin Nucl Med*, 1977, **7**, 59.

45.) L. Koehler, K Gagnon, S. McQuarrie and F. Wuest, *Molecules*, 2010, **15**, 2686-2718.

46.) Positron Emmision Tomography, Quantum Tunnel, http://quantumtunnel.wordpress.com/2012/12/15/positron-emission-tomography-sci-advent-day-14/. (Last Accessed March 2015).

47.) M. E. Phelps and S. R. Cherry, *Clin. Positron Imaging*, 1998, **1**, 31-45.

48.) S. Kalman, *J.Nucl.Med.Technol*, 2002, **30**, 63.

49.) Plane-Definition of Plane by Medical Dictionary, http://medical-dictionary.thefreedictionary.com/plane. (Last Accessed March 2015).

50.) R. Bar-Shalom, A. Valdivia and M. Blaufox, *Semin.Nucl.Med*, 2000, **30**, 150-185.

51.) S. Dresel, PET in Oncology, Springer Berlin Heidelberg, ISBN: 9783540312031.

52.) F. M. Bengal, T. Higuchi, M. S. Javadi and R. Lautamaki, *J.Am.Coll.Cardiol*, 2009, **54**, 1-15.

53.) Y. F. Tai, and P. Piccini, *J Neurol Neurosurg Psychiatry*, 2004, **75**, 669-676.

54.) W. D. Heiss, G. Pawlik, V. Holthoff, J. Kessler and B. Szelies, *Cerebrovasc.Brain Metab.Rev*, 1992, **4**, 1-27.

55.) A. Hempel, M. Henze, C. Berghoff, N. Garcia, R. Ody and J. Schroder, *Psychiatry Research-Neuroimaging*, 2001, **108**, 133-140.

56.) P. M. Matthews, E. A Rabiner, J. Passchier and R. N. Gunn, *Br.J.Clin.Pharmacol*, 2012, **73**, 175-186.

57.) Shortages in supply of Medical Radioisotopes, news.net/2013/05/08/shortages-in supply-of-medical-radioisotopes-the-lobby-to-stop-alternatives-technologies-and-price-fixing-and-iran/. (Last Accessed March 2015).

58.) A. Rahmin and H. Zaidi, *Nucl.Med.Commun*, 2008, **29**, 93-207.

59.) I. Dijkgraaf and O. C. Boerman, *Eur. J. Nucl. Med. Mol*, 2010, **37**, 104-13.

60.) K. Yoshinaga, C. Katoh, O. Manabe, M. Naya, R. deKemp, R. B. Beanlands and N. Tamaki, Molecular Imaging for Integrated Medical Therapy and Drug Development, Springer, 2010, ISBN: 9784431980735.

61.) M. E. Merhige, W. J. Breen, V. Shelton, T. Houston, B. J. D'Aecy and A. F. Perna, *J. Nucl. Med*, 2007, **48**, 1069-1076.

62.) G. A. M. S. van Dongen, G. W. M. Visser, M. N. L. Hooge, E. G. De Vries and L. R. Perk, *Oncologist*, 2007, **12**, 1379-1389.

63.) D. H. Peters and A. Fitton, *Clinical Immunotherapeutics*, 1995, **3**, 395-408.

64.) M. J. W. D. Vosjan, L. R. Perk, G. W. M. Visser, M. Budde, G. E. Kiefer and G. A. M. S. van Dongen, *Nat Protoc*, 2010, **5**, 739-743.

65.) A. M. Issa, *McGill Journal of Medicine*, 2007, **10**, 53-57.

66.) H. Hong, Y. Yang, Y. Zhang and W. Cai, *Curr.Top.Med.Chem*, 2010, **10**, 1327-1248.

67.) I. B. Buchwalow, E. A. Mibib and W. Boecker, *Acta Histochem*, 2005, **107**, 143-148.

68.) E. Gu, W. Chen, P. Burridge and J. C. Wu, *Theranostics*, 2012, **4**, 335-345.

69.) T. Z. Wong, J. L. Lacy, N. A. Petry, T. C. Hawk, T. A. Sporn, M. W. Dewhirst and G. Vlahovic, *Am.J.Roentgenol*, 2008, **190**, 427-432.

70.) M. Roca, E. F. J. de Vries, F. Jamar, O. Israel and A. Signore, *Eur.J.Nucl.Med.Mol.Imaging*, 2010, **37**, 835-841.

71.) M. P. Sandler, Diagnostic Nuclear Medicine, Lippincott Williams & Wilkins, ISBN: 9780781732529.

72.) M. A. Green and J. C. Huffman, *J.Nucl.Med*, 1988, **29**, 417-420.

73.) Indium in 111 Oxyquinoline Solution, Amersham Health Medi Physics, http://dailymed.nlm.nih.gov/dailymed/lookup.cfm?setid=4c52c904-8137-4b10-8a85-d9b96c2d8a00, (Last Accessed March 2015).

74.) A. Signore, M. Sensi, C. Pozzilli, M. Negri, G. Lenzi and P. Pozzilli, *J.Nucl.Med*, 1985, **26**, 612-615.

75.) Periodic Table of Elements: Zirconium-Zr (EnviromentalChemistry.com), http://environmentalchemistry.com/yogi/periodic/Zr.html#Atomic, (Last Accessed March 2015).

76.) Zirconium (Zr) - Chemical properties, Health and Environmental effects, http://www.lenntech.com/periodic/elements/zr.htm. (Last Accessed October 2014).

77.) L. D. Zardiackas, M. J. Kraay and H. L. Freese, Technology & Engineering, ATSM International, 2006, ISBN: 9780803134973.

78.) M. Eagleson, Concise Encyclopedia Chemistry, Walter de Gruyter, 1994, ISBN: 9783110114515.

79.) C. M. Kozak, and P. Mountford, Zirconium & Hafnium: Inorganic & Coordination Chemistry, John Wiley & Sons, Ltd, 2006, ISBN: 9780470862100.

80.) E. Wiberg and N. Wiberg, Inorganic Chemistry, Academic Press, 2001, ISBN: 9780123526519.

81.) M. A. Pell and J. A. Ibers, *J.Am.Chem.Soc*, 1995, **117**, 6284-6286.

82.) A. Lisovskii and M. Eisen, *Topics Organomet Chem*, 2005, **10**, 63-65.

83.) A. F. Wells, Structural Inorganic Chemistry, Oxford University Press, ISBN: 9780198553700.

84.) C. E. Hollway, I. M. Walker and M. Melni, *Rev Inorg Chem*, 1988, **9**, 153-198.

85.) P. K. Mishra, V. Chakravortty and K. C. Dash, *Transit Metal Chem*, 1991, **16**, 73-75.

86.) G. Roza, Zirconium, Rosen Publishing Group, 2009, ISBN: 9781435850705.

87.) H. Braunschweig, K. Radacki and K. Schwab, *Chem.Commun*, 2010, **46**, 913-915.

88.) S. I. Sukhoruchkin and Z. N. Soroko, *Elementary Particles, Nuclei and Atoms*, 2009, **24**, 1901-1905.

89.) S. Watt, Zirconium, Marshall Cavendish Corporation, 2007, ISBN: 9780761426882.

90.) IUPAC, Naturally occurring isotope abundances: Commission on Atomic Weights and Isotopic Abundances report for the International Union of Pure and Applied Chemistry, 1998, 70, Session 217.

91.) J. P. Holland, Y. Sheh and J. S Lewis, *Nucl.Med.Biol*, 2009, **36**, 729-739.

92.) Q. A. Acton, Issues in Applied Physics: 2011 Edition, Scholarly Editions, 2012, ISBN: 9781464963377.

93.) Isotope data for Zirconium-93 in the Periodic Table, Wolfram Research Inc, http://periodictable.com/Isotopes/040.93/index2.p.full.html, (Last Accessed March 2015).

94.) J. Lehto and X. Hou, Chemistry and Analysis of Radionuclides, Wiley, 2011, ISBN: 9783527633029.

95.) J. Peterson, M. MacDonell, L. Haroun and F. Monette, Radiological and chemical fact sheets to support health risk analyses for contaminated areas. Argonne National Laboratory Environmental, Science Division, Lemont, http://www.remm.nlm.gov/ANL_ContaminantFactSheets_All_070418.pdf, (Last Accessed March 2015).

96.) Y. Zhang, H. Hong and W. Cai, *Curr Radiopharm*, 2011, **4**, 131-139.

97.) I. Verel, G. Visser, R. Boellaard, M. Stigter-van Walsum, G. B. Snow and G. A. M. S. van Dongen, *J.Nucl.Med*, 2003, **44**, 1271-1281.

98.) M. Sadeghi, M. Enferadi and M. Bakhtari, *Ann.Nucl.Energy*, 2012, **41**, 97.

99.) J. Zweit, S. Downey and H. L. Sharma, *Appl.Radiat.Isot*, 1991, **42**, 199-201.

100.) S. A. Kandil, I. Spahn, B. Scholten, Z. A. Saleh, S. M. M. Saad, H. H. Coenen and S. M. Qaim, *Appl.Radiat.Isot*, 2007, **65**, 561.

101.) G. Niu, W. Cai and X. Chen, *Front.Biosci*, 2008, **13**, 790-805.

102.) S. B. M. Gaykema, A. H. Brouwers, S. Hovenga, M. N. Lub-de Hooge, E. G. E. de Vries and C. P. Schroder, *J. Clin. Oncol*, 2012, **30**, 74-75.

103.) J. P Holland, V. Divilov, N. H. Bander, P. M. Smith-Jones, S. M. Larson and J. S. Lewis, *J.Nucl.Med*, 2010, **51**, 1293-1300.

104.) The Hague, Committee on Updating of Occupational Exposure Limits, Yttrium and yttrium compounds Health-based Reassessment of Administrative Occupational Exposure Limits, *2000; publicat*, 2000, ISBN: 9055493503.

105.) Yttrium (Y) – Chemical Properties, Health and Enviromental Effects, http://www.lenntech.com/periodic/elements/y.htm. (Last Accessed March 2015).

106.) S. Ghosh, A. Sharma and G. Talukder, *Biol.Trace.Elem.Res*, 1992, **35**, 247-271.

107.) L. D. Zardiackas, M. J. Kraay and H. L. Freese, Titanium, Niobium, Zirconium, and Tantalum for Medical and Surgical Applications, ATSM, ISBN: 9780803134973.

108.) B. Alberts, A. Johnson, J. Lewis, P. Walter, M. Raff and K. Roberts, Molecular Biology of the Cell 4th Edition: International Student Edition, Routledge, 2002, ISBN: 9780815332886.

109.) H. Firouzabadi, N. Iranpoor and B. Karimi, *ChemInform*, 1999, **30**, 321-323.

110.) J. P. Holland, Y. Sheh and J. S. Lewis, *Nucl.Med.Biol*, 2009, **36**, 729-739.

111.) B. G. Yasnitskii, V. A. Oridoroga, I. I. Novik, Y. N. Chebotaev, I. E. Kalashnikova, B. M. Lotvin, S. S. Kirienko, S. I. Kuvshinova, A. G. Balanyan, M. A. Butlerovskii and A. L. Giverts, *Pharm.Chem.J*, 1976, **10**, 1065-1068.

112.) J. P. Greenstein, *J.Am.Chem.Soc*, 1936, **58**, 1314.

113.) A. Albert and J. N. Phillips, *J. Chem. Soc*, 1956, 1294-1304.

114.) W. F. Zeng, Y. S. Chen, M. Y. Chiang, S. S. Chern and C. P. Cheng, *Polyhedron*, 2002, **21**, 1081-1087.

115.) A. Y. Shen, S. N. Wu and C. T. Chiu, *J.Pharm.Pharmacol*, 1999, **51**, 543-548.

116.) A. T. Krueger and B. Imperiali, *ChemBioChem*, 2013;14, **7**, 788-799.

117.) L. M. Surhone, M. T. Timpledon and S. F. Marseken, Tropolone, VDM Publishing, 2010, ISBN: 9786131017049.

118.) M. J. S. Dewar, *Nature*, 1945, **155**, 50-51.

119.) J. R. Scheffer and L Wang, *J.Phys.Org.Chem*, 2000, **13**, 531-538.

120.) A. Brossi, H. J. C. Yeh, M. Chrzanowska, J. Wolff, E. Hamel, C. M. Lin, F. Quin, M . Suffness and J. Silverton, *Med.Res.Rev*, 1988, **8**, 77-94.

121.) D. T. Leblanc and H. A. Akers, *Food Technol*, 1989, **43**, 78.

122.) K. H. Thompson and C. Orvig, *J.Chem.Soc*, 2000, **17**, 2885-2892.

123.) K. H. Thompson, C. Barta and C. Orvig, *Chem.Soc.Rev*, 2006, **35**, 545-556.

124.) M. Barrand, B. Callingham ans R. Hider, *J.Pharm.Pharmacol*, 1987, 39, 203-211.

125.) R. Galanello, *Ther Clin Risk Manag*, 2007, **3**, 795-805.

126.) D. Rund and E. Rachmilewitz, *N.Engl.J.Med*, 2005, **353**, 1135-1146.

127.) E. Yasumoto, K. Nakano, T. Nakayachi, S. R. M. Morshed, K. Hashimoto, H. Kikuchi, H. Nishikawa, M. Kawase and H. Sakagami, *Anticancer Res*, 2004, **24**, 755-762.

128.) F. Guerard, Y. Lee, R. Tripier, L. P. Szajek, J. R. Deschamps and M. W. Brechbiel, *Chem Comm*, 2013, **49**, 1002-1004.

129.) Safety (MSDS) data for oxine, Bio-Cide International, Inc, http://www.bio-cide.com/uploads/OxineMSDS.pdf, (Last Accessed March 2015).

130.) D. F. Lewis and R. C. Fay, *J. Chem. Soc., Chem. Commun*, 1974, **24**, 1046-1047.

131.) L. E. Orgel, An introduction to transition-metal chemistry ligand-field theory, Methuen & Co Ltd, 1960, ISBN: 9780416634402.

132.) D. Tranqui, J. Laugier, P. Boyer and P. Vulliet, *Acta Cryst*, 1978, **34**, 767-773.

133.) R. D. Archer, W. D. Bonds and W. C. Hamilton, *Inorg.Chem*, 1971, **10**, 1773.

134.) P. Kathirgamanathan, S. Surendrakumar, J. Antipán-Lara, S. Ravichandran, V. R. Reddy, S. Ganeshamurugan, M. Kumaraverl, V. Arkley, A.J. Blake and D. Bailey, *J.Mater.Chem*, 2011, **21**, 1762-1771.

135.) Small Lights, Big Impression, *Chemistryworld*, A. Extance, http://www.rsc.org/chemistryworld/2013/05/organic-light-emitting-diodes-oleds, (Last Accessed March 2015).

136.) P. Kathirgamanathan, V. Arkley, S. Surendrakumar, G. Paramaswara, J. Antipán-Lara, , S. Ravichandran, S. Ganeshamurugan, M. Kumaraverl and Y. F. Chan, *Society For Information Display*, 2007, ISBN: 9789810581435.

137.) A. R. Davis and F. W. B. Einstein, *Acta Crystallogr. Sect. B*, 1978, **34**, 2110-2115.

138.) F. D. C. Fim, T. Machado, D. S. De Sá, P. R. Livotto, Z. N. Rocha, N. R. D. S. Basso and G. B. Galland, *J.Polym.Sci. A Polym*, 2008, **46**, 3830-3841.

139.) S. Alshehri, J. Burgess, J. Fawcett, S. A. Parsons and D. Russell, *Polyhedron*, 2000, **28**, 399-405.

140.) M. A. Barrand, B. A. Callingham and R. C. Hider, *J.Pharm.Pharmacol*, 1987, **39**, 203-201.

141.) G. J. Kontoghiorghes, *Analyst*, 1995, **120**, 845-851.

142.) L. N. Sheepard and G. J. Kontoghiorghes, *Arzneimittelforschung*, 1993, **43**, 659-663.

143.) E. L. Muetterties and C. W. Alegranti, *J.Am.Chem Soc*, 1969, **91**, 4420-4425.

144.) W. Y. Hsieh and S. Liu, *Synth React Inorg Me*, 2005, **35**, 61-70.

145.) J. H. Gross and P. Roepstorff, Mass Spectrometry: A textbook, Springer, 2011, ISBN: 9783642107092.

146.) J. T. Watson and O. D. Sparkman, Introduction to mass spectrometry: Instrumentation, applications and strategies for data interpretation, Wiley-Blackwell, 2008, ISBN: 9780470516348.

147.) MIT, Growing Quality Crystals, http://web.mit.edu/x-ray/cystallize.html, (Last Accessed March 2015).

148.) C. Hammond, The Basics of Crystallography and Diffraction, 3rd Edition, Oxfod, 2009, ISBN: 9780199546459.

149.) N. E. Jacobsen, NMR Spectroscopy Explained: Simplified Theory, Applications and Examples for Organic Chemistry and Structural Biology, Wiley, 2007, ISBN: 9780471730965.

150.) D. H. Williams, and I. Fleming, Spectroscopic methods in organic chemistry, McGraw-Hill, 1996, ISBN: 9780077091477.

151.) E. Breitmaier, Structure elucidation by NMR in organic chemistry: a practical guide, Wiley, 2002, ISBN: 9780470850060.

152.) C. Blaire, B. C. Baker and D. T. Sawyer, *Anal Chem*, 1968, **40**, 1945-1951.

153.) J. K. Howie, P. Bosserman and D. T. Sawyer, *Inorg.Chem*, 1980, **19**, 2293-2296.

154.) F. Macdonald and C. H. J. Ford, Molecular Biology of Cancer, BIOS Scientific Publishers Limited, 1997, ISSN: 1859962254.

155.) M. A. Greean and J. C. Huffman, *J.Nucl.Med*, 1988, **3**, 417-420.

156.) A. von Zelewsky, Stereochemistry of Coordination Compounds, John Wiley & Sons, 1996, ISBN: 9780471955993.

157.) M. Roca, E. F. J. de Vries, F. Jamar, O. Israel and A. Signore, *Eur.J.Nucl.Med.Mol.Imaging*, 2010, **37**, 835-841.

158.) P. Griffiths and J. A. De Haseth, Fourier Transform Infrared Spectrometry, John Wiley & Sons, 2007, ISBN: 9780470106297.

159.) R. C. Taylor, E. M. Larsen and D. R. Taylor, *J.Inorg.Nucl.Chem*, 1981, **43**, 293-298.

160.) G. M. Photiadis and G. N. Papatheodorou, *Dalton Trans*, 1998, **21**, 981-989.

161.) Y. T. Li, C. W. Yan and H. S. Guan, *Polyhedron*, 2003, **22**, 3223-3230.

162.) R. L. Frost, M. L. Weier, *J.Raman Spectrosc*, 2003, **34**, 776-785.

163.) T. Gavrilko, R. Fedorovich, G. Dovbeshko, A. Marchenko, A. Naumovets, V. Nechytaylo, G. Puchkovska, L. Viduta, J. Baran and H. Ratajczak, *J.Mol.Struct*, 2004, **704**, 163-168.

164.) A. D. Patel, N. K. Prajapati and J. J. Vora, *Der Pharmacia Sinica*, 2012, **3**, 93-98.

165.) M. M. A. Sekkina and S. M. El Helbawt, *Sci.Ami,51.A*, 1985, **51**, 959-964.

166.) C. C. Wagner, A. C. Gonzalez-Baro, E. J. Baran, *Spectroc.Acta Pt.A-Molec.Biomolec.Spectr*, 2011, **79**, 1762-1765.

167.) Y. Ikegami, *Bull.Chem.Soc.Jpn*, 1963, **36**, 1118-1125.

168.) J. L. Yao, Y. X. Yuan and G. N. Gu, *Spectroc.Acta Pt.A-Molec.Biomolec.Spectr*, 2006, **64**, 1072-1076.

169.) J. Burgess, B. DeCastro, C. Oliveria, M. Rangel and W. Schlindwein, *Polyhedron*, 1997, 16, **5**, 789-794.

170.) K. H. Thompson, J. Chiles, V. G. Yuen, J. Tse, J. H. McNeill and C. Orvig, *J.Inorg.Biochem*, 2004, **98**, 683-690.

171.) B. S. Parajon-Costa, E. J. and E. J. Baran, *Spectroc.Acta Pt.A-Molec.Biomolec.Spectr*, 2013, **113**, 337-339.

172.) B. S. Parajon-Casta, E. J. and E. J. Baran, *Spectroc.Acta Pt.A-Molec.Biomolec.Spectr*, 2011, **78**, 133-135.

173.) C. C. Wagner, B. S. Parajon-Casta, E. J. and E. J. Baran, *Lat Am J Pharm*, 2011, **30**, 1454-1456.

174.) C. Y. Panicker, H. T. Varghese, B. Harikumar and A. Chandran, *Orient J Chem*, 2011, **27**, 1705-1709.

175.) C. Queiros, M. J. Amorim, A. Leite, M. Ferreira, P. Gameiro, B. de Castro, K. Biernacki, A. Magalhaes, J. Burgess and M. Rangel, *Eur.J.Inorg.Chem*, 2011, 131-140.

176.) M. Mohammadpour, A. Sadeghi, A. Fassihi, L. Saghaei, A. Movahedian and M. Rostami, *Res.Pharm.Sci*, 2012, **7**, 171-179.

177.) J. Sebestik, M. Safarik, and P. Bour, *Inorg.Chem,* 2012, **51**, 4473-4481.

178.) F. A. Johnson, E. M. Larsen, C. L. Rollinsion and J. Lindsay, Inorganic Syntheses, Volume 8, Wiley, ISBN: 9780470131671.

179.) H. H. Perkampus, UV-VIS spectroscopy and its applications, Springer-Verlag, 1992, ISBN: 9783540554219.

180.) B. J. Clark, T. Frost and A. Russell, UV Spectroscopy: Techniques, Instrumentation and Data Handling, Springer, 1993, ISBN: 9780412405303.

181.) L. M. A. Monzon, F. Burke and J. M. D. Coey, *J.Phys.Chem.C,* 2011, **115**, 9182-9192.

182.) B. S. Parajón-Costa, E. J. Baran, J. R. R. Sáez-Puche, G. Arrambide and D. Gambino, *J.Coord.Chem*, 2011, **64**, 57-70.

183.) S. Lindsay, High Performance Liquid Chromatography, Wiley, 1992, ISBN: 9780471931157.

184.) W. J. Lough and I. W. Wainer, High Performance Liquid Chromatography: Fundamental Principles and Practice, Blackie Academic & Professional, 1995, ISBN: 9780751400762.

185.) G. B. Saha, Basics of PET Imaging: Physics, Chemistry, and Regulations, Springer, 2005, ISBN: 9780387271286.

186.) C. S. Hambali and P. R. Haddad, *Chromatographia*, 1980, **13**, 633-634.

187.) K. Soroka, R. S. Vithanage, D. A. Phillips, B. Walker and P. K. Dasgupta, *Anal.Chem*, 1978, **59**, 629-636.

188.) F. Z. Lian, Q. Huang, Y. F. Kang, G. W. Zou, S. P. Bi and L. C. Tian, *J.Liq.Chromatogr.Rel.Technol*, 2003, **26**, 273-283.

189.) E. J. Wojtowicz, *J.Pharm.Sci*, 1984, **73**, 1430-1433.

190.) J. P. Larcinese, F. Avaltroni and V. Normand, *J.Chromatogr.Sci*, 2007, **45**, 629-634.

191.) M. Abbas, R. Nawaz, T. Iqbal, M. Ali and M. R. Asi, *Pak.J.Pharm.Sci*, 2012, **25**, 343-348.

192.) Agilent Technologies, Analytical HPLC & UHPLC, Zorbax Eclipse XDB, http://www.chem.agilent.com/en-US/products-services/Columns-Sample-Preparation/LC-LC-MS-Columns/Analytical-HPLC-UHPLC/ZORBAX-Eclipse-XDB/Pages/default.aspx, (Last Accessed March 2015).

193.) Phenomenex, Luna HPLC Column, http://www.phenomenex.com/Products/Part/00D-4162-Y0, (Last Accessed March 2015).

194.) Luna Range HPLC Columns (Phenomenex) https://www.brechbuehler.ch/fileadmin/redacteur/pdf/columns-sampleprep/lc-columns/zhlun.pdf, (Last Accessed March 2015).

195.) Alltima HP Reversed-Phase C18 Hi-Load HPLC Columns, Mandel Scientific Company Inc, http://www.mandel.ca/products/chromatography/Liquid_Chromatography/HPLC_Columns/Alltech_Alltima_HP/Alltima_HP_C18_HiLoad/index.htm, (Last Accessed March 2015).

196.) Alltima - A Column for All Reasons, http://www.bioszeparacio.hu/_user/downloads/HPLC/Alltima1.pdf, (Last Accessed March 2015).

197.) Imtakt USA-Next Generation HPLC Columns, http://www.imtaktusa.com/library/technical_information/4/, (Last Accessed March 2015).

198.) D. Corradini, Handbook of HPLC, Second Edition, Taylor & Francis, 2010, ISBN: 9781420016949.

199.) D. M. Wieland, M. C. Tobes and T. J. Mangner, Analytical and chromatographic techniques in radiopharmaceutical chemistry, Springer-Verlag, 1986, ISBN: 9780387961859.

200.) J. Sherma and B. Fried, Handbook of Thin-Layer Chromatography, Taylor & Francis, 2003, ISBN: 9780824748661.

201.) E. Hahn-Deinstrop, Applied Thin-Layer Chromatography, Wiley, 2007, ISBN: 9783527315536.

202.) S. F. W. Sunderman, *Ann.Clin.Labb.Sci*, 1990, **20**, 12-21.

203.) J. R. Ballinger, B. Gerson and K. Y. Gulenchyn, *Int.J.Rad.Appl.Instrum,A*, 1987, **38**, 665.

204.) J. Debruine, E.Vanroyen, A. Vyth, J. Dejong and J. B. Vanderschoot, *J.Nucl.Med*, 1985, **26**, 925-930.